

Novel strategies for singlet molecular oxygen O₂(¹Δ_g) generation and detection in cells

Roger Bresolí Obach

<http://hdl.handle.net/10803/662972>

ADVERTIMENT. L'accés als continguts d'aquesta tesi doctoral i la seva utilització ha de respectar els drets de la persona autora. Pot ser utilitzada per a consulta o estudi personal, així com en activitats o materials d'investigació i docència en els termes establerts a l'art. 32 del Text Refós de la Llei de Propietat Intel·lectual (RDL 1/1996). Per altres utilitzacions es requereix l'autorització prèvia i expressa de la persona autora. En qualsevol cas, en la utilització dels seus continguts caldrà indicar de forma clara el nom i cognoms de la persona autora i el títol de la tesi doctoral. No s'autoritza la seva reproducció o altres formes d'explotació efectuades amb finalitats de lucre ni la seva comunicació pública des d'un lloc aliè al servei TDX. Tampoc s'autoritza la presentació del seu contingut en una finestra o marc aliè a TDX (framing). Aquesta reserva de drets afecta tant als continguts de la tesi com als seus resums i índexs.

ADVERTENCIA. El acceso a los contenidos de esta tesis doctoral y su utilización debe respetar los derechos de la persona autora. Puede ser utilizada para consulta o estudio personal, así como en actividades o materiales de investigación y docencia en los términos establecidos en el art. 32 del Texto Refundido de la Ley de Propiedad Intelectual (RDL 1/1996). Para otros usos se requiere la autorización previa y expresa de la persona autora. En cualquier caso, en la utilización de sus contenidos se deberá indicar de forma clara el nombre y apellidos de la persona autora y el título de la tesis doctoral. No se autoriza su reproducción u otras formas de explotación efectuadas con fines lucrativos ni su comunicación pública desde un sitio ajeno al servicio TDR. Tampoco se autoriza la presentación de su contenido en una ventana o marco ajeno a TDR (framing). Esta reserva de derechos afecta tanto al contenido de la tesis como a sus resúmenes e índices.

WARNING. The access to the contents of this doctoral thesis and its use must respect the rights of the author. It can be used for reference or private study, as well as research and learning activities or materials in the terms established by the 32nd article of the Spanish Consolidated Copyright Act (RDL 1/1996). Express and previous authorization of the author is required for any other uses. In any case, when using its content, full name of the author and title of the thesis must be clearly indicated. Reproduction or other forms of for profit use or public communication from outside TDX service is not allowed. Presentation of its content in a window or frame external to TDX (framing) is not authorized either. These rights affect both the content of the thesis and its abstracts and indexes.

DOCTORAL THESIS

Title	Novel strategies for singlet molecular oxygen $O_2(^1\Delta_g)$ generation and detection in cells
Presented by	Roger Bresolí Obach
Centre	IQS School of Engineering
Department	Analytical and Applied Chemistry
Directed by	Prof. Santiago Nonell Marrugat and Dr. Rubén Ruiz González

*Diuen que totes les coses
que aprens en la vida són fruit dels errors.
I que gràcies a tantes caigudes
comences a entendre les regles del joc.*

*Diuen que l'home entropessa amb la mateixa pedra
en més d'una ocasió.
I que cada entrebanc és un repte
que cal afrontar sense temor.*

Pau Alabajos

*Quan surts per fer el viatge cap a Ítaca,
has de pregar que el camí sigui llarg,
ple d'aventures, ple de coneixences.
Has de pregar que el camí sigui llarg,
que siguin moltes les matinades
que entraràs en un port que els teus ulls ignoraven,
i vagis a ciutats per aprendre dels que saben.*

*Tingues sempre al cor la idea d'Ítaca.
Has d'arribar-hi, és el teu destí,
però no forçis gens la travessia.
És preferible que duri molts anys,
que siguis vell quan fondegis l'illa,
ric de tot el que hauràs guanyat fent el camí,
sense esperar que et doni més riqueses.*

*Ítaca t'ha donat el bell viatge,
sense ella no hauries sortit.
I si la trobes pobra, no és que Ítaca
t'hagi enganyat. Savi, com bé t'has fet,
sabràs el que volen dir les Ítaques.*

Konstandinos Petru Kavafis – Lluís Llach

*On vas Ulisses si no tens barca,
i ni tan sols saps on para Ítaca?
Només la fermesa de voler alçar-la
no et durà més lluny de la primera onada.*

*On vas Ulisses si no tens barca?
On vas Ulisses sens camarades,
si t'has quedat sol de tant destriar-ne?
Demà tindràs l'esquena baldada
sens haver perdut ni de vista la platja.*

*On vas Ulisses sens camarades?
On vas Ulisses si no tens mapes,
ni diari d'abord, ni calendari de viatge,
esperant que el vent i la benaurança
et dugui a bon port com per art de màgia?*

*Fes primer una barca a la teva drassana,
allà hi trobaràs gent que voldrà acompanyar-te.
No trïis els millors amics sinó gent experimentada:
els millors mariners, de tots la gent més brava.
Tots junts traçarem una ruta clara,
discretament, sense advertir la guàrdia.
Amb tu Ulisses vull fer el viatge!*

*Deixa, Ulisses, de fer memòria
de les virtuts que ens encaminen,
d'assajar la dansa de la victòria
i brandar en terra la bandera de marina.*

*No somiarem més enmig de lluna plena
ni ens discutirem per la forma de l'eina.
Jo també frisso a desplegar la vela
però és a drassanes on ara hi ha feina.
Amb tu Ulisses faré el viatge!*

Aramateix - Francesc Ribera (Titot)

Resum

En aquesta tesi s'han utilitzat diferents estratègies per obtenir control en la producció i detecció de diferents espècies reactives d'oxigen (ROS), especialment per a l'oxigen singlet ($^1\text{O}_2$).

En la primera part de la tesi, l'enfoc principal consisteix en entendre la generació de ROS i intentar potenciar-ne el seu efecte. En primer lloc, demostrem que la modificació de diferents fotosensibilitzadors afegint-hi un catió de trifenilfosfoni com a element diana produeix derivats amb una excel·lent activitat fotoantimicrobiana contra bacteris Gram-positius (*S. aureus* i *E. faecalis*). **En segon lloc,** descobrim una sèrie de nous aspectes de la reacció de “ β -phenyl quenching” per derivats de 9-fenilfenalenona. La fototoxicitat d'aquests derivats ja es troba esmentada en el llibre: “L'origen de les espècies” de C. Darwin. També es suggereix una via metabòlica mediada per la reacció BPQ en la biosíntesi dels pigments vegetals derivats de fluorones. A més, si el grup fenil és substituït per altres grups arils, s'observa diferències en la reacció de BPQ. **En tercer lloc,** s'ha demostrat que diferents antraquinones d'origen natural indueixen fototoxicitat en biofilms de *C. tropicalis* a causa de la generació de $\text{O}_2^{\bullet-}$, tenint l' $^1\text{O}_2$ un rol menor. **En quart lloc,** es demostra el fàrmac antitumoral Doxorubicina produeix quantitats significants d' $^1\text{O}_2$, però es redueix la seva generació quan es complexa amb el ADN. **En cinquè lloc,** s'ha estudiat l'efecte d'adsorció o unió covalent d'un fotosensibilitzador a nanopartícules mesoporoses de sílice. A més a més, s'han derivatitzat per afegir-hi elements diana. **Sisè i últim,** s'ha estudiat les propietats fotoquímiques d'una nova diada que conté un bromo-bodipy com a fotosensibilitzador i trampa química de ROS (que desactiva la capacitat del bromo-bodipy de generar $^1\text{O}_2$). Un cop oxidada la trampa química, la diada recupera la capacitat de generar $^1\text{O}_2$ i causar dany cel·lular. S'observa diferents propietats foto-antitumorals d'aquesta diada en funció de l'estrès cel·lular o de la localització cel·lular.

En la segona part de la tesi, s'ha centrat en la detecció de ROS. En primer lloc, s'han dissenyat, sintetitzat i caracteritzat nanosondes fluorescents per la detecció d' $^1\text{O}_2$ en sistemes biològics. La nanovehiculització elimina algunes de les limitacions de les diferents sondes fluorescents d' $^1\text{O}_2$. En aquest sentit, diverses sondes tals com SOSG, ADPA o furil-vinil-naftooxazol s'han unit covalentment a nanopartícules utilitzant diferents cadenes espaciadores per tal d'optimitzar la seva reactivitat front $^1\text{O}_2$. A diferència de quan es troben lliures en solució, les nanosondes són fàcilment internalitzades per cèl·lules eucariotes i procariotes i es minimitza la interacció amb proteïnes (com per exemple, l'albumina de sèrum boví). Les diferents nanosondes responen a l' $^1\text{O}_2$ generat intracel·lular. Com a prova de concepte, també s'ha desenvolupat una nanosonda fluorescent per la detecció no selectiva de ROS, basada en 2',7'-diclorodihidrofluoresceïna. **En segon lloc,** s'ha caracteritzat la estructura i reactivitat de la sonda fluorescent: CellROX Deep Red. **En tercer lloc,** s'ha desenvolupat la primera sonda d'optoacústica per la detecció de ROS basada en l'oxidació de la tetrametilbenzidina. S'ha aconseguit detectar $^1\text{O}_2$ produït per bacteris utilitzant tal sonda.

Finalment i com a prova de concepte, s'ha dissenyat un “self-reporter” nanofotosensibilitzador. El nanosistema és capaç de produir i detectar $^1\text{O}_2$ simultàniament. Aquest nanodispositiu s'ha utilitzat amb èxit per la fotoinactivació de *S. aureus*, observant-se una correlació entre el canvi de fluorescència de la sonda i la mort bacteriana.

Resumen

En esta tesis se han utilizado distintas estrategias para obtener el control en la producción y detección de diferentes especies reactivas de oxígeno (ROS), especialmente para el oxígeno singlete ($^1\text{O}_2$).

En la primera parte de la tesis, el enfoque principal consiste en entender la generación de ROS e intentar potenciar su efecto. En primer lugar, demostramos que la modificación de distintos fotosensibilizadores, añadiendo un catión de trifenilfosfonio como elemento diana, produce derivados con una excelente actividad fotoantimicrobiana contra bacterias Gram-positivas (*S. aureus* y *E. faecalis*). **En segundo lugar,** descubrimos una serie de nuevos aspectos de la reacción de " β -phenyl quenching" por derivados de 9-fenilfenalenona. La fototoxicidad de estos derivados ya se encuentra mencionada en el libro: "el origen de las especies" de C. Darwin. También se sugiere una vía metabólica mediada por la reacción BPQ en la biosíntesis de los pigmentos vegetales derivados de fluorenonas. Además, si el grupo fenilo es sustituido por otros grupos arilos, se observan diferencias en la reacción de BPQ. **En tercer lugar,** se ha demostrado que distintas antraquinonas de origen natural inducen fototoxicidad en biofilms de *C. tropicalis* debido a la generación de $\text{O}_2^{\bullet-}$, teniendo el $^1\text{O}_2$ un rol menor. **En cuarto lugar,** se demuestra que el fármaco antitumoral Doxorubicina produce cantidades significantes de $^1\text{O}_2$, pero se reduce su generación cuando se compleja con el ADN. **En quinto lugar,** se ha estudiado el efecto de adsorción o unión covalente de un fotosensibilizador a nanopartículas mesoporosas de sílice. Además, se han derivatizado para añadir elementos diana. **Sexto y último,** se han estudiado las propiedades fotoquímicas de una nueva diada que contiene un bromo-bodipy como fotosensibilizador y trampa química de ROS (que desactiva la capacidad del bromo-bodipy para generar $^1\text{O}_2$). Una vez oxidada la trampa química, la diada recupera la capacidad para generar $^1\text{O}_2$ y causar daño celular. Se observan diferentes propiedades foto-antitumorales de esta diada en función del estrés celular o de la localización celular.

La segunda parte de la tesis, se ha centrado en la detección de ROS. En primer lugar, se han diseñado, sintetizado y caracterizado nanosondas fluorescentes para la detección de $^1\text{O}_2$ en sistemas biológicos. La nanovehiculización elimina algunas de las limitaciones de las distintas sondas fluorescentes de $^1\text{O}_2$. En este sentido, varias sondas tales como SOSG, ADPA o furilo-vinilo-naftooxazol se han unido covalentemente a nanopartículas utilizando distintas cadenas espaciadoras para optimizar su reactividad frente $^1\text{O}_2$. A diferencia de cuando se encuentran libres en solución, las nanosondas son fácilmente internalizadas por células eucariotas y procariotas y se minimiza la interacción con proteínas (como por ejemplo con la albúmina de suero bovino). Las distintas nanosondas responden al $^1\text{O}_2$ generado intracelular. Como prueba de concepto, también se ha desarrollado una nanosonda fluorescente para la detección no selectiva de ROS, basada en 2',7'-diclorodihidrofluoresceína. **En segundo lugar,** se ha caracterizado la estructura y reactividad de la sonda fluorescente: CellROX Deep Red. **En tercer lugar,** se ha desarrollado la primera sonda de optoacústica para la detección de ROS basada en la oxidación de la tetrametilbenzidina. Se ha logrado detectar $^1\text{O}_2$ producido por bacterias empujando tal sonda.

Finalmente, y como prueba de concepto, se ha diseñado un "self-reporter" nanofotosensibilizador. El nanosistema es capaz de producir y detectar $^1\text{O}_2$ simultáneamente. Este nanodispositivo ha sido utilizado con éxito para la fotoinactivación de *S. aureus*, observándose una correlación entre el cambio de fluorescencia de la sonda y la muerte bacteriana.

Abstract

In this thesis, different strategies have been used in order to gain control in reactive oxygen species (ROS) production and detection, especially for singlet oxygen ($^1\text{O}_2$).

In the first part of the thesis, the main focus is towards understanding ROS generation and try to potentiate its effect. First, we demonstrate that modification of different photosensitisers with the triphenylphosphonium cation yields derivatives with an excellent photoantimicrobial activity against Gram-positive bacteria (i.e., *S. aureus* and *E. faecalis*). **Second**, we uncover a number of new aspects of β -phenyl quenching reaction in 9-phenylphenalenone scaffold, whose phototoxicity was already mentioned in Darwin's Origin of Species. It is suggested an excited state-mediated metabolic pathway in the biosynthesis of fluorone plant pigments. Moreover, if phenyl moiety is substituted for other aryl groups, it is observed that the electrocyclic ring opening back to ground state ketones have lifetimes between milliseconds and picoseconds. **Third**, we demonstrate that the main photosensitizing mechanism, involved in the photo-induced *C. tropicalis* antibiofilm activity by natural anthraquinones, is via $\text{O}_2^{\bullet-}$ production, whereas $^1\text{O}_2$ participation seems of lesser importance. **Fourth**, we demonstrate that doxorubicin produces significant amounts of $^1\text{O}_2$, however, this is largely suppressed when bound to DNA. **Fifth**, we studied the effect of PS adsorption or covalently bond onto the surface of mesoporous silica nanoparticles. Moreover, we further derivatize them for attach targeting elements. **Sixth and last**, we studied the activation a new dyad comprising a bromo-bodipy, which acts as PS, plus a non-selective ROS chemical trap, which quenches the ability of bromo-bodipy to produce $^1\text{O}_2$. For that aPS we observe a differential behaviour in function of the cellular stress or even in function of the organelle.

In the second part of the thesis, focus has been shifted towards ROS detection. First, we designed, synthesized, and characterized biocompatible fluorescent nanoprobe for $^1\text{O}_2$ detection in biological systems that circumvents many of the limitations of the different molecular $^1\text{O}_2$ fluorescent probes. Under that purpose different $^1\text{O}_2$ probes (Singlet Oxygen Sensor Green, anthracene dipropionic acid and furyl-vinyl-naphthoxazole) were covalently linked to nanoparticles core using different architectures to optimize their response to $^1\text{O}_2$. In contrast to its molecular counterpart, the optimum nanoprobe are readily internalized by prokaryotic and eukaryotic cells and they do not interact with proteins (i.e. bovine serum albumin). Furthermore, the spectral characteristics do not change inside cells, and the probe responds to intracellular generated $^1\text{O}_2$ with the corresponding change in fluorescence. As a proof of concept, a non-selective ROS fluorescent nanoprobe, based on diacetyl 2',7'-dichlorodihydrofluorescein, has been synthesized and successfully used for detecting intracellular ROS. **Second**, we have performed the chemical characterization of the CellROX Deep Red, a new commercial non-selective ROS fluorescent probe, ascertained its putative chemical structure and evaluated its reactivity towards different reactive oxygen/nitrogen species and light in solution. **Third**, we developed the first ROS optoacoustic probe based on the oxidation of tetramethylbenzidine and successfully used for detecting $^1\text{O}_2$ produced by bacteria.

Finally, as proof of concept we have designed a self-reporter nanophotosensitizer. The nanosystem is capable to produce and detect the $^1\text{O}_2$ generated simultaneously. It has been successfully used for *S. aureus* photoinactivation in which a correlation was observed between fluorescent change of the probe and bacterial cellular death.

Agraïments:

“Fa una nit clara i tranquil·la, hi ha la lluna que fa llum, els convidats van arribant i van omplint tota la casa de colors i de perfums (...)”

Bones tardes amics meus tots, majoritàriament els he escrit tornant de Montreal; penseu que són 7 hores de vol que donen per molt. Avis per a navegants, ho he escrit tal com sóc jo, cosa que potser hi ha frases no molt políticament correctes, però són autèntiques i això es el que compta.

(...) I ens ha costat Déu i ajuda arribar fins aquí (...)

Primer de tot vull agrair al **Santi**, probablement sense tu avui no estaríem aquí. M'agradaria agrair-te les hores que has estat picant pedra per tal d'ensenyar-me moltes de les coses que actualment se. Segurament, tot i que jo no m'he n'hagi adonat massa, tu has influït (i crec que molt positivament) a ser la persona que avui sóc, perquè primer són les persones i després ja si de cas la ciència. Ho puc dir sense por a equivocar-me (que és una de les coses que sempre hem dius, tot i tenir la raó tens por a equivocar-te) amb tots aquests anys has de fet professor, mentor, conseller, però també d'amic. I mira que n'hem fet de coses, des de ciència (i crec que de la bona) a shows a les escoles, xarrades filosòfiques, compartir gastronomia... Espero que aquesta relació amb el temps vagi a millor (o com a mínim es mantingui igual). Gràcies una altra vegada.

En segon lloc (com català que sóc i la pela és la pela) vull agrair als fons socials europeus i al secretariat d'universitats i recerca del DEC de la Generalitat de Catalunya per la concessió de la beca que m'ha permès sobreviure durant aquests tres anys de doctorat (2015 FI_B 00315; 2016 FI_B1 00021; 2017 FI_B2 00140). També quiero agradecer al Ministerio de Economía y Competividad los dos proyectos de investigación (CTQ2013-48767-C3-1-R; CTQ2016-78454-C2-1-R) y la Red de Fotoquímica Biológica (CTQ2015-71896-REDT) que han costeado la mayor parte de los experimentos de esta tesis doctoral y mi estancia a Málaga. També vull agrair a l'Institut Químic de Sarrià per costejar l'altra part dels experiments realitzats. Finally, I want to thank the European Society for Photobiology for the fellowships to attend the 16th and 17th Congress of the ESP.

Aquest viatge a Ítaca, va començar un dia de setembre en el llunyà 2008 (i ara estem al 2018; casi 10 anys) on vam passar de Tàrrrega a Barcelona, un gran canvi per cert. Van passar els anys de la llicenciatura on vaig conèixer grans persones (però això avui no toca). Avui i ara toca parlar del grup de fotoquímica (els de tota la vida):

Gràcies **Rubén**, per tots els anys que he tingut el plaer que hagi "codirigit" aquesta tesis. Hi ha una certa part que també és teva. A part de ciència, hem fet altres coses (moltes també van per tu Quimet, però no les repetiré) veure els partits del Barça al Sotavent, fer passejos pel Parque del Retiro (i ho deixo aquí), anar a jugar al billar amb el pitzero de Prada a baix (entre moltes altres coses)... Llàstima que no vaig venir aquell dia que "regalaven" el Jabugo (el Jaumet aquí va ser llest).

Gràcies **Joaquim** (o millor dit Quimet), aquesta vegada he après i no citaré el magnífic Jep Cabestany ehh.... Ets una de les millors persones que he conegut. Crec que no fa falta que digui res més. Allí estas sempre, entusiasta, amb ganes de fer coses, normalment mai dient

que no, normalment liante o viceversa... i això és molt bonic. Que et vagi molt molt bé aquest nou període de vida que iniciem. Nen, siguis tu; no canviïs mai (o si ho fas a millor).

Ara anem per tu **Uri**, tampoc podies faltar en aquesta llista. Potser alguns dies hem tingut els nostres altibaixos però crec que ara tot ha tornat al nivell basal i això per a mi és molt important (espero que el mateix a viceversa). Tal com he dit al Joaquim que no canviï mai, tu has canviat (i molt) des de que et vaig conèixer. No entraré a valorar si a millor o pitjor, tot canvi té les seves coses bones i dolentes. Gràcies pels bons moments que hem compartit i els que espero en un futur i per totes les coses que m'has ensenyat o hem après amb el pas del temps. Tal com diria la Pepa: mejora continua.

Ara anem per tu **Bea**, primer de tot gràcies per aguantar-me aquests anys, sé que ha estat dur, però doncs aquí estem. Espero que et vagi molt be en aquesta nova etapa que comences.

I no hem podia oblidar del megacrack de la sílice, **gran Jaumet**. Per les teves teories, per els moments de riure, per les teves anades d'olla, per parlar sol (que no és gens dolent; jo també ho faig a vegades), per seguir-me a rampinyar, per això i per moltes altres coses, gràcies. A part sense la teva col·laboració i coneixements aquesta tesis tampoc s'hauria realitzat.

Per una banda no hem podia descuidar al companys del laboratori de microbiologia. Primer, gràcies **Montse** per tal d'ajudar-me a planificar els experiments i resoldre tots els meus dubtes quan els he tingut. Per altra banda, també gràcies **Oscar** per estar sempre a punt de donar un cop de mà. Sense tu part d'aquesta tesis no s'hauria realitzat. A part sempre que hem necessitat parlar ho he pogut fer i sempre m'has escoltat i aconsellat.

I no hem puc descuidar la nostra adoptada, la **Eli**. Tot i haver entrat per l'altra porta, crec que t'hem acollit a la perfecció, si no ja ens ho diràs. Gràcies per estar present sempre que t'he necessitat i per comentar tant experiències científiques com no. Espero que en breus estiguem ja en una altra etapa. El mateix m'agradaria dir pel **Raul**, tot i que vas aparèixer més tard, també et dic el mateix que per l'Eli... Gràcies per totes les xerrades.

I ara m'agradaria fer un viatge temporal per la resta:

Quan vaig arribar al grup quan començava 5è (estic parlant de setembre de 2012; fa temps ehhh...), hi havia persones que ara ja no hi són (si si llei de vida ...). Encara ho recordo, el primer dia a lo grande, trencant una cubeta! (com s'ha de fer, per deixar impacte). En aquells temps hi havia l'Adaya que era qui posava "cordura" al grup, perquè si la resta ho teníem que fer, malament anàvem. Allà ballant allò (que no m'hen recordo com és diu) que sembla capoeira però la versió moderna i que estaven que no cagaven... Els primers beures...

I aquí vull introduir una cosa els Provamels eh... **Ester** (Volmer ¿? Gran Joaquim)... tu entre això i el tango ja ho teníem tot solucionat. Gràcies Ester per posar la cordura i la seriositat en aquest grup. I ho complirem un dia anirem a ballar tango (no se quant tinc marge fins a la mort). Només per aguantar-nos ja t'hem d'estar completament agraïts. Però encara hi ha més... sempre estaves allà en mode positiu i preparada per ensenyar uns quants transitoris incunables (tot i que mira que a mi m'agraden).

Els dies van corrent, estava a punt d'acabar 5è i llavors amb el Santi vam decidir provar una síntesis (secció 3.2). Vam pensar amb qui millor ho podem fer que amb la **Carme**, la persona

que m'ha ensenyat la poca química orgànica que sé. Hem va acollir amb els braços oberts i mira que ho vam fer bé que fins i tot vaig obtenir uns mil·ligrams del producte. Has estat una de les millors professores que he tingut (i encara millor persona) t'ho vull agrair. També als nens que voltaven per allí, ehh Lordan i Adam.

Vaig començar el màster and then it arrives my first visitor. Yeah I am talking about you Alena. In that time, I learnt a lot of things from your experience. Also, I learnt some words in German (i.e. papallona is "S+Metall+IN"). Thanks for coming during these four months, it was so useful for me. I remember that first Fotoqs calçotada. Vaig continuar el meu màster, vaig provar de demanar la beca de la Caixa (però sembla que la fotoquímica no ven prou), va néixer la Claudia i l'Adaya va marxar...

Vaig presentar el màster i llavors aquell setembre va arribar el Sr. **Pietro Delcanale**. Sembla que tots els que venien eren físics. Era una altra persona amb seny... Ma que cosa diche, ma que cocha fae!!! Amb el típic moviment italià de la mà. M'estic autocensurant algunes altres frases. Va marcar un abans i després, estava allà a punt per fer el que calia. Al cap de sis mesos hem va saber molt greu que marxessis (però bueno al final has tornat a "Barcelona" i bona companyia que m'has fet alguns dies). Mentrestant, hi havia certs alumnes/as de segon que venien a veure que fèiem (Dientes i sables ehheh Uri; nena hi tornaré més avall).

Llavors va arribar el març i ens van venir un parell de xavals de grau: el **Cormac** que era una persona de "seny" i el **Victor**. El Victor era el meu xavalin de grau i li vaig agafar aprecí (el Jaumet crec que també) i aquells mesos m'ho vaig passar be, amb les seves ocurrències. Del Cormac que n'he de dir, la nova incorporació al grup. N'ha après be del seu mestre. Ja des de el primer moment porta ordre i neteja al laboratori (que certament s'ha de reconèixer que hi ha vegades que és necessari, sobretot quan puja l'entropia, ja que hi ha persones com jo que som altament entròpiques). Van presentar, el Victor apurant a l'últim moment al setembre.

And then in that summer, **Michael** appears (or Mitch for everyone else). The optoacoustic man. A person that can drink 15 coffees per day, with the American mentality. He show me that the things can be done without asking permission. Exactly, going directly to the objective. If it is necessary going to "La Barceloneta" before arriving IQS, you can do that. However, like each visitor I learnt some things from him and he is my friend.

Llavors, ja varen venir els estudiants de màster (Valeriano tranquilo ya llegara tu momento) i ens va arribar la **Lucia**. Aquí nomes puc dir-te una cosa: et demano perdo, per intentar fer química orgànica (reaccions) quan no en tinc ni punyatera idea. Et vas topar amb una paret per culpa meva, però lo important mai vas perdre la il·lusió. I mai m'ho has retret, nomes per això ja estic més tranquil. Gràcies per a tot.

El verano paso, y entonces pon un chileno en tu vida. Nos llegó **Renzo** (si Zanocco; cuyo momento aprovecho para agradecerles a tus padres también que me dejareis entrar en el mundo de los naftozaxoles). Que decir de una persona alegre, pero al mismo tiempo seca. Que consigue una elevada pureza a partir de la recristianización. Si, me enseño a recristalizar, calentando el agua al microondas. Nos fuimos a la Rioja con todos (si a la calle Laurel...), a Hamburgo, Venecia... Muchos buenos recuerdos de esos días. Aun me recuerdo el día de la feria medieval de Vic comiendo las butifarras.

Y cuando ya te ibas, llevo el fenómeno, el Don de Gentes... Mi amigo de Madrid (si... hace 5 años puede que ni me lo creíera) **Valeriano** i també la **Ingrid**. Pero en ese momento me fui un mes a Málaga a terminar el trabajo que empezó Renzo. Tengo que agradecer tanto a Ezequiel como a Paco la cálida bienvenida que me hicieron y lo bien que me trataron durante ese mes. Hago extensiva este agradecimiento a todo su laboratorio en Bionand (Noemí, Anjara, Pablo y Carlos). A part, durant aquell mes hem vaig inflar a menjar porc ibèric d'excel·lent qualitat, clar així és més fàcil estar feliç. I com diria el Jaumet té collons la cosa que vagi a Màlaga i nevi allí i a part facin vaga d'escombriaires.

Si tu **Valeriano**... un tío que tiene una risa distinguible a la legua. Que siempre está allí preparado para contar un chiste. Y aparte compartimos otra afición, la buena comida. Si se tiene que ir a comer un buen txuleton, pos se va (ves quin remei), pinchos, gallegos, asturianos... Si hasta conseguí que te comieras unos caracoles. Mira que me hacen comer estos catalanes en l'Aplec del Caragol... (aún tengo el video) También te tengo que decir que como el rabo de toro de Nuri hay pocas cosas. Nene, probablemente nos unió la comida... pero esto ya no se separa nunca. Pero vamos a lo científico, gracias por ayudarme en el capítulo 5. Por cierto aun no nos ha tocado el Gordo de Navidad solo 50 €, el próximo año será la nuestra (PD: el cachopo estaba muy bueno). Piensa donde vas dejas huella, Cristina aún se acuerda de ti.

Que dir-te a tu Ingrid en aquestes alçades de la pel·lícula, que no t'ho hagi dit en persona. Ets collonuda, tot i que algun dia la pugui liar. Ets directa, si has de dir algo, ho dius... Mai m'has donat un consell dolent... Per això i per molts altres petits detalls, moltes gràcies per formar part d'aquesta aventura.

Clar, després que tornes a Madrid el Valeriano i tant l'Oriole, el Quimet i la Bea fent estades a fora el laboratori es va tornar trist. Sort que va tornar el Cormac a fer el màster i el doctorat; i la Clara. Va tornar l'alegria al laboratori a cop de gralla. Anaves una mica estressat però tot va acabar be (no?). Tothom, va tornar i fins i tot s'hi va afegir per uns dies l'**Oscar Molins**, un molt bon xicot. Vas estar pocs dies i a part repartit en dos tongades, però crec que va ser suficient.

I finalment, si la primavera del 2016 va aparèixer un Valeriano salvaje, la primavera del 2017 va portar vells coneguts per quedar-s'hi. El primer que va arribar va ser el **Marcello** de Parma, un físic que va venir a fer la seva tesis de màster i ha fet combo. El noi va estar molt posat en l'optoacústica, cosa que li agraeixo perquè hem va ajudar en la secció 4.4. Igualment vaig aprofitar per practicar l'Italià. A continuació vull agrair els meus dos nens de grau. **Lluís** i **Nacho** o **Nacho** i **Lluís** l'ordre dels factors no altera els productes. Heu de tenir clar que podeu fer el que vulgueu, perquè sou capaços de tot i si voleu us podreu menjar el món. Lluís sense tu la secció 4.2.5 d'aquesta tesis probablement no s'hauria realitzat i Nacho el mateix dic respecte a la secció 3.2, però això no és el més important hauria perdut la possibilitat de conèixer un parell de persones brillants. M'ha encantat aquest pas de mentor a amic, i tot que ara les paraules no flueixin ja sabeu que vull dir. Espero que això duri en el temps. No vull acabar el paràgraf sense l'altra... si tu **Blanca**, la que faltava... que t'he de dir que no t'hagi dit encara. Tal com hem vas posar l'any passat al TFG que havies guanyat un gran amic, m'agradaria tornar-t'ho per dir-te: he guanyat una gran amiga de tot cor. T'has guanyat la meua confiança i això és difícil. Ha passat un any i uns quants quilometres de diferencia i sembla que s'ha mantingut. Tu també faràs el que et proposis amb la teva vida, sobretot si

ets capaç de deixar de banda les teves pors. Sóc pesat ho sé. De la primavera del 2017 no m'he penedeixo en cap cas d'haver-vos relacionat tant amb vosaltres tres.

L'estiu va passar i va aparèixer l'**Elena**, una noia molt maja que sempre porta alegria a la sala, sempre explorant els diminutius amb i. Al matí sempre esta allí (a la tarda no tant) amb ganes de fer les coses be. Al mismo tiempo y por la otra puerta apareció **Angel**, el palentino, una persona muy maja, siempre dispuesto a ayudar a todo el mundo. Si un día te regala filipinos, otro xicles o otro cafés. Que esto pueda continuar por años y que cuando os visite os vea con la misma ilusión. Aquí no hem puc deixar el **Pinilla**, un noi alegre que ens compra amb embotits de guijuelo i que sempre esta disposat a col·laborar.

On 25th of October, I went to Montreal. First, I want to thank Prof. **Gonzalo Cosa**, para acogerme en su grupo, enseñarme muchos conceptos sobre microscopia y como se trabaja en otro grupo distinto del nuestro. Also, I thank **Julia** and **Kevin** for introducing me in the dormant PS project. Julia synthetized the molecules for me, and Kevin helped me in all the biological experiments. Kevin hasta la victoria siempre. Also during my stage there I make good friends. **Yasser** (2 chileno de 3) que te tengo que decir, todos los Ollys que hicimos. **Vicky**, because there I won a real friend, see you soon in Munchen.

Cuando volví de Montreal, apareció otro chileno en mi vida... Com es nota l'excel·lent relació de Santi amb Xile. Se llamaba Francisco, pero **Pancho** para los amigos (y Panchito de pequeño). Que decirte Pancho, te hemos llevado a hacer muchos eventos, pero te has pensado porque? Si porque te lo mereces y teniendo el carácter latino aún mejor. I ja anem acabant, finalment arriba en **Ruben**, el meu últim TFG, ha estat un plaer també coneixe't i poder compartir aquest treball amb tu. Malauradament, per motius temporals no ha estat possible incloure'l en aquesta tesis, però allà queda.

Anem acabant, m'agradaria agrair a certes persones de fora de l'entorn de l'Institut Químic de Sarrià. **Eloi** i **Jaume** que us he de dir exactament... Fa 25 anys que ens coneixem i des de llavors heu estat presents en tot el que hem fet. Moltes gràcies per estar aquí. **Andrea** i **Neus** per aguantar-los respectivament. **Olga**, **Imma** i **Pat** també crec que us mereixeu com a mínim un esment i a la resta també ehh...

Finalment però no menys importants, vull agrair a muns pares perquè m'han permès arribar fins aquí, dient-me que si a la majoria de vegades. Perquè segurament una gran part de la meva mentalitat i caràcter actual l'heu forjat vosaltres. Per una banda, gràcies per deixar-me estudiar aquí i per l'altra perquè sempre us he tingut al cantó tant a les bones com a les madures. Aquestes paraules també les vull estendre a mon padrí, que ell també ha estat al cantó sempre.

Per això us dic: "Sou molt bona gent"

"(...) Oh, benvinguts, passeu passeu, ara ja no falta ningú, o potser sí, ja me n'adono que tan sols hi faltes tu, també pots venir si vols, t'esperem, hi ha lloc per tots. El temps no compta, ni l'espai, qualsevol nit pot sortir el sol."

List of abbreviations

$^1\text{O}_2$	Singlet Oxygen ($\text{O}_2(^1\Delta_g)$)
$^3\text{O}_2$	Ground state Oxygen ($\text{O}_2(^3\Sigma_g^-)$)
$\text{O}_2^{\bullet-}$	Superoxide radical anion
$\bullet\text{OH}$	Hydroxyl radical
Φ_F	Fluorescence quantum yield
Φ_T	Triplet quantum yield
Φ_P	Phosphorescence quantum yield
Φ_Δ	Singlet oxygen quantum yield
τ	Lifetime
τ_S	Singlet lifetime
τ_T	Triplet lifetime
τ_Δ	Singlet oxygen lifetime
ADPA	Anthracene Dipropionic acid
aPDT	Antimicrobial Photodynamic therapy
APTES	(3-aminopropyl)triethoxysilane
AQ	Anthraquinone
BDE	Bond dissociation energy
BPQ	Beta phenyl quenching
BSA	Bovine serum albumin
CFU	Colony forming units
CSNP	Compact silica nanoparticles
DCFH-DA	Diacetyl 6''-carboxy-2',7'-dichlorodihydrofluorescein
DFT	Density functional theory
DMEM	Dulbecco's modified Eagle's medium
Doxo	Doxorubicin
EDC	1-(3-dimethylaminopropyl)-3-ethylcarbodiimide hydrochloride
F	Fluorescence

Hyp	Hypericin
IC	Internal conversion
IR	Infrared
ISC	Intersystem crossing
LFP	Laser Flash photolysis
LIOAS	Laser-induced optoacoustic spectroscopy
k_q	Quenching rate constant
MB	Methylene Blue
MDPyTMPyP	5-mono(N-decyl-4-pyridyl)-10,15,20-tri(N-methyl-4-pyridyl)-21H,23H-porphine tetrachloride
NHS	N-hydroxysuccinimide
miniSOG	mini-Singlet oxygen generator
MSNP	Mesoporous silica nanoparticle
NMB	New methylene blue
NOX	Furyl-vinyl-naphthoxazole
NP	Nanoparticle
((OEt)₃-Si-L-NH₂)	N-(4,7,10-trioxa-13-tridecaneamine)-N'-(3-(triethoxysilyl)-propyl)-urea
OPO	Optical parametric oscillator
P	Phosphorescence
PBS	Phosphate buffered saline (pH 7.4)
PDT	Photodynamic therapy
PER(PPh₃⁺)₂	Perylene-3,9(10)-diylbis(triphenylphosphonium) bromide
PET	Photoinduced electron transfer
PhA	Pheophorbide a
PN	Phenalenone
PN1	9-Phenyl phenalenone
PN1D	9-Perdeuterophenyl phenalenone
PN2	9-(p-methoxyphenyl) phenalenone
PN3	9-(o,o'-dimethylphenyl) phenalenone
PN4	9-Pyridil phenalenone
PN5	9-Furyl phenalenone
PN6	9-Thionyl phenalenone

PN7	9-Pyridinium phenalenone
PN-ATZ	Aminothiazolo[4,5-c]phenalenone
PN-NCS	6-isothiocyanate phenalenone
PN-NO₂	9-(o-nitrophenyl) phenalenone
PNPPh₃⁺	(2-((1-oxo-1H-phenalen-2-yl)methoxy)ethyl) triphenylphosphonium bromide
PNS	1H-Phenalenone sulfonate
PN-thiourea	1-butyl-3-(1-oxo-1H-phenalen-6-yl)thiourea
PS	Photosensitizer
Q	Quencher
RB	Rose Bengal
RNS	Reactive nitrogen species
ROS	Reactive oxygen species
Rub	Rubiadin
Rub-Me	Rubiadin-1-methyl ether
SAGUA	(1-((1-oxo-1H-Phenalen-2-yl)methyl)-1-methyl-guanidinium chloride
SAPYR	(2-(4-pyridinyl)methyl)-1H-phenalenone
SOLD	Singlet oxygen luminescence dosimetry
SOSG[®]	Singlet Oxygen Sensor Green
SOTD	Singlet oxygen trapping dosimetry
TCNE	Tetracyanoethylene
TCSPC	Time-correlated single photon counting
TEMPO	(2,2,6,6-Tetramethylpiperidin-1-yl)oxyl
TEOS	Tetraethyl orthosilicate
Tiron	1,2-dihydroxybenzene-3,5-disulfonate
TMB	3,3',5,5'-Tetramethylbenzidine
TPP	Triphenylphosphonium
TSB	Tryptic Soy Broth
v.r.	Vibrational relaxation

Index

1. Introduction	25
1.1. Light as a reagent	27
1.2. Reactive oxygen species	31
1.3. Singlet oxygen	32
1.3.1. Structure, Generation and Properties	32
1.3.2. Detection	34
1.3.3. Reactivity	37
1.3.4. Applications	39
1.4. Photodynamic Therapy	40
1.4.1. Photodynamic therapy of cancer	42
1.4.2. Antimicrobial photodynamic therapy	44
1.5. Objectives	46
2. General materials, techniques and methods	49
2.1. Materials	51
2.2. Spectroscopic techniques	52
2.2.1. Steady-state optical techniques	52
2.2.2. Time-resolved optical techniques	53
2.2.3. Light sources	60
2.3. General photoinactivation protocol	61
2.4. General synthesis characterization	62
3. New strategies to increase the $^1\text{O}_2$ efficiency against living systems	65
3.1. Introduction	67
3.2. Triphenylphosphonium cation: a neglected functional group for aPDT	68
3.3. Reevaluating natural-occurring PS	75
3.3.1. Why natural products?	75
3.3.2. Darwin mystery; Naturally-occurring phenalenones	77
3.3.3. β -Phenyl quenching photochemical reaction (BPQ)	80
3.3.4. β -phenyl quenching of 9-phenylphenalenones: a novel photocyclization reaction with biological implications	81
3.3.5. Reprofilling: 9-Heteroaryl-phenalenones as novel photochromic family	88
3.3.6. Reprofilling: 9-Phenyl-phenalenone photoreactivity as student laboratory experiment for understanding laser flash photolysis experiments	96
3.3.7. Reprofilling: 9-(o-nitrophenyl)-phenalenone as an uncaging agent	103
3.3.8. Phenalenone as singlet oxygen labelling agent	109

3.3.9. Naturally-occurring anthraquinones	112
3.4. Nanoparticles as a PS carrier agent	117
3.4.1. Why nanoparticles?	117
3.4.2. Silica nanoparticles	118
3.4.3. Methylene Blue-loaded MSNP	119
3.4.4. Rose Bengal-loaded MSNP	125
3.5. Photodynamic synergistic effect	129
3.6. Reactive oxygen species mediated activation of a dormant singlet oxygen photosensitizer in HeLa cells	135
4. Novel strategies for $^1\text{O}_2$ and other ROS detection in biological systems	145
4.1. Why can be $^1\text{O}_2$ traps an alternative to near-infrared phosphorescence to detect $^1\text{O}_2$?	147
4.2. Small particles, big improvement: the use of nanoprobe for reactive oxygen species detection in biological media	149
4.2.1. Nanoparticles protect the fluorescent probes	149
4.2.2. NanoSOSG: a nanostructured fluorescent probe for the detection of intracellular $^1\text{O}_2$	150
4.2.3. NanoADPA: a nanostructured fluorescent probe for the detection of intracellular $^1\text{O}_2$	158
4.2.4. NanoNOX: A turn-on fluorescence nanoprobe for $^1\text{O}_2$ detection	168
4.2.5. NanoDCFH-DA: a silica-based nanostructured unspecific fluorescent probe for the detection of reactive oxygen species in biology	173
4.3. Unravelling CellROX [®] Deep Red: a nonspecific reactive oxygen species fluorescent probe	182
4.4. Tetramethylbenzidine: a photoacoustic probe for reactive oxygen species detection	190
5. A self-reporting nanophotosensitizer	201
5.1. $^1\text{O}_2$ dosimetry	203
5.2. Aim of the study	205
5.3. Experimental section	205
5.4. Assessment of ADPA-MSNP-RB as a self-reporter nanophotosensitizer	206
6. General discussion and outlook	209
7. General conclusions	221
8. Bibliography	227
9. Annexes	251

Chapter I

General introduction: Light as a reagent

*Pinto les notes d'una havanera
blava com l'aigua d'un mar antic.
Blanca d'escuma, dolça com l'aire,
gris de gavines, daurada d'imatges,
vestida de nit.*

*Miro el paisatge, cerco paraules,
que omplin els versos sense neguit.
Els pins m'abracen, sento com callen,
el vent s'emporta tot l'horitzó.*

*Si pogués fer-me escata
i amargar-me a la platja
per sentir sons i tardes del passat,
d'aquest món d'enyorança,
amor i calma, perfumat de lluna, foc i rom*

*Si pogués enfilar-me a l'onada més alta
i guarnir de palmeres el record,
escampant amb canyella totes les cales
i amb petxines fer-lis un bressol*

*Els vells em parlen plens de tendresa,
d'hores viscudes amb emoció.
Joves encara, forts i valents,
prínceps de xarxa, herois de tempesta,
amics del bon temps.*

Castor Pérez i Gloria Cruz

1.1. Light as a reagent

Light has been used as a healing agent for centuries.^{1,2} Ancient cultures like Egyptians, Greeks, Hindus and Aztecs worshiped the sun under different names: Ra, Helios, Aruṇa or Tonatiuh. In the Ebers Papyrus, the oldest maintained medical document dating from 1550 BC, it is described how to treat depigmented lesions and skin discoloration using a powder of different plants and the sunlight (Figure 1.1). Another historical reference of medicinal uses of the sun light is found in one of India's sacred books, Atharva-Veda dating back from 1400 BC, vitiligo was treated using extracts of certain plants followed by some time of sunlight exposure.³

The use of sunlight for treatment was classically named Heliotherapy, whose name comes from Helios, the Greek god of sun. It was introduced by Hippocrates (460-370 BC), who learned about the healing power of sunlight during his journeys to Egypt.⁴ However, after the Roman Empire the heliotherapy fall into disuse due to the raise of Christianity alongside its monotheistic creed. It reappeared in some Islamic regions during the Early Middle Ages, well-documented by the Persian scholar and physician Avicenna (980-1037 AD).¹⁻⁴



Figure 1.1 Ancient Egyptians worshiped the sun, Helios, due to its healing power. Reproduced from reference 2.

What have in common heliotherapy,⁵ photosynthesis⁶ and vitamin D biosynthesis?⁷ In all cases the molecules involved can absorb light.^a Figure 1.2 shows a simplified version of Jablonski diagram with the main-processes that occur after photon absorption.

^a A photon is an elementary particle, which has zero rest mass, spin 1, no electric charge and it is stable. The energy and momentum of a photon depend only on its frequency (or inversely on its wavelength).

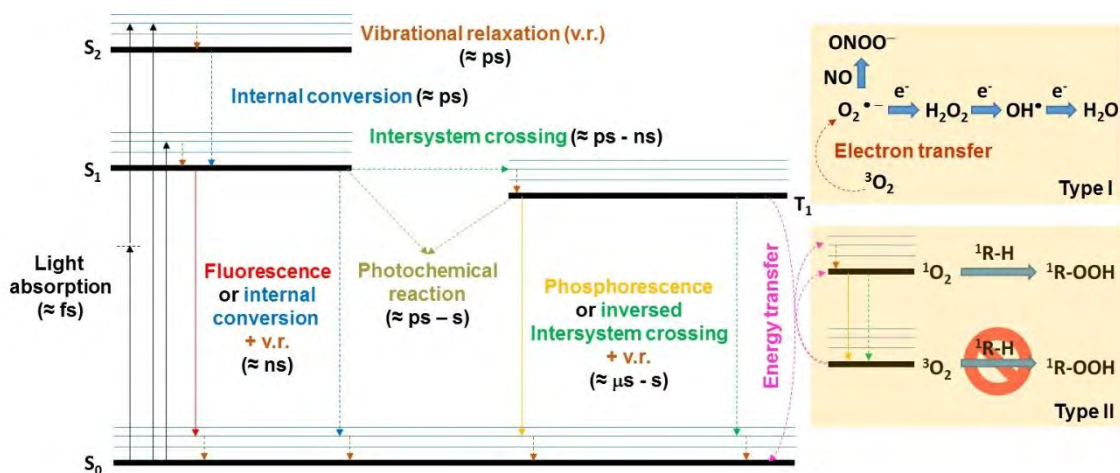


Figure 1.2 Jablonski diagram depicting the main photophysical and photochemical processes and their most-likely timescales. Solid lines correspond to transitions involving radiative processes whilst dashed lines are non-radiative.

After a molecule absorbs a photon (or multiple photons in non-linear optics; see section 4.2.4.2), the molecule is promoted to an excited state.⁸ Only the transitions where spin angular momentum is conserved are allowed.⁹ Closed-shell organic molecules have singlet spin multiplicity in the ground state, so the transitions that are spin-allowed are from S_0 to S_1 , S_2 , (...), S_n . Absorption phenomena starts from the lowest vibrational level of S_0 because the vast majority of molecules are in this level at room temperature. Notwithstanding, forbidden electronic transitions can also occur, but with very low probability.

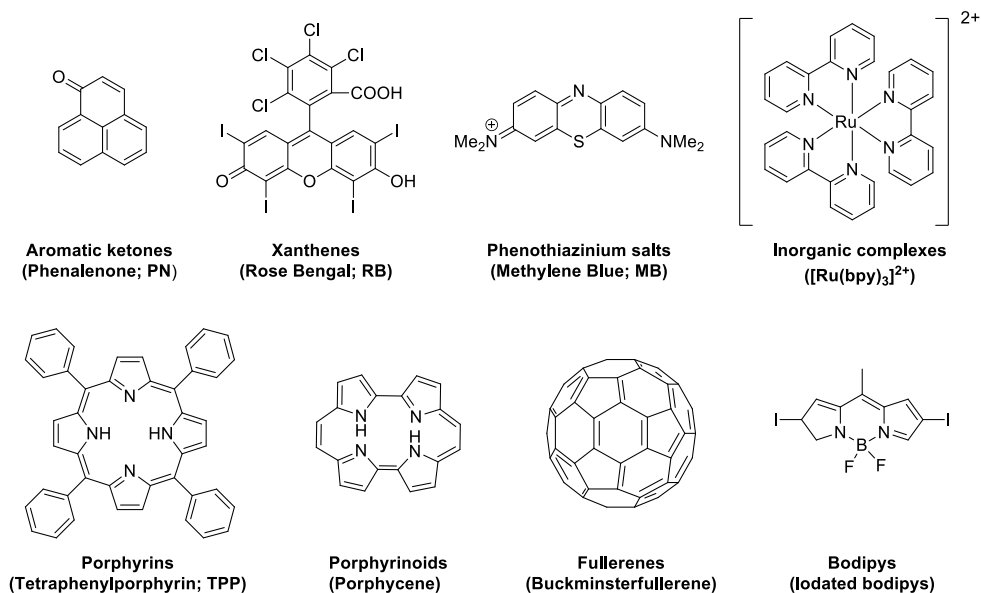
Once the dye is in the excited state, it decays to its ground state through different pathways.¹⁰ Generally, they can be classified into three main groups:

- **Radiative processes**: The excited molecule decays to the ground state emitting electromagnetic radiation. Depending on the spin multiplicity this radiative process can be allowed or forbidden. These processes are depicted in figure 1.2 as solid lines.
 - **Fluorescence (F)**: Radiative transition between states of the same spin multiplicity (typically from S_1 to S_0). Fluorescence emission does not depend on the excitation wavelength (Kasha / Vavilov's rules).¹¹
 - **Phosphorescence (P)**: Radiative transition between states of different spin multiplicity (typically from T_1 to S_0).¹²
- **Non-radiative processes**: The excited state species decay returning the excess of energy as heat. They obey their own set of selection rules. These processes are depicted in figure 1.2 as dashed lines.
 - **Vibrational relaxation (v.r.)**: process in which the excess of vibrational energy of a state is released as heat through collisions.
 - **Internal conversion (IC)**: isoenergetic transition between two electronic states of the same spin multiplicity, followed by vibrational relaxation.
 - **Intersystem crossing (ISC)**: isoenergetic transition between two electronic states with different spin multiplicity. This transition is in principle forbidden, however spin-orbit coupling can be large enough to make it

possible (i.e. in $n \rightarrow \pi^*$ transitions as described by El-Sayed rules).¹³ Also ISC is favored in the presence of heavy atoms.¹⁴

- **Other processes:** The dye in the excited state can competitively participate in chemical reactions, that are thus called photochemical.¹⁵ Of specific interest to this thesis is the photodynamic action, in which a substrate is oxidized by the combined action of light, oxygen and an excited-state dye, referred to as photosensitizer (PS).^{16–18}

The most commonly used PS for photodynamic applications are depicted in Scheme 1.1.



Scheme 1.1 Structure of standard PSs for photodynamic applications.

The chemical structure of PS will determine its behavior and properties. As example, in eukaryotic cells a PS with anionic substituents localizes in the cytoplasm and upon illumination, it relocates in the nucleus. However, a PS with cationic substituents targets the mitochondria. An ideal PS for photodynamic therapy should have the following characteristics:¹⁹

- High absorption coefficients in the 600-900 nm region, which allows the maximum light penetration thorough the tissue with minimum light scattering.
- High triplet quantum yield (Φ_T), with a long triplet lifetime (τ_T) and a triplet state energy higher than 94 KJ/mol in order to be capable to transfer energy to $^3\text{O}_2$ for generating singlet molecular oxygen ($\text{O}_2(^1\Delta_g)$ or $^1\text{O}_2$).
- High quantum yield of generation of ROS, particularly $^1\text{O}_2$.
- Low dark toxicity.
- Good solubility in water, or at least in non-toxic solvents, for its administration.

Different types of PS have been developed. They can be classified in three different categories:

- **First generation:** These compounds are not chemically pure, cause prolonged patient photosensitivity and present low absorbance in the red part of the

spectrum. Porphimer sodium (Photofrin[®]) is the most successful example of this category.^{20,21}

- **Second generation:** These compounds are chemically pure and have better absorption in the red region. This second generation includes compounds like benzoporphyrins (e.g., Visudyne[®]) or chlorins (e.g., Temoporfin[®]).^{22,23}
- **Third generation:** These compounds have incorporated targeting agents so the PSs affinity for tumors has increased. Also, it is possible to target specific subcellular compartments or other strategies to increase the selectivity of the PS (i.e. activatable PS).²⁴⁻²⁶

Recently, genetically-encoded PSs are fluorescent proteins that encase a PS and have therefore the ability to generate ROS when irradiated with light. The first examples of such proteins are KillerRed^{27,28} and miniSOG²⁹ (the abbreviation of mini Singlet Oxygen Generator). Once expressed in a cell, miniSOG has the ability to bind as cofactor the flavin mononucleotide (FMN), which is ubiquitously found in any type of cells. It has been reported to generate ¹O₂ ($\Phi_{\Delta} = 0.03$) and other ROS upon blue-light irradiation. Several miniSOG derivatives have been recently developed, reporting much higher ROS productions rates than the original.

1.2. Reactive oxygen species

It is known that certain derivatives of oxygen are highly toxic to cells.³⁰ They are collectively known as Reactive Oxygen Species (ROS).³¹ Formally, the most common ROS includes hydrogen peroxide (H_2O_2), singlet oxygen ($^1\text{O}_2$), superoxide radical anion ($\text{O}_2^{\bullet-}$) and hydroxyl radical ($\bullet\text{OH}$), as well as hypochlorous acid and hypochlorite ions (HClO and ClO^- , respectively). Incorporation of alkoxy ($\text{RO}\bullet$), peroxy ($\text{ROO}\bullet$), organic hydroperoxides (ROOH) and semiquinone ($\text{SQ}^{\bullet-}$) are also frequently encountered within the definition of ROS. Typically, also they are classified as free radicals and non-radical species.

ROS are highly oxidant species that participate in oxidative damage on proteins, nucleic acids lipids and other biomolecules.^{32,33} Usually, ROS are adventitiously produced in several metabolic processes of aerobic organisms.³⁴ ROS oxidant effects are usually controlled by the cell's own antioxidant defenses,^{35,36} which can be both enzymatic (i.e. superoxide dismutase together with catalase)³⁷ or non-enzymatic (i.e. vitamin E or glutathione).³⁸

When such regulation mechanisms are insufficient or overwhelmed, an accumulation of free ROS takes place inside cells.³⁹ This can lead to irreversible damage that can cause cellular death. The unbalance between oxidant and antioxidant species is known as oxidative stress, and is related to different severe pathologies (cancer, diabetes, aging...).³⁹⁻⁴¹ Nevertheless, when produced in a controlled way, ROS have also been reported to play a vital role in cells such as protein modifications, cell adhesion regulation and immune system control.⁴² As explained in section 1.1, in addition to endogenous sources such as mitochondria, peroxisomes, lipoxygenases or cytochrome P450, ROS can also be produced exogenously.⁴³ Environmental sources include ultraviolet light, ionizing radiation or pollutants. An alternative is to produce them by irradiation of a PS in the presence of oxygen.

Reactive Nitrogen Species (RNS) have similarities with ROS.⁴⁴ They are derived from nitric oxide (NO). Formally, the most common RNS includes peroxynitrite (ONOO^-), nitrosoperoxy carbonate (ONOOCO_2^-), dinitrogen trioxide (N_2O_3) and nitrogen dioxide (NO_2) among others.⁴⁵ Like ROS, they are highly reactive and when they are overproduced cause nitrosative stress.⁴⁶ The consequences of nitrosative stress can include mitochondrial dysfunction, altered structure and function of critical protein mediators, and cell injury or death.⁴⁷⁻⁴⁹ From all RNS, peroxynitrite is the most reactive and potentially injurious because it has powerful oxidizing and nitrating actions.⁵⁰

The ROS mostly studied in this doctoral dissertation is $^1\text{O}_2$, which is therefore described in detail in section 1.3.

1.3. Singlet oxygen

1.3.1. Structure, Generation and Properties

“Since its discovery by Kautsky and Bruijn in 1931, singlet oxygen has remained a central research subject.”^{51,52}

Despite its simplicity, molecular oxygen ($^3\text{O}_2$; ($\text{O}_2(^3\Sigma_g^-)$)) exhibits unusual properties respect to its magnetic behavior, energy-transfer processes, chemical reactivity and spectroscopy.⁵³ This is due to the particular electronic configuration of its ground and excited states. Unlike other homomolecular molecules, $^3\text{O}_2$ has an open-shell electronic configuration with two unpaired electrons.

Singlet oxygen (formally $\text{O}_2(^1\Delta_g)$; hereafter $^1\text{O}_2$) is the first excited state from molecular oxygen.^{53–56} $^1\text{O}_2$ lies 94.3 kJ/mol above the ground state (Figure 1.3).⁵⁷ $^1\text{O}_2$ has an orbital angular momentum of 2 and its symmetry is pair. As result of its high electronegativity, $^1\text{O}_2$ is an excellent electron acceptor and a poor electron donor.^{58–60} Moreover, the addition of an electron to $^1\text{O}_2$ generates other ROS (i.e. $\text{O}_2^{\bullet-}$).

The second excited state of molecular oxygen also has singlet spin electronic distribution ($\text{O}_2(^1\Sigma_g^+)$) and is 63 kJ/mol higher in energy than $^1\text{O}_2$ (Figure 1.3).¹⁵ $\text{O}_2(^1\Sigma_g^+)$ is very short lived (only 130 ns in CCl_4)⁶¹ and is deactivated to the lower singlet state ($\text{O}_2(^1\Delta_g)$) so fast that it has a very small chance to react intermolecularly.⁶²

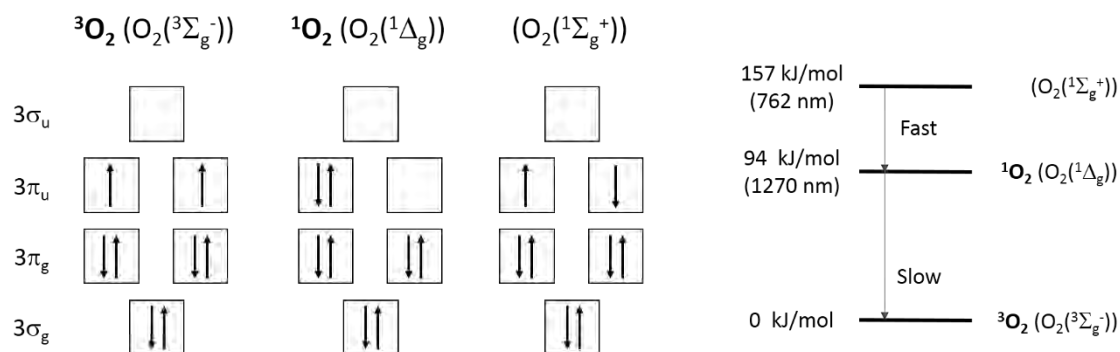
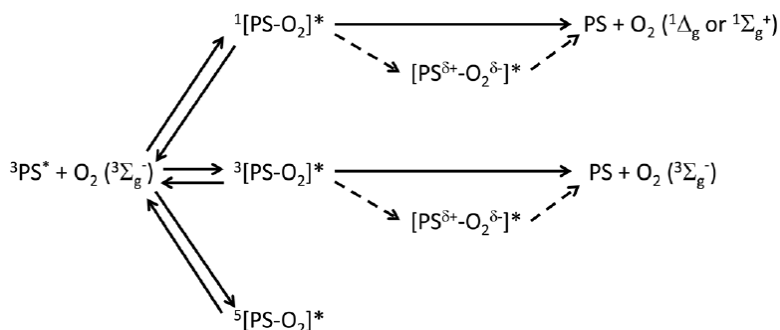


Figure 1.3 Left: Electronic configuration of ground state molecular oxygen ($^3\text{O}_2$; $\text{O}_2(^3\Sigma_g^-)$) and its two first excited states: $^1\text{O}_2$; $\text{O}_2(^1\Delta_g)$ and $\text{O}_2(^1\Sigma_g^+)$. Right: Jablonski diagram for molecular oxygen.

$^1\text{O}_2$ can be generated through several chemical reactions, including some enzymatic processes, reactions involving other ROS such as H_2O_2 , ClO^- or $\text{O}_2^{\bullet-}$ or by thermal decomposition of ozonides or organic endoperoxides.⁶³ The most common strategy to produce $^1\text{O}_2$ is by energy transfer from a long-lived excited state to $^3\text{O}_2$. Due to the long-lifetime requirement, it is mainly the triplet state of a PS the one that can be quenched by relative low concentrations of $^3\text{O}_2$.^{64–66} Scheme 1.2 shows the mechanism of quenching of the PS triplet state ($^3\text{PS}^*$) by $^3\text{O}_2$.⁶⁷

In the first step, an encounter complex/pair between the $^3\text{PS}^*$ and $^3\text{O}_2$ is formed by collision. The complex can have a spin multiplicity of 1, 3 or 5 and may dissociate or in the case of the singlet exciplex, proceed to generate $^1\text{O}_2$ (either in $^1\Delta_g$ or $^1\Sigma_g^+$). The products of the triplet complex are the PS and molecular oxygen in ground state. There are no reactive channels for the quintuplet complex. The relative contribution to the singlet and triplet channels depends on the molecular properties of the PS and the

polarity of the solvent, often due to the presence of charge-transfer components in the quenching mechanism. For effective energy transfer to occur, the energy gap between the triplet and the ground state must be above 94 kJ/mol (for $^1\Delta_g$) or 157 kJ/mol (for $^1\Sigma_g^+$). Normally, the greater the energy dissipation required, the slower the quenching rate of the triplet by 3O_2 .⁶⁸



Scheme 1.2 Mechanism for the quenching of the triplet state by 3O_2 . Reproduced from reference ⁶⁹.

An additional 1O_2 generation pathway is possible if the singlet-triplet energy gap is higher than 94 kJ/mol.⁷⁰ In that case, the PS in S_1 can transfer energy to 3O_2 in order to generate 1O_2 and the PS in the excited triplet state, which can further evolve to produce a second molecule of 1O_2 . Indeed, that is the reason why it is possible to have a Φ_Δ bigger than 1 for some poliaromatic scaffolds (i.e. rubrene, dicyanoanthracene or pyrene among others).⁷¹⁻⁷³

1.3.2. Detection

On the basis of $O_2(^1\Delta_g)$ and $O_2(^1\Sigma_g^+)$ energy levels, luminescence decays can be detected at 1270 nm ($O_2(^1\Delta_g) \rightarrow ^3O_2$) and at 762 nm ($O_2(^1\Sigma_g^+) \rightarrow ^3O_2$) respectively.⁷⁴ Among them the most probable to detect is the radiative transition of $O_2(^1\Delta_g) \rightarrow ^3O_2$. 1O_2 near-infrared phosphorescence detection at 1270 nm was first observed experimentally in the late 1970s by Salokhiddinov *et al.*⁷⁵ Since then, it has gained popularity for detecting 1O_2 by a direct methodology.⁷⁶ Time-resolved near-infrared phosphorescence not only allows the confirmation of its presence, but also the study of its formation and decays kinetics (Figure 1.4).⁷⁷

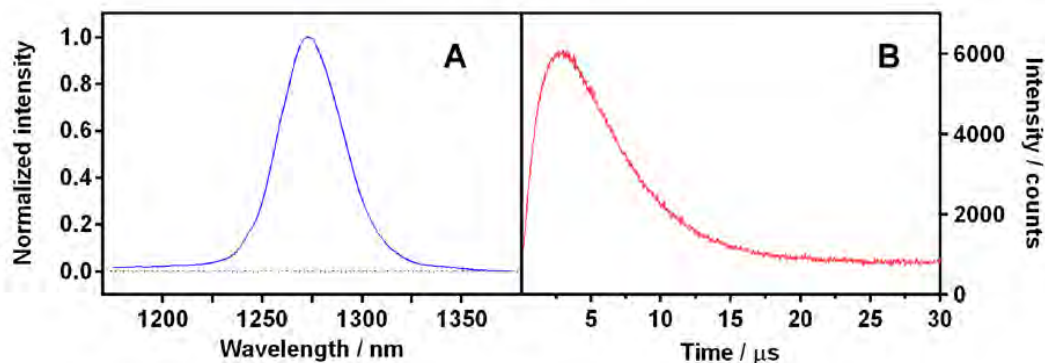


Figure 1.4 A: Near-infrared phosphorescence spectrum of 1O_2 . Time-resolved phosphorescence 1O_2 signal in water. Reproduced from reference ⁷⁸.

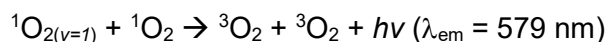
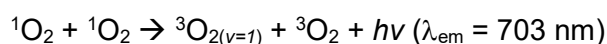
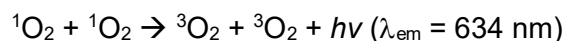
The determination of such parameters can provide interesting information about the microenvironment where 1O_2 is generated (τ_Δ) or information about its precursors (τ_T).^{78,79} Moreover, some researchers go beyond measurements in homogeneous or heterogeneous and study 1O_2 phosphorescence spatially-resolved.^{80,81} This is a robust, specific, non-invasive and direct method; however, it suffers from very weak signal due to the low 1O_2 phosphorescence quantum yield ($\Phi_{P;^1O_2}$), particularly in biological media ($\Phi_P < 1 \times 10^{-6}$).^{82,83}

The pure radiative lifetime of the $^1O_2 \rightarrow ^3O_2 + h\nu$ transition is around 2700 seconds.⁸⁴ The solvent dependence of the 1O_2 radiationless deactivation rate constant (k_d) is quite remarkable.⁸⁵ A qualitative explanation of these remarkable effects is available if it is assumed that the rate of deactivation depends most strongly on the frequency of the vibrations of the solvent that couple with 1O_2 and this coupling determines the k_d .⁸⁶⁻⁸⁸ As a general rule, k_d follows the next solvent trend:⁵⁶

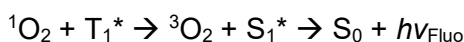
	O-H	>	C-H (aromatic)	>	C-H (aliphatic)	>	O-D	>	C-D	>	C-Halogen
k_d ($M^{-1}s^{-1}$)	2900		1500		300		100		20-10		(<0.6)

Due to high solvent dependence onto k_d , the 1O_2 lifetime (τ_Δ) and $\Phi_{P;^1O_2}$ show also a strong solvent dependence.

If $^1\text{O}_2$ is present in high concentrations, additional emission bands can be observed at 579, 634 and 703 nm.⁸⁹ They are assigned to the emission of $^1\text{O}_2$ dimers (dimol).^{b,90}



Another alternative is the so-called, $^1\text{O}_2$ -sensitized delayed fluorescence. It is the delayed emission from excited singlet states of a PS, which are repopulated by energy transfer from $^1\text{O}_2$.⁹¹

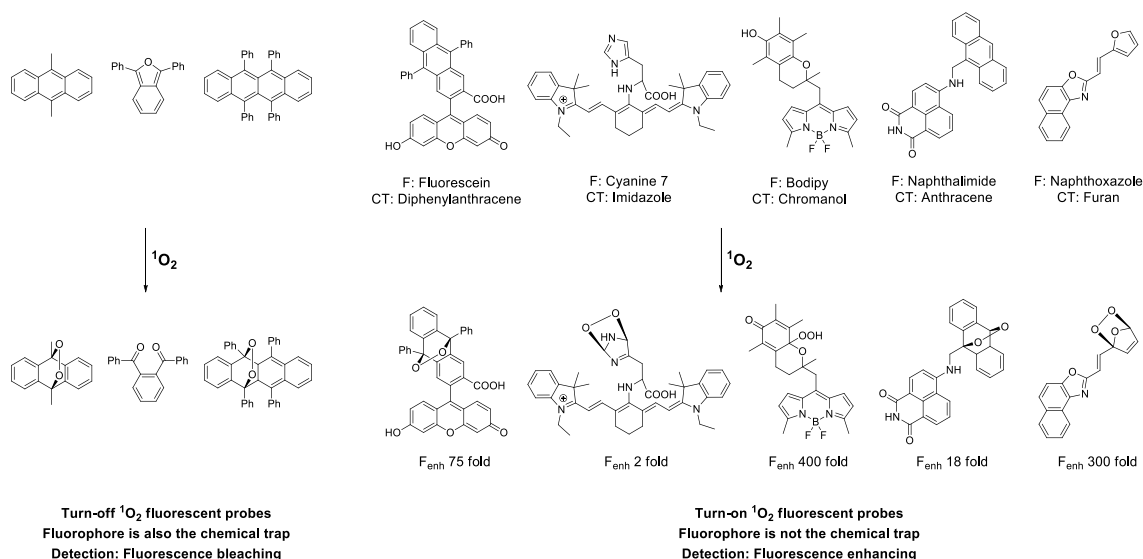


Additionally, $^1\text{O}_2$ can also be studied using photothermal techniques (i.e. laser-induced optoacoustic spectroscopy⁹² or photothermal lensing⁹³), but the need of specialized equipment and the lack of specificity towards $^1\text{O}_2$ makes them less useful to a general public.

The main alternative to near-infrared phosphorescence for $^1\text{O}_2$ detection is the use of $^1\text{O}_2$ chemical traps that allow monitoring $^1\text{O}_2$ by spectroscopic techniques (mainly absorbance,⁹⁴ fluorescence,⁹⁵ chemiluminescence^{96,97} and electronic paramagnetic resonance⁹⁸). Oxidation of the chemical acceptor by $^1\text{O}_2$ leads to a structural change (e.g., formation of endoperoxides, dioxetanes, or other O_2 -adducts), which can further evolve to other oxidized compounds, changing thereby their spectroscopic signature.

The most common probes are the fluorescent ones (Scheme 1.3).⁹⁹ Early attempts to use fluorescence to monitor $^1\text{O}_2$ production were based on the fluorescence decrease of aromatic acceptors such as dimethylantracene,¹⁰⁰ rubrene¹⁰¹ or diphenylisobenzofuran.¹⁰² Since 2000, more efficient $^1\text{O}_2$ fluorescent probes have been reported based on dyads composed of a chemical trap plus a fluorophore. In a first generation of “turn-on” fluorescent probes, the fluorophore fluorescence is quenched by the $^1\text{O}_2$ chemical trap (normally via photoinduced electron transfer). Once the chemical trap has reacted with $^1\text{O}_2$, the fluorophore is no longer quenched and recovers its intrinsic fluorescence.¹⁰³ Several combinations of fluorophores and $^1\text{O}_2$ chemical traps have been designed. Among them, SOSG[®] (Singlet Oxygen Sensor Green; a fluorescein-anthracene dyad; see section 4.2.2.1 for a detailed description about SOSG[®] properties) is commercially available and used widely.^{95,104,105}

^b The dimol emission results when two $^1\text{O}_2$ molecules forms a dimer and it emits only one photon. This dimol emission is produced by a simple collisional process without activation energy.



Scheme 1.3 Representative “turn-off” and “turn-on” $^1\text{O}_2$ fluorescent probes. They are described in the following references.^{100–103,106–109}

Recently, the previous “turn-on” concept has been improved to yield higher contrast. Here, the fluorescent moiety is linked to the $^1\text{O}_2$ chemical trap through an extended π -conjugated system, resulting in fluorescence quenching due to intramolecular charge transfer. $^1\text{O}_2$ mediated oxidation of the trapping moiety results in the formation of new chemical entities whose spectra are different from those of the non-oxidized dyad.^{109,110} In principle, such an approach could induce an infinite contrast. The advantages and drawbacks of the near-infrared phosphorescence and fluorescent probes are compared in section 4.1).

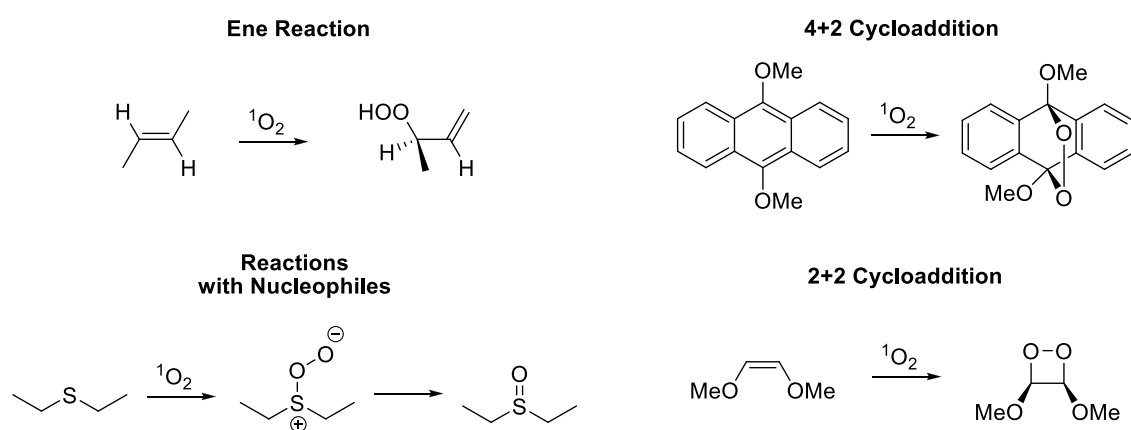
Chemiluminescence probes, in turn, possess the attractive advantage that do not need to be photoactivated, therefore background fluorescence and scattering interferences are eliminated.^{96,97} However, they suffer from lower sensitivity than fluorescent probes.

1.3.3. Reactivity

$^1\text{O}_2$ is a highly reactive molecule. The quantum-mechanics explanation is that closed-shell organic compounds present a singlet spin electronic distribution, so there is not any spin restrictions in their reaction with $^1\text{O}_2$ due to spin momentum conservation. This fact results in a much faster process than reaction with $^3\text{O}_2$ which this reaction is spin forbidden.



Specifically, $^1\text{O}_2$ is highly electrophilic reagent. $^1\text{O}_2$ reacts preferentially with electron-rich substrates containing π -electrons on a carbon framework or at a heteroatom center.¹¹¹ Scheme 1.4 depicts the reactivity of $^1\text{O}_2$ towards organic compounds.



Scheme 1.4 Examples of four main types of $^1\text{O}_2$ reactions with organic substrates.

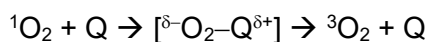
- **Ene reaction:** The product of the Ene reaction is an allylic hydroperoxide. It is formed by addition of $^1\text{O}_2$ to a sp^2 -hybridized carbon of the alkene substrate and the subsequent hydrogen abstraction from a distal allylic carbon.¹¹²⁻¹¹⁴
- **$^1\text{O}_2$ reaction with nucleophiles:** Reactions of $^1\text{O}_2$ towards different heteroatom containing organic molecules have been studied. These studies includes organo-sulfur compounds,¹¹⁵ phosphines,¹¹⁶ nitrogen compounds,^{117,118} or organometallic complexes¹¹⁹ among others.
- **4+2 Cycloaddition:** Electron rich s-cis dienes react with $^1\text{O}_2$ to form endoperoxides.¹²⁰ The resulting endoperoxides are formed stereospecifically in analogy to the products formed in the more common Diels–Alder reactions. The formed aromatic endoperoxides can undergo retro-Diels–Alder reactions to release both $^1\text{O}_2$ and $^3\text{O}_2$.^{121,122}
- **2+2 Cycloaddition:** Electron rich double bonds react with $^1\text{O}_2$ to form dioxetanes.¹²³ The 2+2 cycloaddition is always in competence with Ene reaction.¹²⁴

Alternatively to $^1\text{O}_2$ deactivation through chemical reaction, physical pathways are very common for deactivation of $^1\text{O}_2$. This physical quenching typically is in competition with chemical reaction. $^1\text{O}_2$ can be quenched physically via two different pathways:

- **Energy transfer:** If quencher's triplet excitation energy lies below that of $^1\text{O}_2$, then $^1\text{O}_2$ efficiently transfer its energy to the quencher returning to $^3\text{O}_2$.^{125,126} As example, carotenes are very efficient $^1\text{O}_2$ energy transfer quenchers and why are so important in photosynthetic systems for control its oxidation.¹²⁷



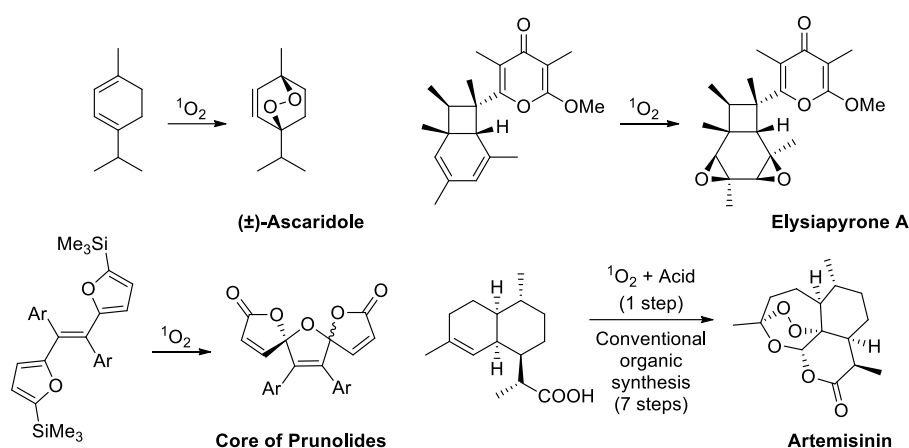
- **Charge transfer:** Electron rich molecules also can favor the relaxation of $^1\text{O}_2$ via partial charge transfer.⁵⁹ Amines,¹²⁸ sodium azide¹²⁹ or metal quelates¹³⁰ are examples of $^1\text{O}_2$ charge transfer quenchers.



1.3.4. Applications

$^1\text{O}_2$ has gained ample attention due to its pivotal role in a large variety of chemical and biological processes e.g., plant signaling, organic synthesis, food and beverage oxidation, or photodynamic therapy (PDT; see section 1.4).^{131–135}

In the field of organic synthesis, $^1\text{O}_2$ is a very useful oxidant reactant (see examples in scheme 1.5). Since the early pioneering work of Schenck and Ziegler on the formation of (\pm)-ascaridole using $^1\text{O}_2$ as co-oxidant.¹³⁶ Since then, $^1\text{O}_2$ has served as an important preparative tool in the synthesis of many natural products and other compounds of special interest. In scheme 1.5, it is exposed four different examples ((\pm)-ascaridole, Elysiapyrone A,¹³⁷ Prunolides core¹³⁸ and Artemisinin^{139,140}) where $^1\text{O}_2$ has been the key reagent for that synthetic pathway. I want to remark a recent work about Artemisinin synthesis (drug against malaria) where it can be reduced its synthesis from 7 conventional organic steps to one using $^1\text{O}_2$ as reactant.¹⁴⁰



Scheme 1.5 Different examples of the natural products organic synthesis where $^1\text{O}_2$ has been used as a reagent.

Another field where $^1\text{O}_2$ has an important role is in food and beverages photodegradation.^{134,141} The deleterious effects of $^1\text{O}_2$ may be summarized as the oxidation of unsaturated fatty acids and oils,¹⁴² reversion flavor in soybean oil,¹⁴³ the formation of unpleasant off-flavors specially in milk,¹⁴⁴ losses of different vitamins^{145,146} and the bleaching of pigments such as myoglobin in meats.^{147,148} Similar consequences present $^1\text{O}_2$ when it is generated inside beverages.^{149,150} Figure 1.5 shows the formation of $^1\text{O}_2$ in some beverages upon ultraviolet irradiation.

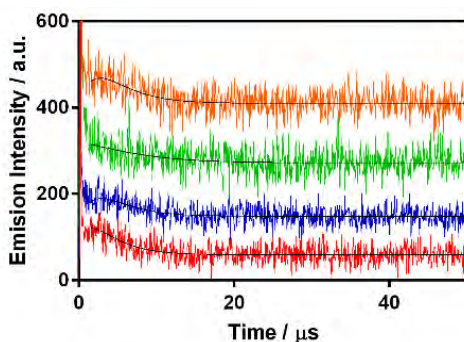


Figure 1.5 $^1\text{O}_2$ generation by different beverages under UV (355 nm) excitation. Coffee (red), sweet wine (moscatell; blue), cola soda (green) and beer (orange).

1.4. Photodynamic Therapy

In the winter semester of 1897-98, Oskar Raab, a medical student in Munich, found out that acridine dye was more toxic against paramecia^c on clear days compared to rainy days. This led to the conclusion that light had an enhancing effect towards paramecia killing. Moreover, paramecia were inactivated even more efficiently if the solutions were kept near a bright window. Oskar Raab and his mentor, Hermann von Tappeiner set the basis of photodynamic therapy (PDT). They hypothesized that light can be converted to some type of chemical energy thanks to certain substances.^{151,152} The surprising result was published in 1900 and stimulated further activity in the field.¹⁵³

In 1903, Niels Ryberg Finsen, a Danish physician, was awarded the Nobel Prize for his treatment of *lupus vulgaris*^d using eosin and light.¹⁵⁴ Two years later, von Tappeiner and Jesionek, a German dermatologist, published clinical data using different PSs in the treatment of lupus and skin cancer.¹⁵⁵ Von Tappeiner also reported that ³O₂ is necessary for the reaction to occur and he was the first to coin the term photodynamic therapy (PDT).¹⁵⁶ Afterwards, Meyer-Betz injected himself with 200 mg of hematoporphyrin. No dark response was recorded until he exposed himself to sunlight and suffered erythema and oedema.¹⁵⁷ Since then, thousands of studies have been published in the PDT field against cancer, bacterial infections or viruses (Figure 1.6).

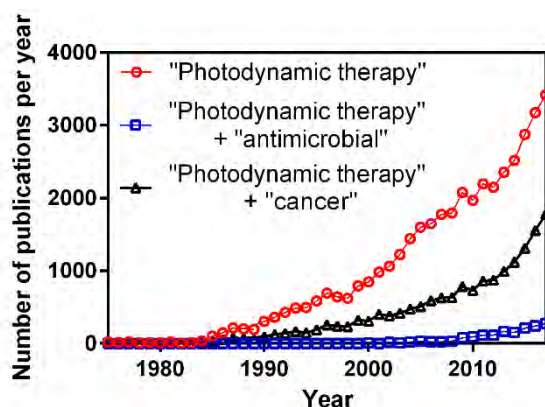


Figure 1.6 Number of publications per year according to Web of Science for the following searches: "Photodynamic therapy" (red circles); "Photodynamic therapy" and "antimicrobial" (blue squares); "Photodynamic therapy" and "cancer" (black triangles). Visited on February 26, 2018.

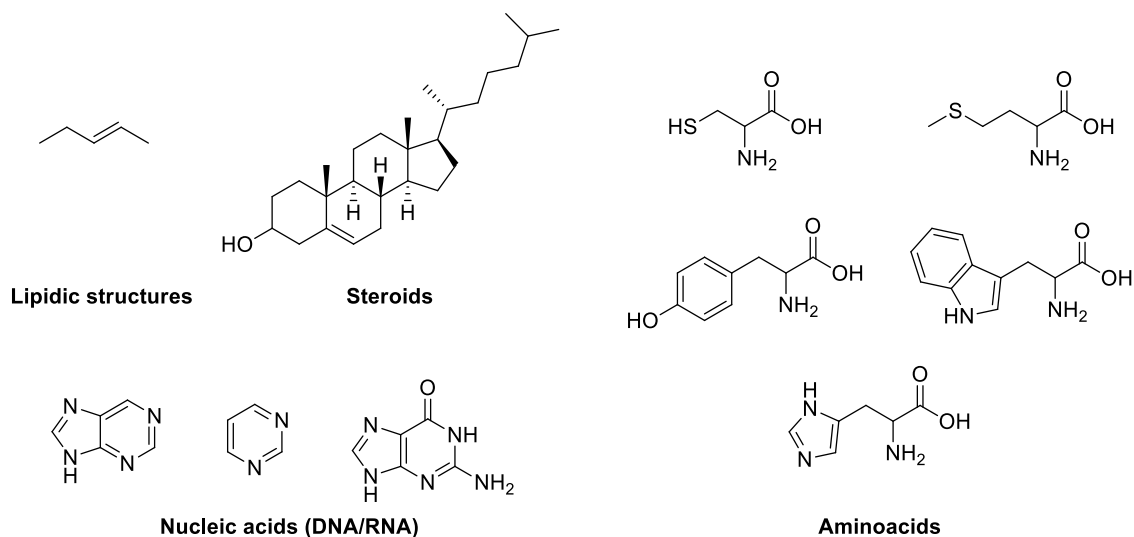
It is now well established that PDT involves the combination of a PS, some source of irradiation (commonly visible light) and ³O₂ to bring about a therapeutic effect. Each of these factors is harmless alone, but when the three are combined produces lethal cytotoxic ROS agents that can inactivate tumoral/bacterial cells.

PDT is an excellent alternative treatment to conventional antitumoral drugs against cancer or to antibiotics against antimicrobial infections.^{131,158-160} PDT takes advantage of the high reactivity of ROS towards a vast array of molecules and biomolecules, particularly lipids,¹⁶¹ proteins¹⁶² and nucleic acids^{163,164} (Scheme 1.6) and their ability to diffuse through biological medium, which allows them to reach distant targets from the

^c Paramecia are single-celled eukaryotic protozoa that are naturally found in aquatic habitats. They are the most studied species of protozoa. The strain used by Raab was *paramecium caudatum*.

^d *Lupus vulgaris* are cutaneous tuberculosis skin lesions with nodular appearance. It is the most common Mycobacterium tuberculosis skin infection.

site of generation inside a cell and cause remote oxidative damage.¹⁶⁵ This leads to DNA/RNA damage, protein miss-function and/or damage to cellular membranes respectively.



Scheme 1.6 Most frequently photooxidable biomolecules. They are lipids, steroids (i.e. cholesterol), nucleic acids (i.e. purine, pyrimidine, and guanine) and aminoacids (i.e. cysteine, methionine, tyrosine, tryptophan, and histidine).¹⁶¹⁻¹⁶⁴

Davies analyzed the distribution of oxidative damage based on abundance and rate constants and concluded that proteins are the most important targets (Figure 1.7).

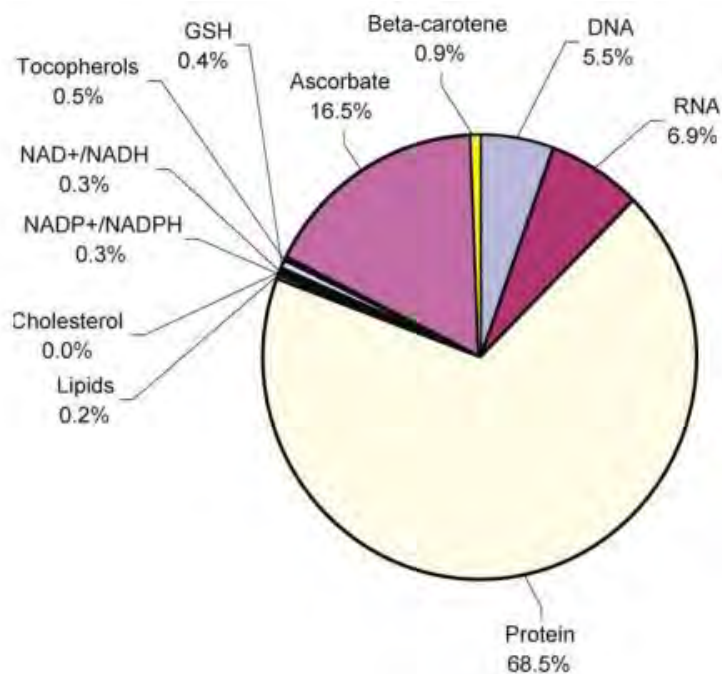


Figure 1.7 Predicted consumption of $^1\text{O}_2$ by intracellular targets calculated and the average concentration of each component within a typical leukocyte cell. Reproduced from reference ¹⁶⁶.

1.4.1. Photodynamic therapy of cancer

Cancer is a group of cell-diseases characterized by a non-regulated cellular growth. In the first stages, it is localized in otherwise healthy tissues and expands to neighboring tissues or even to other body organs through metastasis.¹⁶⁷ This disorder starts in a single cell that suffers additional changes that give it a survival power much higher than non-mutated cells. According to World Health Organization (WHO):¹⁶⁸

“Cancer is one of the leading causes of morbidity and mortality worldwide, with approximately 14 million new cases in 2012. Cancer is the second leading cause of death globally, and was responsible for 8.8 million deaths in 2015. Globally, nearly 1 in 6 deaths is due to cancer. The number of new cases is expected to rise by about 70% over the next 2 decades.”

The most deadly cancers are those of the lung (1.69 million deaths), liver (788 000 deaths), colorectal (774 000 deaths), stomach (754 000 deaths) and breast (571 000 deaths), among others.¹⁶⁹ Therefore, several drugs have been developed and used to cure (or at least to enhance the life quality of cancer patients).¹⁷⁰ However, these treatments are not fully efficient and can produce several side effects.¹⁷¹

PDT is a particularly attractive alternative to conventional antitumoral drugs due to its fundamental specificity and selectivity. It presents a dual selectivity produced by both a preferential partition-in of the PS by cancerous cells and its intrinsic ability to produce ROS only in the specific illuminated region.¹⁷²⁻¹⁷⁴ Unfortunately, other minor side effects have been detected such as skin photosensitization.^{175,176}

PDT can trigger any of the four main cell death pathways: apoptosis, necrosis, paraptosis and autophagy.¹³¹ Apoptosis is a generally major cell death modality in cells responding to PDT.¹⁷⁷ PDT killing effect is further potentiated by damage to the microvasculature (hemorrhage followed by the formation of platelet aggregates), which further restricts ³O₂ and nutrient supply.¹⁷⁸ Finally, tumor cell death is accompanied of cell-signaling cascades and the release of cell fragments cytokines and/or inflammatory mediators. They further stimulates the immune system to recognize and kill the few survival cancerous cells after the treatment (Figure 1.8).^{179,180}

^e **Apoptosis** or “active cell death” is morphologically characterized by chromatin condensation, cleavage of chromosomal DNA into internucleosomal fragments, cell shrinkage, membrane blabbing and formation of apoptotic bodies without plasma membrane breakdown.

Necrosis or “passive cell death” is morphologically characterized by vacuolization of the cytoplasm, swelling and breakdown of the plasma membrane resulting in an inflammatory reaction due to release of cellular contents and pro-inflammatory molecules.

Paraptosis is characterized by the formation of vacuoles in the cytoplasm, along with mitochondrial swelling, reminiscent of necrosis, a somewhat primitive path to cell death. However, what sets paraptosis apart from necrosis is its requirement for new RNA and protein synthesis, suggesting that it, like apoptosis, represents a distinct and programmed biochemical event.

Autophagy is characterized by a massive vacuolization of the cytoplasm.

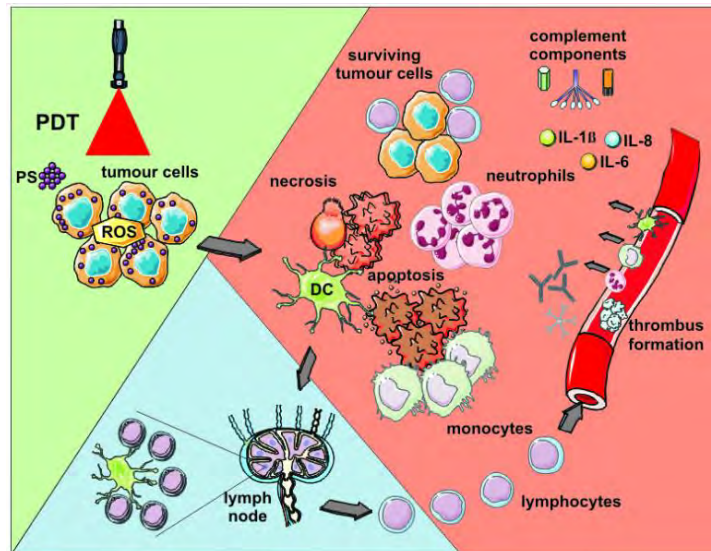


Figure 1.8 PDT-induced effects in tumor cells. Reproduced from reference ¹³¹.

For non-superficial tumors, the ideal PS should present absorption in the red or near-infrared region (600-1000 nm), the so-called therapeutic window, is where the tissues absorb and scatter less.¹⁸¹ Light absorption is mainly due to oxyhemoglobin, water and melanin.¹⁸²

The PS subcellular localization, is a key parameter in cancer PDT. Oliveira *et al* showed that a poor, yet mitochondria-localized PS (cresyl violet), has superior photokilling efficiency than a better PS localized in the lysosomes (methylene blue).¹⁸³ As a rough approximation, lipophilic PSs tend to localize in membranes structures, hydrophilic PSs in lysosomes, and cationic PSs in mitochondria and nuclei.^{184,185}

1.4.2. Antimicrobial photodynamic therapy

Since the discovery of penicillin from the mold *Penicillium notatum* by Alexander Fleming in 1928, antibiotics are used to kill bacteria that cause illness and diseases.¹⁸⁶ Several diseases that caused death before the discovery of penicillin, can nowadays be effectively treated with antibiotics. According to World Health Organization (WHO):¹⁸⁷

“Antibiotic resistance is growing, and we are fast running out of treatment options. If we leave it to market forces alone, the new antibiotics we most urgently need are not going to be developed in time.”

The rapid increase of antibiotic resistance among pathogenic bacteria has stimulated an effort in the development of new antibacterial therapies against which bacteria are unlikely to develop resistance.^{188,189} Antimicrobial photodynamic therapy (aPDT), also called often photodynamic inactivation (PDI) or photo-antimicrobial chemotherapy (PACT) is regarded as a potential alternative to antibiotics, because its multitargeting mode of action difficult the appearance of bacterial resistance.^{190–192} The requirements of an ideal PS for aPDT have to fulfill also with the requirements of an ideal antibacterial drug as described by Paul Ehrlich, the father of chemotherapy.¹⁹³

“In order to use chemotherapy successfully, we must search for substance which have an affinity for the cells of the parasites and a power of killing them greater than the damage such substances cause to the organism itself ... This means ... we must learn to aim, learn to aim with chemical substances.”

Paul Ehrlich

Different groups of bacteria exist^f. Gram-positive and Gram-negative bacteria differ in the composition of their cell wall, which gives different response to antimicrobial agents (Figure 1.9).¹⁹⁴ Gram-positive bacteria can easily uptake neutral or anionic PS and can be easily photoinactivated by them. Instead, Gram-negative bacteria are relatively impermeable to neutral or anionic PS due to their highly negative charged surface.^{195–198}

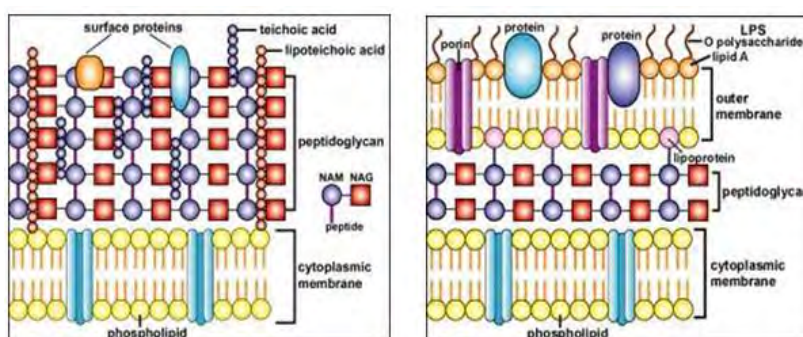


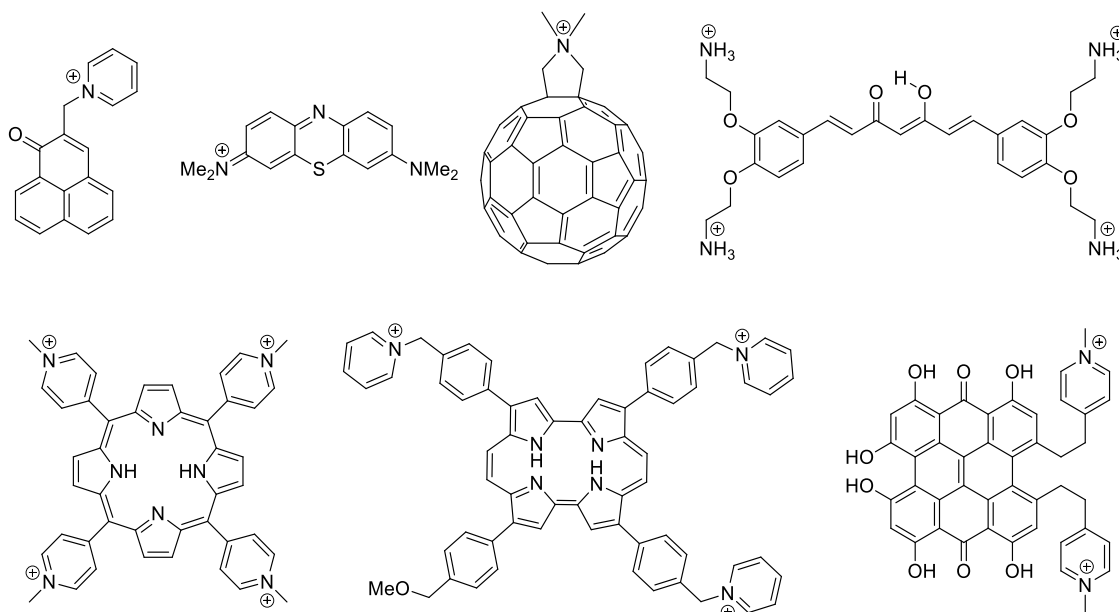
Figure 1.9 Representative Gram-positive (left) and Gram-negative (right) bacterial cell wall. Reproduced from reference ¹⁹⁹.

^f Bacteria can be divided in two main groups based on Gram staining. Gram staining differentiates bacteria by their cell wall structure and chemical composition. Gram-negative bacteria cell wall is more complex than Gram-positive bacteria, because in addition to peptidoglycan they have an additional layer, so-called outer membrane, followed by different polyliposaccharides. This outer membrane acts as a selective permeability barrier.

Different studies have shown that PS positively-charged at physiological pH are active against both Gram-positive and Gram-negative bacteria.¹⁶⁰ Thus, cationic phenothiazine,^{200,201} porphyrins,¹⁹⁵ porphycenes,²⁰² phthalocyanines,^{203,204} hypericin,²⁰⁵ phenalenone,^{206–208} curcuminoids²⁰⁹ or fullerenes²¹⁰ containing positively charged moieties have been synthesized and successfully tested *in-vitro* against Gram-positive and Gram-negative bacteria (Scheme 1.7).

Moreover, some studies used different PS conjugated with poly-L-lysine (a polycationic polymer under physiological conditions) and demonstrated their photo-antimicrobial activity against Gram-positive and Gram-negative bacteria.²¹¹ This conjugate could be the simplest example of a nanoparticulate system.

During the last years, different approaches that use nanoparticulate systems (NPs) have emerged to enhance the effectiveness of aPDT.^{212–214} It is easy to control their size, ζ -potential[§] and surface decoration to further improve their biological activity.²¹⁵ NPs can be used to improve the delivery of the PS to the bacteria and the inactivation kinetics, or they can be used as PSs by themselves (see section 3.4.1 for further information).



Scheme 1.7 Representative cationic PS used for aPDT.^{195,200–210}

To sum up, since PDT was established for antimicrobial purposes several authors pointed out the fact that when a cationic PS is administered to Gram-negative bacteria it has better affinity for the cell wall and then the results after light treatment are better than for anionic dyes.^{195–198}

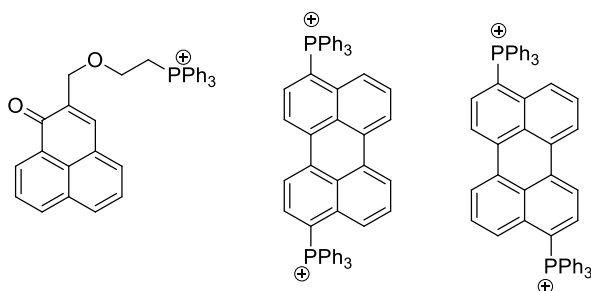
[§] ζ -potential is the potential difference existing between the surface of a solid particle immersed in a conducting liquid and the bulk of the liquid. It is used for quantification of the electrical charge of the NPs.

1.5. Objectives

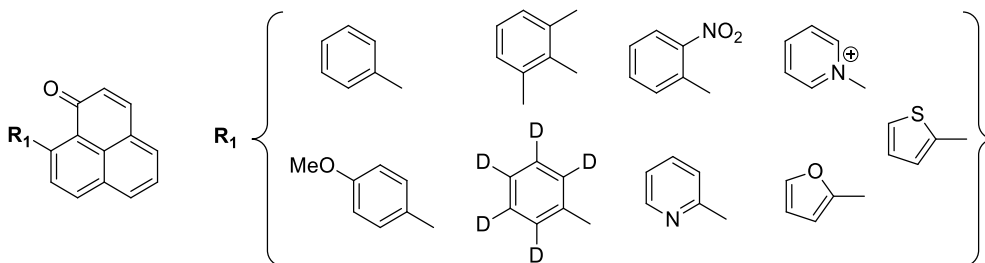
“It shines better when everything has darken.”
Rabindranath Tagore

The main objective of this thesis is to study the behavior of reactive oxygen species, especially singlet oxygen, $^1\text{O}_2$, in different biological environments. The studies range from the characterization of novel targeted photosensitizers to the detection of $^1\text{O}_2$ using different probes. The specific objectives are:

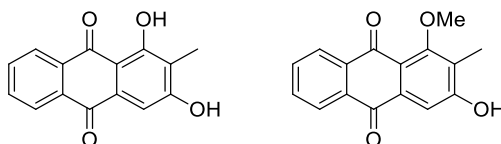
- **O1:** Study of the photophysical and photo-antimicrobial properties of novel triphenyl-phosphonium targeted photosensitizers.



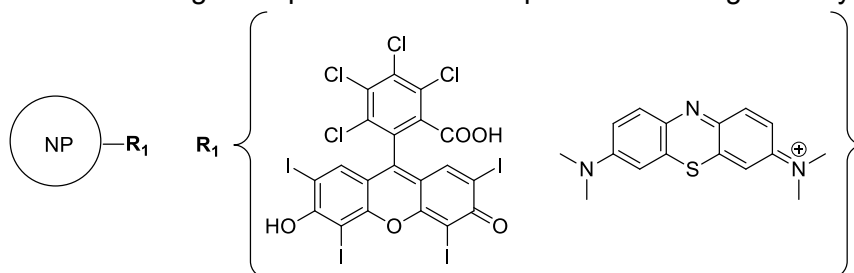
- **O2:** Study of the photophysical and photochemical properties of several 9-aryl- and heteroaryl-phenalenones



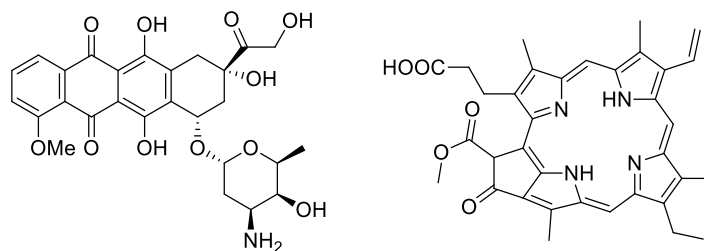
- **O3:** Study of the photophysical and photochemical properties of two-naturally occurring anthraquinones.



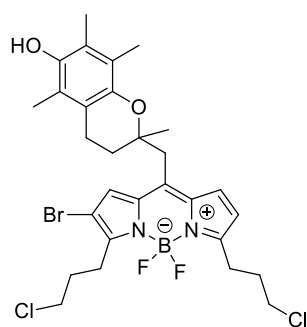
- **O4:** Study of the photophysical and photo-antimicrobial properties of different photosensitizers using mesoporous silica nanoparticles for drug delivery.



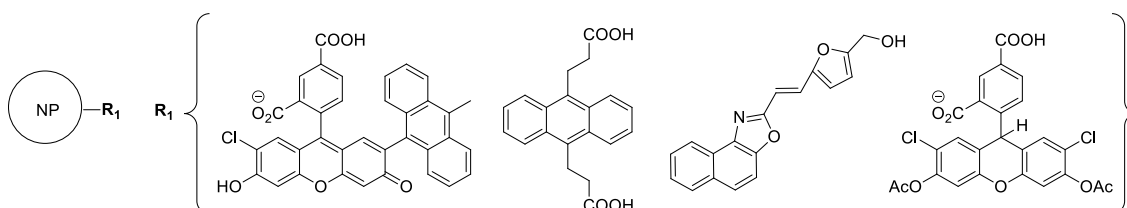
- **O5:** Study of the photophysical and photochemical properties of the antineoplastic drug doxorubicin and assessment of its photo-antineoplastic properties alone or in combination with a photosensitizer.



- **O6:** Study of the photophysical, photochemical and photo-antineoplastic properties of ROS-activatable photosensitizers.

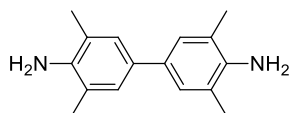


- **O7:** Development of nanoencapsulated $^1\text{O}_2$ fluorescent probes.

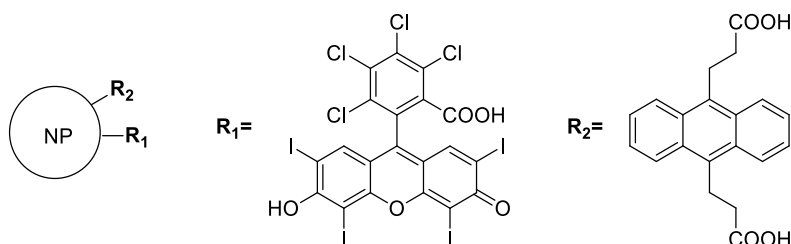


- **O8:** Study of the structure, properties and reactivity of CellROX Deep Red[®], a novel fluorescent probe for detecting ROS.

- **O9:** Development of a $^1\text{O}_2$ probe for photoacoustic imaging.



- **O10:** Development of a self-responsive $^1\text{O}_2$ nanophotosensitizer.



Chapter II

General materials, techniques and methods

*If you can't fly then run,
if you can't run then walk,
if you can't walk then crawl,
but whatever you do you have to keep moving forward.*

Martin Luther King Jr.

2.1. Materials

All solvents were from Scharlau (Barcelona, Spain), except the deuterated ones, which were purchased from Sigma-Aldrich (St Louis, MO, USA). All reagents were used without further purification.

Acrylamide 99%, ammonium persulfate (APS), (3-aminopropyl)triethoxysilane (APTES), anthracene, sodium dioctyl sulfosuccinate (AOT), bovine serum albumin (BSA), copper sulphate, cetyltrimethylammonium chloride solution (25 wt % in H₂O; CTAC), Crystal Violet (CV), d-mannitol, DNA sodium salt from calf thymus, doxorubicin (Doxo), 1-(3-dimethylaminopropyl)-3-ethylcarbodiimide hydrochloride (EDC), hydrogen peroxide (H₂O₂), D-mannosamine hydrochloride, 2-methylnaphthoxazole, 5-(hydroxymethyl)furan-2-carbaldehyde, methylene blue (MB), Mohr salt ((NH₄)₂SO₄·6H₂O), 3-(4,5-dimethylthiazol-2-yl)-2,5-diphenyl-2H tetrazolium bromide (MTT), new methylene blue (NMB), N-hydroxysuccinimide (NHS), pheophorbide a (PhA), phenalene (PN), potassium superoxide (KO₂), quinine sulphate (QS), rose bengal (RB), sodium azide (NaN₃), sodium hypochlorite solution (50 g/L of NaClO), sodium nitroprusside (Na₂[Fe(CN)₅NO]) tetracyanoethylene (TCNE), N,N,N,N-tetramethylethylenediamine (TEMED), tetraethyl orthosilicate (TEOS), 1,2-dihydroxybenzene-3,5-disulfonate (Tiron), *meso*-tetraphenylporphyrin (TPP), *meso*-tetra(4-sulfonatophenyl)porphine tetrasodium salt (TPPS₄), *meso*-tetra(*N*-methyl-4-pyridyl)porphine tetratosylate salt (TMPyP), tetramethylbenzidine (TMB), 3-(triethoxysilyl)propyl isocyanate, 4,7,10-trioxa-1,13-tridecanediamine, were purchased from Sigma-Aldrich (St. Louis, Missouri, USA).

Flavin mononucleotide (FMN) was purchased from ChromaDex™ (Irvine, California, USA). Perdeuterobromobenzene was purchased from Cambridge Isotope Laboratories (Andover, MA). Singlet oxygen sensor green (SOSG) and CellROX Deep Red were purchased from Life technologies Invitrogen (Alcobendas, Spain). ADPA was supplied by Chemodex (St. Gallen, Switzerland). N,N'-methylenebis(acrylamide) and Brij 30® were obtained from Fluka Analytical (Gillingham, United Kingdom). Hexamethylindodicarbocyanine iodide (Cy5 core), diacetyl 6''-carboxy-2',7'-dichlorodihydrofluorescein (DCFH-DA) were purchased from Santa Cruz Biotechnology (Dallas, Texas, USA). Fetal Bovine Serum was purchased from Greiner Bio-One (Frickenhausen, Germany). B-PER cell lysis reagent was purchased from Thermo-Fischer (Waltham, USA).

Phosphate Buffered Saline (PBS; Fisher Scientific BP399-1, adjusted pH=7.4) was purchased from Fisher Bioreagents (Geel, Belgium). Tryptic Soy Broth (TSB) and Agar (Bacteriology grade) were purchased from Panreac AppliChem (Castellar del Vallès, Spain). Dulbecco's modified Eagle's medium (DMEM) with 4.5 g/L glucose, fetal bovine serum (FBS), trypsin solution C (0.05%) with EDTA (0.02%) and phenol red, L-glutamine 200 mM, and penicillin (10000 units/ml)-streptomycin (10 mg/ml) solution were supplied by Biological Industries (Kibbutz Beit Haemek, Israel). The DMEM 1 g/L glucose without phenol red, Cell Tracker Green CMFDA Dye and B-PER cell lysis were supplied by Thermo Fisher Scientific (Waltham, Massachusetts, USA). The HEPES buffer 1M in 0.85% NaCl was supplied by Lonza (Basel, Switzerland). The sterilized cell culture material was supplied by LabClinics S.A. (Barcelona, Spain).

1H-Phenalen-1-one sulfonate (PNS) was synthesized as described in reference 216.

2.2. Spectroscopic techniques

2.2.1. Steady-state optical techniques

Absorbance spectra were recorded in a Cary 6000i UV-Vis-NIR spectrophotometer (Agilent Technologies, Santa Clara, CA, USA).

Fluorescence emission and excitation spectra were recorded in a Fluoromax-4 spectrofluorometer (Horiba Jobin-Yvon, Edison, NJ, USA). Excitation and detection were performed at 90° for optically diluted solutions ($A < 0.05$ to avoid inner filter effects in the measurement of fluorescence).

Emission spectra of the different irradiation sources used were recorded in a BLACK-Comet CXR-50 spectrophotometer (StellarNet, Tampa, Florida, USA).

Fluorescence quantum yield (Φ_F) were determined from the comparison of the area under the corrected emission curves of optically-matched solutions of the sample and a suitable reference (Eq. 2.1).¹⁰

$$\Phi_{F;sample} = \frac{F_{sample} \cdot n_{sample}^2}{F_{reference} \cdot n_{reference}^2} \Phi_{F;reference} \quad Eq. 2.1$$

Where F_i is the fluorescence intensity integrated over the entire emission spectrum and n_i is the refractive index of the solvent used.

2.2.2. Time-resolved optical techniques

2.2.2.1. Time-correlated single photon counting (TCSPC)

Time-Correlated Single Photon Counting (TCSPC) is the most commonly used technique for singlet state lifetime determination.^{217–219} It is based on the detection of single photons of a periodical light signal, the measurement of the detection times of the individual photons and the reconstruction of the waveform from the individual time measurements.

The TCSPC technique makes use of the fact that for low-level, high-repetition-rate pulses, the produced light intensity is so low that the probability of detecting one photon in one signal period is much less than one.²²⁰ Therefore, it is not necessary to provide for the possibility of detecting several photons in one signal period. It is sufficient to record the photons, measure their arrival time in the signal period, and build up a histogram of the photon times as depicted in figure 2.1.

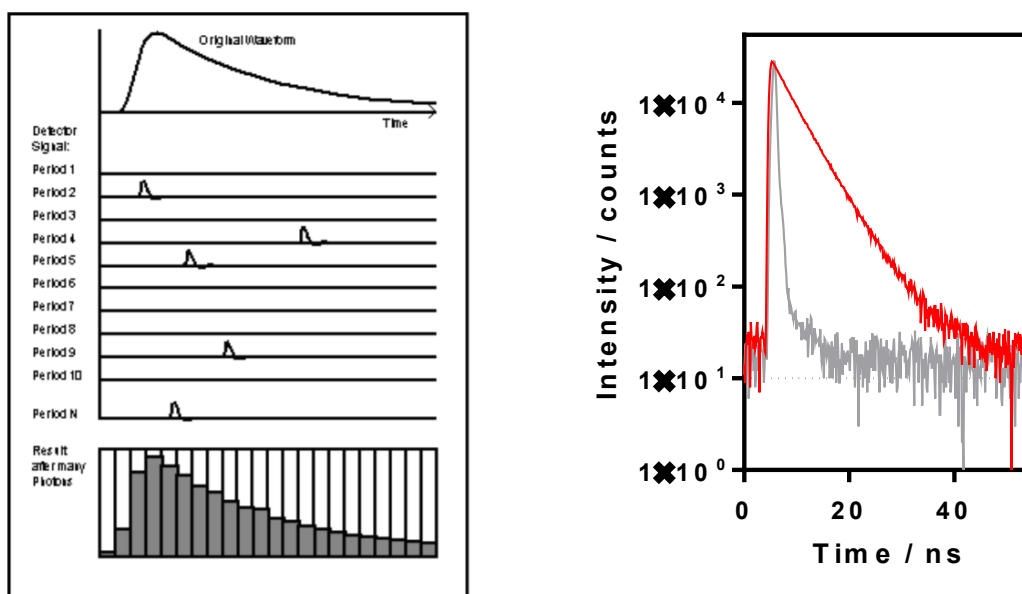


Figure 2.1 Left: schematic representation of the TCSPC technique. Reproduced from reference ²²¹. Right: Time-resolved fluorescence (TRF) decay for a fluorophore. Grey trace represent the instrument response function (IRF).

Time-resolved fluorescence decays were registered with a TCSPC system (Fluotime 200, PicoQuant GmbH, Berlin, Germany). The samples can be excited at different wavelengths (290, 375, 405, 457, 502, 596, 654 nm) by means of a picosecond-pulsed LEDs or Laser working at a 10 MHz repetition rate. Fluorescence decays were acquired at the emission maxima, and they were analyzed using PicoQuant FluoFit c4.6.5 data analysis software. The counting frequency was always kept below 1%.

The deconvolution of the TCSPC fluorescence signal using the instrument response function (IRF; reference sample: ludox in water, which directs a small fraction of the excitation beam into the detection path) and a kinetic model yields the appropriate kinetic parameters, e.g., the singlet lifetime (Figure 2.1).²²²

For time-resolved anisotropy studies, Glan-Taylor polarizers were placed both at the entrance and exit ports of the sample chamber. Anisotropy decay $r(t)$ were calculated using Eq. 2.2.^{10,223}

$$r(t) = \frac{VV(t) - G \cdot VH(t)}{VV(t) + 2G \cdot VH(t)} \quad \text{Eq. 2.2}$$

Where $VV(t)$ and $VH(t)$ denote fluorescence decay kinetics of the sample measured using V polarized exciting light and detecting the emission components polarized V and H, respectively. G is an instrument- and wavelength-dependent correction factor that compensates for the polarization bias of the detection system. The precise G-factor is determined by treating the additionally measured $HV(t)$ and $HH(t)$ curves (Eq. 2.3)

$$G = \frac{\int HV(t) dt}{\int HH(t) dt} \quad \text{Eq. 2.3}$$

2.2.2.2. Time-resolved near-infrared phosphorescence

This technique is commonly used for directly and specifically monitoring the formation and decay of $^1\text{O}_2$, the measurement of its lifetime (τ_Δ) and its quantum yield of formation (Φ_Δ).^{76,78,224} It is based on the detection of the weak $^1\text{O}_2$ phosphorescence, centered at 1270 nm as explained in the section 1.3.2.

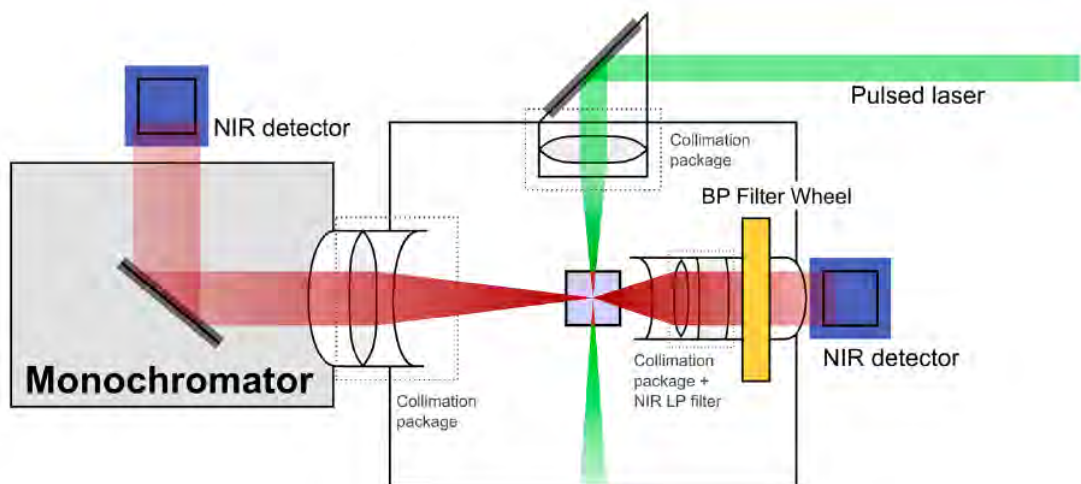


Figure 2.2 Typical optical setup for detection of near-infrared phosphorescence using either a monochromator (left arm) or a filter wheel containing different band-pass filters (right arm). Reproduced from reference ⁷⁸.

Time-resolved near-infrared phosphorescence decays were acquired with a customized Fluotime 200 system (Figure 2.2; PicoQuant GmbH, Berlin, Germany). A diode pulsed Q-switched Nd:YAG laser (FTSS355-Q, CrystaLaser, Berlin, Germany) working at 1 or 10 kHz repetition rate and emitting at 532 or 355 nm (1.2 or 0.5 μJ per pulse, respectively) or a pulsed AO-Z-473 solid state AOM Q-switched laser (Changchun New Industries Optoelectronics Technology Co., Changchun, China) working at 2 kHz repetition rate at 473 nm (<1.5 μJ per pulse) were used for sample excitation. In the case of the pulsed Nd:YAG laser, a 1064-nm rugate notch filter (Edmund Optics, Barrington, NJ, USA) and an uncoated SKG-5 filter (CVI Laser Corporation, East Albuquerque, NM, USA) were placed at the exit port of the laser to remove any residual component of its fundamental emission in the near-infrared region. The luminescence exiting from the sample was filtered by a 1100 nm long-pass filter (Edmund Optics, Barrington, NJ, USA) and a narrow band pass filter at 1275 nm (BK-1270-70-B, bk Interferenzoptik Elektronik GmbH, Nabburg, Germany). A thermoelectric-cooled near-infrared sensitive photomultiplier tube assembly (H9170-45, Hamamatsu Photonics, Hamamatsu, Japan) was used as detector. Photon counting was achieved with a multichannel scaler (NanoHarp 250, PicoQuant GmbH, Berlin, Germany). The count histograms were built up until a sufficient signal-to-noise ratio was attained.

The time dependence of the $^1\text{O}_2$ phosphorescence with the signal intensity $S(t)$ is described by Eq. 2.4, where τ_T and τ_Δ are the lifetimes of the photosensitizer triplet state and of $^1\text{O}_2$, respectively, and $S(0)$ is a quantity proportional to $^1\text{O}_2$ quantum yield (Φ_Δ) as shown in Eq. 2.5; κ is a proportionality constant, which includes electronic and geometric

factors k_R is the 1O_2 radiative rate constant, E is the incident laser energy, and A is the sample absorbance at the excitation wavelength.

$$S(t) = S(0) \frac{\tau_\Delta}{\tau_\Delta - \tau_T} \left(e^{-\frac{t}{\tau_\Delta}} - e^{-\frac{t}{\tau_T}} \right) \quad Eq. 2.4$$

$$S(0) = \kappa k_r \phi_\Delta E (1 - 10^{-A}) \quad Eq. 2.5$$

Two different procedures have been used for determining ϕ_Δ . The first one involved measuring the $S(0)$ values for a series of solutions of increasing absorbance and then plotting $S(0)$ versus the sample absorption factor ($1-10^{-A}$), which should yield linear plots. Then ϕ_Δ value was obtained by comparison of the slopes of such plots for a suitable reference and the PS, using Eq 2.6.

$$\phi_{\Delta;PS} = \frac{Slope_{PS}}{Slope_{Ref}} \phi_{\Delta;Ref} \quad Eq. 2.6$$

The other procedure involved comparing the $S(0)$ values of solutions of the PS and the reference optically-matched at the excitation wavelength, as described by Eq. 2.7.

$$\phi_{\Delta;PS} = \frac{S(0)_{PS}}{S(0)_{Ref}} \phi_{\Delta;Ref} \quad Eq. 2.7$$

The rate constants for the global 1O_2 quenching (k_q) were determined by measuring τ_Δ as a function of the concentration of the quencher. Thus, a plot of the reciprocal lifetime vs concentration should yield a straight line whose slope is k_q .

τ_T was determined, when possible, by fitting an exponential (or poly-exponential if multiple species were present) to the emission signal obtained at a wavelength where the triplet state of the photosensitizer emits (typically in the near-infrared region).

2.2.2.3. UV-Vis nanosecond laser flash photolysis

Laser Flash Photolysis (LFP) is a pump-probe laboratory technique, in which a sample is firstly excited by a nanosecond pulsed-laser light (called pump-pulse). This strong pulse generates excited states, which can further evolve through a photochemical reaction. Afterwards, the absorption of light (called analyzing-beam) by the sample is recorded to monitor relaxation or possible photoinduced chemical reaction processes initiated by the pump-pulse.^{225,226} This technique was developed in the 40s and 50s by Manfred Eigen, Ronald George Wreyford Norrish and George Porter and they won the 1967 Nobel Prize in Chemistry for this invention.^{227–229}

Transient absorption spectra was recorded in a LFP home-built system (Figure 2.3). A nanosecond-pulsed Nd:YAG laser (Continuum Surelite 10, San José, USA) operated at the 2nd or 3rd harmonic (λ_{exc} 532 or 355 nm, 10 mJ/pulse) was used as the pump-pulse to excite the sample. The energy of the pulse was varied by changing the laser Q-switch delay. The energy of the pulse was measured by diverting a small fraction of the beam onto a Laser Precision Corporation energy meter.

The analyzing beam was produced by a 75W short arc Xe lamp (Photon Technology International, Birmingham, NJ, USA). A 10 cm water filter was placed in the analyzing beam in order to remove any near infrared emission before sample irradiation. Changes in the analyzing beam intensity (and therefore sample absorbance changes) were detected with a dual-grating monochromator (mod. 101, Photon Technology International, Birmingham, NJ, USA) coupled to a UV-Vis photomultiplier (PTI 710, Photon Technology International, Birmingham, NJ, USA). Three slits (one before and two after the sample holder) were placed to control the analyzing beam intensity, and avoid saturating the photomultiplier. The photomultiplier signal was fed to an oscilloscope (Lecroy WaveSurfer 454, Irvington, NY, USA) through a DC50 Ω coupled port for digitizing and averaging (typically between 10 and 100 shots) and finally transferred to a PC for data storage and analysis.

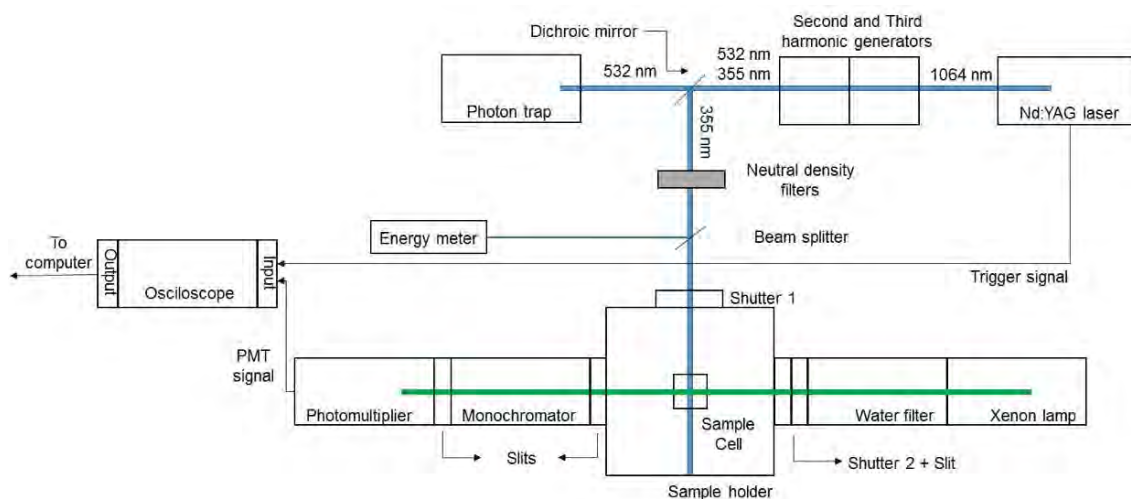


Figure 2.3 Optical setup for our LFP home-built system. Blue and green lines are the pump-pulse and the analyzing-beam respectively.

Three different kinetics traces (signal, blank and reference) were acquired for each LFP experiment performed. Signal trace ($S(t)$) is collected with shutter 1 and 2 open and it is the former LFP experiment. Blank trace ($B(t)$) is collected only with shutter 2 open to detect baseline deviations. Reference trace ($R(t)$) is collected only with shutter 1 open to detect the intrinsic fluorescence and/or phosphorescence of the sample. Then, the differences in absorbance (ΔA) are calculated accordingly to Eq. 2.8.

$$\Delta A(t) = \log\left(\frac{I_I}{I_T}\right) = \log\left(\frac{B(t)}{S(t) - R(t)}\right) \quad \text{Eq. 2.8}$$

Where I_I and I_T are the light intensity received and transmitted by the sample respectively. The full system was operated by a computer using a LabView-based home-written software.

2.2.2.4. Laser-induced optoacoustic spectroscopy

Laser-induced optoacoustic spectroscopy (LIOAS) monitors the pressure changes induced by the heat emitted by non-radiative deactivation processes of an excited molecule as well as by chemical reactions after excitation of the samples.^{92,230}

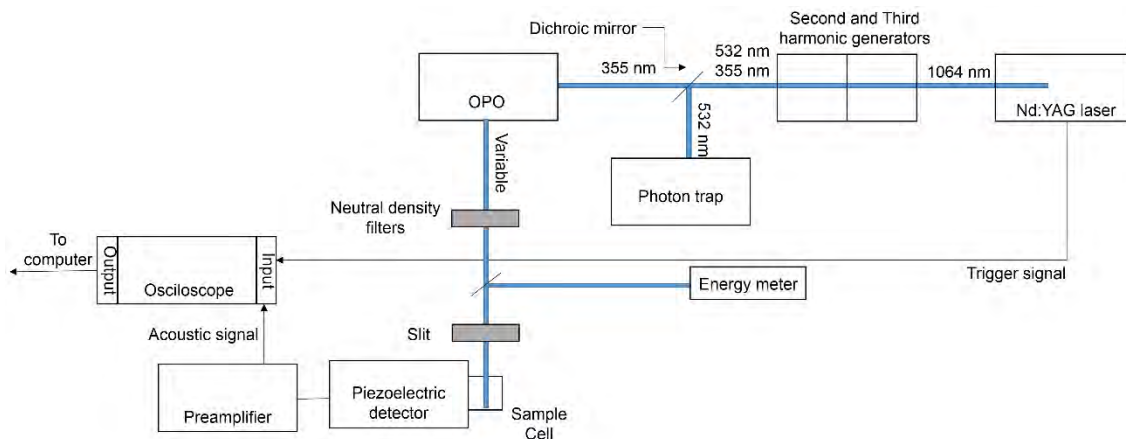


Figure 2.4 Optical setup for our LIOAS home-built system.

The LIOAS signals were recorded in a home-built system (Figure 2.4). A nanosecond-pulsed Nd:YAG laser (Continuum Surelite 10, San José, USA) operated at 3rd harmonic (λ_{exc} 355 nm, 10 mJ/pulse) coupled to an optical parametric oscillator (OPO^h; Continuum SL OPO, San José, USA) was used to excite the sample. The resulting beam was passed through a 1 mm-slit to create a rectangular line source. Samples were measured using a piezoelectric detector 9310 (Quantum Norhtwest, WA, USA) attached to an absorbance cuvette in right-angle geometry. The analog signal was amplified using a Panametrics 5662 Preamp (Olympus, Japan) and passed to a Lecroy WaveSurfer 454 oscilloscope which performed digitalization and signal averaging over 1000 shots per measurement.

^h An optical parametric oscillator (OPO) is a parametric oscillator that oscillates at optical frequencies. It converts an input laser wave with E_{in} into two output waves of lower energy (E_{out1} and E_{out2}) by means of second-order nonlinear optical interaction.

$$E_{in} = E_{out1} + E_{out2}$$

2.2.3. Light sources

For the irradiation experiments reported in this thesis, different light sources were used. The emission wavelength was chosen to match the absorption spectrum of the PS (Figure 2.5). Fluence rates were routinely measured using a power meter (Ophir Laser Power Meter model AN/2, North Andover, MA, USA).

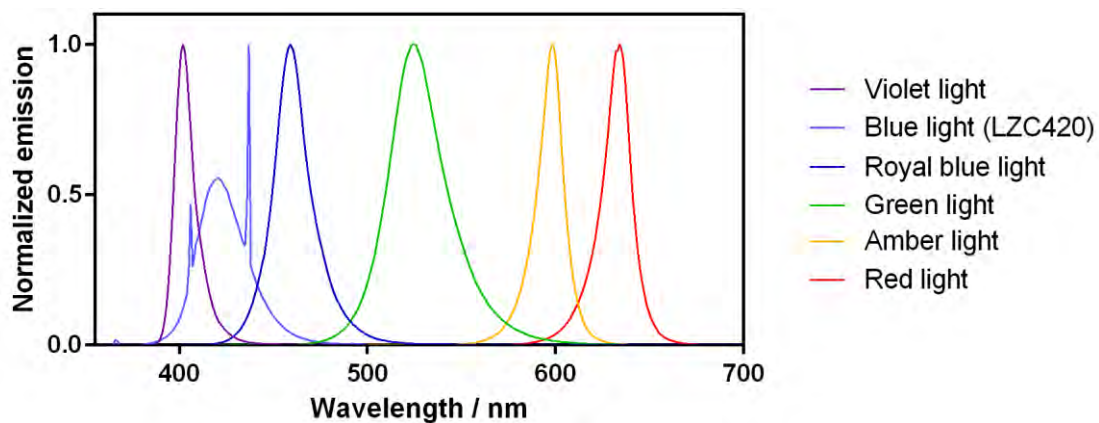


Figure 2.5 Emission spectra of the different light sources. Violet light (402±6 nm; 12.8 mW/cm²), blue light (LZC420; 421±15 nm; 10.2 mW/cm²), royal blue light (459±10 nm; 14.0 mW/cm²), green light (524±17 nm; 7.5 mW/cm²), amber light (598±8 nm; 4.2 mW/cm²) and red light (634±8 nm; 7.8 mW/cm²).

2.3. General photoinactivation protocol

Different bacterial strains have been used in this doctoral thesis. In each section, the bacterial strains will be specified. Unless stated, the culture media used for growing the bacterial cells was Tryptic Soy Broth (TSB). The different bacterial strains were grown overnight at 37 ± 1 °C. Then, 100 μ L of the culture were grown in 10 mL of fresh TSB until reaching the desired optical density at 600 nm (OD_{600}). Afterwards, bacteria were harvested by centrifugation (5000 rpm, 10 min) and resuspended in sterile PBS, maintaining the same concentration of bacteria.

1 mL of the bacterial cell suspensions in PBS, were poured to a 1.5 mL sterile microtube and was used for the irradiation control. To check that the light is not toxic itself and all the death can be attributed to the PS, this microtube will not contain PS. Then, for every concentration of photosensitizer, 1 mL of the bacterial cell suspension was poured to 2 microtubes.

The microtubes containing bacteria were harvested by centrifugation (5000 rpm, 10 min). Afterwards, bacterial cells were resuspended in 1 mL of PBS with the desired concentration of PS, which was dissolved in sterile PBS or DMSO. Following this, bacterial cell suspensions were incubated in the dark at 37 °C during a known-amount of time in an orbital shaker. After the incubation, aliquots of 300 μ L were poured into a 96 well plate. After that, samples were irradiated without the lid with the corresponding lamp until reach the desired fluence or maintained in the dark for the same period. The specific lamp used and the fluence delivered will be quoted at each section.

Then, the aliquots were diluted using 96-well plates: 300 μ L of the aliquots were placed in each well, and 30 μ L of them were poured into another well with 270 μ L of new PBS, this was repeated 6 times for every aliquot, until reaching a 10^{-6} dilution factor.

Next, 10 μ L of every dilution (the original aliquots and the consecutive dilutions) were spread on Tryptic Soy Agar (TSA). Finally, the plates were incubated aerobically at 37 ± 1 °C for 24 hours and after the incubation, the colony forming units (CFU) were counted and the dilution factor was considered.

A minimum of the three independent experiments per experimental condition were performed, with three plates inoculated for each replica, to a minimum total of nine recounts.

2.4. General synthesis characterization

¹H-NMR spectra were recorded on a Varian 400 spectrometer (400 MHz; Palo Alto, CA, USA) using residual solvent as internal standard.²³¹ The multiplicity is reported as s = singlet, d = doublet, t = triplet, q = quadruplet and m = multiplet. All of the coupling constants are reported in hertz. ¹³C-NMR spectra were recorded on the same instrument, and chemical shifts were measured relative to solvent resonances as internal standard.²³¹

Size and ζ -potential of the synthesized SNPs were measured using a Nano-ZS Zetasizer equipment (Malvern Instruments Ltd, Worcestershire, UK). For size examination, a diluted aliquot in ethanol was measured. For ζ -potential examination, a diluted aliquot in Milli-Q water was measured.

Infrared spectra of the organic compounds or NPs supported on a potassium bromide disk were recorded using a Nicolet Magna 560 FTIR spectrophotometer (Thermo Electron Corporation, Waltham, MA, USA).

Organic elemental analysis of the different nanoparticles synthesized were recorded in a EURO EA-3000 Elemental Analysis (Eurovector, Pavia, Italy).

Chapter III

New strategies for increasing $^{1}\text{O}_2$ efficiency against living systems

*Estima el teu ofici,
la teva vocació, la teva estrella,
allò pel que serveixes, allò en què realment
ets un entre els homes,
esforça't en el teu quefer
com si de cada detall que penses,
de cada paraula que dius,
de cada peça que poses,
de cada cop de martell que dones,
en depengués la salvació de la humanitat.
Perquè en depèn, creu-me.*

*Si oblidant-te de tu mateix
fas tot el que pots en el teu treball,
fas més que un emperador que regeix
automàticament els seus estats;
fas més que el qui inventa teories universals
només per satisfer la seva vanitat,
fas més que el polític, que l'agitador, que el que governa.*

*Pots desdenyar tot això i l'adobament del món.
El món s'adobaria bé tot sol, només que cadascú
fes el seu deure amb amor, a casa seva.*

Joan Maragall

3.1. Introduction

ROS are cytotoxic species due to their oxidant properties, as introduced in the introduction chapter. Since more than 100 years ago, ROS have been used to treat diseases such as cancer, bacterial and fungal infections, as well as for virus inactivation.²³² Although several reviews about PDT in connection with ROS have been published,^{131,158–160} some questions about $^1\text{O}_2$ (and other ROS) remain unanswered in the PDT field.

It is widely known that cationic PS are excellent photoantimicrobial agents against Gram-positive and Gram-negative bacteria, whilst neutral/anionic PS are “only” effective against Gram-positive bacteria (with the corresponding exceptions).^{195,233} In section 3.2 we study the effect of triphenyl-phosphonium targeting moiety -a highly-lipophilic cation- for its use in aPDT.

Nowadays, the main pharmaceutical agencies, like the American Food and Drug Administration (FDA) or the European Medicines Agency (EMA), impose many restrictions for the approval of new synthetic drugs, whilst if the compound has a natural origin the restrictions are lower.^{234,235} In section 3.3, we re-evaluate the use of some naturally-occurring PSs based on aromatic ketones. In connection with this, we studied the mechanism of the β -phenyl quenching reaction and show that the 9-aryl phenalenone scaffold can be used to engineer a new family of photochromic compounds as well as for uncaging purposes.

In the last few years, nanotechnology has gained a fundamental role in the biosciences. In the nanometric scale, several materials present different properties than in the macroscopic scale, and this is used advantageously by nanomedicine to improve conventional treatments.^{212–214} In section 3.4, we study the interaction between different PSs and mesoporous silica NPs as well as their ability to produce $^1\text{O}_2$ and their photo-antimicrobial properties.

In the last few years, some studies have appeared that propose the combination of various PSs with different subcellular localization to reduce the therapeutic dose.^{236–238} Similar studies have also appeared that combine a classical antineoplastic agent with a PS.^{239–241} In section 3.5 we study the interaction and the photophysical properties of an antineoplastic drug (Doxorubicin) and a PS (Pheophorbide a), as well as the effect of a combined treatment.

Selectivity of PDT results from the preferential uptake of the PS by the tumour tissue by passive and/or active targeting.²⁴² In addition, ROS will only be produced when $^3\text{O}_2$, PS and light are together. Using an activatable PS (aPS), another layer of selectivity is added, whereby the aPS will be able to generate $^1\text{O}_2$ only when an additional specific stimulus is present.^{69,243} In section 3.6 we study the activation of an aPS by ROS both in solution and in HeLa cells.

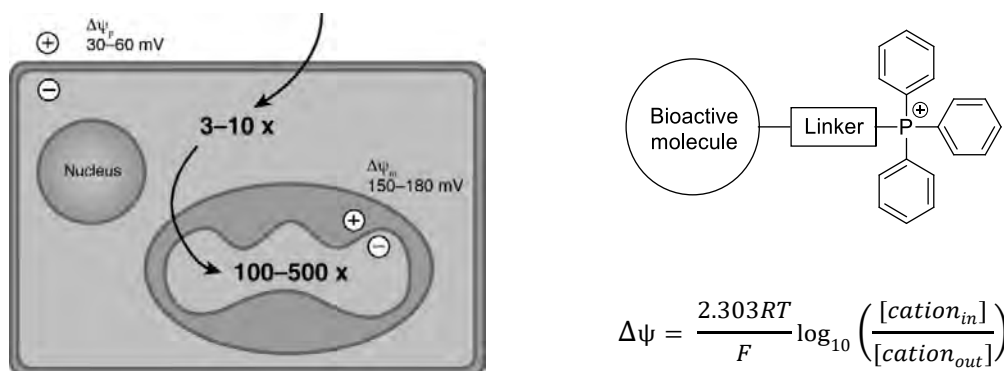
3.2. Triphenylphosphonium cation: a neglected functional group for aPDT

(Adapted from: **R. Bresolí-Obach**,⁺ I. Gispert,⁺ D. García-Peña,⁺ S. Boga, Ò. Gulías, M. Agut, M.E. Vázquez and S. Nonell, Triphenylphosphonium cation: a valuable functional group for antimicrobial photodynamic therapy, *J. Biophotonics*. **2018**, e201800054; ⁺These authors contributed equally to this work.)

The work described in this section has been carried out in collaboration with Universidade de Santiago de Compostela (Santiago de Compostela, Spain).

3.2.1. Why triphenylphosphonium cation?

Delocalized lipophilic cations (i.e. triphenylphosphonium (TPP)) have a large hydrophobic surface area and delocalized charge distribution that results in weakened solvation enthalpy, which allows them to easily penetrate through biological membranes.^{244–246} Once inside the cells, they are driven to the mitochondria by the large electrochemical potential generated by the electron transport chain.²⁴⁷ TPPs cations accumulate inside mitochondria according to the Nernst equationⁱ (Figure 3.1).²⁴⁸ There will be a ~10-fold preferential accumulation of TPPs within mitochondria for every ~60 mV increase in membrane potential ($\Delta\psi$). Therefore, the mitochondrial $\Delta\psi$ is typically 150–180 mV,²⁴⁹ so there will be more than 100-fold preferential accumulation of TPPs derivatives into the mitochondrial matrix (Figure 3.1).



$$\Delta\psi = \frac{2.303RT}{F} \log_{10} \left(\frac{[cation_{in}]}{[cation_{out}]} \right)$$

Figure 3.1 Left: Uptake of TPPs derivatives by mitochondria within cells. In a first step, TPP derivate is uptaken from the extracellular environment into the cytoplasm driven by the plasma membrane potential. From the cytoplasm the TPP derivate is further accumulated into mitochondria, driven by the mitochondrial membrane potential. The mitochondrial and plasma membrane potentials ($\Delta\psi$) are indicated. Reproduced from reference ²⁴⁸. Right: Chemical structure of a mitochondrial targeted molecule and the Nernst equation adapted for this system.

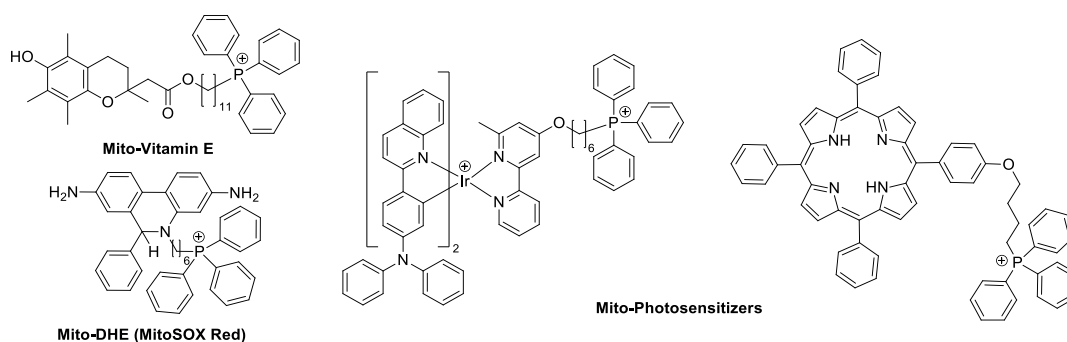
The use of TPPs conjugated bioactive molecules in mitochondrial biology was reinvented and refined by Murphy and coworkers.^{250–253} TPPs cations have been used to deliver fluorescent probes, antioxidants or pharmacophores to mitochondria. Moreover, this strategy leads to numerous patent applications and publications.^j

ⁱ Nernst equation is an electrochemical equation that relates the reduction potential of an electrochemical reaction to the standard electrode potential, temperature, and chemical activities of the chemical species undergoing reduction and oxidation process. Furthermore, Nernst equation has a physiological application when used to calculate the potential of an ion to cross a biological membrane.

^j By searching the term “triphenylphosphonium” AND “mitochondria” AND “targeting” in the Google Patents database, 574 patent applications have been identified (visited on 06-04-2018). Among them,

The photokilling ability of the $^1\text{O}_2$ produced is dependent from the place where it has been generated. As example, a poor $^1\text{O}_2$ PS (i.e. crystal violet) is much more effective killing HeLa cells than a good $^1\text{O}_2$ PS (i.e. methylene blue) because crystal violet is localized in mitochondria whilst methylene blue is distributed around the cell.¹⁸³ Even more, synthetic fluorophores such as MitoTracker series (specially Deep Red) can be highly phototoxic to cells even for relatively short irradiation times.²⁵⁴

PS subcellular localization is indeed as important as the photosensitizing properties in terms of overall cell killing. Therefore, mitochondrial localization is a highly desirable property for the development of more efficient PS for antitumoral PDT.¹⁶⁰ Since then different mitochondrial targeted PS have been synthesized and tested against tumoral cells (Scheme 3.1).^{255,256}



Scheme 3.1 Different examples of TPPs-based mitochondria targeted molecules (i.e. Vitamin E analogue,²⁵³ $\text{O}_2^{\bullet-}$ fluorescent probe (MitoSOX Red)²⁵⁷ or inorganic²⁵⁵/organic²⁵⁶ PS).

Given the similarities between mitochondria and bacteria,^{k258} we set out to assess the potential of TPP as a targeting unit for the development of new photoantimicrobials. To our best knowledge, there has not been yet published any study that study the potential of TPP as a targeting unit for aPDT. Moreover, in bibliography, only two studies are found using TPP-based antibiotics derivatives. They are efficient against Gram-positive bacteria, but not against Gram-negative.^{259,260} Herein we report the optical, photophysical, and photoantimicrobial properties against Gram-positive and Gram-negative microbial cells in vitro of (2-((1-oxo-1H-phenalen-2-yl)methoxy)ethyl) triphenylphosphonium bromide, (PNPPH_3^+). Additionally, to further demonstrate the value of the TPP group for the development of new compounds with photoantibacterial properties, we also synthesized and tested the perylene-3,9(10)-diylbis(triphenylphosphonium) derivatives ($\text{PER}(\text{PPh}_3^+)_2$), which, in contrast to phenalenone, are highly fluorescent but poor $^1\text{O}_2$ photosensitisers.²⁶¹

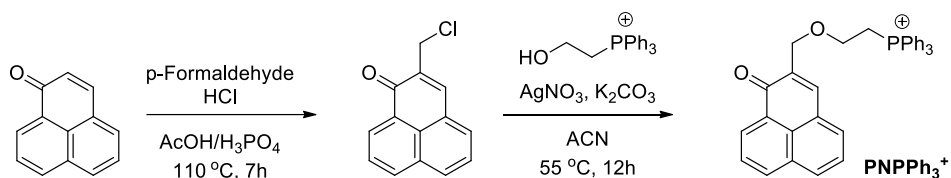
almost 50% have a filing date later than 2013. By searching the term “triphenylphosphonium” AND “mitochondria” AND “targeting” in the Web of Science, 385 research articles have been identified (visited on 06-04-2018)

^k Mitochondria (together with chloroplasts) are unique organelles because they contain their own DNA. It is believed that they were once free-living bacterial organisms that were absorbed by eukaryotic cells at some point in the planet's history. This is known as the endosymbiosis theory (endosymbiosis is a symbiotic relationship between two organisms where one lives inside the other).

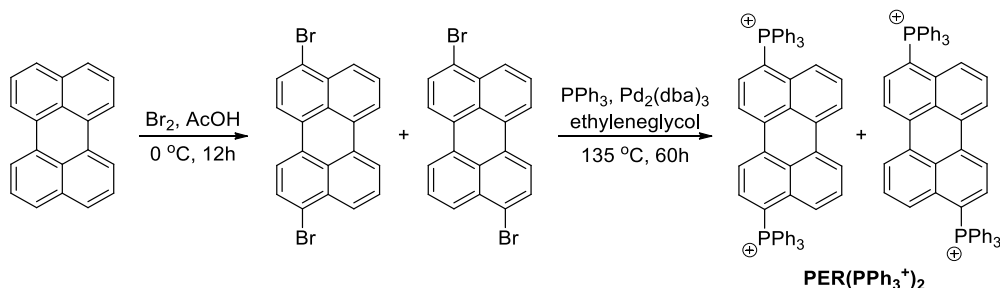
3.2.2. Experimental

3.2.2.1. Synthesis of PNPPH_3^+ and $\text{PER}(\text{PPh}_3^+)_2$

The compounds used in this section have been synthesized in the group of Dr. M. Eugenio Vázquez (Universidade de Santiago de Compostela, Spain). Their synthetic routes are described in Scheme 3.2 and 3.3. For $\text{PER}(\text{PPh}_3^+)_2$ inseparable 9- and 10-substituted mixture was obtained even for bromo and triphenylphosphonium perylene derivatives.



Scheme 3.2 Synthesis of (2-((1-oxo-1H-phenalen-2-yl)methoxy)ethyl)-triphenylphosphonium (PNPPH_3^+).



Scheme 3.3 Synthesis of perylene-3,9-diylbis(triphenylphosphonium) and perylene-3,10-diylbis(triphenylphosphonium) inseparable mixture derivatives ($\text{PER}(\text{PPh}_3^+)_2$).

3.2.2.2. Specific photoinactivation conditions

Three different strains, two Gram-positive, *Staphylococcus aureus* (*S. aureus*; ATCC 29213) and *Enterococcus faecalis* (*E. faecalis*; ATCC 27285) and one Gram-negative, *Escherichia coli* (*E. coli*, ATCC 25922) were used in this study. The cell culture were grown in fresh TSB until reaching an OD₆₀₀ of 0.2 for both *E. faecalis* and *E. coli* and 0.3 for *S. aureus*. The different used PSs were delivered dissolved in DMSO.

The different bacterial strains were irradiated for 218 seconds in the photoreactor which contains LZC420 fluorescent lamps (420 ± 10 nm; for a total fluence of 1.2 J·cm⁻²) or for 720 seconds under LED Par 64 Short V2 lamp blue led (463 ± 11 nm; for a total fluence of 10 J·cm⁻²) or maintained in the dark for the same period.

3.2.2.3. ¹O₂ measurements with bacterial cells

In all the experiences, bacterial cell suspensions in PBS were incubated with 10 μM of PS in the dark at 37 °C during 10 minutes. Then, the bacterial cell suspensions were poured into quartz cuvette and their ¹O₂ phosphorescence kinetic traces were measured at 1275 nm. Afterwards, the samples were centrifuged and both the supernatant and the pellet had their ¹O₂ phosphorescence decay measured again.

3.2.3. Results

In a first step, the photophysical properties of PNPPH_3^+ and $\text{PER}(\text{PPh}_3^+)_2$ have been studied. PNPPH_3^+ displayed absorbance maxima at 363 nm ($\epsilon = 8900 \text{ M}^{-1}\text{cm}^{-1}$) and 400 nm ($\epsilon = 7200 \text{ M}^{-1}\text{cm}^{-1}$; Figure 3.2a), which enabled the use of UV-A, violet or blue light sources for its excitation. In agreement with the properties of phenalenone, PNPPH_3^+ was found weakly fluorescent ($\Phi_F = 0.015$ in PBS) and the emission spectrum shows a maximum at 494 nm. More importantly, PNPPH_3^+ shows a high ability to produce $^1\text{O}_2$ ($\Phi_\Delta = 0.73$ in PBS; Figure 3.2b) and high photostability, losing less than 30% of its absorbance after being exposed to a fluence of 50 J/cm^2 at 420 nm, which is more than 40-fold higher than the intensity used in the antimicrobial studies.

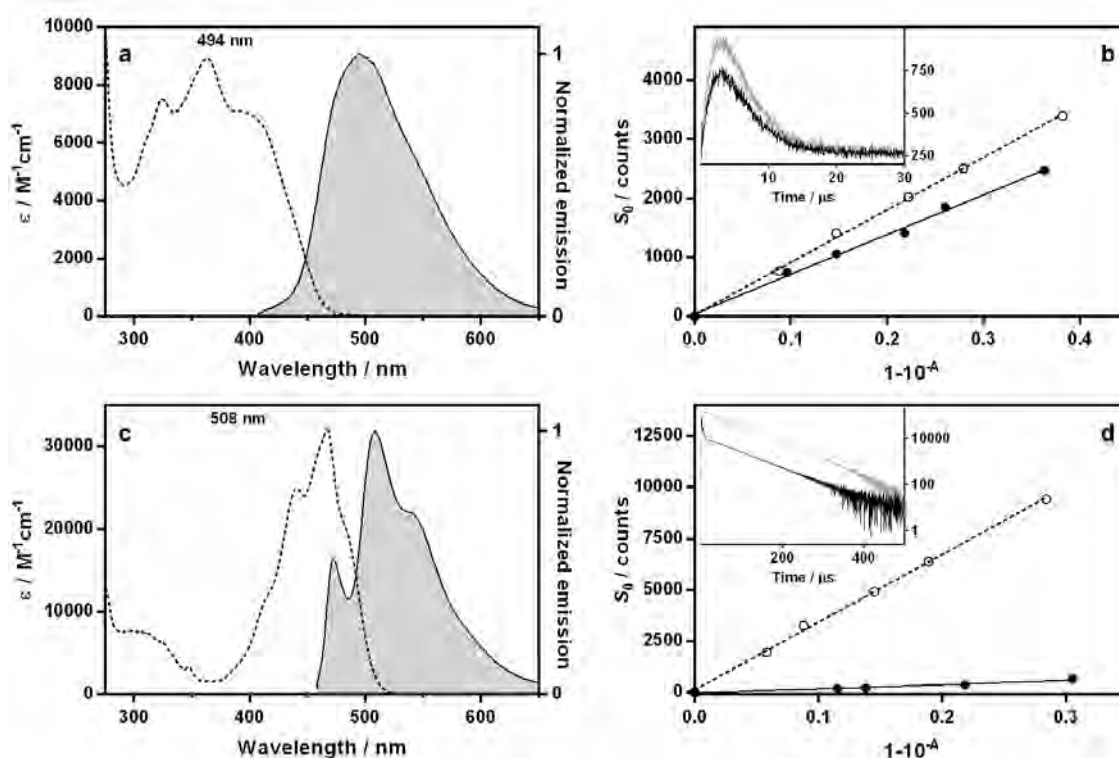


Figure 3.2: Left. Absorption (dashed line) and emission (solid line, filled curve) spectra of PNPPH_3^+ (a) and $\text{PER}(\text{PPh}_3^+)_2$ (c) in PBS. Right. Determination of Φ_Δ . Dependence of the $^1\text{O}_2$ phosphorescence intensity (S_0) on the sample absorption factor ($1-10^{-4}$) for PNPPH_3^+ or $\text{PER}(\text{PPh}_3^+)_2$ (b or d respectively; solid line) and the reference PNS or flavin mononucleotide (dashed line; $\Phi_\Delta = 0.97^{216,262}$ and $0.56^{263,264}$ respectively) in PBS; $\lambda_{\text{exc}} = 355$ and 473 nm respectively. Inset: Kinetic traces for $^1\text{O}_2$ phosphorescence signals for optically matched samples of the PNS (grey) and PNPPH_3^+ (black) (b) or flavin mononucleotide (grey) and $\text{PER}(\text{PPh}_3^+)_2$ (black) (d). Due to the low Φ_Δ of $\text{PER}(\text{PPh}_3^+)_2$, the optically-matched traces for inset d were recorded in d-PBS and plotted in logarithmic scale to obtain a clearer kinetic trace.

On the other side, $\text{PER}(\text{PPh}_3^+)_2$ presents a broad absorbance band between 400-500 nm with an absorbance maximum at 467 nm ($\epsilon = 32000 \text{ M}^{-1}\text{cm}^{-1}$; Figure 3.2C). In agreement with the photophysical properties of perylene, $\text{PER}(\text{PPh}_3^+)_2$ was highly fluorescent ($\Phi_F = 0.98$ in PBS) with an emission maximum at 508 nm whilst poor $^1\text{O}_2$ generation is detected ($\Phi_\Delta = 0.034$ either in PBS or deuterated-PBS; Figure 3.2D).

The aPDT activities of PNPPH_3^+ and $\text{PER}(\text{PPh}_3^+)_2$ were tested towards two different Gram-positive bacteria, *S. aureus* and *E. faecalis* and one Gram-negative species, *E. coli*. Bacterial cell suspensions with PNPPH_3^+ or $\text{PER}(\text{PPh}_3^+)_2$ at concentrations ranging

from 0.5 to 10 μM for *S. aureus* and *E. faecalis* and from 1 to 50 μM for *E. coli* were incubated in the dark at 37 °C for 10 minutes, and irradiated with blue light (420 and 463 nm for PNPPH_3^+ and $\text{PER}(\text{PPh}_3^+)_2$ respectively in order to achieve a better spectral overlap. The neutral PN, the anionic PNS and the neutral unsubstituted perylene were used as controls (Figure 3.3).

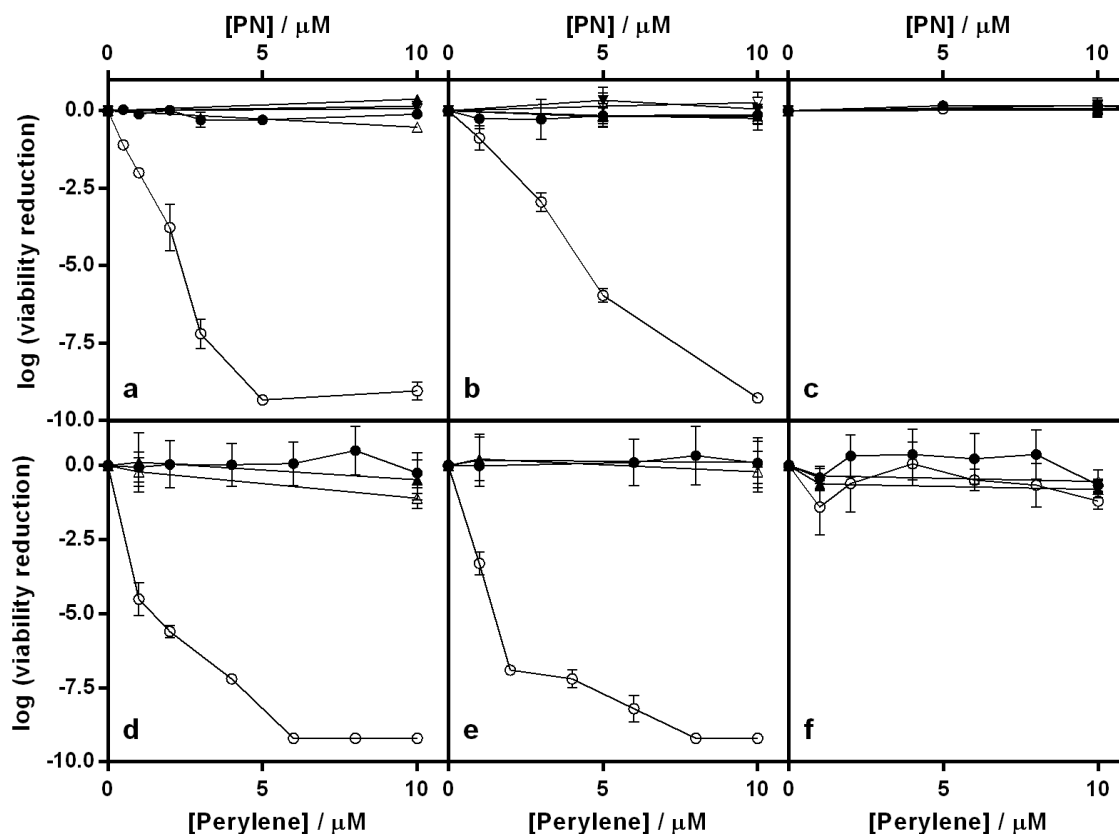


Figure 3.3 Survival curves of *S. aureus* (a/d), *E. faecalis* (b/e) and *E. coli* (c/f). (a-c): incubated with different concentrations of PNPPH_3^+ (circles), PN (up triangle) and PNS (down triangle) in the dark (closed symbols) and irradiated with blue light (420 ± 10 nm; 1.2 Jcm^{-2} ; open symbols). (d-f): incubated with different concentrations of $\text{PER}(\text{PPh}_3^+)_2$ (circles) and perylene (up triangle) in the dark (closed symbols) and irradiated with blue light (463 ± 11 nm; 10 Jcm^{-2} ; open symbols).

PNPPH_3^+ , for both *S. aureus* and *E. faecalis* at the very low light fluence of 1.2 Jcm^{-2} , shows strong photoantimicrobial activity in a concentration-dependent manner. Specifically, for *S. aureus*, a viability reduction of $9\log_{10}$ is achieved at a concentration of $5 \mu\text{M}$, whereas a reduction of at least $\geq 3\log_{10}$ (99.9% reduction), considered biologically relevant in the guidelines of hand hygiene, is reached with a PNPPH_3^+ concentration of $2 \mu\text{M}$. The results for *E. faecalis* are similar, in this case $10 \mu\text{M}$ being required to achieve $9\log_{10}$ cell viability reduction and $3 \mu\text{M}$ to achieve $3\log_{10}$. In addition to these remarkable results, it is worth mentioning that PNPPH_3^+ shows no dark toxicity in any of these bacteria, even at the highest concentration tested. Moreover, neutral PN and anionic PNS, which are endowed with even higher Φ_{Δ} values,²⁶² do not kill even $1\log_{10}$ *S. aureus* or *E. faecalis*, thus confirming the targeting effect of the cationic TPP unit.

Regarding the performance of $\text{PER}(\text{PPh}_3^+)_2$, similar photoantimicrobial activity is observed without dark toxicity, although the light fluence used (10 J/cm^2) is higher due to its much lower Φ_{Δ} (c.a. 20 fold). The $\geq 3\log_{10}$ and $9\log_{10}$ reductions are achieved with concentrations of $<1 \mu\text{M}$ and $6 \mu\text{M}$ for *S. aureus* and $<1 \mu\text{M}$ and $8 \mu\text{M}$ for *E. faecalis*

respectively. Nonetheless, no photoantimicrobial effect is observed for the neutral perylene. Furthermore, both PNPPh_3^+ and $\text{PER}(\text{PPh}_3^+)_2$ are not able to photoinactivate *E. coli* cells up to 50 μM concentration.

Overall, PNPPh_3^+ appears more effective than SAPYR, and shows comparable efficiency to SAGUA. On the other hand, and in contrast with the nitrogen-based cationic derivatives, PNPPh_3^+ was ineffective against *E. coli* at all concentrations tested. It is worth mentioning, that this comparison with SAPYR and SAGUA is by taking the experimental data from references.^{265–267} This small difference observed could be due to slightly differences in the photoinactivation protocols used in the two different laboratories. A similar comparison cannot be made for $\text{PER}(\text{PPh}_3^+)_2$ because, to our best knowledge, no photoantimicrobial assays have been reported using cationic nitrogen-based perylene cationic derivatives.

The ineffectiveness against *E. coli* suggests that triphenylphosphonium-modified PSs cannot pass through the lipopolysaccharide barrier, which is consistent with the reported behaviour of TPP in *E. coli* by Hirota *et al.*,²⁶⁸ and of phenothiazine derivatives incorporating a TPP moiety reported by Dunn *et al.*²⁵⁹ Therefore, the external lipopolysaccharide receives the majority of $^1\text{O}_2$ produced, and no killing effect is achieved in this case. The neutral PN and perylene, as well as the anionic PNS did not cause any measurable cell death either because $^1\text{O}_2$ is generated in bulk medium for these cases.

In order to rationalise the above observations, $^1\text{O}_2$ production by PNPPh_3^+ was studied for the three tested microorganisms under the same conditions as those used for the photoinactivation assays. For the three-bacterial species tested, the $^1\text{O}_2$ phosphorescence signals showed the same kinetics of formation and decay (Figure 3.4 and Table 3.1). This experiment has not been realized for $\text{PER}(\text{PPh}_3^+)_2$ due to its poor $^1\text{O}_2$ generation.

Table 3.1 Kinetic analysis of figure 3.4 $^1\text{O}_2$ phosphorescence traces: τ_{Δ} and τ_{τ} values.

	PNS				PNPPh_3^+			
	Not centrifugated		Supernatant		Not centrifugated		Supernatant	
	$\tau_{\Delta} / \mu\text{s}$	$\tau_{\tau} / \mu\text{s}$	$\tau_{\Delta} / \mu\text{s}$	$\tau_{\tau} / \mu\text{s}$	$\tau_{\Delta} / \mu\text{s}$	$\tau_{\tau} / \mu\text{s}$	$\tau_{\Delta} / \mu\text{s}$	$\tau_{\tau} / \mu\text{s}$
PBS	3.5	2.2	----	----	3.4	2.3	----	----
<i>S. aureus</i>	4.1	1.9	4.0	2.1	3.5	2.5	3.7	2.2
<i>E. faecalis</i>	3.9	2.2	3.9	2.3	3.9	2.0	3.7	2.0
<i>E. coli</i>	3.6	2.5	3.8	2.3	3.7	2.2	4.0	2.0

This indicates that the microenvironment of the photosensitiser where $^1\text{O}_2$ is generated is similar for the three strains, which is surprising given the different structure of their cell walls. The kinetic rate constants were indistinguishable from those in a bacteria-free PBS solution, suggesting that PNPPh_3^+ is in the external part of the cell wall in all cases. When the cells were separated by centrifugation, $^1\text{O}_2$ was observed in the supernatant but not in the re-suspended pellet, also suggesting that the interaction between PNPPh_3^+ and the bacterial cell wall is very weak in all cases.

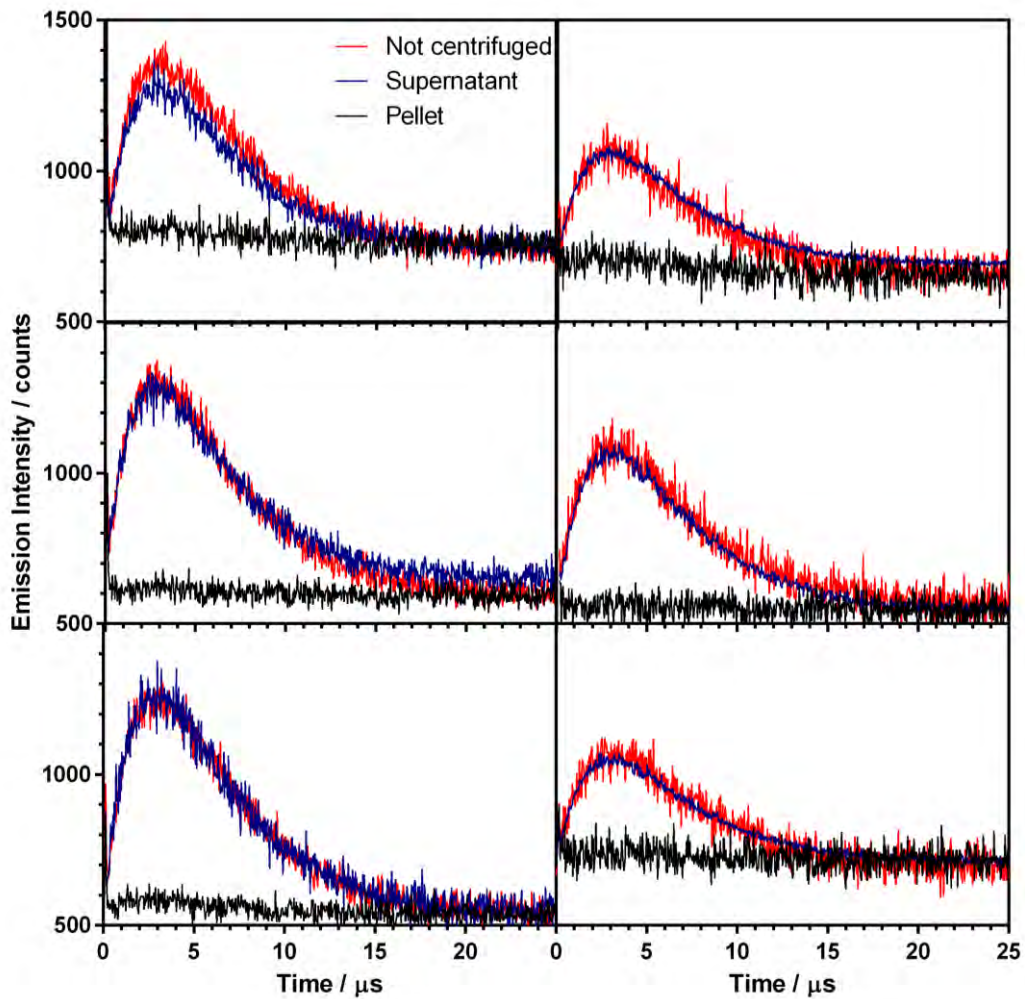


Figure 3.4 $^1\text{O}_2$ phosphorescence kinetics decay for PNPPH_3^+ (left) and reference PNS (right) in *S. aureus* (top), *E. faecalis* (middle), *E. coli* (down). Red line is the kinetics trace after the 10 minutes of co-incubation. Blue and black lines are the kinetics traces after bacterial centrifugation for the supernatant and the pellet resuspended respectively.

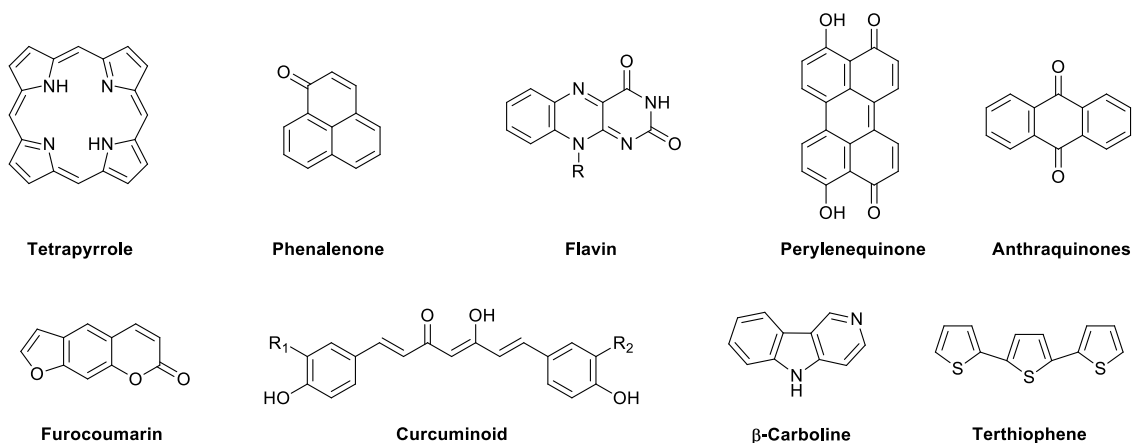
3.3. Revaluating naturally-occurring PSs

3.3.1. Why natural products?

(Adapted from: B. Rodríguez-Amigo, O. Planas, **R. Bresolí-Obach**, J. Torra, R. Ruiz-González and S. Nonell; Chapter 2: Photosensitisers for Photodynamic Therapy: State of the Art and Perspectives; in Photodynamic Medicine: From Bench to Clinic, RSC Publishing, 2017.)

Nature has been a source of medicinal products for millennia, with many useful drugs developed from plant sources. Plants, in particular, have formed the basis of sophisticated traditional medicine systems, with the earliest records, dating from around 2600 BCE, documenting the uses of approximately 1000 plant-derived substances in Mesopotamia.^{269,270} These include oils of *Cedrus* species (cedar) and *Cupressus sempervirens* (cypress), *Glycyrrhiza glabra* (liquorice), *Commiphora* species (myrrh), and *Papaver somniferum* (poppy juice), all of which are still used today for the treatment of ailments ranging from coughs and colds to parasitic infections and inflammation. Following discovery of the penicillin's, drug discovery from microbial sources occurred and diving techniques in the 1970s opened the seas.²⁷¹ So, natural product structures play a significant role in drug discovery.²⁷²

Returning into the PDT field, several naturally-occurring dyes are endowed with photodynamic activity and are therefore being currently investigated as photo-antimicrobial and/or photo-anticancer purposes.^{273,274} Scheme 3.4 shows the more-common chemical structures of naturally-occurring dyes that are being used as PS.



Scheme 3.4 The most common naturally-occurring dyes considered for PDT.

Several naturally-occurring tetrapyrroles macrocycles with possible photodynamic activity have been isolated.²⁷³ For example silkworm excreta, a well-known ancient Chinese medicine, contains chlorophyll degradation products with known phototoxic properties such as 10-hydroxypheophytin *a*.²⁷⁵ The most-used naturally-occurring tetrapyrroles are protoporphyrin IX, pheophorbide *a* and pyropheophorbide *a*. Several *in-vitro* and *in-vivo* studies have demonstrated that protoporphyrin IX and both pheophorbides have photodynamic activity against cancer cells.²⁷⁶ In addition, the semisynthetic derivative pyropheophorbide *a* methyl ester has proved useful, e.g., against lung-cancer.²⁷⁷

Phenalenone derivatives are one of the main focus of this thesis and their photosensitizing properties are described in section 3.3.2.

Flavin derivatives are present in almost every type of cells, mainly as riboflavin, FMN and FAD. They are common cofactors in enzymes and plant and bacteria photoreceptors.^{278,279} The flavin core is water-soluble and it is known to generate both $^1\text{O}_2$ and $\text{O}_2^{\bullet-}$.²⁸⁰ Endogenous flavins are devoid of any significant phototoxicity owing to their binding to proteins that provide efficient deactivation pathways for their excited states.²⁸¹ Exogenous riboflavin can induce oxidative stress upon UV-A or visible exposure²⁸² and can photooxidise several different natural antioxidants²⁸³ and drugs,²⁸⁴ which can affect their biological activity.

Recently, some authors have mutated some flavin-binding proteins to act as endogenous PS.²⁸⁵ Their photosensitising properties remained unexplored until the development of miniSOG²⁸⁶ (Figure 3.5), the first genetically-encoded flavoprotein engineered for the endogenous production of $^1\text{O}_2$, although it can also produce other ROS species (i.e. $\text{O}_2^{\bullet-}$).^{287,288} Since the development of miniSOG, novel protein variants with improved properties have been developed for many applications such as *in vivo* advanced imaging techniques, electron microscopy, optogenetics, or PDT.^{289–291} The endogenous production of $^1\text{O}_2$ has been demonstrated to induce fatal damage in both bacterial and mammalian cells,^{292,293} inactivation of target proteins²⁹⁴ and damaging genomic DNA²⁹² upon blue light illumination. For these reasons, there is a growing interest on the development of new FbFPs that photosensitise $^1\text{O}_2$ more efficiently, and some successful examples have already been reported.^{295,296}

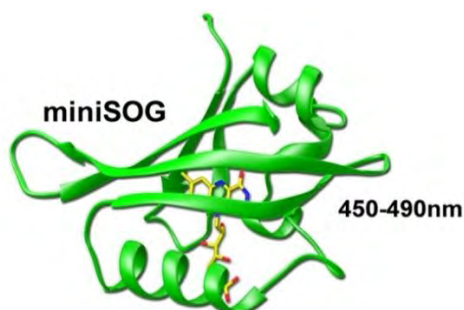


Figure 3.5 The flavin-binding protein: miniSOG structure.

Perylenequinones are aromatic diketones with extended conjugation.²⁷³ Hypericin is a red-coloured photoactive pigment that is isolated from the plant *Hypericum perforatum* (Saint John's wort or pericó, which is widely distributed in Països Catalans).²⁹⁷ *Hypericum* extracts have been used recurrently by ancient Chinese medicine²⁷³ and their phototoxicity was discovered after noticing the relationship between cattle skin photosensitivity and ingestion of *Hypericum* plants.²⁹⁸ Since then, hypericin has been identified as a photodynamic agent and explored as a therapeutic agent for several cancer types, as well as an antiviral and an antibacterial agent.²⁹⁹ One of the main drawbacks of these PSs is their poor water solubility, which leads to the formation of aggregates devoid of any photosensitising activity. In order to overcome this shortcoming, PS is delivered in suitable nanocarriers such as liposomes, nanoparticles or proteins.^{300–302}

The previous exposed dyes are the most common and studied. However, only in plants more than 100 natural phototoxins have been identified so far, belonging to more than 35 different plant families.^{273,303}

3.3.2. Darwin mystery; Naturally-occurring phenalenones

(Adapted from: **R. Bresolí-Obach**; Fotociclació de 9-fenil-fenalenones: Caracterització de productes i mecanisme de reacció; Master Thesis supervised by Dr. Santi Nonell, 2014)

In Charles Darwin's treatise "On the Origin of the Species" the observation of photodynamic toxicity originating from plants was described based on the ingestion of *Lachnanthes tinctoria* by pigs (Figure 3.6).³⁰⁴

"I shall have to show that constitutional peculiarities of the strangest kind, entailing liability to the action of certain poisons, are correlated with the colour of the skin. I will here give a single case, on the high authority of Professor Wyman; he informs me that, being surprised at all the pigs in a part of Virginia being black, he made inquiries, and ascertained that these animals feed on the roots of the Lachnanthes tinctoria, which colours their bones pink, and, excepting in the case of the black varieties, causes the hoofs to drop off."

On the Origin of the Species - Charles Darwin

The phototoxicity of phenalenone derivatives is described in Charles Darwin's treatise "On the origin of the species", where he reported the observation by farmers of the deleterious effects of the plant *Lachnanthes tinctoria* on white, but not black, pigs.³⁰⁴ Almost a century later, lachnanthocarpone and other phenalenone derivatives were isolated from that plant and identified as the main phototoxic compounds.³⁰⁵

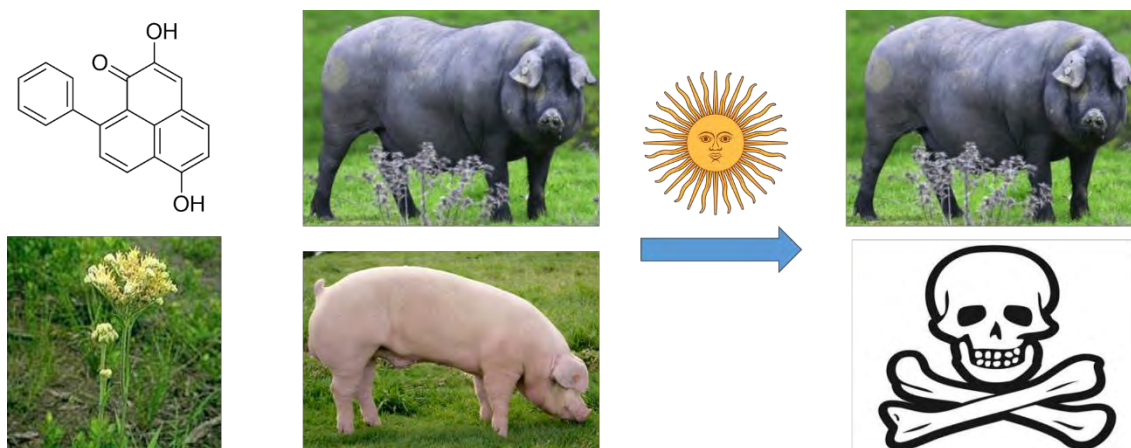
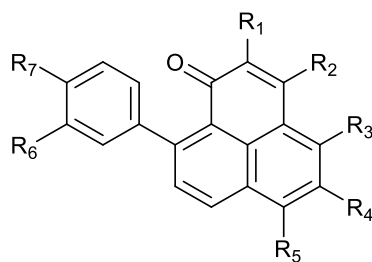


Figure 3.6 Ingestion of *Lachnanthes tinctoria* (plant left) by white and black pigs. Upon sun exposure white pigs suffer from phototoxicity of the plant, whilst black pigs not. Lachnanthocarpone (chemical structure, top right) is the major substance which has been isolated from *Lachnanthes tinctoria*.

Unsubstituted phenalenone produces $^1\text{O}_2$ with quantum yield $\Phi_{\Delta} \approx 1$ in both polar and non-polar solvents.^{262,306,307} Since then, several phenalenone derivatives, mainly 4- and 9-phenyl substituted derivatives, have been isolated from plants and fungi.^{274,308,309} More than 30 9-phenyl-phenalenones derivatives have been isolated from plants (*Musaceae*, *Haemodaracea*, *Pontederiaceae* and *Strelitziaceae*; Table 3.2).

Table 3.2 Naturally-occurring 9-phenylphenalenones. D = Dimer bond; Glu = O-Glucoside.



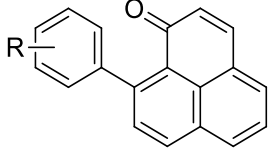
	R ₁	R ₂	R ₃	R ₄	R ₅	R ₆	R ₇	Ref.	Name
1	OH	H	H	H	H	H	H	310	Anigorufone
2	OMe	H	H	H	H	H	H	311	Methoxyanigorufone
3	OH	H	H	H	H	H	OH	310	Hydroxyanigorufone
4	OH	H	H	H	H	H	OMe	312	4'-O-methylanigorufone
5	OMe	H	H	H	H	H	OH	313	
6	OMe	H	H	H	H	H	OMe	313	
7	OH	H	H	H	H	OH	OH	314	Dihydroxyanigorufone
8	OH	H	H	H	H	OMe	OH	315	Musanolone F
9	OMe	H	H	H	H	OMe	OMe	313	
10	OH	OH	H	H	H	H	OH	315	Musanolone E
11	OH	H	OH	H	H	H	H	316	
12	OH	H	OH	H	H	H	OH	317,318	Thyrsiflorin
13	OH	H	OH	H	H	OH	OH	318	
14	OMe	H	OH	H	H	H	H	312	
15	OMe	H	Glu	H	H	H	H	318	
16	OMe	H	R ₁₀	H	H	H	H	318	
17	OH	H	OH	OMe	H	H	H	314	
18	OH	H	OMe	H	OMe	H	H	319	Haemodoronol
19	OH	H	H	OH	OH	H	H	320	Lachnanthoside aglycone
20	OMe	H	H	OH	OH	H	H	320	
21	OH	H	H	OMe	OH	H	H	318	Haemocorin aglycone
22	OH	H	H	OH	OMe	H	H	314	Anigozanthin
23	OH	H	H	OH	O-GluGlu	H	H	321	Lachnanthoside
24	OMe	H	H	OMe	OH	H	H	322	Xiphidone tautomer
25	OMe	H	H	OH	OMe	H	H	319,323	Haemoxiphidone
26	OMe	H	H	OMe	OMe	H	H	319,324	
27	O-GluGlu	H	H	OMe	OH	H	H	325	Haemocorin
28	O-Celobiose	H	H	OMe	OH	H	H	321	
29	OMe	H	H	OMe	H	H	H	319	
30	OH	H	H	H	OH	H	H	320	Lachnanthocarpone
31	OMe	H	H	H	OMe	H	H	319,326	Lachnanthocarpone dimethyl ether
D1	OH	H	H	D	D	H	H	327	Lachnanthospirone
D2	OH	D	H	H	H	H	H	328	3,3'-bis-anigorufone dimer
D3	OH	D	H	H	H	H	OH	310,328	3,3'-bis-hydroxyanigorufone dimer

Lachnanthocarpone is classified as a plant phototoxin. These phototoxins play a key role in plant self-defence against bacterial as well as fungal infections²⁷⁴ and can be classified as phytoanticipins and phytoalexins.³²⁹ Phytoanticipins are already present in the plant and are released upon mechanical exposure. On the other hand, phytoalexins are secondary metabolites which can be accumulated upon microbial/fungal attack. It was found that the phenalenones' antifungal activity, e.g., against *Fusarium oxysporum*, could be enhanced by light.^{274,330,331}

Then the next question, why nature uses 9-phenylphenalenones instead of the unsubstituted PN skeleton? The answer could be that the presence of phenyl group in position 9 decreases the Φ_{Δ} relative to that of unsubstituted phenalenone (Table 3.3).³³⁰ The lower Φ_{Δ} facilitates the controlled $^1\text{O}_2$ generation to avoid self-sensitization damage. Intramolecular deactivation of triplet carbonyls by phenyl moieties has been well documented in non-rigid systems and is called β -phenyl quenching (BPQ, see section 3.3.3.)

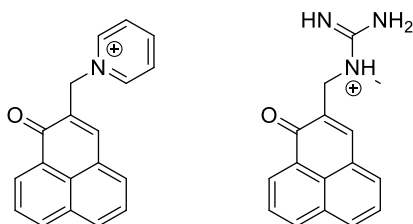
Table 3.3 τ and Φ_{Δ} for different 9-phenylphenalenones in acetonitrile.

Compound	τ / ns	Φ_{Δ}	Refs
4-OMe (PN2)	80	0.01	309,330,332
H (PN1)	160	0.08	309,330,332
2,2'-Me (PN3)	800	0.14	309,333,334
2-NO ₂ (PN-NO ₂)	17000	0.51	332-334
Phenalenone core (PN)	38000	1	262,306,307



Recently, other synthetic phenalenones derivatives have also attracted the interest for aPDT by attaching nitrogen-based cationic moieties to them. Cieplik *et al.*,²⁶⁷ were the first to synthesize cationic phenalenones and prove their effect against Gram-positive and Gram-negative bacteria. These phenalenones are water soluble, whilst keep high Φ_{Δ} . Afterwards, Maisch *et al.*,²⁶⁶ have also reported a cationic derivative of phenalenone (2-(4-pyridinyl)methyl)-1H-phenalene-1-one (SAPYR; Scheme 3.5) and other cationic derivatives for use in dentistry owing to their almost neutral colour and photodynamic activity against key buccal pathogens such as *Actinomyces naeslundii*, *Streptococcus mutans*, *Enterococcus faecalis* and *Aggregatibacter actinomycetemcomitans*.

The photo-antimicrobial activity against oral key pathogens was due to the positively charged moiety, the pyridinium cation substituent. More recently, Maisch *et al.*²⁶⁵ have reported a better phenalenone with a guanidinium group (1-((1-oxo-1H-Phenalen-2-yl)methyl)-1-methyl-guanidinium chloride, also named SAGUA (Scheme 3.5). It was tested against *Actinomyces naeslundii*, *Streptococcus mutans*, *Enterococcus faecalis*, *Staphylococcus aureus* and *Escherichia coli*.



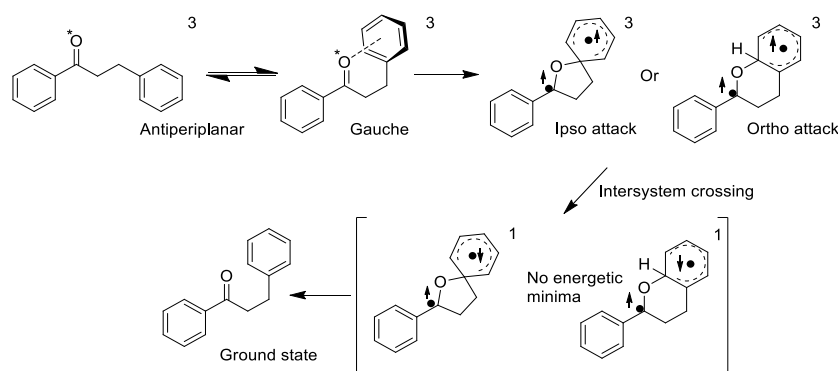
Scheme 3.5 Chemical structures for SAPYR (left) and SAGUA (right).

3.3.3. β -Phenyl quenching photochemical reaction (BPQ)

(Adapted from: **R. Bresolí-Obach**, and S. Nonell, Una visión moderna sobre la desactivación de cetonas aromáticas por beta-fenilos, *Afinidad*. **2016**, 574, 90)¹

In 1970, three independent manuscripts reported that the triplet lifetime of different propiophenones was shorter when there was a phenyl moiety in the β -position of the aromatic carbonyl.^{335–337} From these experimental facts, they claimed that: the n,π^* triplet excited states of aryl ketones bearing a phenyl ring in the β -position, (i.e. β -phenylpropiophenone), are quenched very efficiently by an intramolecular reaction called β -phenyl quenching (BPQ).^{336,338}

Afterwards, Scaiano *et al* observed that β -phenylpropiophenones were much more photostable than other aromatic ketones.³³⁹ They proposed that should exist some type of interaction between $^3(n,\pi^*)$ orbital from aromatic ketone and the phenyl moiety, followed by the formation of an intermediate which reverts to the original ketone with a very short lifetime ($\tau < 20$ ps).³⁴⁰ Generally, electron-withdrawing substituents in the β -phenyl ring significantly slow down the reaction, whereas π -electron donors such as a methoxy group in the para position of the β -phenyl ring increase the rate of BPQ.³⁴¹



Scheme 3.6 Proposed addition-ISC-relaxation mechanism for BPQ in 3-phenylpropiophenone scaffold.³⁴²

In 2008, Bucher proposed a possible mechanism for BPQ combining computational calculations with the previous exposed experimental data (Scheme 3.6).³⁴² He proposed that BPQ occurs by addition of the carbonyl to the ipso (preferred) or ortho (less favourable) carbon atoms of the β -phenyl ring, yielding intermediary triplet biradicals. This π addition requires that the ketone and phenyl substituents should be in a gauche arrangement ($\theta \approx 60^\circ$), while the thermodynamically favourable antiperiplanar arrangement ($\theta \approx 180^\circ$) does not allow for such an interaction.

After the addition, the aromaticity of the system is lost, due to the formation of a sp^3 carbon. Moreover, this addition has a certain charge transfer character from the carbonyl to the aromatic system. The triplet and singlet energies are nearly degenerated for these biradicals, thus allows an efficient intersystem crossing to the singlet manifold. On the singlet hypersurface, both biradicals are not minima at the levels of theory used in that study. This fastens the return to the ground-state original ketones once the singlet manifold is reached.

¹ I want to acknowledge AIQS for the P. Salvador Gil 2014 Award in chemistry category and for allowing me publishing a review in the journal *Afinidad*.

3.3.4. β -Phenyl quenching of 9-phenylphenalenones: a novel photocyclisation reaction with biological implications

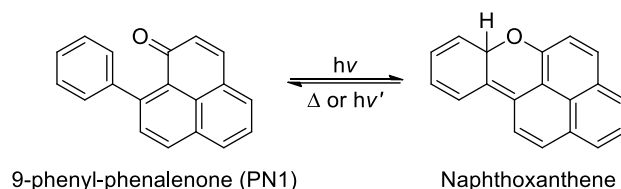
(Adapted from: G. Bucher, **R. Bresoli-Obach**, C. Brosa, C. Flors, J.G. Luis, T.A. Grillo and S. Nonell, β -Phenyl quenching of 9-phenylphenalenones: a novel photocyclisation reaction with biological implications, *Phys. Chem. Chem. Phys.*, **2014**, *16*, 18813)

This work described in this section was carried out in collaboration with the University of Glasgow (United Kingdom), IMDEA Nanociencia (Madrid, Spain), the Universidad de La Laguna (Tenerife, Spain) and the Secció d'Esteroides (Institut Químic de Sarrià, Spain).

3.3.4.1. Introduction

The BPQ reaction has been studied mainly in β -phenylpropiophenones scaffolds (see section 3.3.3.).^{336,339–347} However, in 2006, C. Flors *et al* published evidences of an intramolecular charge-transfer process in the excited states of 9-phenylphenalenones. This process offers a new-competitive pathway in counterposition to $^1\text{O}_2$ production.³³² The described intramolecular charge-transfer complex, in the view of BPQ reaction could be an electronic rearrangement of the biradical intermediate.

Moreover, a recent work proposed that the described intramolecular charge-transfer complex is 1H-2-6aH-naphtho[2,1,8-mna]xanthene (hereafter naphtoxanthene),³⁴⁸ which could be formed in a formal 6- π electrocyclic intramolecular photocyclization of PN1 through BPQ mechanism (Scheme 3.7). The generated naphtoxanthene reverts thermally to PN1 within few microseconds. Contrary to β -phenylpropiophenone, the naphtoxanthene ground state is a minimum in the hypersurface, so its chemical/physical characteristics can be fully studied.



Scheme 3.7 Proposed BPQ reaction for 9-phenylphenalenone (PN1).

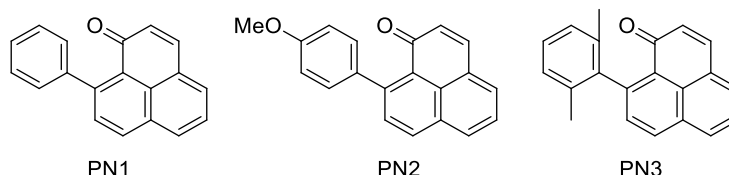
So, from a fundamental point of view, the rigidity of 9-phenyl-phenalenones provides a unique framework for extending the current knowledge on BPQ of aromatic ketones³³⁴ and expands the scope of its applications outside its uses for PDT.^{274,330}

With all the previous considerations in mind, we studied the singlet and triple excited states of 9-phenylphenalenones in order to unveil the role of BPQ in the photochemistry of PN1. Moreover, we studied spectroscopically and chemically-trapped the naphtoxanthene generated in order to prove the presence of this intermediate.

3.3.4.2. Experimental part

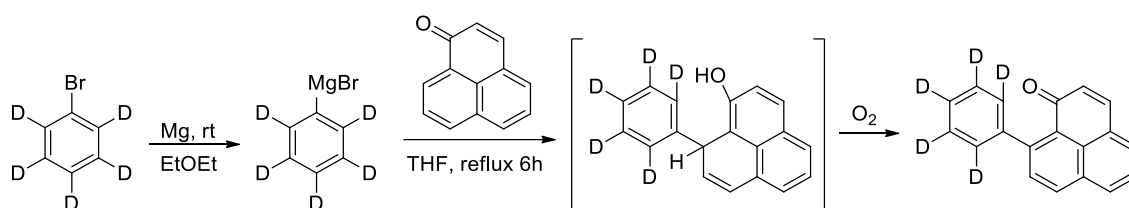
3.3.4.2.1. Synthesis of 9-phenylphenalenones

9-Phenyl-phenalenone (PN1), 9-(4-methoxyphenyl)-phenalenone (PN2) and 9-(2,2'-dimethylphenyl)-phenalenone (PN3) were synthesized as described elsewhere (see Scheme 3.8 for their chemical structures).^{349,350}



Scheme 3.8 Chemical structures for PN1, PN2 and PN3.

9-Perdeuterophenyl-phenalenone (PN1D) was synthesized as described below (Scheme 3.9).



Scheme 3.9 Synthesis of 9-perdeuterophenyl-phenalenone.

A solution of perdeutero-bromobenzene (354 mg, 2.19 mmol, 0.7M) in diethyl ether (3 mL) was added dropwise to a suspension of magnesium turnings (78 mg, 3.2 mmol) in diethyl ether (2 mL). The reaction mixture was stirred and heated at reflux for 20 min and then cooled to room temperature. The Grignard's reagent was added to a stirred solution of PN (284 mg, 1.58 mmol) in THF (12 mL). The reaction mixture was stirred and heated at reflux for 6 h. The reaction mixture was cooled to room temperature, and then quenched with an aqueous saturated solution of NH₄Cl (10 mL) and extracted with EtOAc (3 x 15 mL). The combined organic extracts were washed with H₂O, brine (15 mL) and dried (Na₂SO₄). Removal of solvent under vacuo followed by silica gel column flash chromatography (Ethyl acetate:hexane, 1:3) afforded 9-perdeuterophenyl-phenalenone (96 mg, 24%) as a yellow solid.

¹H-NMR: δ 8.17 (1H, d, J = 8.0 Hz, H-7), 8.04 (1H, dd, J = 1.0, 8.0 Hz, H-6), 7.78 (1H, dd, J = 1.0, 7.0 Hz, H-4), 7.69 (1H, d, J = 9.5 Hz, H-3), 7.62 (1H, dd, J = 7.0, 8.0 Hz, H-5), 7.60 (1H, d, J = 8.0 Hz, H-8), 6.59 (1H, d, J = 9.5 Hz, H-2).

¹³C-NMR: δ 185.93 (C-1), 147.78 (C-9), 140.54 (C-3), 133.87 (C-7), 131.90 (C-9a), 131.88 (C-6), 131.77 (C-8), 131.55 (C-4), 130.68 (C-2), 128.67 (C-3a), 128.53 (C-9b), 126.52 (C-6a), 126.20 (C-5).

GC-MS (EI, 70 eV): M/Z (%; fragment) 261 (24; M⁺), 260 (27; M⁺-H), 259 (100; M⁺-D), 230 (11; M⁺-H-COH).

3.3.4.3. Photochemical intermediate (naphthoxanthene) characterization

Evidence for the proposed BPQ pathways was derived from spectroscopic measurements. Photolysis of PN1 ($\lambda_{\text{exc}} = 395 \text{ nm}$; matrix-isolated in Ar at $T = 10 \text{ K}$) led to the formation of a red matrix with new UV-Vis absorption bands at $\lambda_{\text{max}} = 501$ and 290 nm (Figure 3.7). The obtained spectrum is similar to that observed at room temperature by transient absorption, $\lambda_{\text{max}} = 520 \text{ nm}$, and is consistent with the calculated UV-Vis spectrum of naphthoxanthene (B3LYP/6-31G(d)), which shows maxima at 345 and 565 nm (Figure 3.7, inset). Under all photolytic conditions tested, conversion to naphthoxanthene was partial only, indicating the presence of a photostationary equilibrium between PN1 and naphthoxanthene for that irradiation wavelength. Subsequent photolysis ($\lambda_{\text{exc}} 530 \text{ nm}$) resulted in the complete disappearance of the new bands, and to the reversion of the matrix colour to yellow.

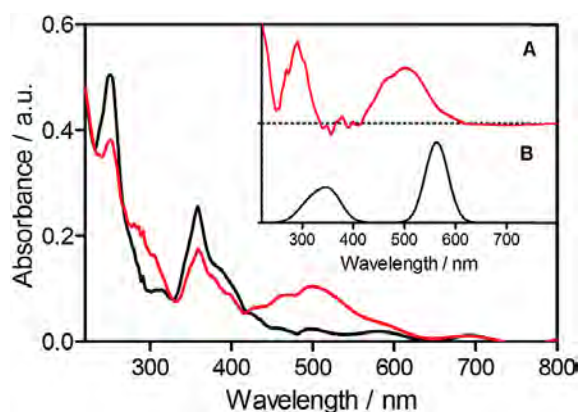


Figure 3.7 UV-Vis absorption spectrum of PN1, matrix-isolated in Ar at $T = 10 \text{ K}$, before and after photolysis (black and red lines respectively; $\lambda_{\text{exc}} 395 \text{ nm}$, 20 min). Inset: (A) difference absorption spectrum. (B) calculated spectrum of naphthoxanthene.

Additional confirmation of the nature of the BPQ process was obtained from the study of oxygen and substitution effects on its kinetics. Figure 3.8 shows the transient absorbance signals obtained upon excitation of PN1, PN2 and PN3 in argon- and air-saturated acetonitrile, which are assigned to the formation and decay of their corresponding naphthoxanthenes.

PN2 forms and decays faster than the unsubstituted PN1, ($\tau_{\text{rise}} 80 \text{ ns}$ vs. 160 ns ; $\tau_{\text{decay}} 1.8 \mu\text{s}$ vs. $8 \mu\text{s}$, respectively), consistent with the trends in the production of $^1\text{O}_2$ (see table 3.3), a process competing with BPQ, for two different series of 9-phenyl phenalenone derivatives. Specifically, we found that Φ_{Δ} increases when the electron donating ability of the phenyl substituent decreases.

On the other hand, PN3 forms and decays more slowly ($\tau_{\text{rise}} = 800 \text{ ns}$; $\tau_{\text{decay}} = 12 \mu\text{s}$), a clear indication that the steric constraints imposed by the methyl groups control the reaction in this case. Moreover, the strong but incomplete inhibition of the transient signal by oxygen in air-saturated solutions is a clear indication that both the singlet and triplet states can undergo BPQ in all three compounds. This is consistent with previous ultrafast transient absorption data, which showed that for PN1 the naphthoxanthene is also formed from the singlet state in 13 ps in acetonitrile.³³²

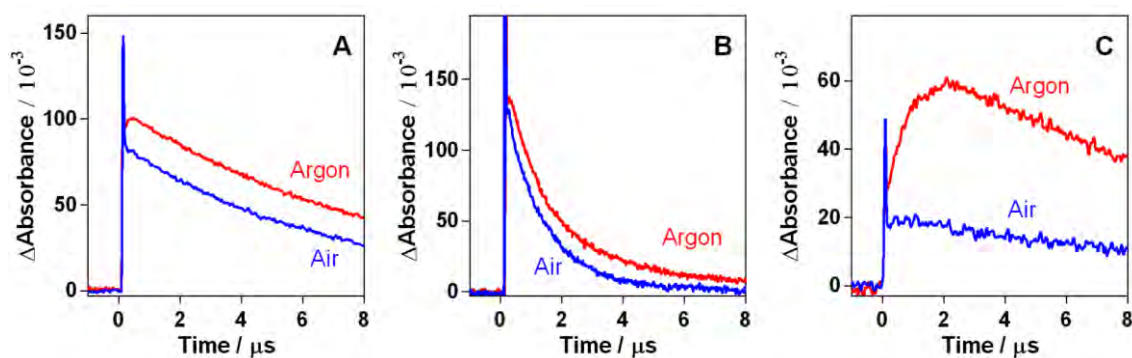


Figure 3.8 Transient absorption of PN1 (A), PN2 (B) and PN3 (C) in acetonitrile. λ_{exc} 355 nm; λ_{obs} 520 nm.

Considering that PN1 is a good scaffold for BPQ, we decided to study the effect of the solvent proticity and polarity in BPQ reaction. For that purpose, the formation and deactivation of naphthoxanthene in thirteen different solvents with different polarity and proticity were studied. An increase of the PN1 triplet lifetime (from 90 to 250 ns) and a reduction of naphthoxanthene lifetime (from 20 to 2.5 μ s) were observed when the solvent polarity was increased (Figure 3.9). Furthermore, no significant effect of the solvent proticity could be observed in the triplet lifetime whilst only a slight increase in the naphthoxanthene lifetime could be noticed. These experimental data are in agreement with those reported for β -phenylpropiophenones.^{343,351}

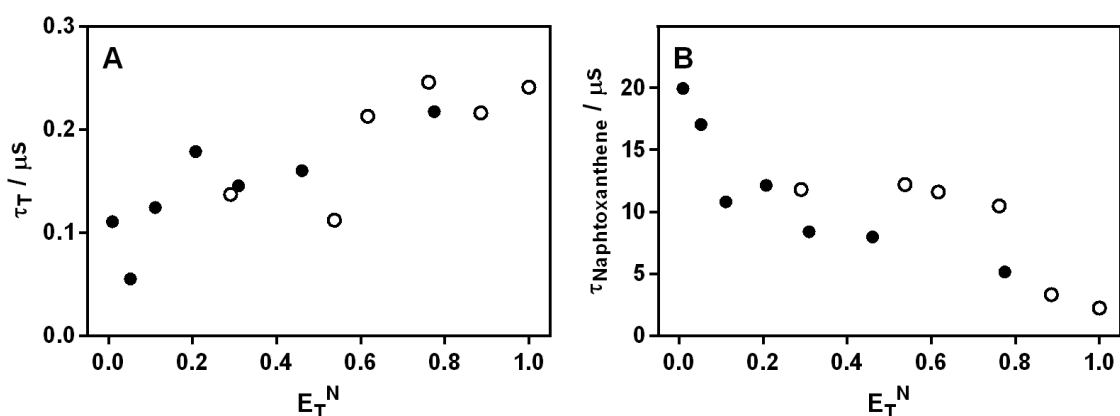


Figure 3.9 Triplet PN1 (A) and naphthoxanthene (B) lifetime vs Normalized Reichardt's solvent polarity parameter (E_T^N) for different solvents. Closed circles for aprotic solvents (A). Open circles for protic solvents (P). Solvents tested (increasing polarity ordered according to E_T^N):^{352,353} hexane (A), 1-octene (A), benzene (A), tetrahydrofuran (A), 2,4-dimethyl-3-pentanol (P), dichloromethane (A), acetonitrile (A), 1-octanol (P), 1-propanol (P), methanol (P), formamide (A), 2,2,3,3-tetrafluoro-1-propanol (P) and water (P).

Finally, the effect of viscosity on the BPQ reaction was also studied. For that purpose, the formation and deactivation of naphthoxanthene in different methanol:glycerol mixtures was studied (Figure 3.10). The results indicate an increase of the PN1 triplet lifetime with the viscosity, which seems logical because the rotation of C_9 -Ph bond should be hampered by viscosity. Likewise, the naphthoxanthene lifetime is also reduced when the viscosity is increased.

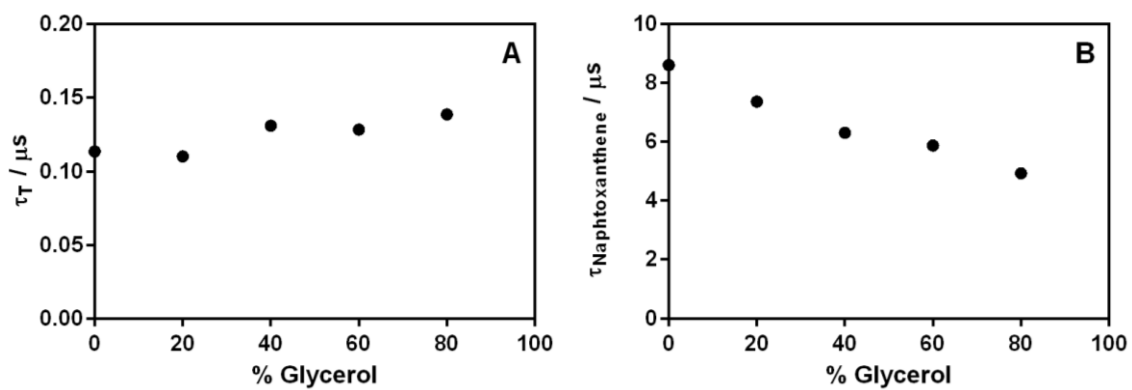
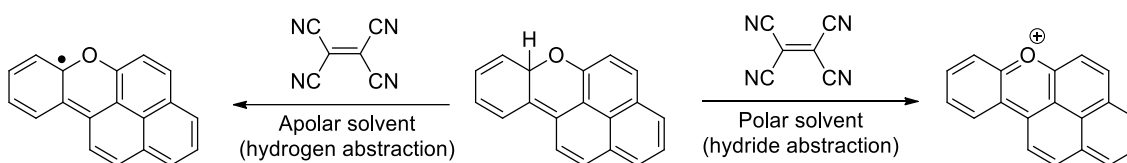


Figure 3.10 Triplet (A) and naphthoxanthene (B) lifetime vs % of glycerol in methanol:glycerol mixtures.

3.3.4.4. Naphthoxanthene trapping experiments

Computational calculations predicted that the C(sp³)-H bond in naphthoxanthene should be exceedingly weak, with a bond dissociation energy of only 28.8 kcal/mol. So it should be possible to trap it with a suitable hydrogen and/or hydride abstractor such as tetracyanoethylene (TCNE)^m (Scheme 3.10).^{354,355}



Scheme 3.10 Reaction pathways upon reaction of naphthoxanthene with TCNE in function of the solvent polarity.

In the light of the computational calculations, the products formed in the photolysis of PN1 in the presence of TCNE were investigated by UV-Vis and ¹H-NMR spectroscopies, employing benzene and acetonitrile (as apolar and polar solvents, respectively).

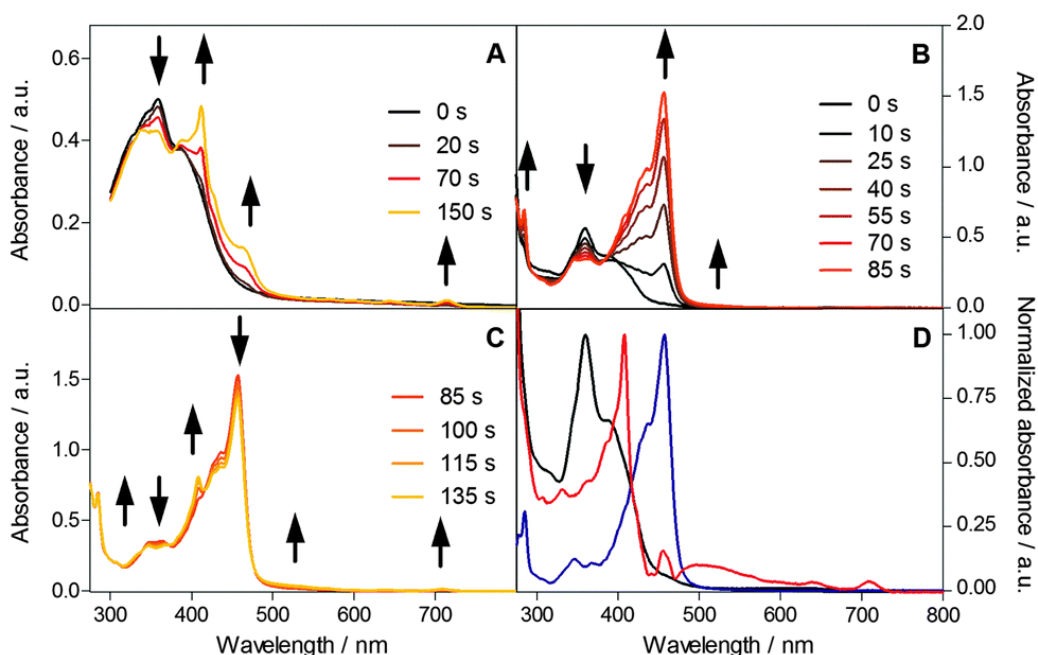


Figure 3.11 UV-Vis spectral changes upon laser photolysis of PN1 (A_{355} of 0.5) in the presence of 150 μ M TCNE in argon-saturated solutions. (A) In benzene. (B) In acetonitrile at early photolysis stages. (C) In acetonitrile at later photolysis stages. (D) Deconvoluted spectra.

Upon 355 nm laser excitation of an argon-saturated PN1-TCNE solution in benzene, two new absorption bands appeared at $\lambda_{\text{max}} = 408$ and 460 nm (Figure 3.11A). When the experiment was conducted in acetonitrile, the 460 nm band dominated at early stages of the photolysis (Figure 3.11B) and the 408 nm band appeared at later stages (Figure 3.11C). Deconvolution of the UV-Vis spectra yielded pure spectra of the two species (Fig. 3.11D), which are in excellent agreement with those of naphthoxanthenyl radical and naphthoxanthenium cation, obtained independently by chemical synthesis.³⁴⁸

^m Cyano groups have low energy π^* orbitals, and the presence of four such groups, with their electron-withdrawing π systems linked (conjugated) to the central C=C double bond, gives rise to an excellent electron/hydrogen acceptor.

Consistent with this assignment, the 408 nm species was not observed under an atmosphere of air as one would expect for a carbon-centred radical, whereas the 460 nm band was still present. Prolonging the irradiation, both with laser and with the UV chamber, led to a complex mixture of products.

As a final piece of evidence, PN1D, the 9-perdeuterophenyl analogueⁿ of PN1 was synthesized and studied by laser flash photolysis and ¹H-NMR spectroscopy (Figure 3.12). While the lifetimes of the two naphthoxanthenes were roughly the same (8 and 7 μs, respectively), the TCNE quenching rate constant for the deuterated naphthoxanthene was 2.3-fold smaller ($5.2 \times 10^6 \text{ M}^{-1}\text{s}^{-1}$ vs. $1.2 \times 10^7 \text{ M}^{-1}\text{s}^{-1}$). The TCNE quenching rate constant in benzene was the same as in acetonitrile.

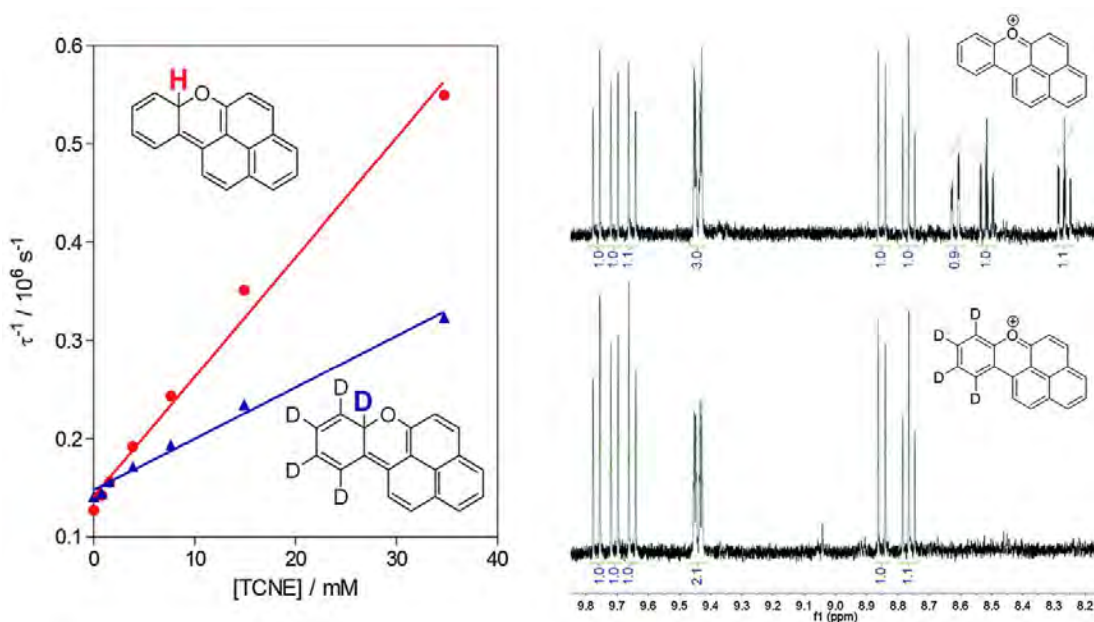


Figure 3.12 Left: Plot of the reciprocal lifetime of naphthoxanthenes vs. the concentration of TCNE in argon-saturated acetonitrile at room temperature. Right: ¹H-NMR spectra in acetone-*d*₆ of PN1 (top) and its perdeuterophenyl analogue PN1D (bottom) after photolysis in the presence of 5 mM TCNE in argon-saturated acetonitrile at room temperature.

The ¹H-NMR spectrum of the photolysis products of PN1 and PN1D in argon-saturated acetonitrile in the presence of 5 mM TCNE (Figure 3.12 right) are consistent with those of the corresponding naphthoxanthenium cations.³⁴⁸ The spectrum of deuterated-naphthoxanthenium cation lacks the signals of four (but not all five) phenyl protons relative to the spectrum of non-deuterated, which is consistent with a proton having been previously abstracted by TCNE.

ⁿ I proposed to synthesize the 9-perdeuterophenyl analogue in order to prove that the hydrogen abstraction was the limiting kinetic step for that reaction. The hydrogen or deuterium abstraction rate should be different due to kinetic isotopic effects. This change in rate results from heavier isotopologues having a lower velocity/mobility and an increased stability from the higher dissociation energies when compared to the compounds containing lighter isotopes.^{634,739} The kinetic isotopic effect is extremely large in the H/D pair because deuterium is almost two-fold heavier than hydrogen (2.014 vs 1.008 amu, respectively).

3.3.5. Reprofileing: 9-Heteroaryl-phenalenones as a novel photochromic family

(Adapted from: **R. Bresolí-Obach**, C. Flors, J.G. Luis, T.A. Grillo, G. Bucher and S. Nonell, 9-Aryl-Substituted Phenalenones: Reversibly Switchable T-Type Photochromic Coumpounds, in preparation.)

The results reported in this section have been carried out in collaboration with the University of Glasgow (United Kingdom), IMDEA Nanociencia (Madrid, Spain) and the Universidad de La Laguna (Tenerife, Spain).

3.3.5.1. Introduction

For centuries, nature has awarded scientists with a rich repertoire of materials and systems that can reversibly adjust their structure and properties in response to environmental stimuli, such as camouflage in chameleons or colour changes in echinoderms animals.³⁵⁶ Molecules with photochemically switchable properties play a crucial role in modern applications (Figure 3.13). Some examples may include their use as functional molecules, assemblies, and materials used in optoelectronic devices for data storage and logic operations as well as biotechnological and pharmacological applications, especially for optogenetics.^{357–360} Furthermore, these compounds are key molecules for some super-resolution microscopy techniques, like STORM or PALM.^{361,362} Properties that can be switched include, among others, UV/Vis absorption, magnetic state, mesoscopic properties or surface tension.^{363–367}

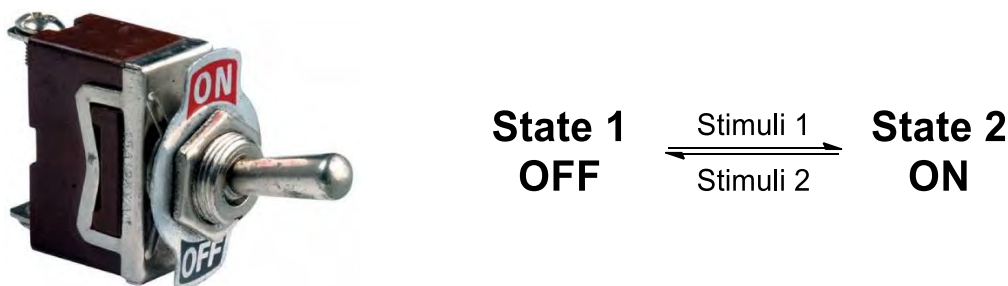
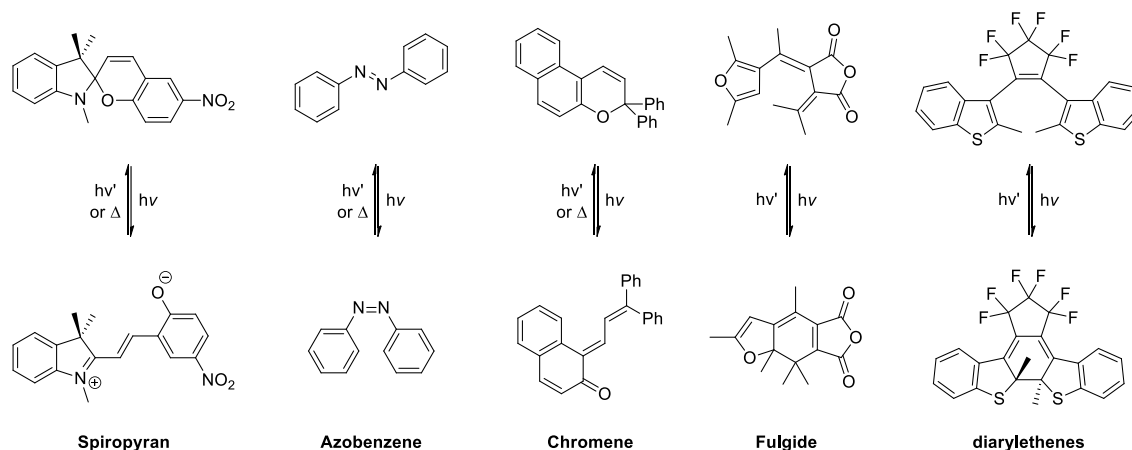


Figure 3.13 Concept of a molecular switch.

Among the different forms of external inputs that can influence the switch compound, light can present some advantages, as for example it can be controlled with high spatial and temporal resolution and it can be applied in an external and non-invasive fashion.³⁶⁸ So, photochromic switches, also called photoswitches, are widely used. Formally, a photoswitch is a molecule that is able to reversibly photoisomerize between at least two different (meta)-stable isomers with markedly different properties.³⁶⁹

Two main families of photoswitches are distinguished (Scheme 3.11). P-type switches are only photochemically reversible; they do not thermally revert to the initial isomer even at elevated temperature. Fulgides³⁶⁰ and diarylethenes³⁶⁰ belong in this group. T-type switches are photochemically and thermally reversible. In this case, the photochemically generated isomer reverts thermally to the initial form, which can last from nanoseconds to months in the temporal scale. Examples for T-type photochromic switches would be azobenzenes,³⁷⁰ stilbenes,³⁷¹ chromenes,³⁷² or spiropyrans.³⁷³



Scheme 3.11 Some important families of photochromic compounds and their photochromic reactions.

The main photochemical reactions for photoswitches are: i) cis-trans isomerization (i.e. azobenzenes or stilbenes), ii) interconversion between closed and open forms (i.e. spiropyrans, diarylethenes, and chromenes) or iii) photo-tautomerism.³⁵⁹ This results in a change in geometry, spectroscopic properties, charge distribution, polarity among others properties of the sample.^{374–377}

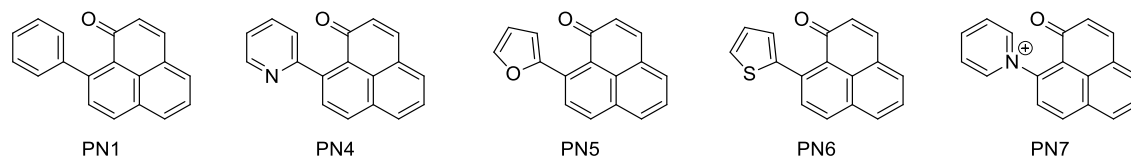
For use in real-time information transmitting systems, photochromic switches of T-type with very rapid thermal reversion lifetimes are required.³⁷⁸ The photochemically generated isomer should therefore be short-lived, ideally with a lifetime smaller than microseconds range.³⁷⁹ Considerable advances have been made towards azobenzene-based photochromic switches, where the kinetics of the thermal cis-azobenzene to trans-azobenzene isomerization have been accelerated down to the microsecond range.^{380–382}

In this sub-chapter, we study different 9-heteroaryl-phenalenones by nanosecond laser flash photolysis as a model for a new family of T-type photochromic switches. The differences in the electronic distribution of the 9-heteroaryl moiety changes the rate of photo-cyclization and descyclization allowing the modulation of the non-thermodynamically stable isomer lifetime from the range of picoseconds to milliseconds.

3.3.5.2. Experimental part

3.3.5.2.1. Synthesis of 9-aryl-phenalenones

9-Phenyl-phenalenone (PN1), 9-pyridil-phenalenone (PN4), 9-furyl-phenalenone (PN5), 9-thionyl-phenalenone (PN6) and 9-pyridinium-phenalenone (PN7) were synthesized as described elsewhere.^{350,383} (see Scheme 3.12 for their chemical structures).



Scheme 3.12 Chemical structures for PN1, PN4, PN5, PN6 and PN7.

3.3.5.3. β -phenyl quenching reaction in 9-aryl-phenalenones

The photophysical and photochemical properties of PN1 and PN 4-7 are collected in table 3.4.

Table 3.4 Optical and photophysical properties of PN1 and PN4-PN7 and their corresponding naphthoxanthenes in different argon saturated-solvents (^ahexane, ^btoluene, ^cacetonitrile, ^dmethanol and ^ePBS).

	$\lambda_{\text{abs,max}} / \text{nm}$	$\tau_T / \mu\text{s}$	$\tau_{\text{naphthoxantene}} / \mu\text{s}$	Singlet contribution	Triplet contribution	$k_q^{\text{TCNE}} / \text{M}^{-1}\text{s}^{-1}$
PN1	530 ^b 520 ^c	0.12 ^b 0.16 ^c	20 ^a 11 ^b 8 ^c 8 ^d	0.78 ^b 0.72 ^c	0.22 ^b 0.27 ^c	1.2×10^7 ^b 1.2×10^7 ^c
PN4	525 ^b 515 ^c	0.26 ^b 0.64 ^c	29 ^a 20 ^b 14 ^c 7 ^d	0.63 ^b 0.76 ^c	0.37 ^b 0.24 ^c	3.2×10^6 ^c
PN5	445 ^b 430 ^c	0.45 ^b 0.60 ^c	30×10^3 ^a 14×10^3 ^b 11×10^3 ^c 11×10^3 ^d	0.90 ^b 0.89 ^c	0.10 ^b 0.11 ^c	2.1×10^5 ^c
PN6	470 ^b 460 ^c	0.38 ^b 0.53 ^c	28×10^3 ^a 18×10^3 ^b 12×10^3 ^c 10×10^3 ^d	0.92 ^b 0.91 ^c	0.08 ^b 0.09 ^c	1.2×10^5 ^c
PN7	585 ^e	50 ^e	7×10^{-5} ^e	1	0	----

For PN1 and PN4-PN6, τ_T is more than one order of magnitude smaller than for free PN, whilst for PN7 the triplet lifetime is longer than PN. This advocates that the BPQ reaction is strongly favorable from the triplet state, when the 9-position aromatic ring it is at least neutral or electronically rich. Furthermore, as we proved recently for naphthoxanthene,³⁸⁴ the corresponding naphthoxanthenes of PN4-PN6 can also be generated from the singlet state. Further, experimental evidence for this statement is the biexponential kinetics in naphthoxanthenes formation (Figure 3.14).

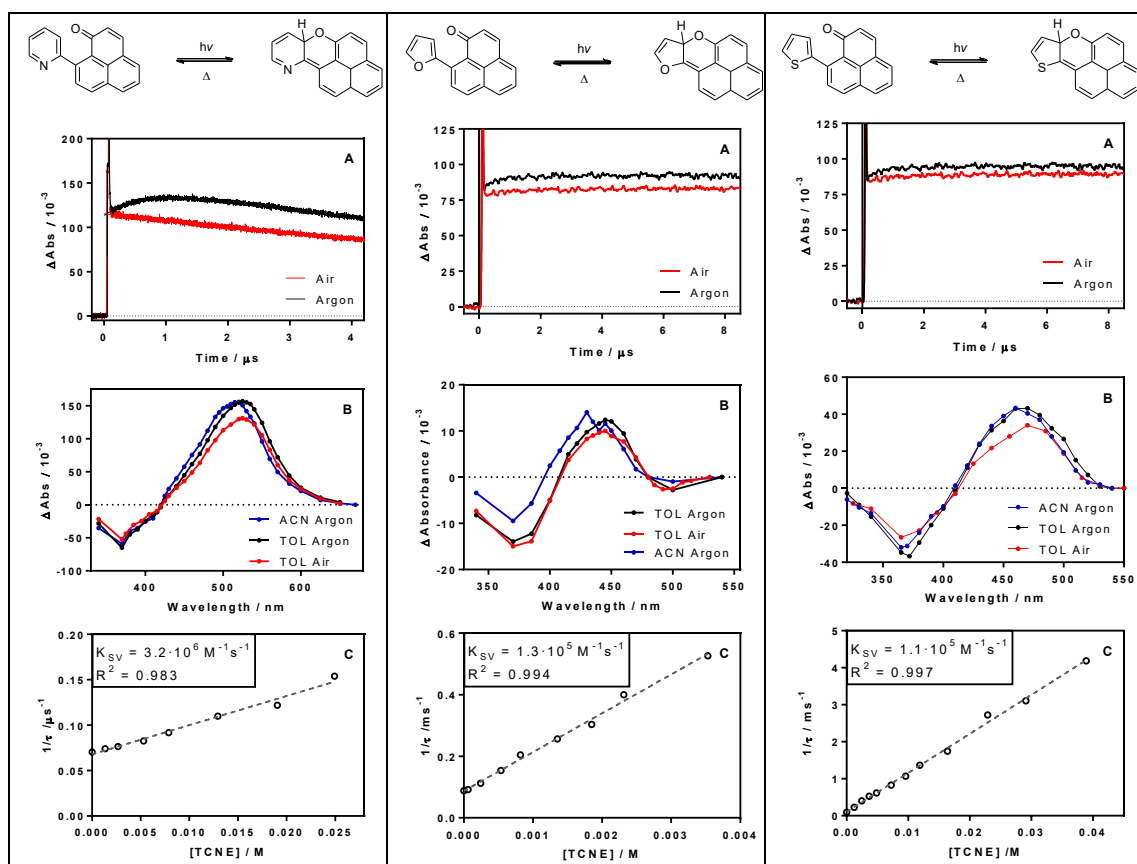


Figure 3.14 left: PN4; middle: PN5; right: PN6. (a) Transient absorption in air and argon-saturated acetonitrile. λ_{exc} 355 nm. (b) Transient absorption spectra in argon-saturated acetonitrile, argon-saturated toluene and air-saturated toluene. (c) Plot of the reciprocal lifetime of corresponding naphthoxanthene vs the concentration of TCNE in argon-saturated acetonitrile at room temperature.

A special case is PN7, where no experimental evidence for the formation and decay of the corresponding naphthoxanthene is detected in the range of nanoseconds to seconds by transient absorption spectroscopy. Femtosecond transient absorption experiments (Figure 3.15) reveal a singlet lifetime of 4.4 ps, which is 7-fold shorter than that of free PN ($\tau_s = 29$ ps) and 2.25 fold shorter than that of PN1. This strongly suggests that the BPQ reaction from the singlet state is highly favored when the β -aryl-moiety is positive charged.

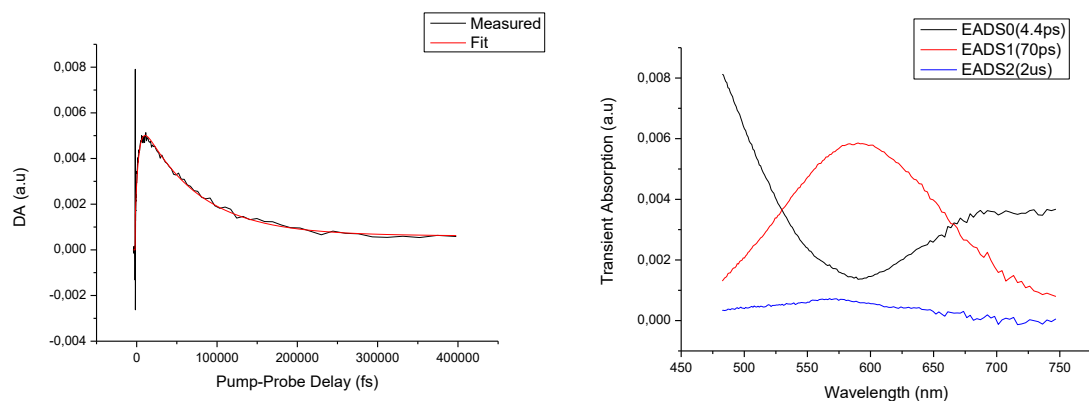


Figure 3.15 Femtosecond transient studies of PN7. Left: Transient absorption in air-saturated PBS. Right: Deconvoluted spectra for the different components. λ_{exc} 355 nm. This data has been acquired by Dr. Cristina Flors in IMDEA Nanociencia (Madrid, Spain).

However, the BPQ reaction does not occur to any measurable extent from its triplet state, as indicated by the following evidences: (Figure 3.16): i) the microsecond transient absorption spectrum matches that of $^3\text{PN}^*$, ii) the microsecond transient can be quenched by $^3\text{O}_2$ with a rate of $3 \times 10^8 \text{ M}^{-1} \text{ s}^{-1}$, iii) its τ_T in argon-saturated PBS is $50 \mu\text{s}$ which is even longer than for free PN^{332} and iv) its Φ_Δ in air and oxygen saturated PBS is 0.08 for both cases, which is approximately equal to Φ_T .

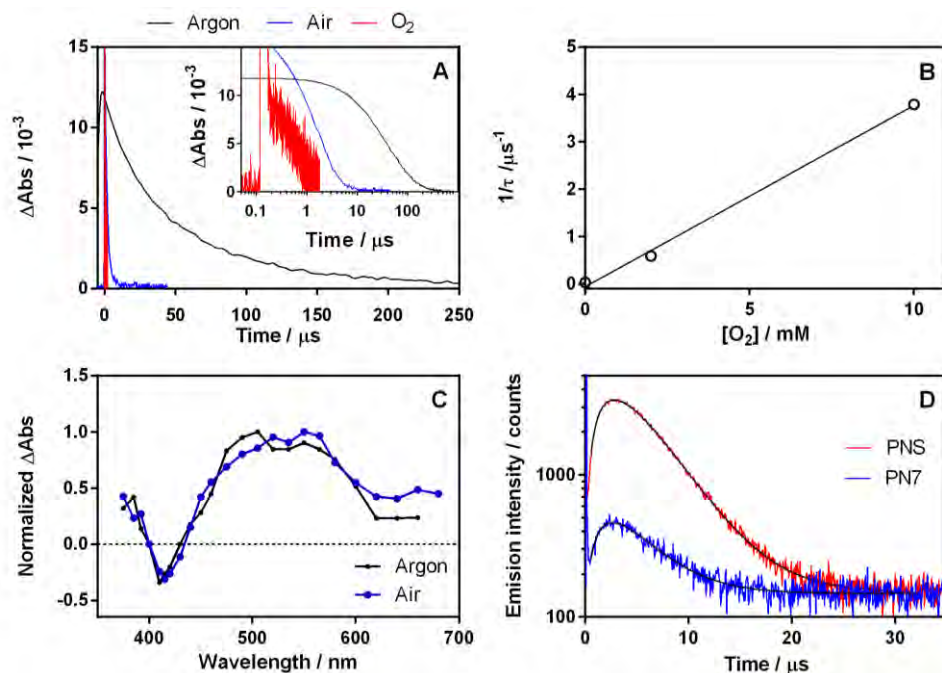


Figure 3.16 (A) Microsecond-transient absorption spectra of PN7 in argon- (black), air- (blue) and oxygen- (red) saturated PBS. Inset: The same data represented in logarithmic scale. (B) Plot of the reciprocal lifetime of PN7 vs the concentration of $^3\text{O}_2$ in PBS at room temperature. (C) Transient absorption spectra of PN7 in argon- and air-saturated PBS. (D) Kinetic traces for $^1\text{O}_2$ phosphorescence signals for optically matched samples of the PNS (red; $\Phi_\Delta = 0.97^{216,262}$) and PN7 (blue).

Experimental characterization of photo-generated naphthoxanthenes was derived from LFP experiments. The absorption maxima of them are between 430 to 585 nm. In one hand, the blue-shift of furyl and thiophene naphthoxanthenes is due to the reduction of the conjugation of the electronic π -system. In the other hand, the red-shift of pyridinium naphthoxanthenes is due to the presence of a positive charge in the chromophore moiety.

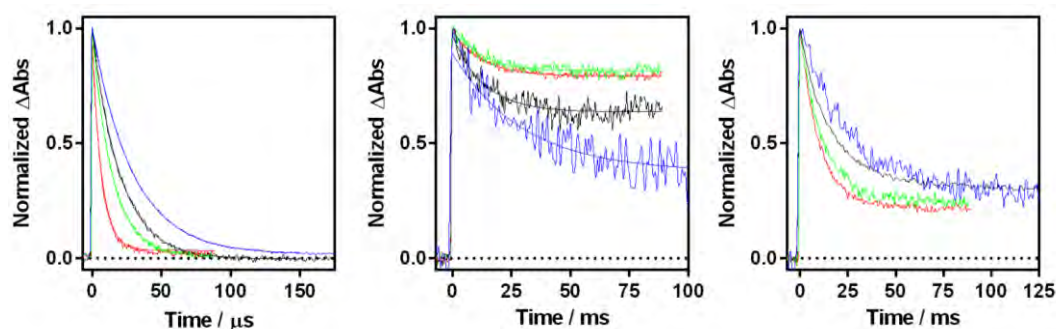


Figure 3.17 Transient absorption spectra of PN4 (left; $\lambda_{\text{obs}} = 520 \text{ nm}$), PN5 (middle; $\lambda_{\text{obs}} = 440 \text{ nm}$) and PN6 (right; $\lambda_{\text{obs}} = 460 \text{ nm}$) in argon-saturated solvents (hexane (blue), toluene (black), acetonitrile (green) and methanol (red)).

Information of the thermal stability of naphthoxanthenes was obtained by transient absorption spectroscopy (Figures 3.15 and 3.17). Pyridine substitution seems to have little impact to its stability in comparison with phenyl substitution (a slightly increase from 17 to 11 μ s). Furan or thiophene substitution increase 1000-fold its lifetime, from microseconds to milliseconds; whilst for pyridinium substitution decreases its lifetime to only 70 picoseconds. As a whole, heteroaromatic substitution on position 9 allows to modulate the naphthoxanthene lifetime in more than 8 orders of magnitude.

Also we have studied the photoproducts formed in the photolysis of naphthoxanthenes in the presence of TCNE. In comparison with PN1, the reaction rate constant k_q^{TCNE} is one order of magnitude smaller for pyridyl- and 2 orders for furyl and thienyl-substituted PNs. Additionally, the reactivity of pyridyl-substituted naphthoxanthene towards 8 mM TCNE was followed by steady-state UV-Vis spectroscopy. Upon laser excitation of PN4 in air and argon saturated acetonitrile, two new bands appeared at 435 and 458 nm (Figure 3.18) which are attributed to the formation of naphtho[2',1',8':4,5,6]chromeno[3,2-b]pyridin-6-ium cation. This compound was characterized by 1 H-NMR without further purification and is structurally elucidated.

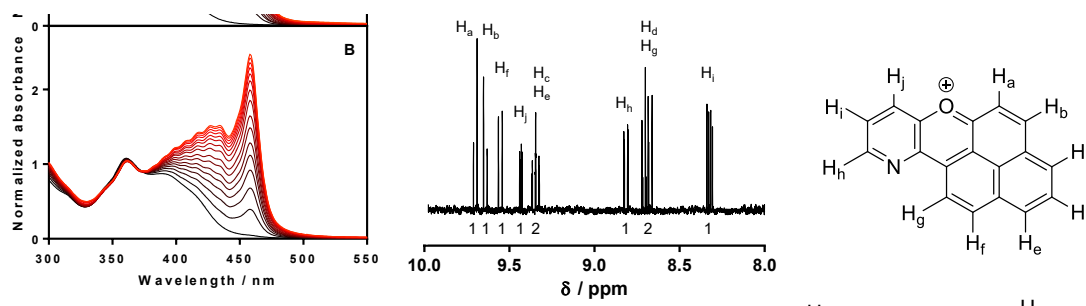


Figure 3.18 Left: UV-Vis spectral changes upon laser photolysis of PN4 in the presence of 80 μ M TCNE in argon-saturated acetonitrile. Middle: 1 H-NMR spectrum of the photoproduct. Right: Proposed chemical structure for the photoproduct generated.

Finally, we have checked the photostability of PN1 and PN4-6 under the same conditions by submitting them to hundreds of cycles of exposure to 355 nm pulsed light (10 mJ per pulse) in air-saturated acetonitrile. Figure 3.19 shows their photobleaching in acetonitrile at 25 $^{\circ}$ C. PN1 is the most photostable derivative. The substitution of the phenyl by a pyridyl seems to slightly reduce its photostability, whilst the substitution by a furyl or thienyl reduces its signal by 50% after only 50 or 100 cycles respectively.

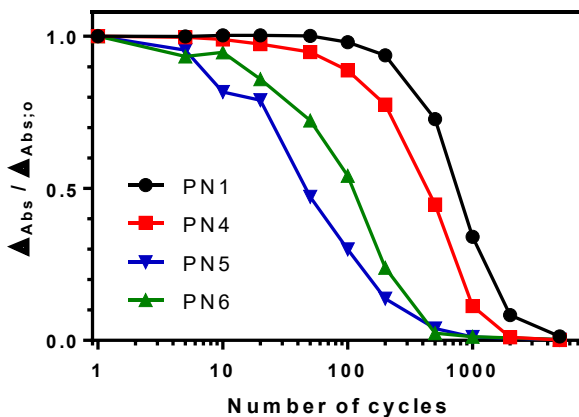


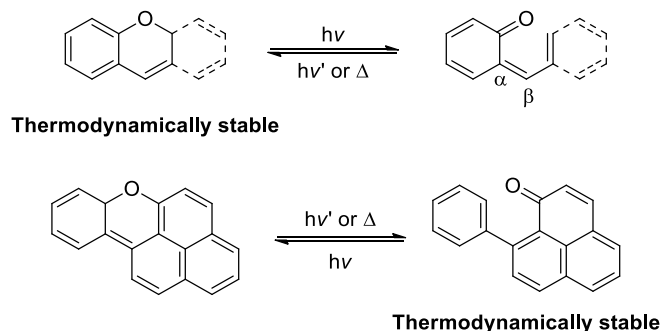
Figure 3.19 Photostability of PN1 and PN4-6 upon pulsed 355 nm laser irradiation cycles (10 mJ per cycle) in aerated-acetonitrile.

3.3.5.4. 9-Aryl-phenalenones as inversed-chromenes

The previously presented data strongly advocate that 9-aryl-phenalenones are a good scaffold for developing a new type of photochromic system. Ultraviolet irradiation of PN1-PN7 renders the corresponding naphthoxanthene derivatives via a 6- π electrocyclic intramolecular photocyclization (BPQ).

This study shows that BPQ reaction is not restricted to phenyl groups but can rather be extended to other aromatic heteroaryl moieties such as pyridyl, furyl, thienyl and pyridinium. Thus, by modulating the heteroaryl substitution of the position 9, it is possible to change the naphthoxanthene lifetime over nine orders of magnitude, from tens of picoseconds to tens of milliseconds.

It is interesting to note that the BPQ reaction and the posterior electrocyclic ring opening reaction are similar reactions to the ones that occur with the photochromic chromenes family (i.e. naphthopyrans, benzopyran or oxazines).^{372,385-387} For these compounds, the most stable isomer is the 2H-chromene core and upon light illumination undergoes by a photo-electrocyclic ring opening to obtain a $\alpha,\beta,\gamma,\delta$ -unsaturated ketone core. A deeper structural analysis of the unsaturated ketone, allows observing that it has a vinyl group in β -position of the ketone, which can revert to the original chromene core by a BPQ reaction either thermally or photochemically (Scheme 3.13).



Scheme 3.13 Photochemical reaction pathway for 2H-chromene core and PN1.

Taking into account this observation, it can be postulated that 9-aryl-phenalenones are photochromic compounds acting as inverted-chromenes. The main reason for this inversion in reactivity is that the phenalenone core is an aromatic ketone and consequently its stability is increased by the aromaticity of the system. In contrast, for the chromene case, the ketone is no longer stabilized by aromaticity while the cyclic structure is aromatic,^{372,388} even if the β -substituent is vinylic or aryl, ³⁸⁹ although for aryl substituents it can further photochemically evolve through an *ipso* BPQ addition.^{390,391}

3.3.6. Reprofilig: 9-Phenyl-phenalenone photoreactivity as student laboratory experiment for understanding laser flash photolysis experiments

(Adapted from: **R. Bresolí-Obach**, and S. Nonell, Unravelling a mechanism of photocyclization and decyclization reaction by laser flash photolysis experiments, in preparation (**intended for J. Chem. Ed.**))

ESTIMADES i estimats mestres:

Gràcies per la vostra vocació artesana, la de fer les coses ben fetes pel gust de fer-les ben fetes. Per entendre que la vostra feina no acaba quan ho heu explicat, sinó quan ho han entès.

Per la il·lusió amb què enceteu el curs, dient com diem tots que fa mandra, però sentint íntimament les ganes de començar. Per l'esforç que feu per treure el màxim de cada alumne, confiar-hi i reforçar-los l'autoestima.

Pels xèrres que heu de fer pendants dels que tenen dificultats a casa, sabent que en una societat meritocràtica això no ha de perjudicar la igualtat d'oportunitats a l'escola. Pel sentit de l'humor, que us permet combinar el repte més transcendent de la humanitat -educar les criatures- amb els somriures que ho fan tot més fàcil.

Per entendre que el món connectat no és res que ens hagi de fer por, si ho fem servir com a palanca per augmentar la motivació. Per tenir clar que en el món connectat també s'ha de saber desconnectar. Per la paciència que teniu amb els pares. Per l'estima que teniu pels nostres fills. Per no desanimar-vos per més motius que tingueu, sabent que la vostra missió és massa important per permetre-us el luxe d'abaixar la guàrdia.

Per tot el que heu preparat i pensat perquè aquest any us surti encara millor que l'anterior. Per no tenir por d'innovar. Per compartir experiències amb altres mestres, per formar-vos i assumir que heu de formar aprenents permanents, que avui a les aules s'hi va a aprendre a aprendre.

Carles Capdevila – Carta d'agraïment als bons mestres artesans (Diari Ara; 13-09-2015)

En els castellers, els més grans i forts estan a baix a la pinya i ajuden als més petits a ser el més alts del món per un moment i poder tocar el cel amb la mà.

Això de forma desinteressada (o com a mínim ho vull creure) és el que ha fet moltíssims mestres: transmetre el seu coneixement. En aquest sentit vull agrair a tots els mestres que he tingut, fent especial esment al Dr. Santi Nonell que ha fet de "mestre artesà" ensenyant al seu "aprenent" des d'aquell setembre de 2009 en aquella primera classe de Química Física a segon de carrera.

I com tot en aquesta vida, tot ha de fluir. Per tant, considero que un cop arribat a aquest nivell s'havia de fer alguna activitat per tal d'ajudar els nous estudiants a adquirir nous conceptes.

Si aquest secció o les diferents sessions experimentals realitzades durant aquests anys han servit per ajudar a algú a comprendre la fotòlisis làser de llampec (en anglès Laser Flash Photolysis) aquesta tesi doctoral ja haurà valgut la pena.



3.3.6.1. Aim of the study

In order to explain the aim of this “special” section, I want to remember two different quotes. The first one is from Maimonides, who was a medieval Sephardic Jewish philosopher from Al-Andalus; the second is from Benjamin Franklin, one of Founding Fathers of the United States.

“Give a man a fish and you feed him for a day; teach a man to fish and you feed him for a lifetime”

“An investment in knowledge pays the best interest”

Although the first quote is 600 years older than the second one, the two sentences have a similar meaning: education is essential for improving the “value” of a person. Societies have improved their life quality with education and when the education disappeared (i.e. Europe in the Middle Age) their life quality diminished substantially.

I believe that helping “knowledge transfer” to the younger students should be necessarily a part of a PhD thesis. This can be achieved by mentoring younger undergraduates or master students (in my case), but also through outreach activities involving school-children. Demonstrations of science (and chemistry in particular) can be interesting and funny in the same time or designing (and improving) some laboratory experiences. For this last purpose, we decided to design a laboratory experience for the photochemistry based with section 3.3.2.3.

In one hand, laser flash photolysis (LFP, the technique used mainly in this laboratory experience) is a pump-probe laboratory technique, in which a sample is firstly excited by a pulsed-laser light (called pump-pulse). This strong pulse generates excited states, which can further evolve thorough a photochemical reaction. Afterwards, the absorption of light (called analysing-beam) by the sample is recorded in order to monitor relaxation or possible photoinduced chemical reaction processes initiated by the pump-pulse.

This technique was developed in the 40s and 50s by Manfred Eigen, Ronald George Wreyford Norrish and George Porter, who won the 1967 Nobel Prize in Chemistry for this invention²²⁷⁻²²⁹ and is honorary PhD by IQS. The idea of LFP was born out of cameras developed during and shortly after the Second World War, which were used to take pictures of fast moving planes, rockets and missiles. Since then, use and refinement of LFP techniques allowed to scientific community to understand light-induced processes in organic molecules, polymers, nanoparticles, semiconductors, photosynthesis, signalling, or light-induced conformational changes in different biological systems.³⁹²⁻³⁹⁵

In the other hand, the importance of photochemical BPQ reaction studied in laboratory experience is deeply explained in the previous sections.^{309,342}

This experiment was successfully completed by 27 master students during the academic period from 2013 to 2017. This laboratory experiment has been included as part of the curriculum in photochemistry course at master level at Institut Químic de Sarrià (Universitat Ramon Llull, Barcelona, Spain). Students did work individually or in groups of two-three to complete their assigned project tasks.

3.3.6.2. Student laboratory protocols

PN1 and TCNE solution are prepared in acetonitrile, either by the students or staff (depending on available time of the class; solution 1 and 2 respectively). The concentration of these solutions are 100 μM and 1 M respectively. In order to vary the concentration of oxygen, a stream of oxygen 5.0 or argon 5.0 was flowed into the solution under gentle stirring for approximately 30 minutes.

3.3.6.2.1. Basic LFP experiments

i) Argon, air or oxygen-saturated solution 1 is excited with 355 nm nanosecond pulsed laser. The absorbance changes are monitored at 520 nm with two different time-windows, 2 and 50 μs , in order to collect properly the rise and the decay kinetics, respectively. The data collected is fitted with equation 3.1, which is a triexponential curve used for fitting the kinetics of some intermediates where its formation or decay can occur through two different processes.

$$y(t) = -A_1 e^{\frac{-t}{\tau_1}} - A_2 e^{\frac{-t}{\tau_2}} + A_3 e^{\frac{-t}{\tau_3}} \quad \text{Equation 3.1}$$

A_1 , A_2 and A_3 are the pre-exponential factors and τ_1 , τ_2 and τ_3 are the lifetimes of the different species. Note to students that A_1 and A_2 are negatives whilst A_3 is positive because they represent rises and decay respectively.

ii) With air-saturated solution 1 used in the previous experiment, controlled volumes of solution 2 are added for obtain different TCNE concentrations (recommended: 0, 5, 10, 15 and 22 μM). Each solution is excited with 355 nm nanosecond pulsed laser and the absorbance changes are followed at 520 nm with a time window of 50 μs . Due to chosen time-scale, only the decay is collected, so it should be adjusted with a monoexponential equation 3.2.

$$y(t) = A_3 e^{\frac{-t}{\tau_3}} \quad \text{Equation 3.2}$$

From decay lifetime shortening, it is calculated the quenching rate of naphthoxanthene by TCNE using a Stern-Volmer like plot, accordingly to equation 3.3.

$$\frac{1}{\tau} = \frac{1}{\tau_0} + k_q [\text{TCNE}] \quad \text{Equation 3.3}$$

Where τ is decay lifetime in function of TCNE concentration, τ_0 is the decay lifetime in absence of TCNE and k_q is the quenching rate of TCNE. This equation is directly derived from Stern-Volmer equation (Equation 3.4).³⁹⁶

$$\frac{\tau_0}{\tau} = 1 + \tau_0 k_q [\text{TCNE}] \quad \text{Equation 3.4}$$

3.3.6.2.2. Complementary LFP experiments

i) Argon-purged solution 1 is excited using a 355 nm nanosecond pulsed laser. The absorbance changes are followed at different wavelengths in the range from 300 to 600 nm (recommended step interval of 20-50 nm) with a time-window of 50 μ s.

ii) 100 μ M PN solution in argon-purged acetonitrile is prepared. This sample is excited using a 355 nm nanosecond pulsed laser. The absorbance changes are followed at 520 nm with a time-window of 200 μ s in order to measure PN triplet lifetime.

iii) Quantum mechanics calculations can be performed using the Gaussian09 suite of programs.³⁹⁷ Naphthoxanthene energy minima can be optimized at the density functional theorem B3LYP/6-31G(d) level of theory.³⁹⁸ Afterwards, time-dependent-DFT B3LYP/6-31G(d) can be used to estimate the energy of naphthoxanthene singlet excited states.³⁹⁹

iv) In a quartz-cuvette, 3 mL of an argon-purged acetonitrile solution containing 100 μ M PN1 and 20 mM TCNE are irradiated with UV-A or blue light (at a fluence of approximately 10 mW/cm²) for 120 minutes. Ideally, every 5-10 minutes an absorption spectrum should be recorded in order to reconstruct naphthoxanthenium cation formation kinetics.

v) ¹H-NMR spectrum could be recorded after removal of solvent under vacuum from the solution obtained in the previous experiment, dry and redissolve it in deuterated acetonitrile or acetone. ¹H-NMR spectrum should be similar to the one depicted in figure 3.12.

3.3.6.3. Student laboratory experience argumental tale

It is well-known that PN has a Φ_T and Φ_A of 1 in a vast variety of solvents, whereas when the hydrogen situated in position 9 is replaced by a phenyl group, Φ_T and Φ_A decrease dramatically.^{305,330,332} This clearly suggests that an additional deactivation pathway has to occur in competition with triplet and 1O_2 generation. Different laser flash photolysis experiments are proposed in order study this competitive pathway.

In a first step, kinetic traces of PN1 dissolved in argon-saturated acetonitrile are collected (Figure 3.20). A biexponential rise and monoexponential decay are fitted by a mathematical kinetic analysis with lifetimes of <0.01, 0.16 and 8 μ s respectively. This triexponential observed kinetics is in concordance with the formation and posterior evolution of the naphthoxanthene intermediate generated. It can be assumed that the intermediate decays to PN1, because it is not observed any absorbance changes between 350 to 600 nm after 50 μ s. Furthermore, PN1 kinetic trace is completely different to PN where only a monoexponential decay is observed with a lifetime of 38 μ s, which is attributed to triplet state decay. This assumption is further confirmed because this trace is quenched by oxygen.

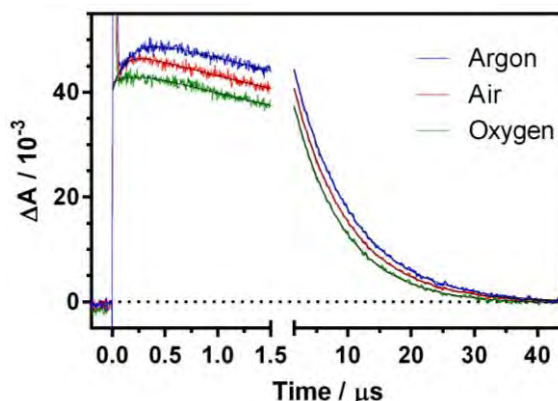


Figure 3.20 Transient absorption kinetics of PN1 in argon-, air- or O_2 -saturated acetonitrile (blue, red and green line respectively). λ_{exc} 355 nm; λ_{obs} 520 nm.

The students should identify if any of the observed kinetics for PN1 can be attributed to the triplet state. It is well-known that triplet state in absence of external quenchers (i.e. oxygen) can live from hundreds of nanoseconds up to several seconds.⁶⁶ Therefore, kinetics traces of PN1 has also been recorded in air- and oxygen-saturated acetonitrile (Figure 3.20). Under presence of oxygen, a biexponential rise and monoexponential decay model is still valid. From them, only the slow rise is oxygen dependent (Table 3.5), therefore this decay is somehow associated to the triplet state. It is observed a quenching in its lifetime (dynamic quenching) plus a partial inhibition of the transient signal (static quenching), which is a clear indication that for PN1 both singlet and triplet states can undergo BPQ.

Table 3.5 Obtained lifetimes from a triexponential kinetic data analysis.

Gas-saturated acetonitrile	τ_1 / μ s	τ_2 / μ s	τ_3 / μ s
Argon	< 0.01	0.16 ± 0.02	9.2 ± 0.8
Air	< 0.01	0.10 ± 0.01	8.7 ± 1.0
Oxygen	< 0.01	0.09 ± 0.02	8.8 ± 0.7

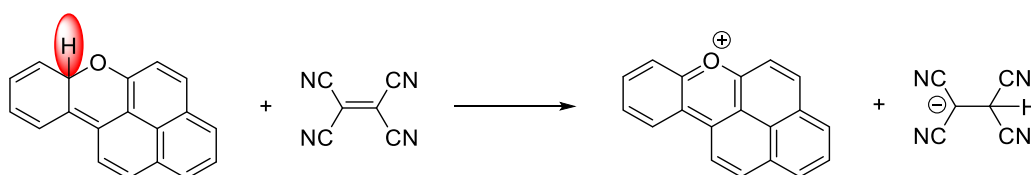
The BPQ reaction is further confirmed because the singlet and triplet lifetimes of PN1 decrease relative to the unsubstituted PN (Table 3.6). Moreover, the shortening in τ_S reduces the probability to populate the triplet state, whereas, the shortening in τ_T reduces the probability of transferring energy from triplet towards 3O_2 to generate 1O_2 . This is fully consistent with lower Φ_A values obtained for PN1 (and other substituted 9-phenylphenalenones) in comparison with the unsubstituted PN.

Table 3.6 τ_S and τ_T of PN and PN1 in acetonitrile. For the singlet state the data is taken from reference ³³². For the triplet state the acetonitrile is purged with argon. Φ_A values are taken from reference ^{262,332}.

Compound	τ_S / ps	τ_T / μ s	Φ_A
PN	29	38 ± 3	1.00
PN1	10	0.16 ± 0.02	0.08 ± 0.02

The previous proposed LFP experiment confirms the presence of naphthoxanthene that reverts to PN1 with a lifetime of 8 μ s in acetonitrile, but do not give any information about the structure of naphthoxanthene. Naphthoxanthene optical properties can be studied by recording its transient absorption spectrum and it should be compared with the expected BPQ product, which can be obtained by density functional theory calculations. It is observed a good match between the experimental and calculated spectra, but this is not enough for confirming its structure.

The next step should be trapping naphthoxanthene with a chemical scavenger. Taking into account its short lifetime, this scavenger should be highly reactive and used in the millimolar concentration range to efficiently trap it. Naphthoxanthene has a C-H bond in the unique sp^3 carbon and it disrupts its planarity and conjugation. If this H is abstracted, then aromaticity is fully recovered and consequently stability is enlarged. Taking into account this driving-force, TCNE has been chosen as scavenger because it is an excellent hydride abstractor.^{354,355} TCNE reacts with naphthoxanthene to generate a highly stable naphthoxanthenium cation (Scheme 3.14).



Scheme 3.14 TCNE reactivity towards the BPQ reaction product.

Then, a series of PN1 kinetics decays with increasing TCNE concentration is recorded by the students (Figure 3.21A). The lifetime of the decay is clearly quenched upon consecutive TCNE addition, whilst the amplitude not. This data supports that only naphthoxanthene is scavenged by TCNE. Furthermore, the TCNE quenching rate constant for PN1 is $(1.2 \pm 0.2) \times 10^7 \text{ M}^{-1}\text{s}^{-1}$ by Stern-Volmer like plot (Figure 3.21B). Moreover, naphthoxanthenium cation formation can be monitored by steady-state spectroscopy (i.e. absorption or $^1\text{H-NMR}$) from PN1 UV-A photolysis in presence of 20 mM TCNE.

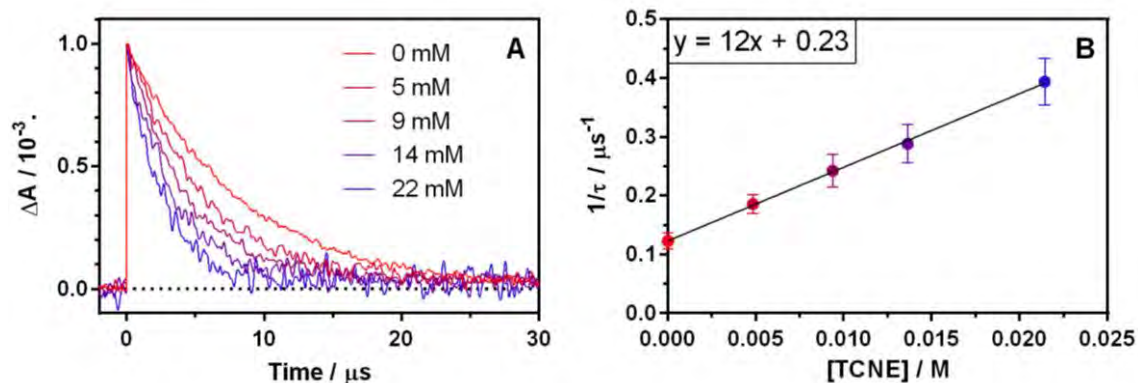
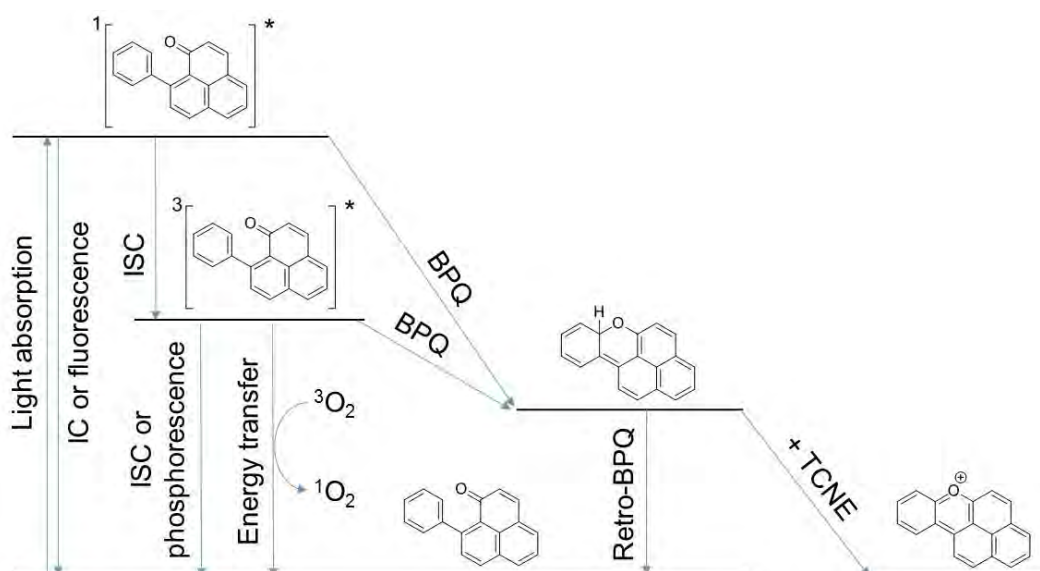


Figure 3.21 (A): Transient absorption kinetics of **1** in air-saturated acetonitrile with increasing concentration of TCNE. (B): Plot of the reciprocal lifetime of the BPQ reaction product vs. the concentration of TCNE in air-saturated acetonitrile. λ_{exc} 355 nm; λ_{obs} 520 nm.

From all the proposed experiments and rationalizing the results obtained, students should be capable to propose a mechanism similar to scheme 3.15. PN1 under UV-light excitation promotes to its first excited singlet state. There it can evolve to naphthoxanthene through BPQ reaction, to triplet state via intersystem crossing or decay to ground state. This last pathway is almost discarded due to its short τ_s . The generated triplet state can also evolve to naphthoxanthene through BPQ or decay to ground state via energy transfer to oxygen for generating $^1\text{O}_2$. All these previous exposed processes occurs in less than one microsecond after photon absorption. Afterwards, naphthoxanthene evolves spontaneously to PN1 via retro-BPQ reaction with a lifetime of 8 μs . For further characterization of naphthoxanthene, it can be scavenged with a hydride abstractor, such as TCNE, to generate naphthoxanthenium which is a stable cation.



Scheme 3.15 The different deactivation pathways for the excited states of PN1.

3.3.7. Reprofilng: 9-(o-nitrophenyl)-phenalenone as an uncaging agent

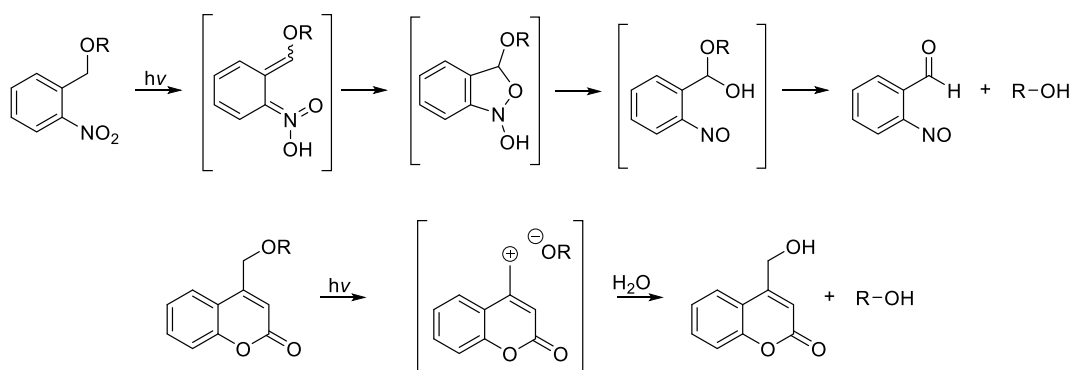
(Adapted from: **R. Bresolí-Obach**, O. Gulias, M. Agut, G. Bucher and S. Nonell, 9-(o-nitro)-phenalenone as an uncaging agent, in preparation).

The results reported in this section have been carried out in collaboration with the University of Glasgow (United Kingdom).

3.3.7.1. Photouncaging compounds

Caged compounds are light-sensitive probes that functionally encapsulate biomolecules in an inactive form.^{400–402} Typically, the molecule of interest is chemically modified with a photoremovable protecting group. The size of the protecting group hampers the interaction between the biomolecule and its corresponding biological receptor. Illumination of these compounds results in the release of the protecting group and consequently the release of the caged-biomolecule. The term “caging” was coined in 1978 by J. F. Hoffman.⁴⁰³

A good photoremovable protecting group should have high absorption coefficients at wavelengths higher than 300 nm (ideally in the visible part of the spectrum), the photoreaction should occur with high quantum yield and be clean -without the appearance of byproducts and/or radicals.⁴⁰² Many photo-uncaging reactions proceed via a cascade of non-stable intermediates, which further evolve to release the desired biomolecule.^{404,405} Until now, several photoremovable protecting groups have been developed. Among them, 2-nitrobenzyl^{406,407} and coumarinyl^{408,409} derivatives are by far the most commonly used (Scheme 3.16).



Scheme 3.16 Photouncaging mechanism for 2-nitrobenzyl⁴⁰⁴ and coumarinyl⁴⁰⁵ derivatives, where R is the caged compound.

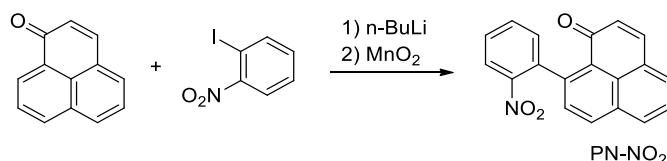
Why are the caged compounds so useful? The ability to release a selected biomolecule with light allows to study its impact in cellular biology.⁴¹⁰ For that, several examples of caged biomolecules (i.e. neurotransmitters,⁴¹¹ nucleotides,⁴⁰⁷ ATP⁴⁰⁶) have been developed. In the last years, optogenetics, which is a biological technique that uses light to control cells, has gained a pivotal role in bioscience research.^{412,413} Several caged-drugs have been synthesized for optogenetics purposes.^{414–416}

In this section, we have studied the photophysical and photochemical properties of 9-(o-nitrophenyl)-phenalenone (PN-NO₂). As proof of concept, we expect that 9-phenylphenalenone could be a good photouncaging scaffold due to the low expected C(sp³)-NO₂ energy bond in the naphthoxanthene intermediate.

3.3.7.2. Experimental part

3.3.7.2.1. Synthesis of 9-(o-nitrophenyl)phenalenone

9-(o-nitrophenyl)phenalenone (PN-NO₂) was a gift from Prof. Kiyoshi Fukuhara (National Institute of Health Sciences, Setagaya-ku, Japan) as described in reference ⁴¹⁷. PN-NO₂ synthetic route is described in Scheme 3.17



Scheme 3.17 Synthesis of 9-(o-nitrophenyl)phenalenone (PN-NO₂).

3.3.7.2.2. Specific photoinactivation conditions

Two different strains, one Gram-positive, *Staphylococcus aureus* (*S. aureus*; ATCC 29213) and one Gram-negative, *Escherichia coli* (*E. coli*, ATCC 25922) were used in this study. The cell culture were grown in fresh TSB until reaching an OD₆₀₀ of 0.4 for both bacteria. The different used PSs were delivered dissolved in dimethylsulfoxide.

The different bacterial strains were irradiated in the photoreactor which contains LZC420 fluorescent lamps (420 ± 10 nm; 10.2 mW/cm²) or maintained in the dark for the same period.

3.3.7.3. Photochemical reactivity of PN-NO₂

The absorption spectra of PN-NO₂ was recorded in different solvents (Figure 3.22) and it has the typical profile of a 9-phenyl substituted phenalenone. PN-NO₂ does not present any emission either in acetonitrile or benzene at room temperature, which is in agreement with other 9-substituted phenalenones.

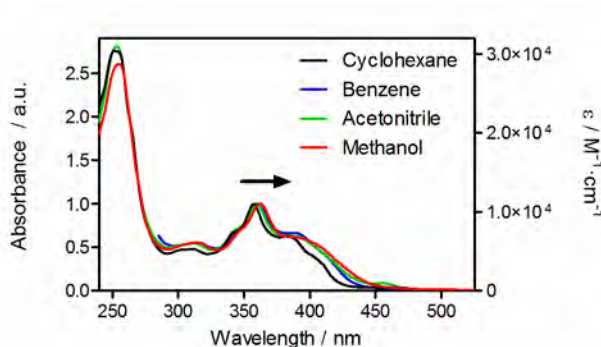


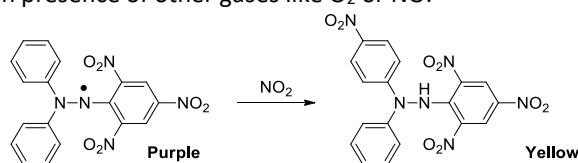
Figure 3.22 Absorption spectra of PN-NO₂ in cyclohexane, benzene, acetonitrile and methanol.

Surprisingly, PN-NO₂ was not photostable at all. The photoproduct generated upon 355 nm pulsed-laser irradiation is dependent of solvent polarity (Figure 3.23).

In argonated-saturated apolar solvents (i.e. cyclohexane or benzene) a sharp band at 412 nm appears upon UV irradiation, whilst in aerated-atmosphere the new band becomes much broader. In addition, this band can be bleached by addition of (2,2,6,6-tetramethylpiperidin-1-yl)oxyl (TEMPO) or methanol. The spectrum of the photoproduct resembles that of the naphthoxanthene radical. Finally, the release of NO₂ could be detected.^o These experimental observations suggest that the naphthoxanthenyl radical is formed under these conditions.

In argonated-saturated polar solvents (i.e. acetonitrile) a sharp band at 460 nm and a shoulder at 430 nm appear upon UV irradiation. In this case, addition of O₂ to the system seems to have a minor role. The generated photoproduct could be purified by thin layer chromatography and identified as the naphthoxanthenium cation by ¹H-NMR analysis. Furthermore, the release of NO₂⁻ upon PN-NO₂ photolysis in water was detected by the Griess test.^p

^o Nitrogen dioxide (NO₂) is scavenged by 2,2-diphenyl-1-picrylhydrazyl radical (DPPH).^{740,741} This reaction is selective towards NO₂ in presence of other gases like O₂ or NO.^{742,743}



^p Nitrite (NO₂⁻) is highly reactive towards aromatic amines to generate diazonium salts, which can further react with another amine to obtain a diazo dye.^{744,745} Griess test takes advantage of azo coupling to detect NO₂⁻.

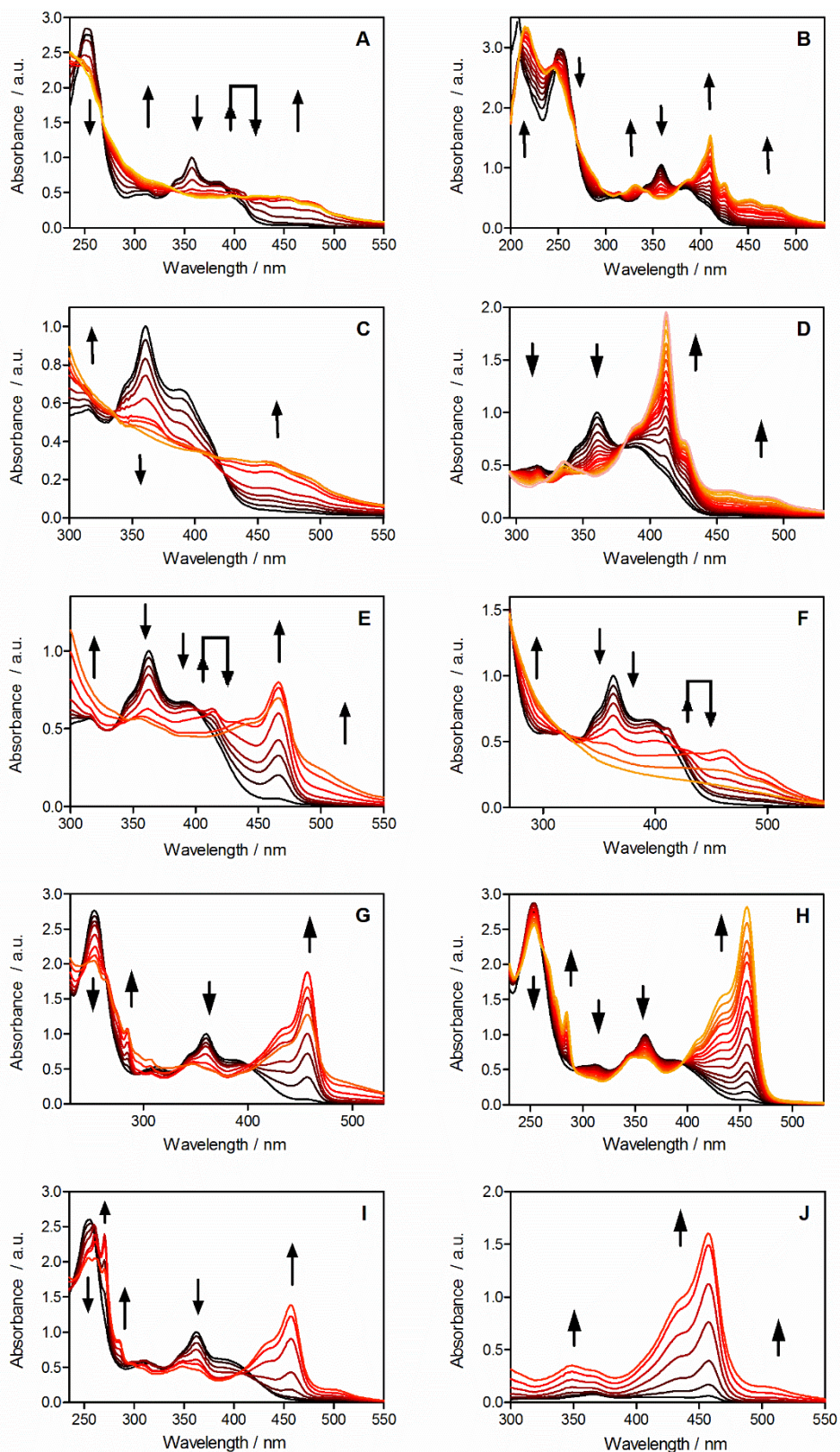
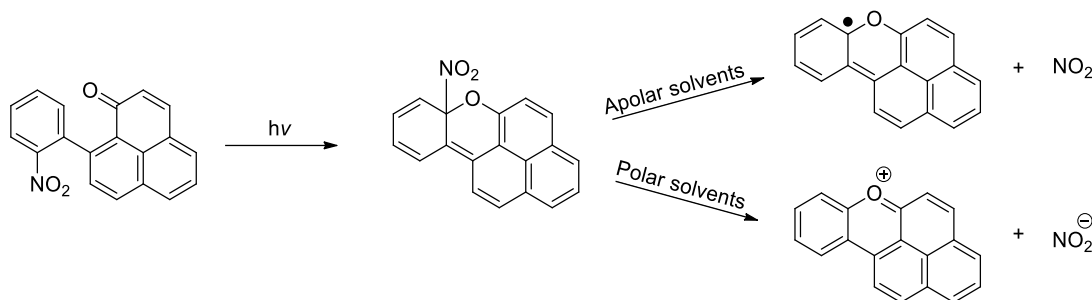


Figure 3.23 UV-Vis spectral changes of PN-NO₂ upon laser photolysis ($\lambda_{exc} = 355$ nm). (A) In air-saturated cyclohexane. (B) In argon-saturated cyclohexane. (C) In air-saturated benzene. (D) In argon-saturated benzene. (E) In argon-saturated benzonitrile. (F) In argon-saturated dimethyl sulfoxide. (G) In air-saturated acetonitrile. (H) In argon-saturated acetonitrile. (I) In air-saturated methanol. (J) In air-saturated methanol:water mixture (1:3).

In argon-saturated “medium” polarity solvents (i.e. benzonitrile or dimethylsulfoxide) the formation of the naphtoxanteny radical and the naphthoxanthenium cation is detected simultaneously. In scheme 3.18 the proposed photochemical reactivity for PN-NO₂ according to the results obtained in photolysis experiments is depicted.



Scheme 3.18 Proposed photochemical reactivity for PN-NO₂ in function of the solvent polarity.

Our collaborators at the University of Glasgow carried out DFT calculations³⁹⁸ in order to observe the feasibility of the proposed mechanism (Figure 3.24). Those calculations indicate that the formation of nitro-naphthoxanthene is fairly favourable. The homolytic and/or heterolytic rupture of the C(sp³)-NO₂ bond evolve to the naphthoxanteny radical or naphthoxanthenium cation, respectively, presents almost no activation barrier. Nitro-naphthoxanthene should have a lifetime of few picoseconds according to the calculations.

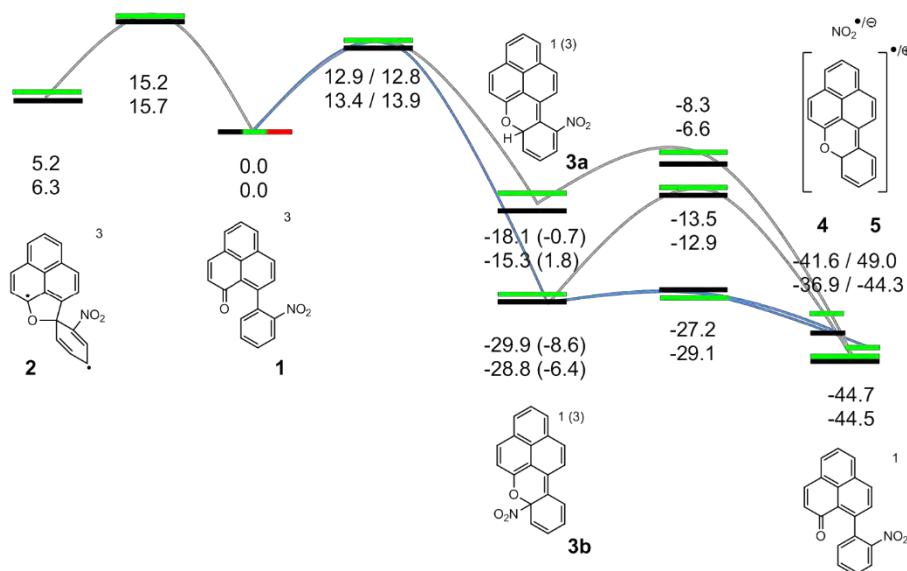


Figure 3.24 Reaction pathways after triplet excitation of PN-NO₂. Free Gibbs free energy are given in kcal/mol relative to the triplet state. Without brackets: singlet state. In brackets: triplet state. In ordinary font/black bar: gas phase. In italics/green bar: in acetonitrile. The different solid lines connecting the different states is provided as a visual aid only (blue line is the preferred reaction pathway). This data has been calculated by Dr. Götz Bucher in WestCHEM, School of Chemistry, University of Glasgow (Glasgow, United Kingdom).

Finally, we decided to study the photo-antimicrobial properties of PN-NO₂ due to its capacity for uncage NO₂⁻ in water. In a first series of experiments, we observed that NO₂⁻ release has no effect on *S. aureus* survival rate (Figure 3.25). Similar results were obtained for *E. coli*.

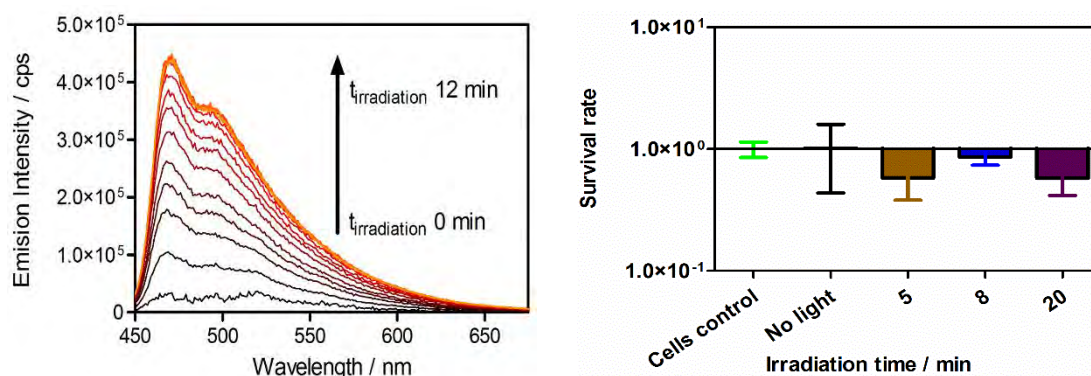


Figure 3.25 Left: 1 μM PN-NO₂ fluorescence changes upon irradiation at 375 nm at very low fluences (<0.1 mJ/cm² after 20 minutes of irradiation) in the presence of *S. aureus*. Right: *S. aureus* survival rate from the previous experiment.

In a second series of experiments, PN-NO₂ showed strong photoantimicrobial activity for both *S. aureus* and *E. coli* respectively (Figure 3.26). Specifically, for *S. aureus*, a viability reduction of 3log₁₀ was achieved at a fluence of 15 J/cm² whilst for *E. coli* it was achieved at 10 J/cm². The PN-NO₂ photo-antimicrobial effect is mediated by ¹O₂, because it is enhanced when PBS is replaced with deuterated-PBS.

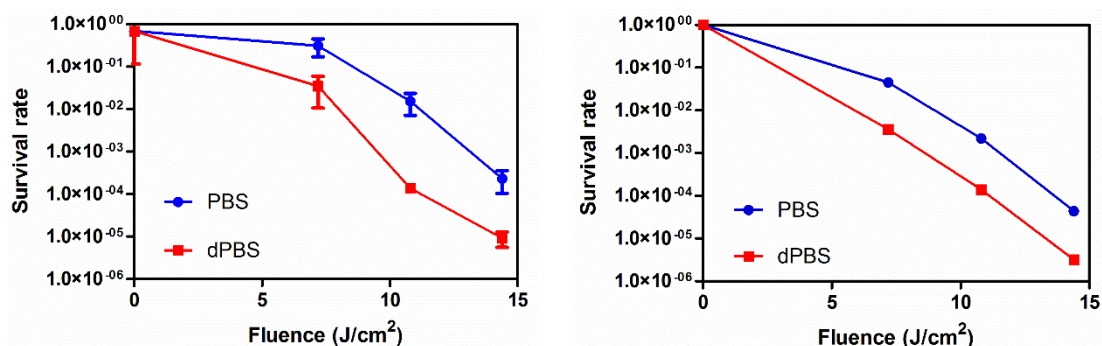


Figure 3.26 Survival curves of *S. aureus* (left), and *E. coli* (right). The bacteria was incubated with 1 (*S. aureus*) and 10 (*E. coli*) μM of PN-NO₂ and irradiated with blue light (420 ± 10 nm) in PBS or dPBS (blue and red lines respectively).

Taking together the two series of experiments, it would seem that under these conditions the naphthoxanthemium cation acts as PS. It has a Φ_{Δ} of 0.15 in PBS. Naphtoxanthemium cation has different promising properties for PDT: i) it is planar; ii) the positive charge is completely delocalized around all the molecule and iii) it is fluorescent ($\Phi_F = 0.52$) which opens the door to use it as a theranostic PS.

3.3.8. Phenalenone as singlet oxygen labelling agent

3.3.8.1. Introduction

Fluorescent tags or labels are widely used to tag proteins and antibodies, nucleic acids (i.e. DNA or RNA) and other relevant biomolecules (Figure 3.27).⁴¹⁸⁻⁴²² Typically, they are used to follow the labelled biostructure in a complex medium. The fluorophore selectively binds to a specific region or functional group on the target molecule and can be attached chemically (i.e. organic fluorophores) or biologically (i.e. a fluorescent protein).⁴²³ For attaching an organic fluorophore to a biomolecule, click-chemistry reactions, such as that of isothiocyanate with amino residues,^{424,425} maleimide with cysteine-reduced thiol groups,^{426,427} and carbodiimide with carboxy groups, are commonly used.⁴²⁸

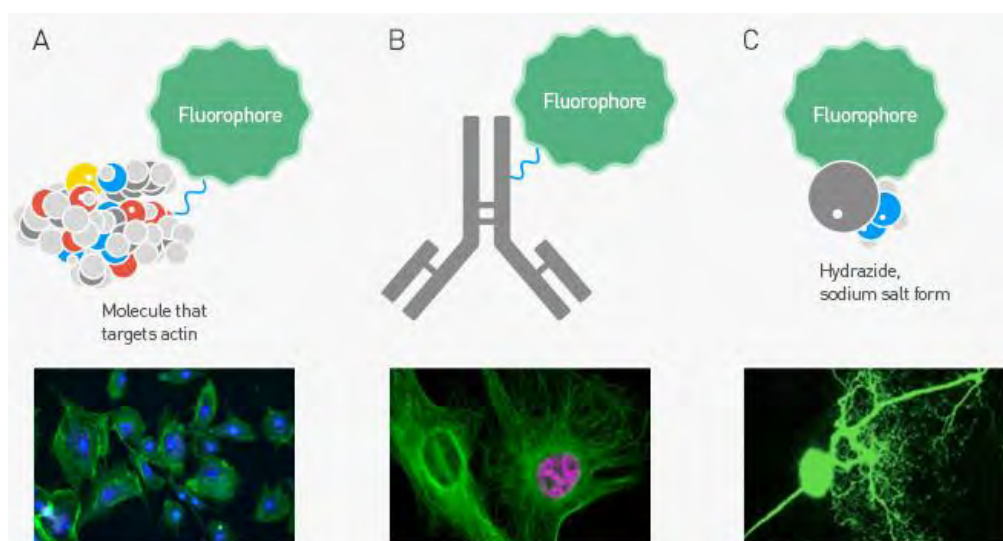


Figure 3.27 Labelling fluorophores to biostructures. Reproduced from reference ⁴²⁹.

If instead of a fluorescent tag a PS is used it might function as a theranostic labels.^{430,431} These compounds are fluorescent and able to generate $^1\text{O}_2$, therefore they can be used to signal the location of the labelled-biomolecule and generate ROS at the site.⁴³² Among them, chromogenic theranostic labels, which after conjugation to biomolecules undergo a substantial shift in the absorption and fluorescence spectra, are highly desired to differentiate the covalently bound from those that are not.^{431,433,434}

In this section, we have derivatized the phenalenone core in order to synthesize a theranostic tag and studied its photophysical properties and its capacity to generate $^1\text{O}_2$.

3.3.8.2. Experimental procedures

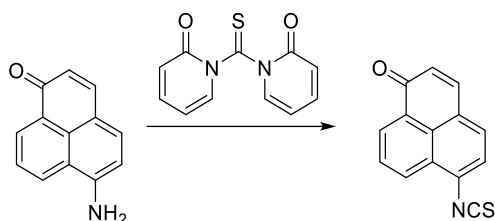
3.3.8.2.1. Synthesis of 6-isothiocyanate-phenalenone (PN-NCS)

To a solution of 6-aminophenalenone (5.7 mg, 0.035 mmol) in CH₂Cl₂ (8 mL) was added 1,1'-thiocarbonyldi-2(1H)-pyridone (23 mg, 3 eq, 0.10 mmol). The mixture was stirred 16 h at room temperature. The solvent was evaporated and the mixture was purified by chromatography with silica column eluting with a 1:1 mixture of ethylacetate and cyclohexane to provide 6-isothiocyanate-phenalenone (PN-NCS) as an orange product (4.5 mg, 0.030 mmol, 75 %; Scheme 3.19).

¹H-NMR (CDCl₃): δ 8.67 (dd, J = 7.4, 1.2 Hz, 1H), 8.48 (dd, J = 8.3, 1.2 Hz, 1H), 7.93-7.84 (m, 1H), 7.74-7.65 (m, 2H), 7.50 (d, J = 7.7 Hz, 1H), 6.72 (dt, J = 9.8, 0.4 Hz, 1H).

¹³C-NMR (CDCl₃): δ 185.2, 141.0, 131.8, 131.5, 131.1, 129.9, 129.8, 129.3, 128.4, 128.4, 128.3, 127.2, 124.4.

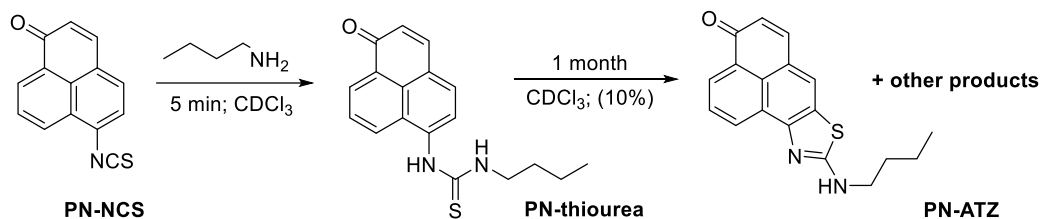
IR (KBr disk): 3087, 2068, 1637, 1585, 1573, 1242, 854, 767 cm⁻¹.



Scheme 3.19 Synthesis of 6-isothiocyanate-phenalenone.

3.3.8.3. Reactivity and photochemical properties of ¹O₂ phenalenone-based label

6-isothiocyanatephenalenone (PN-NCS) was synthesized from 6-aminophenalenone using 1,1' thiocarbonyldi-2(1H)-pyridone⁴³⁵. PN-SCN can react efficiently with different aliphatic amines (n-butylamine and morpholine) to achieve the corresponding thioureas (Scheme 3.20).



Scheme 3.20 Reactivity of PN-NCS against aliphatic amines.

Under the same experimental conditions PN-NCS does not react with aromatic amines (i.e. aniline). Even more, at room temperature after 1 month in solution the generated thiourea can further cyclize to generate a aminothiazolo[4,5-c]phenalenone (PN-ATZ) with around 10% yield. This cyclization has been followed by ¹H-NMR (Figure 3.28) and confirmed by the disappearance of H-5 signal and the change in the multiplicity of H-4 from a doublet to a singlet.

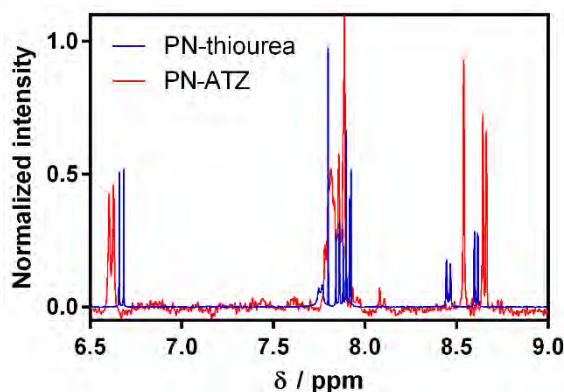


Figure 3.28 $^1\text{H-NMR}$ spectra for PN-thiourea and PN-ATZ in acetone- d_6 .

The photophysical properties of PN-thiourea and PN-ATZ have been characterized (Figure 3.29). A red-shift in the absorption spectra for PN-thiourea in comparison with bare PN could be observed. It is highly interesting because PN-thiourea has its absorption band in the blue region instead of ultraviolet. Moreover, like PN, PN-thiourea is not fluorescent ($\Phi_F < 10^{-3}$) and is still capable to generate $^1\text{O}_2$ ($\Phi_\Delta = 0.70$ in methanol).

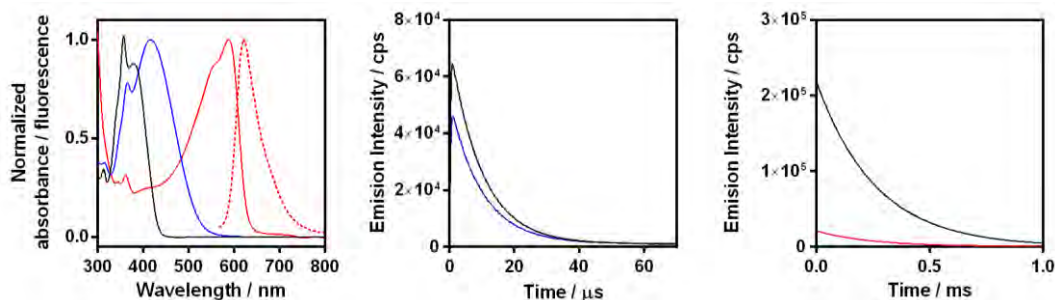


Figure 3.29 Photophysical properties of PN (black), PN-thiourea (blue) and PN-ATZ (red). Left: Absorption and fluorescence spectra. Middle: Time-resolved $^1\text{O}_2$ phosphorescence of optically matched solutions of PN (black; $\Phi_\Delta = 1^{262,306,307}$) and PN-thiourea (blue) in CH_3OH . $\lambda_{\text{exc}} = 355$ nm. Right: Time-resolved $^1\text{O}_2$ phosphorescence of optically matched solutions of TMPyP (black; $\Phi_\Delta = 0.74^{436,437}$) and PN-ATZ (red) in deuterated- CH_3OH . $\lambda_{\text{exc}} = 532$ nm.

For PN-ATZ, the red-shift is even stronger. PN-ATZ absorbance spectrum presents a maximum at 588 nm. PN-ATZ, although it conserves the PN core, is highly fluorescent ($\Phi_F = 0.78$) and has a much lower capacity to generate $^1\text{O}_2$ ($\Phi_\Delta = 0.07$ in deuterated-methanol).

3.3.9. Naturally-occurring anthraquinones

(Adapted from: J. Marioni,⁺ **R. Bresolí-Obach**,⁺ M. Agut, L.R. Comini, J.L. Cabrera, M.G. Paraje, S. Nonell and S.C. Nuñez-Montoya, On the mechanism of *Candida tropicalis* biofilm reduction by the combined action of naturally-occurring anthraquinones and blue light, *PLoS ONE*, **2017**, *12*, e0181517.; ⁺These authors contributed equally to this work.)

The results reported in this section have been carried out in collaboration with the Universidad Nacional Córdoba (Argentina).

3.3.9.1. Introduction

Heterophyllaea pustulata Hook f. is plant originary from South-America that grows in the Andean region of northwestern Argentina and Bolivia between 2500 and 3000 m above sea level. It is popularly locally known as “cegadaera”, “ciegadaera” o “saruera” (Figure 3.30). Natural intoxication by “cegadaera” has been reported for rabbit, equine, bovine and goat-like individuals as dermatitis and blindness in severe cases, without direct death of the animals confirmed.⁴³⁸

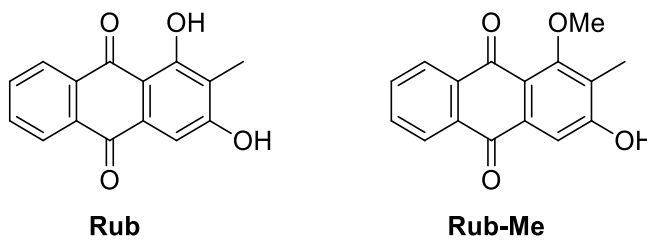


Figure 3.30 Left: Photograph of *Heterophyllaea pustulata* Hook f. plant. The photograph is reprinted from reference ⁴³⁹. Right: Chemical structure of Rubiadin (Rub) and Rubiadin-1-methyl ether (Rub-Me).

In the 2000s, Nuñez-Montoya *et al* identified the phototoxic compounds in *H. pustulata*. They found that 9,10-anthraquinone derivatives (AQs; Figure 3.30) were the predominant metabolites, whereas a minority of other structures were present belonging to the flavonoid and iridoid groups.^{440,441} Afterwards, as it could have been expected based on their structure,⁴⁴² these naturally-occurring AQs presented photosensitizing properties of $^1\text{O}_2$ and/or $\text{O}_2^{\bullet-}$.^{443,444} They used *H. pustulata* plant extracts or the corresponding purified AQs in order to photoinactivate Herpes Simplex Virus Type I,⁴⁴⁵ *Candida tropicalis*,^{446,447} or MCF-7 breast cancer.⁴⁴⁸

We set out to identify the reactive intermediates involved in the photo-induced *C. tropicalis* biofilm viability reduction by two natural AQs: rubiadin (Rub) and rubiadin-1-methyl ether (Rub-Me). Under that purpose we identify, if the *C. tropicalis* biofilm photoinactivation is mediated by type-I or type-II mechanism using spectroscopic techniques.

3.3.9.2. Experimental procedures

3.3.9.2.1 Extraction and purification of anthraquinones used

Rub and Rub-Me were purified from benzene extracts of *H. pustulata* using a methodology described previously in Universidad de Cordoba (Argentina).⁴⁴¹ The purity was 94% for both AQs, as established by HPLC analysis.⁴⁴⁶

3.3.9.2.2 *Candida tropicalis* biofilm growth

Stock solution of *Candida tropicalis* NCPF 3111 (*C. tropicalis*; National Collection of Pathogenic Fungi, Bristol, UK, strain N° 2), suspended in Sabouraud dextrose broth (SDB) with 10% glycerol (cryoprotectant), was kept at -80 °C. In order to ensure purity and viability of yeasts before its use, they were plated in Sabouraud dextrose agar (SDA) and then were incubated overnight in Falcon tubes at 37 °C with SDB.⁴⁴⁷

Biofilm formation was achieved adapting the method of O'Toole and Kolter using flat-bottomed 96-well microplates.⁴⁴⁹ Strain suspension (1×10^7 cells/mL) in SDB was inoculated in pre-treated microplates with 50% (v/v) Fetal Bovine Serum, and then were incubated 90 minutes at 37 °C. After removing the non-adhered cells and adding fresh culture medium, the incubation of microplates was resumed at the same temperature during 48 h without stirring to obtain a dense biofilm.

3.3.9.2.3. Spectroscopic measurements of *C. tropicalis* biofilms

Dense biofilms were developed on a square glass plate (1x1 cm) in a 24-well microplate and then 56 µM AQs were added dissolved in DMSO. Final DMSO concentration was kept always below 1%. After the incubation period, the supernatants were removed, the biofilms were washed twice with sterile PBS and the glass plates were introduced vertically in the spectroscopic cuvettes at 45 degrees relative to the excitation light beam. Then the appropriate aqueous buffer (PBS or d-PBS) was carefully added to fill the cuvette. Controls containing sessile cells of *C. tropicalis* without anthraquinones in d-PBS were performed. In agreement with the report by Berry *et al*, d-PBS had no effect on the biofilm biomass compared to PBS.⁴⁵⁰ Spectroscopic measurements were carried out without stirring to prevent mechanically disturbing the biofilms.

3.3.9.3. Photophysical properties of naturally-occurring anthraquinones

The absorption spectra of Rub and Rub-Me in chloroform, PBS, planktonic yeast and biofilms of *C. tropicalis* are shown in Figure 3.31. The absorption spectra in chloroform should be representative for anthraquinones that are not aggregated, whilst in PBS anthraquinones are completely aggregated. The spectra in PBS and planktonic yeast were similar, with broader, red-shifted bands relative to CHCl_3 solutions. The red-shift is more pronounced for Rub-Me. The spectra in biofilms showed a behaviour intermediate between CHCl_3 and PBS. Once it is known where Rub and Rub-Me absorbed and their aggregation degree in planktonic yeast and biofilms of *C. tropicalis*, it is possible to detect if they are able to generate $\text{O}_2^{\cdot-}$ and/or $^1\text{O}_2$ under such conditions.

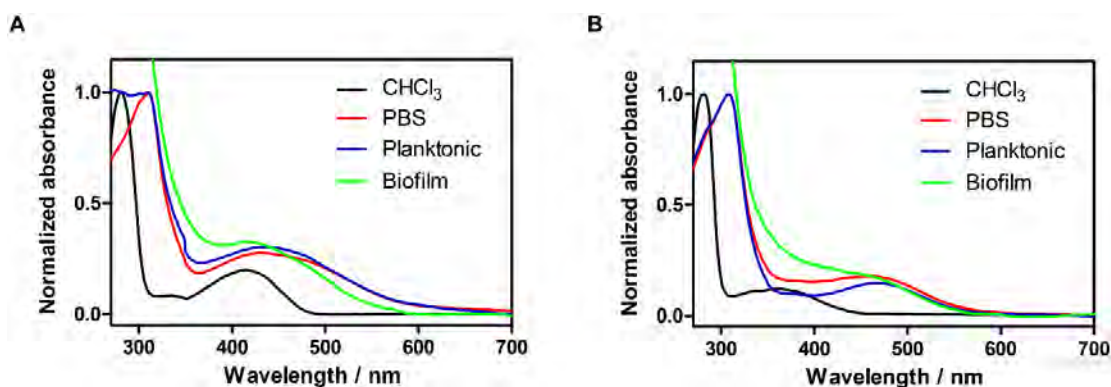


Figure 3.31 Absorption spectra of rubiadin (A; Rub) and rubiadin 1-methyl ether (B; Rub-Me) in CHCl_3 , PBS, planktonic yeast and biofilms of *C. tropicalis*.

For detecting the generation of $\text{O}_2^{\cdot-}$, it is necessary to study the formation of the triplet state, the ketyl radical and the radical anion of the AQs (^3AQ , AQ^{\cdot} and $\text{AQ}^{\cdot-}$ respectively) by transient absorption spectroscopy in CHCl_3 and biofilms (Figures 3.32, 3.33).

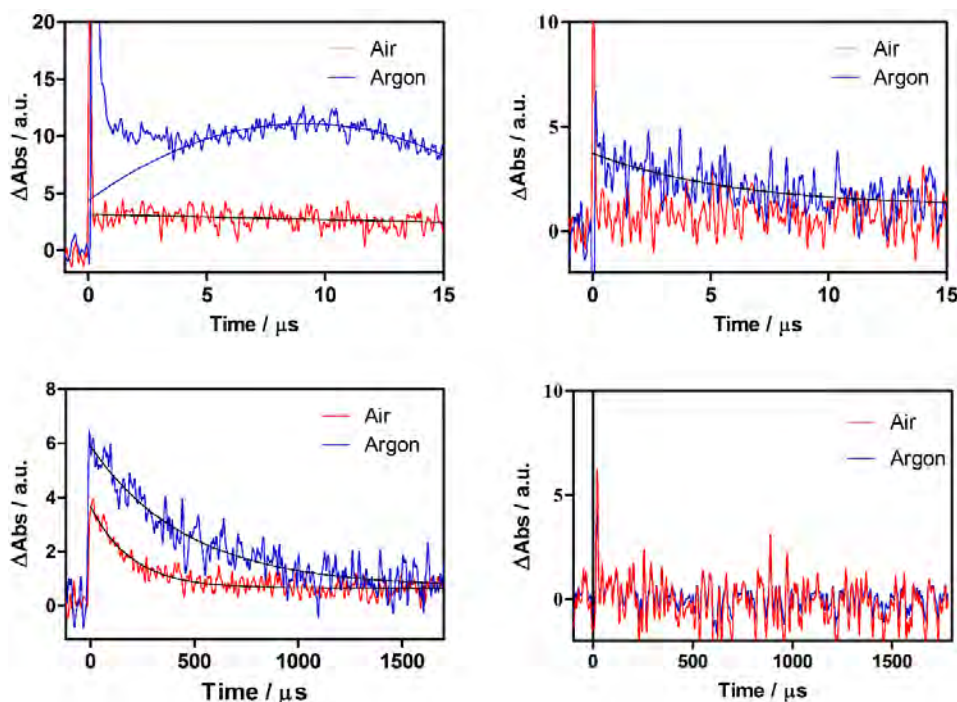


Figure 3.32 Transient absorption of Rub-Me in argon- and air saturated- CHCl_3 solutions. Signals recorded at 550 nm (left) correspond to $\text{AQ}^{\cdot-}$, whereas signal at 675 nm (right) correspond to ^3AQ .

The corresponding wavelengths were 675 nm (^3AQ), 450 nm (AQ^*) and 550 nm ($\text{AQ}^{\bullet-}$).⁴⁵¹ It was not possible to detect AQ^* or $\text{AQ}^{\bullet-}$ for Rub in any of the above systems, whereas large $\text{AQ}^{\bullet-}$ signals could be observed for Rub-Me in CHCl_3 solutions (Figure 3.32). In argon-saturated CHCl_3 the transient rose with lifetime 4 μs and lived 450 μs , whereas in air-saturated solutions the rise was much faster and the lifetime was decreased to 150 μs . This indicates that $\text{AQ}^{\bullet-}$ is formed from ^3AQ and $^3\text{O}_2$ quenches it, presumably leading to the production of $\text{O}_2^{\bullet-}$.

In the case of biofilms, $\text{AQ}^{\bullet-}$ could be detected only when the cells were incubated for 3 hours (Figure 3.33). The lifetime of the transient was 170 μs in air-saturated samples. No evidence for the presence of ^3AQ in biofilms could be derived from transient absorption measurements (Figure 3.33).

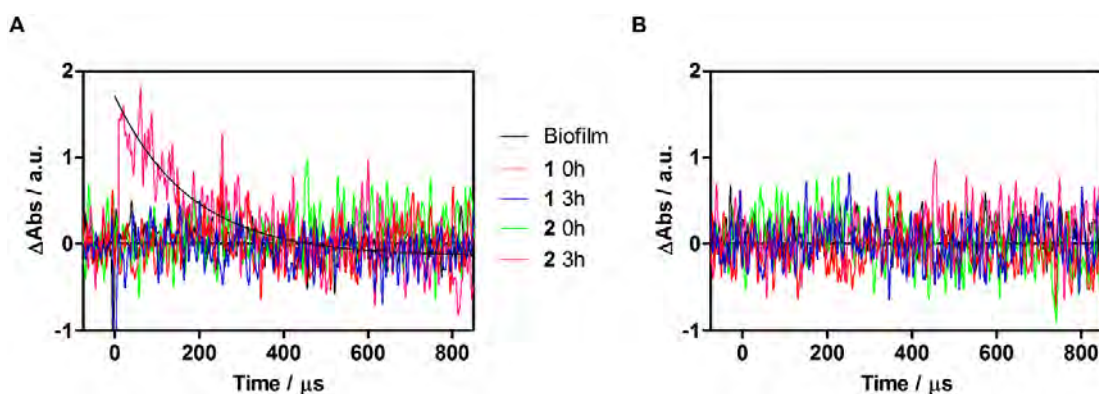


Figure 3.33 Transient absorption of air saturated- *C. tropicalis* biofilms with Rub, Rub-Me at $t = 0$ and 3 hours of incubation and biofilm alone. Signals recorded at 550 nm correspond to $\text{AQ}^{\bullet-}$ (A), whereas signal at 675 nm correspond to ^3AQ (B).

$^1\text{O}_2$ has been studied by detecting its near-infrared phosphorescence. Clear signals could be observed for Rub and Rub-Me in CHCl_3 and PBS. The ϕ_{Δ} values in CHCl_3 (0.34 and $<10^{-3}$ for Rub and Rub-Me, respectively) were already reported by Nuñez-Montoya *et al.*^{443,444} In PBS, they were $\phi_{\Delta} < 0.01$ for Rub and $\phi_{\Delta} = 0.02$ for Rub-Me.

Luminescence signals could also be recorded in biofilms (Figure 3.34) and they were assigned to $^1\text{O}_2$ based on the spectral distribution (disappearance of the signal at 1325 nm, where $^1\text{O}_2$ shows almost no phosphorescence), and on the lengthening of the decay lifetime upon solvent deuteration.

Observation of $^1\text{O}_2$ indicates that ^3AQ is indeed formed, even if the concentration is too small to produce a transient absorption signal. By comparing the intensity of the phosphorescence signals for the two AQs, it is apparent that Rub-Me generates approximately threefold more $^1\text{O}_2$ than Rub in biofilms (Figure 3.34).

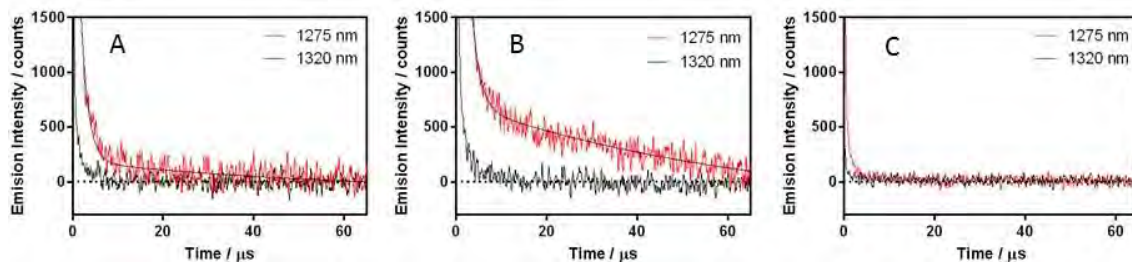


Figure 3.34 $^1\text{O}_2$ kinetics of Rub (A), Rub-Me (B) and no anthraquinone (C) in *C. tropicalis* biofilm observed at 1275 nm and at 1325 nm (negative control) in biofilms incubated with dPBS.

Simultaneously in the University of Cordoba, they showed that biofilms incubation with AQs and exposure to light induced higher levels of $\text{O}_2^{\bullet-}$. Moreover, biofilm viability is not reverted when it is incubated with sodium azide (a good $^1\text{O}_2$ scavenger)¹²⁹ but Tiron (a good $\text{O}_2^{\bullet-}$ and $\bullet\text{OH}$ scavenger)⁴⁵² reduces significantly anthraquinones phototoxicity (Figure 3.35).

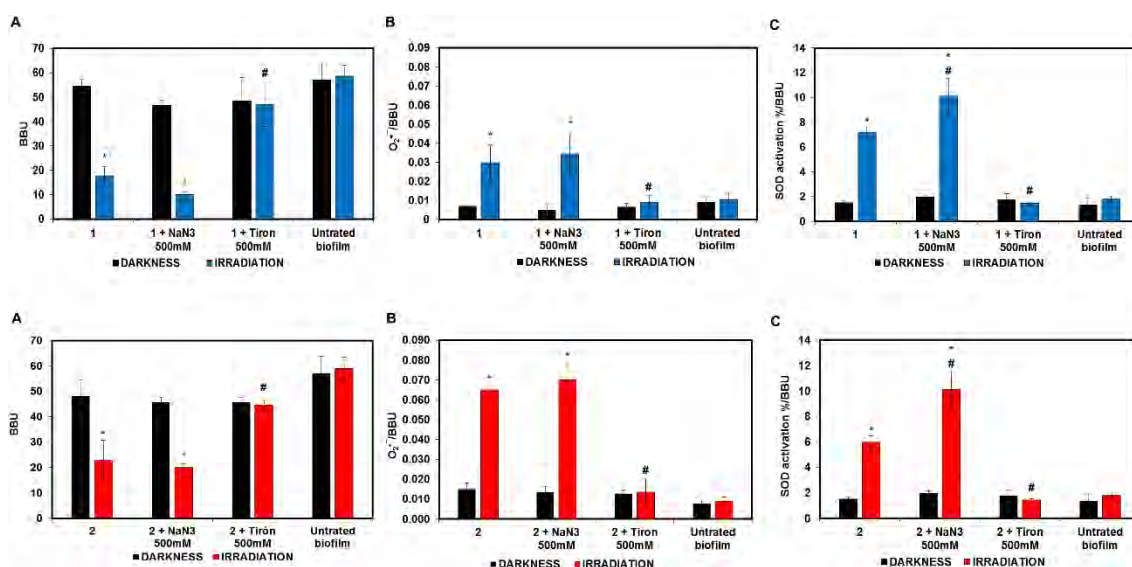


Figure 3.35 (A) Photo-induced *C. tropicalis* biofilm reduction by Rub (top) and Rub-Me (bottom) in the presence of the specific ROS quenchers sodium azide and Tiron. (B) Superoxide radical production in *C. tropicalis* by AQ alone and in the presence of quenchers. (C) SOD activation in *C. tropicalis* biofilms by AQ alone and in the presence of quenchers. This data has been obtained by Dr. Juliana Marioni and Dr. Susana C. Núñez Montoya in Universidad Nacional de Córdoba (Córdoba, Argentina).

From these cellular experiments together with our spectroscopic experiments, it can be concluded that prompt $\text{O}_2^{\bullet-}$ produced by photosensitization, but not $^1\text{O}_2$, is the main responsible for the perturbation of the oxidative balance of the cell, which leads to *C. albicans* cellular death.

3.4. Nanoparticles as delivery agents for photosensitisers

3.4.1. Why nanoparticles?

Nanoparticles (NPs) are systems whose size can vary from a few to hundreds of nanometers.^{453,454} Generally their size is designed according to its purpose. NPs designed for drug delivery can have different sizes, shapes and can be made of different materials. The physicochemical characteristics of each NP determine its loading capacity, the stability of both the NPs and the drug, its release profile, and its targeting ability.^{455–457}

The most common NPs used for drug delivery systems are micelles, liposomes, metallic, polymeric or silica scaffolds.^{458,459} When NPs are introduced in medical applications, not only their composition but also their physical properties like size, polarity or ζ -potential are important factors that determine their activity.^{457,460}

NPs containing PS have some advantages over free PS.^{212–214} Lower concentrations of PS are needed, the possibility of drug resistance, is reduced and selectivity is enhanced. In addition, the NP matrix is non-immunogenic, prevents the dimerization of the PS and the NP can increase the solubility of the PS in water or biological media.⁴⁶¹ Different types of NPs have already been used as PS carriers for PDT^{213,462–464} and four main types of interaction between the PS and the NP have been reported (Figure 3.36):

- **PS embedded or encapsulated inside the NP:** These NPs have been used to deliver the PS into the desired cell and improve its biological activity. Biocompatible and biodegradable matrices such as liposomes, poly(lactic-co-glycolic acid), or cyclodextrins are considered of particular interest because they allow the use of PDT in medical situations.^{465,466}
- **PS covalently-bound onto the surface of the NP:** When the PS is linked to the NP it is not uniformly distributed over the cell but in clusters, thus it locally generates ROS leading to a higher local effect than the free PS even if the overall concentration might be lower.^{467,468} Moreover, this strategy allows to bind insoluble PS to water-soluble NPs.
- **PS adsorbed onto the surface of NP:** This system is simpler than the previous category but has the disadvantage that the PS can leach under some conditions.⁴⁶⁹
- **NPs that act as PS:** One prime example are the porphysomes, spherical nanovesicles that are formed from self-assembled porphyrins.^{470,471} Once uptaken by cells, they release the porphyrin units that can then act as PS. Other examples could be photoactive inorganic nanoparticles (i.e. titanium dioxide),⁴⁷² carbon-based nanostructures (i.e. carbon dots)⁴⁷³ or metallic NPs (i.e. gold or silver nanoclusters).⁴⁷⁴

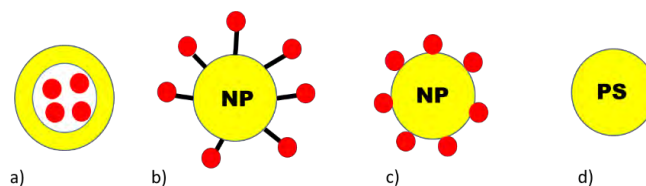
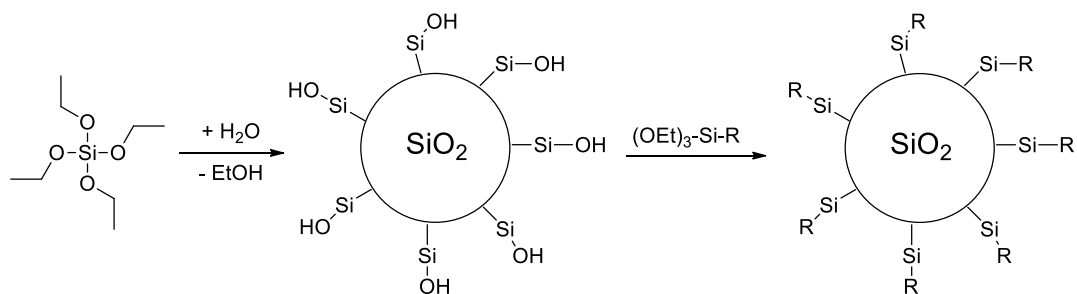


Figure 3.36 Schematic representation of the different interactions NP-PS. a) PS embedded or encapsulated, b) PS covalently linked onto the surface, c) PS adsorbed, d) NPs as the PS.

3.4.2. Silica nanoparticles

Silicon dioxide (SiO_2 ; also known as silica from the Latin *Silix*) is an attractive material for photomedicine because it is optically transparent, chemically inert, mechanically stable and fairly biocompatible.⁴⁵⁷ Furthermore, the surface of silica is easily functionalizable by grafting its surface with different functional groups (Scheme 3.21).⁴⁷⁵ This easy surface functionalization is due to the presence of highly reactive silanol moieties on the surface.



Scheme 3.21 Synthesis of silica NPs and its further superficial derivatization, where R can be: $-\text{NH}_2$, $-\text{NHS}$, $-\text{NCO}$, $-\text{OH}$, $-\text{SH}$, $-\text{I}$, or $-\text{COOH}$ among others.

In the late 60s, Dr. Stöber developed a methodology to synthesize compact spherical NPs with uniform size, in the range between 50 nm to 2 μm in diameter.⁴⁷⁶ In all the synthetic procedures, the most important steps are the hydrolysis and the polycondensation of the tetraalkoxysilane precursors.

The next step in complexity is the synthesis of mesoporous silica NPs (MSNP). Porosity increases the specific surface of the NPs and allows the permeability of entrapped drugs and small molecules. Although they were patented in 1971,⁴⁷⁷ MSNP remained almost unnoticed for more 20 years. They were rediscovered by two independent research groups, which allowed to synthesize porous silica material with well-ordered structure by a highly reproducible method.^{478–480} Since then, many studies have investigated different parameters (i.e. temperature, pH, templating agent, reaction time) in order to finely tailor the silica morphology.^{481–483}

Other key parameters for MSNPs are their particle size and ζ -potential, which strongly influence cell membrane permeability and the fate of the NPs in the cell.^{484,485} As an example, in non-phagocytic cells the uptake is limited to NPs of diameter smaller than a few hundred of nanometers, whilst phagocytic cells are capable to internalize particles up to a few microns.⁴⁸⁶

MSNP have emerged as promising vectors for PDT since binding of a PS to a MSNP can increase its $^1\text{O}_2$ generation efficiency.^{487–489} Finally, it is possible to further functionalize MSNP surface with different targeting groups in order to gain higher selectivity.⁴⁹⁰

3.4.3. Methylene Blue-loaded MSNP

(Adapted from: O. Planas,⁺ **R. Bresolí-Obach**,⁺ J. Nos,⁺ T. Gallavardin, R. Ruiz-González, M. Agut and S. Nonell, Synthesis, photophysical characterization, and photoinduced antibacterial activity of methylene blue-loaded amino- and mannose-targeted mesoporous silica nanoparticles, *Molecules*, **2015**, *20*, 6284; ⁺These authors contributed equally to this work.)

3.4.3.1. MB history for PDT

In 1876, methylene blue (MB) was first synthesized by Heinrich Caro when he was working for BASF.⁴⁹¹ In those days, the chemical companies were interested in the discovery of new dyes to tint clothes. Until the discovery of synthetic dyes, only the wealthiest people could afford to buy natural dyes for their clothes and the diversity of colours was slight. As example, why is the mozzetta of cardinals scarlet? and why is the mozzetta of bishops purple? The reason is not ecclesiastical, is monetary. The dyes used for tinting their mozzettas were carminic acid and indigo respectively and the first one was much more expensive than the second one.

For that reason, in the first years after its synthesis MB was only used as dye. MB has been widely used to distinguish Gram-positive and Gram-negative bacteria,⁴⁹² to stain living organisms,⁴⁹² to treat methemoglobinemia.⁴⁹³ MB as PS has been used for a large variety of applications including energy conversion and PDT.⁴⁹⁴ It belongs to the phenothiazinium class of compounds. Its characteristic blue colour is caused by a strong absorption band in the red region of the spectrum with molar absorptivity around $8.5 \times 10^4 \text{ M}^{-1}\text{cm}^{-1}$ at its maximum.⁴⁹⁵ Regarding to its photosensitizing properties, it is useful due to its high $\Phi_{\Delta} \sim 0.5$ in polar solvents.

Although MB has been approved for its therapeutic use by the United States Food and Drug Administration (FDA), the use of MB has been limited by its lack of activity when used *in vivo*.^{201,496} The weak MB pharmaceutical effect results in part from poor eukaryotic cellular internalization and its easy reduction to the non-coloured leukomethylene blue in biological systems.

However, these drawbacks are minor against bacteria.²⁰⁰ Exactly, MB is one of the most commonly studied antimicrobial PS in the literature. It has received regulatory approval for aPDT of dental infectious diseases like periodontitis or caries,^{497,498} and is under clinical investigation for nasal decontamination and chronic sinusitis in some countries. As a result of its excellent photo-antimicrobial activity, several MB derivatives with different lipophilicity have been synthesized and tested against different bacteria.⁴⁹⁹ Among them, the most used are the so-called New Methylene blue and Toluidine Blue.⁵⁰⁰

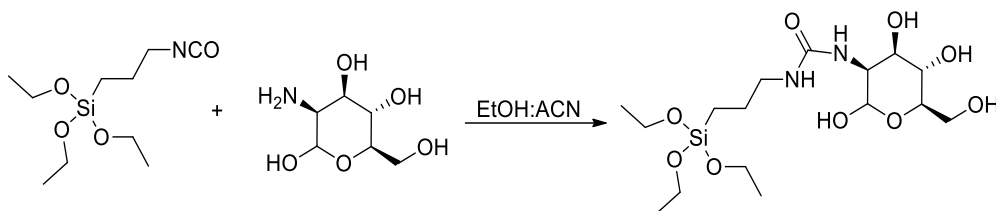
We therefore set out to investigate the effectiveness of MB-encapsulated targeted MSNPs in the inactivation of two Gram-negative bacteria. Specifically, we have decorated MSNP with two different targeting motifs, amino groups (AMSNP) and mannose sugars (MMSNPs), loaded them with MB, and evaluated their photophysical properties and photodynamic activity against *E. coli* and *P. aeruginosa*.

3.4.3.2. Experimental part

3.4.3.2.1. Synthesis of N-(D-Mannose)-N'-(3-(triethoxysilyl)propyl)-urea and 3-(Triethoxysilyl)propyl isocyanate in 1:3 Molar Ratio.

3-(triethoxysilyl)propyl isocyanate (212 mg, 0.81 mmol) was added to a solution of D-mannosamine hydrochloride (58 mg, 0.27 mmol) and Na₂CO₃ (32 mg, 0.30 mmol) in a mixture of 4 mL of acetonitrile and 2 mL of EtOH. The solution was stirred for 5 h at room temperature and solvent was removed under reduced pressure. Finally, the crude was diluted with 2 mL of EtOH and used without further purification (Scheme 3.22).

IR (KBr disk): 3431, 2929, 1652, 1402, 1076 cm⁻¹.



Scheme 3.22 Synthesis of N-(D-Mannose)-N'-(3-(triethoxysilyl)propyl)-urea.

3.4.3.2.2. Synthesis of the nanoparticles.

Synthesis of MSNP. One hundred twenty microliters of ammonia solution (30% w/w, 1.9 mmol) were added to a solution of water (65 mL), EtOH (11.5 mL), and CTAC (7.97 mmol). The mixture was heated at 48 °C and stirred at 1000 rpm for 30 min. Then, 7.3 mL of TEOS (32.7 mmol) were added dropwise and the reaction was left stirring at 48 °C for 2 h. The crude was left aging for 24 h at room temperature. Afterwards, 20 mL of HCl (37% w/w) were added under stirring and kept at room temperature for 12 h. MSNP were obtained after centrifugation at 6000 rpm for 30 min and were put in suspension in EtOH (ultrasounds). This extraction procedure was repeated 3 times and the final nanoparticles were stored in 95 mL of EtOH at room temperature.

Synthesis of AMSNP. Nineteen milliliters of MSNP were centrifuged for 30 min at 6000 rpm and the pellet suspended in 2 mL of EtOH under sonication. Next, 2 mL of a solution of 3-(triethoxysilyl)propyl isocyanate (212 mg, 0.81 mmol) were added dropwise under vigorous stirring (1000 rpm). The mixture was kept at 33 °C for 24 h and centrifuged at 6000 rpm for 30 min. The solvent was removed and the solid was suspended with 19 mL of water 3 times. Finally, the AMSNPs were washed 3 times with 19 mL of EtOH and stored at room temperature.

Synthesis of MMSNP. Nineteen milliliters of MSNP were centrifuged for 30 min at 6000 rpm and the pellet suspended in 2 mL of EtOH under sonication. Next, 2 mL of the solution of N-(D-mannose)-N'-(3-(triethoxysilyl)propyl)- urea and 3-(triethoxysilyl)propyl isocyanate in a 1:3 molar ratio were added dropwise under vigorous stirring (1000 rpm). The mixture was kept at 33 °C for 24 h and centrifuged at 6000 rpm for 30 min. The solvent was removed and the solid was suspended with 19 mL of water 3 times. Finally, the MMSNPs were washed 3 times with 19 mL of EtOH and stored at room temperature.

Loading of MB onto MSNP, AMSNP, or MMSNP. Two milliliters of a stock 1-mM MB solution in ethanol were added to 19 mL of each set of the nanoparticle suspensions. The mixture was stirred at 800 rpm for 48 h and the nanoparticles were isolated through repeated centrifugations. Several washes with EtOH were performed until a white supernatant was achieved.

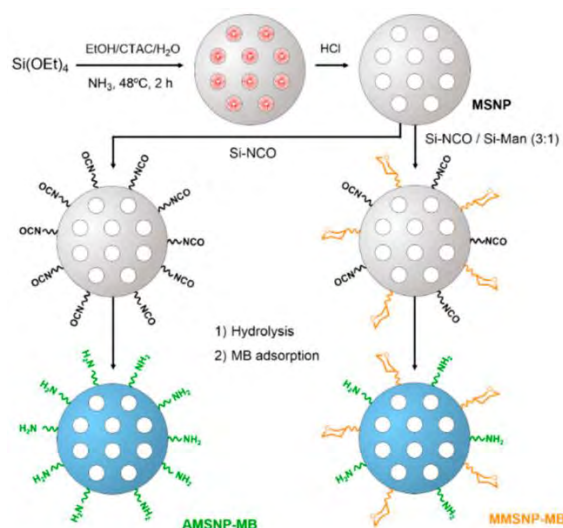
AMSNP-MB: Size: 200 nm; ζ -potential: -25 mV.

MMSNP-MB: Size: 180 nm; ζ -potential: -20 mV.

3.4.3.2.3. Microbial Strains and Growth Conditions

Escherichia coli (*E. coli*; CECT 101) and *Pseudomonas aeruginosa* (*P. aeruginosa*; CECT 116) were obtained from the Spanish Type Culture Collection (CECT, Paterna, Spain). Bacterial cells were grown overnight in sterile tryptic soy broth at 37 °C. Stock inoculum suspensions were prepared in LB and adjusted to an OD₆₀₀ of 0.4 for *E. coli* and 0.6 for *P. aeruginosa* (equivalent to ca. 10⁸ colony-forming units/mL).

3.4.3.3. Results



Scheme 3.23 Synthesis of MSNP, AMSNP-MB, and MMSN-MB.

The procedure for the synthesis of mesoporous silica nanoparticles (MSNPs), as well as their functionalization with amino- and mannose-moieties, is illustrated in scheme 3.23. MSNPs were prepared via the sol-gel process under high dilution conditions. Afterwards, the bare MSNP were decorated with external amines or d-mannose with the corresponding silanes. Finally, MB was adsorbed to the two MSNP. The modified MSNPs were characterized by their size and ζ -potential as well as by infrared-spectroscopy, which confirms the conjugation of d-mannose by an urea bond.

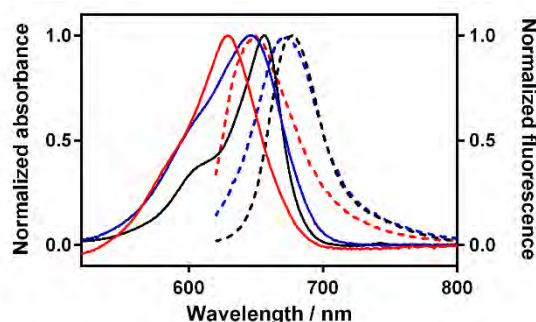


Figure 3.37 Absorption (solid line) and emission (dashed line) spectra of free MB (A; black), AMSNP-MB (B; red), and MMSN-MB (C; blue) in EtOH.

Once the MSNPs are synthesized and derivatized, it has been studied its photophysical properties. Figure 3.37 shows the visible absorption and fluorescence spectra of free MB, AMSNP-MB, and MMSN-MB in EtOH. The spectra of AMSNP-MB and MMSN-MB are blue-shifted relative to those of free MB. This indicates that all MB is adsorbed on the surface of the nanoparticles, where it experiences a different microenvironment. Consistent with this, the relative intensity between the shoulder and the maximum of the absorption bands also varies from compound to compound, leading to less-structured bands for AMSNP-MB and MMSN-MB.

Time-resolved fluorescence decays were recorded at the maximum of the emission bands. While the decay was monoexponential for free MB, biexponential decays were observed for MB adsorbed onto the nanoparticles, which suggests two different

populations of the PS. The relative amplitudes of the two components are given in table 3.7 and it is noteworthy that the dominant emission is the one with the longest lifetime, roughly twice as long as that observed for free MB.

Table 3.7 Decay kinetics and relative intensity of all tested nanoparticles in ethanol.

	Component	τ_s / ns	Amplitude (%)
MB	1	0.8	100
	2	---	---
AMSNP-MB	1	0.8	33
	2	1.5	67
MMSNPs-MB	1	0.7	13
	2	1.4	87

Pulsed-laser irradiation of MB, AMSNP-MB, and MMSNPs-MB suspended in ethanol produced clear time-resolved $^1\text{O}_2$ phosphorescence signals (Figure 3.38). The $^1\text{O}_2$ signal for MB grew with a lifetime of 0.2 μs and decayed monoexponentially with a time constant of 15 μs . An additional rise component was needed to fit the data for MB associated to the MSNPs. Specifically, the $^1\text{O}_2$ signal for AMSNP-MB was found to show biphasic growth kinetics with time constants of 0.2 μs and 3.3 μs , respectively, and decayed monoexponentially with a time constant of 26 μs (Figure 3.38A). The lifetimes were slightly longer for MMSNPs-MB: 0.2 μs , 4.6 μs , and 34 μs , respectively (Figure 3.38B).

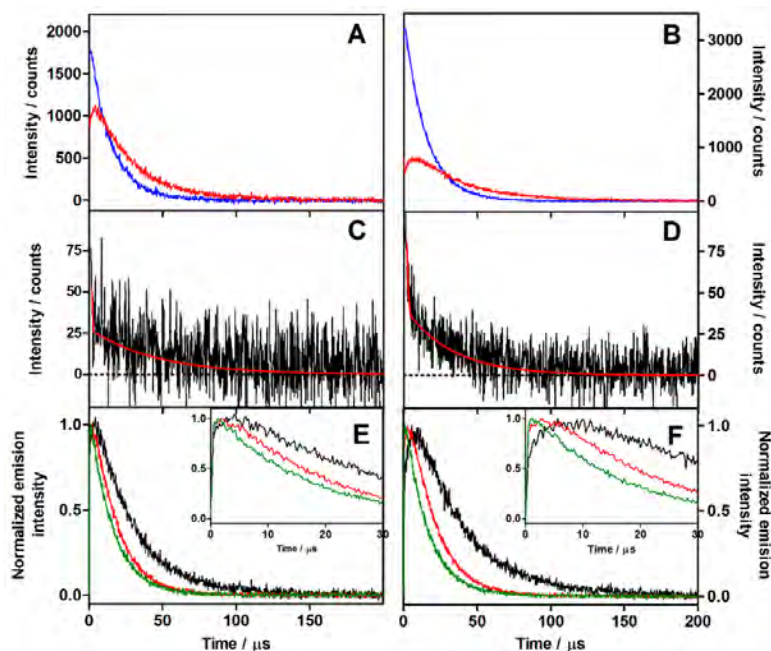


Figure 3.38 (A) Time-resolved $^1\text{O}_2$ phosphorescence ($\lambda_{\text{obs}} = 1270$ nm) of optically matched solutions of MB (blue) and AMSNP-MB (red). (B) Time-resolved $^1\text{O}_2$ phosphorescence of optically matched solutions of MB (blue) and MMSNPs-MB (red) at 532 nm. (C) Time-resolved phosphorescence emission at 1110 nm of AMSNP-MB. (D) Time-resolved phosphorescence emission at 1110 nm of MMSNPs-MB. (E) Normalized time-resolved $^1\text{O}_2$ phosphorescence of AMSNP-MB in air (black) oxygen saturated (red) and in 100 mM acetic acid aerated-solution (green). (F) Normalized time-resolved $^1\text{O}_2$ phosphorescence of MMSNPs-MB in air (black), oxygen saturated (red), and in 100 mM acetic acid aerated-solution (green). $\lambda_{\text{exc}} = 532$ nm.

In order to assign the observed lifetimes, additional emission decays were recorded at 1110 nm, where the phosphorescence from MB's triplet state can be monitored independently. The signal was found to decay biexponentially with time constants 0.2 μs and 24 μs for AMSNP-MB, and 0.2 μs and 35 μs for MMSNPs-MB (Figure 3.38C,D), which

match two of the three components observed in the $^1\text{O}_2$ phosphorescence signals at 1270 nm. This is consistent with two MB populations, as observed in the fluorescence experiments. Moreover, the very different lifetimes indicate very different exposure to oxygen for the two triplets. Comparison of the two individual components shows that the $^1\text{O}_2$ signal arises mainly from the longer-lived triplet in the nanoparticle's mesopores, where oxygen diffusion is more difficult, while the contribution from MB molecules bound to the outer surface of the NP is comparatively less important (less than 10%). This was confirmed by saturation of the suspensions with $^3\text{O}_2$, which completely eliminated the shortest component and reduced the lifetime of the longest one to 16 μs for AMSNP-MB and 18 μs for MMSNP-MB (Figure 3.38E,F).

Returning to the $^1\text{O}_2$ phosphorescence signals at 1270 nm, it must be concluded that the third component (3.3 μs for AMSNP-MB and 4.6 μs for MMSNP-MB) corresponds to the decay of $^1\text{O}_2$ in each suspension. The τ_{Δ} in the MSNPs suspensions (3.3 μs for AMSNP-MB and 4.6 μs for MMSNP-MB) is substantially shorter than in ethanol ($15.5 \pm 3.5 \mu\text{s}$).⁵⁷ Three contributions may account for this observation: (i) quenching by free amino groups on the nanoparticle surface,^{501,502} (ii) quenching by hydrogen-bonded water and silanol groups in the mesopores,^{503,504} and (iii) enhancement of these processes by the increased wall collision frequency in the narrow silica mesoporous channels.⁵⁰⁴ This was confirmed by addition of 100 mM acetic acid, which protonated the amino groups of the nanoparticle surface, rendering them cationic with the concomitant release of MB due to electrostatic repulsion. Under such conditions, the $^1\text{O}_2$ phosphorescence signals showed the same kinetics as those for free MB in ethanol (Figure 3.38E,F).

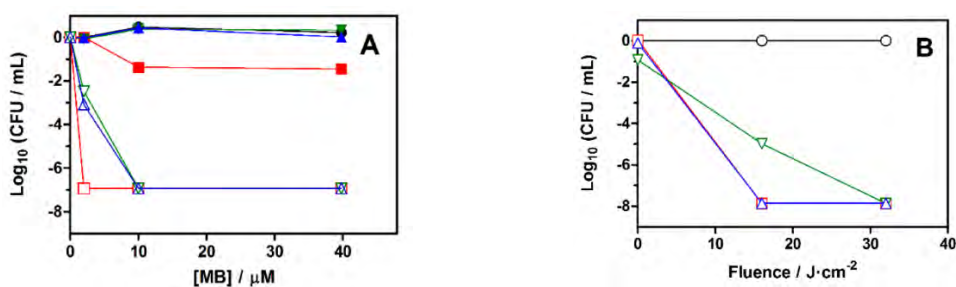


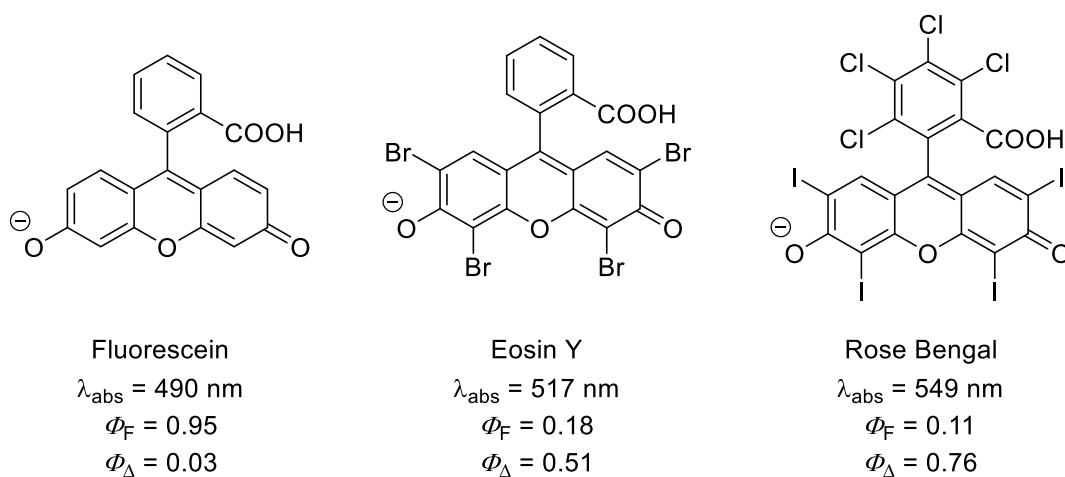
Figure 3.39 (A) Survival curves of *E. coli* incubated with different concentrations of MB in the dark (closed symbols) and after being exposed to a red light treatment (open symbols; $634 \pm 8 \text{ nm}$; 16 J/cm^2). (B) Survival curves of *P. aeruginosa* incubated with $10 \mu\text{M}$ MB after receiving increasing red light fluences ($634 \pm 8 \text{ nm}$; 7.8 mW/cm^2). Control experiments and cells incubated with free MB, AMSNP-MB, and MMSNP-MB are represented by circles, squares, inverted triangles, and triangles, respectively.

Finally, to assess the photo-antibacterial potential of the nanostructures, a series of microbiological assays were conducted on *E. coli* and *P. aeruginosa* suspensions. In the absence of light, MB, incubated for 30 min at $2 \mu\text{M}$ concentration, induced no dark toxicity to *E. coli* irrespective of the vehicle used for delivery. However, when the MB concentration was increased to $10 \mu\text{M}$, and even more so at $40 \mu\text{M}$, it was observed that free MB reduced the survival fraction by almost 2-log_{10} , whereas MB bound to the nanosystems was still devoid of any measurable dark toxicity (Figure 3.39). This is in line with previous results for other drug delivery systems.^{301,302} Irradiation of the bacteria pre-incubated with MB with a 16 J/cm^2 fluence of red light reduced their survival fraction in a concentration-dependent manner, MB in free form being more phototoxic than when associated to the nanoparticles. There was no appreciable difference between the two types of nanoparticles (Figure 3.39).

3.4.4. Rose Bengal-loaded MSNP

3.4.4.1. Importance of Rose Bengal

Rose Bengal (RB) is a xanthene derivative from fluorescein. It can be traced back to Basel, Switzerland, where in 1882, German patent No. 32584 was granted to Ghnem for a new family of wool dyes.⁵⁰⁵ Exactly, Ghnem took different halogens and added them to fluorescein to produce molecules with different colours. The addition of halogens shifted the absorbance spectrum to the red, reduced its Φ_F and increased its capability to produce 1O_2 (Scheme 3.24).⁵⁰⁶ This is coherent because in the end Br and I atoms are heavy atoms. It is known that the presence of such heavy atoms favours intersystem crossing towards fluorescence or internal conversion.^{14,507–509;q}



Scheme 3.24 Chemical structures of fluorescein, Eosin Y and Rose Bengal with their bibliographical λ_{abs} , Φ_F and Φ_{Δ} in water.^{506,510}

Since then, RB has been used widely for PDT against cancer and bacteria.^{468,511,512} Moreover, RB is approved for its use in clinics, but not in PDT field (i.e. its sodium salt is used in eye drops to stain damaged conjunctiva and corneal cells and thereby identify damage to the eye).^{513,514} Despite this, the use of RB in clinics for PDT should be easier to for its approval than other PS.

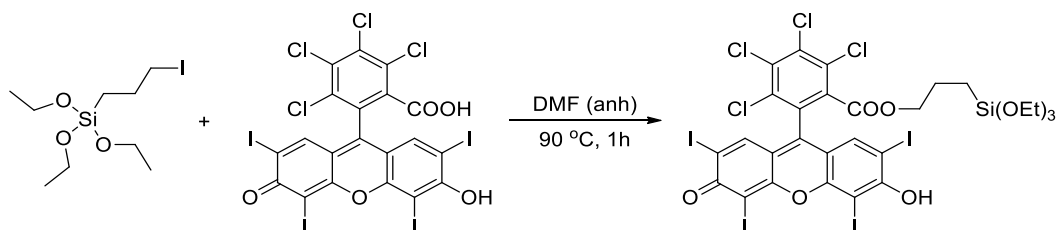
We therefore set out to investigate 1O_2 generation by MSNP which have been further functionalized for bonding RB (MSNP-RB). Specifically, we have synthesized a RB-silane which is grafted onto the MSNP surface. Finally, we have evaluated their photophysical properties and photodynamic activity against *S. aureus* and *E. coli*.

^q Transitions between pure spin states of different multiplicity are forbidden by the spin selection rule. There are, however, numerous examples in the literature of spin-forbidden or intercombinational transitions occurring in organic molecules. The occurrence of such transitions results from spin-orbit coupling, a relativistic phenomenon which induces a quantum mechanical mixing of states of different multiplicity. Thus, the spin states involved in an intercombinational transition are not pure states, but possess a small admixture of states of other multiplicities. Qualitatively, spin-orbit coupling arises from the interaction of the spin magnetic moment of an electron and the magnetic field resulting from the apparent motion of the nucleus. Since the magnitude of the nuclear magnetic field is directly proportional to the nuclear charge and hence to the atomic number, spin-orbit coupling increases with increasing atomic number.

3.4.4.2. Experimental

3.4.4.2.1. Synthesis of 3-(triethoxysilyl)propyl-2,3,4,5-tetrachloro-6-(6-hydroxy-2,4,5,7-tetraiodo-3-oxo-3H-xanthen-9-yl)benzoate.

Rose Bengal (2,3,4,5-tetrachloro-6-(6-hydroxy-2,4,5,7-tetraiodo-3-oxo-3H-xanthen-9-yl)benzoic acid; 47 mg, 0.05 mmol) was dissolved in 1 mL of anhydrous DMF. 3-iodopropyltriethoxysilane (30 mL, 0.153 mmol) was added and the solution was stirred during 1 hour at 90 °C. The crude was used without further purification (Scheme 3.25).



Scheme 3.25 Synthesis of 3-(triethoxysilyl)propyl-2,3,4,5-tetrachloro-6-(6-hydroxy-2,4,5,7-tetraiodo-3-oxo-3H-xanthen-9-yl)benzoate.

3.4.4.2.2. Synthesis of MSNP-RB

MSNP were synthesized as described in section 3.4.2.1.

Mesoporous silica nanoparticles (MSNP, 100 mg in 12 mL of ethanol) were added to 200 μ L of the previous reaction mixture. The reaction crude was stirred at 1000 rpm and room temperature for 24 hours. The resulting nanoparticles were washed by centrifugation with ethanol (12000 rpm, 20 minutes) until the supernatant ethanol was colourless.

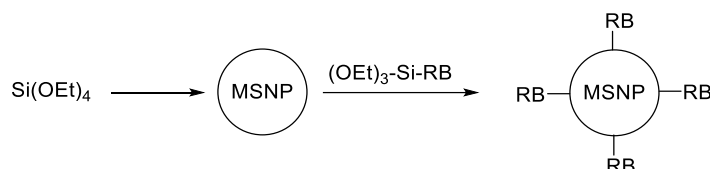
MSNP-RB: Size: 173 nm

ζ -potential: -20.7 mV.

IR (KBr): 3412, 2900, 1732 (s C=O), 1658, 1456, 1324 and 1236 cm^{-1} .

3.4.4.3. Results

The procedure for the synthesis of mesoporous silica nanoparticles (MSNPs), as well as their further functionalization with RB, is illustrated in Scheme 3.26. MSNPs were prepared via the sol-gel process under high dilution conditions. Afterwards, the bare MSNP were decorated with RB with the corresponding silane. It is known that RB is reactive towards bromo-alkane derivatives to generate the corresponding ester bond between RB and the corresponding alkane.⁵¹⁵ The modified MSNPs were characterized by their size and ζ -potential as well as by infrared-spectroscopy, which confirms the conjugation of RB by an ester bond.



Scheme 3.26 Synthesis of MSNP and MSNP-RB.

Absorption and fluorescence spectra of MSNP-RB were recorded in ethanol, and compared to absorption/fluorescence spectra of RB in EtOH and in PBS (Figure 3.40). In the three cases, the absorbance spectra has the same profile, however MSNP-RB maximum is shifted to the red 10 nm in comparison to free RB. Regarding to fluorescence it is also observed the red-shift when RB is bond to MSNP.

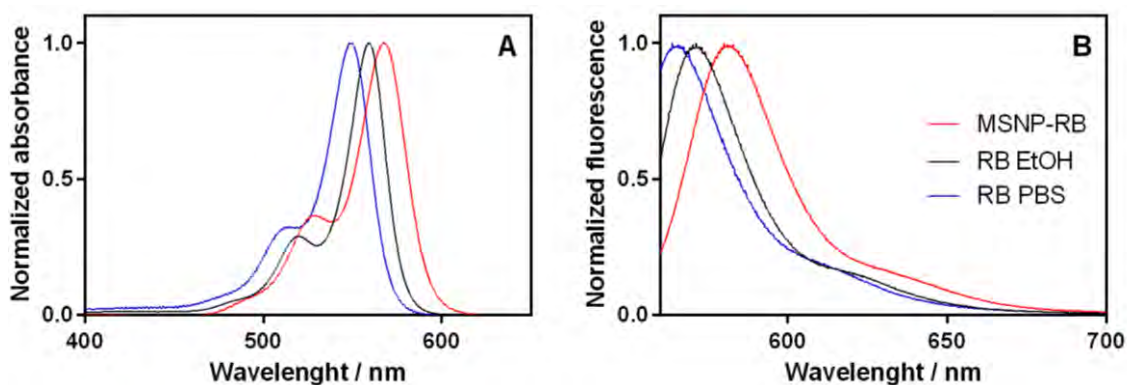


Figure 3.40 Absorption (A) and fluorescence (B) spectrum of MSNP-RB in EtOH (red line) and RB in EtOH and PBS (black and blue lines respectively).

Pulsed-laser irradiation of RB and MSNP-RB suspended in ethanol produced clear time-resolved $^1\text{O}_2$ phosphorescence signals (Figure 3.41), which are quenched in presence of 25 mM NaN_3 . Data analysis of the kinetic traces reveals that MSNP-RB produces $^1\text{O}_2$ in a lower rate than RB (almost 3 times less). In difference to AMSNP-MB and MMSNP-MB, for MSNP-RB it is only observed one population for $^1\text{O}_2$ generation. Furthermore, τ_T is longer in MSNP-RB than for free RB (1.1 vs 0.5 μs respectively).

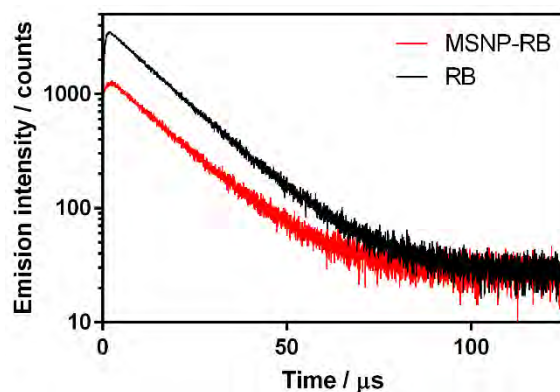


Figure 3.41 Time-resolved $^1\text{O}_2$ phosphorescence of optically matched solutions of MSNP-RB and RB (red and black lines respectively) in EtOH.

Using $^1\text{O}_2$ data fit, the triplet quenching constant by oxygen was calculated as $6.0 \times 10^8 \text{ M}^{-1}\text{s}^{-1}$, which is slightly smaller than processes controlled by diffusion. This confirms the protective effect of MSNP scaffold against $^3\text{O}_2$.

Photoantimicrobial preliminary results with the synthesized NPs have been obtained. MSNP-RB are not toxic in dark conditions against *S. aureus* and *E. coli*. Unfortunately, MSNP-RB are less phototoxic than free RB for both microbial species. This is with concordance with the minor production of $^1\text{O}_2$ by MSNP-RB in comparison with free RB (Figure 3.42).

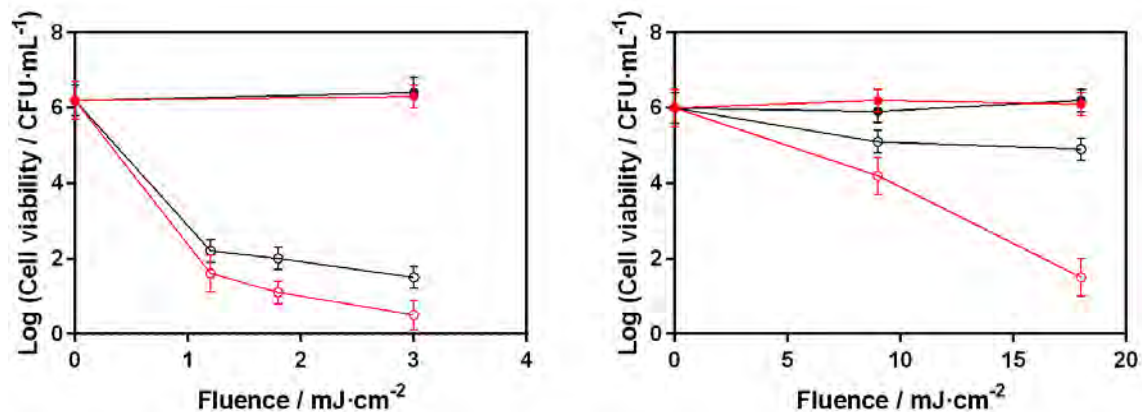


Figure 3.42 Cell viability of *S. aureus* (left) and *E. coli* (right). PS concentration was $0.5 \mu\text{M}$ and $5 \mu\text{M}$ for *S. aureus* and *E. coli* respectively. The bacteria was incubated with RB (red circles) and MSNP-RB (black circles) in the dark (closed symbols) and irradiated with green light ($524 \pm 17 \text{ nm}$; open symbols).

3.5. Photodynamic synergistic effect^r

(Adapted from: R. Ruiz-González, P. Milán, **R. Bresolí-Obach**, J.C. Stockert, A. Villanueva, M. Cañete and S. Nonell, Photodynamic synergistic effect of Pheophorbide a and Doxorubicin in combined treatment against tumoral cells, *Cancers*, **2017**, *9*, 18)

The results reported in this section have been carried out in collaboration with the Universidad Autónoma de Madrid (Madrid, Spain).

3.5.1 Introduction

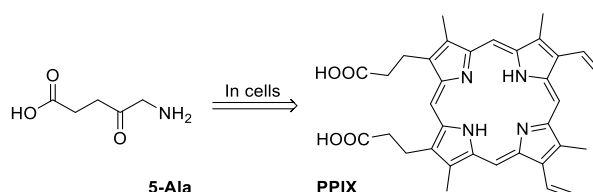
Recent approaches in anticancer therapies include the application of combined chemotherapeutic drugs, delivered together in order to reduce the individual toxicity of each drug (and ultimately side effects) and decrease the likelihood of generating resistance.^{516,517} Combination of different anticancer therapies is also being actively explored^{240,241} as different cell signaling pathways are simultaneously activated. Hence, tumor cells are destroyed in a more efficient manner by additive or synergistic effect of both treatments, allowing a reduction in the dose of the most toxic therapeutic agent.^{240,241}

The combination of a chemotherapeutic drug with a PS is an increasingly growing area of study *in vitro*, *in vivo* or even in clinical trials.⁵¹⁸ One of the first studies was conducted by Peterson *et al* and evaluated the interaction between doxorubicin and meso-chlorin e₆ monoethylene diamine (Mce₆) against human epithelial ovarian carcinoma, showing additive or synergic effects depending on the dose at which each of the therapeutic agents was administered.⁵¹⁹ Datta *et al* studied the photodynamic effect of 5-aminolevulinic acid^s in combination with mitomycin C on J82 bladder cell lines, either regular or mitomycin resistant. In this scenario, results on cell viability indicated a higher sensitivity to PDT for the mitomycin-sensitive cell line. Moreover, the combination treatment resulted in enhanced effect when the chemotherapeutic agent was given first both for parental and mitomycin-sensitive cells.⁵²⁰

Another study was the application of cisplatin and porfimer sodium to L5178Y lymphoma cells where the authors described a marked synergistic effect and increased apoptosis death.⁵²¹ In the same line, low doses of cisplatin or gemcitabine in combination with HpD-based or indocyanine-green-based PDT achieved additive or synergic effect in lung and breast cancer cells, respectively.^{522,523} These treatments not only significantly increase cell inactivation but also reduce the concentrations of PS and, more importantly, the antineoplastic agent.⁵²⁴ Notwithstanding, in some combinations of both therapies there

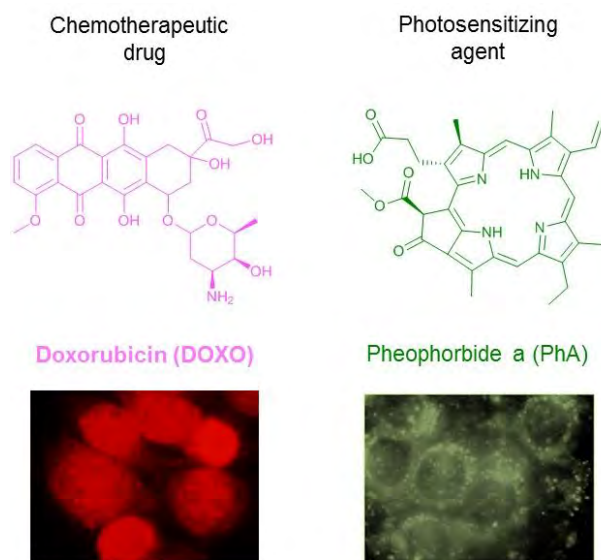
^r Aquesta secció va especialment dedicada a les meves avies que varen morir de càncer quan jo era petit. I per totes aquelles persones pròximes que han sofert aquesta malaltia.

^s 5-aminolevulinic acid is an endogenous non-protein aminoacid which is the biosynthetic precursor of the hemo group.⁷⁴⁶ In mammalian cells it evolves to protoporphyrin IX, which acts as PS.



may be produced antagonistic effect as described for Erlotinib or Cetuximab when applied in combination with PDT using meso-tetraphenylporphine.⁵²⁵

Due to the relevance of cancer in our society and taking into account that the combination of a chemotherapeutic drug with a PS is a hot topic nowadays, we decided to study the combination of Pheophorbide a^t (PhA; as PS) with doxorubicin^u (Doxo; as traditional antineoplastic agent) (Scheme 3.27). It has been determined the photophysical properties of the two compounds and for Doxo also they have been determined in presence of DNA.



Scheme 3.27 Chemical structure and sub-cellular localization of the chemotherapeutic drug: Doxorubicin (Doxo) and the photosensitizing agent: Pheophorbide a (PhA).

^t Pheophorbide a (PhA) is a photosensitive chlorophyll metabolite with immunostimulant activity,⁷⁴⁷ which at adequate concentrations causes apoptosis of tumour cells.⁷⁴⁸ Despite its negligible toxicity to healthy cells in the dark, exposure to light elicits apoptosis, cell cycle arrest at sub-G1, abolition of antiapoptotic protein Bcl-2, cytochrome-C release to the cytosol and activation of procaspases 3 and 9.⁷⁴⁹ PhA has been shown to induce apoptosis in Jurkat leukaemia cells, human hepatocellular carcinoma or uterine carcinosarcoma in photodynamic treatments.^{750,751}

^u Doxorubicin (or Adriamycin; Doxo) is a non-selective anthracycline antibiotic class I whose mechanism of action is the inhibition of enzymes responsible for DNA replication. This drug intercalates in the DNA double helix and interferes with topoisomerases I and II, thereby preventing the binding of the DNA strands and leading to cell death.⁵²⁶ Doxo is often used in the treatment of solid tumours; however, it has significant side effects such as cardiomyopathies.⁷⁵²

3.5.4. Photophysical properties of doxorubicin and pheophorbide a

As a first approach, we measured the absorption and fluorescence spectra of solutions of Doxo and PhA in ethanol and water, taken as simple models of the cell membrane and the cytoplasm, respectively (Figure 3.43). In EtOH, both the absorption and fluorescence spectra show narrow structured bands and the fluorescence excitation spectra match with the corresponding absorption spectra (Figure 3.43a,b). These observations indicate that both compounds exist as monomers.

In contrast, the absorption spectra in water (Figure 3.43c) show broader and non-structured bands, red-shifted in the case of Doxo and blue-shifted for PhA. Notwithstanding, the fluorescence emission (Figure 3.43) and excitation (Figure 3.43c, inset) spectra are very similar to those recorded in EtOH, although much weaker in intensity, particularly for PhA. These findings clearly indicate that both compounds exist as a mixture of fluorescent monomers and essentially non-fluorescent aggregates in aqueous solutions (J-type in the case of Doxo and H-type PhA).^v

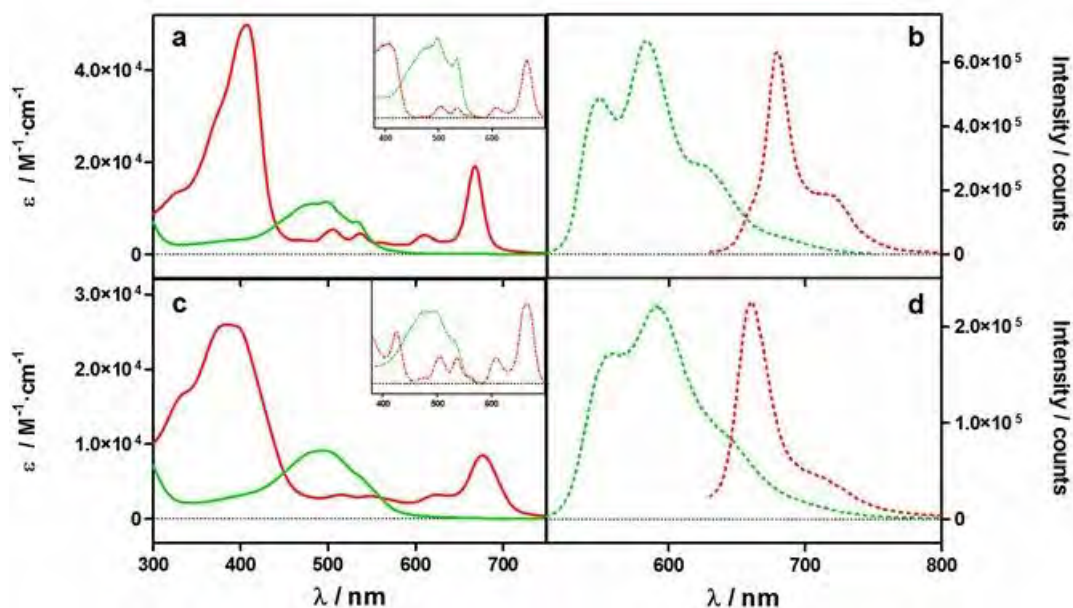


Figure 3.43 Absorption (a,c) and fluorescence (b,d) spectra of Doxo (green) and PhA (red) in EtOH (a,b) and water (c,d). $\lambda_{exc;DOXO}$ 455 nm and $\lambda_{exc;PhA}$ 610 nm. Insets: (a, c) Excitation spectra of the fluorescence at 705 nm for PhA and 610 nm for Doxo.

Figure 3.44 shows the fluorescence decays for Doxo (green traces) and PhA (red traces). In EtOH, Doxo decays with a biexponential function with time constants 1.4 ns (93% weight) and 4.3 ns (7% weight). In deuterium oxide (D_2O), however, only one lifetime (4.0 ns) was needed to adequately fit the decay. On the other hand, PhA shows a monoexponential decay in EtOH with lifetime 5.9 ns, whereas the weak emission in

^v The self-association of dyes in solution is a frequently encountered phenomenon in dye chemistry owing to strong intermolecular van der Waals-like attractive forces between the molecules. The aggregates in solution exhibit distinct changes in the absorption band as compared to the monomeric species. The bathochromically shifted J-bands and hypsochromically shifted H-bands of the aggregates have been explained in terms of molecular exciton coupling theory. They may aggregate in a parallel way (plane-to plane stacking) to form a sandwich-type arrangement for H-aggregates or in a head-to-tail arrangement (end-to end stacking) to form a J-aggregates. Further information in reference ⁷⁵³.

D₂O showed two components with lifetimes 4.8 ns (61 % weight) and 2.6 ns (31 % weight).

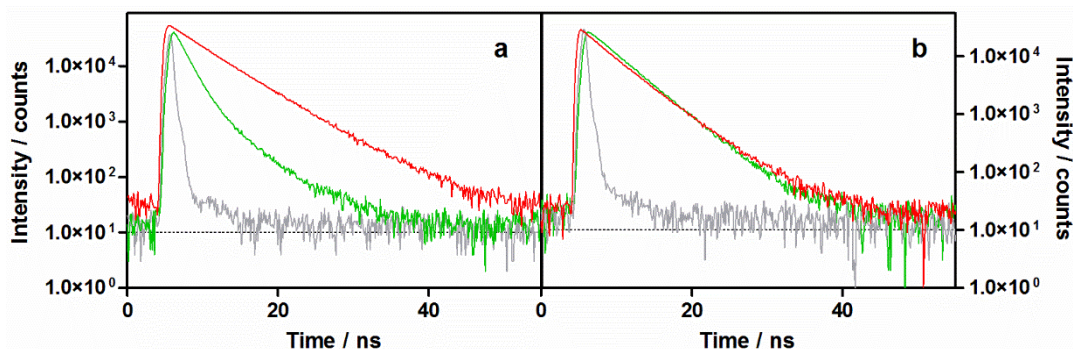


Figure 3.44 Time-resolved fluorescence decays for Doxo (green; λ_{exc} 504 nm; λ_{obs} 660 nm) and PhA (red; λ_{exc} 654 nm; λ_{obs} 710 nm) in EtOH (a) and D₂O (b). Grey traces represent instrument response function.

The strong fluorescence of Doxo suggests that it might generate ROS upon exposure to light. Its capacity to photosensitize ¹O₂ was assessed in D₂O and EtOH by time-resolved near-infrared ¹O₂ phosphorescence. The luminescence observed is assigned to ¹O₂ because the transient is completely quenched in presence of sodium azide. As shown in Figure 3.45, Doxo does indeed generate ¹O₂ with quantum yield Φ_{Δ} = 0.03 in EtOH and Φ_{Δ} = 0.01 in D₂O, irrespective of the excitation wavelength (λ_{exc} 473 or 532 nm). Regarding to PhA generates higher amounts of ¹O₂ with a Φ_{Δ} of 0.61 and 0.04 in EtOH and D₂O respectively. The decrease of Φ_{Δ} for both compounds in D₂O is consistent with the occurrence of aggregation in this solvent.

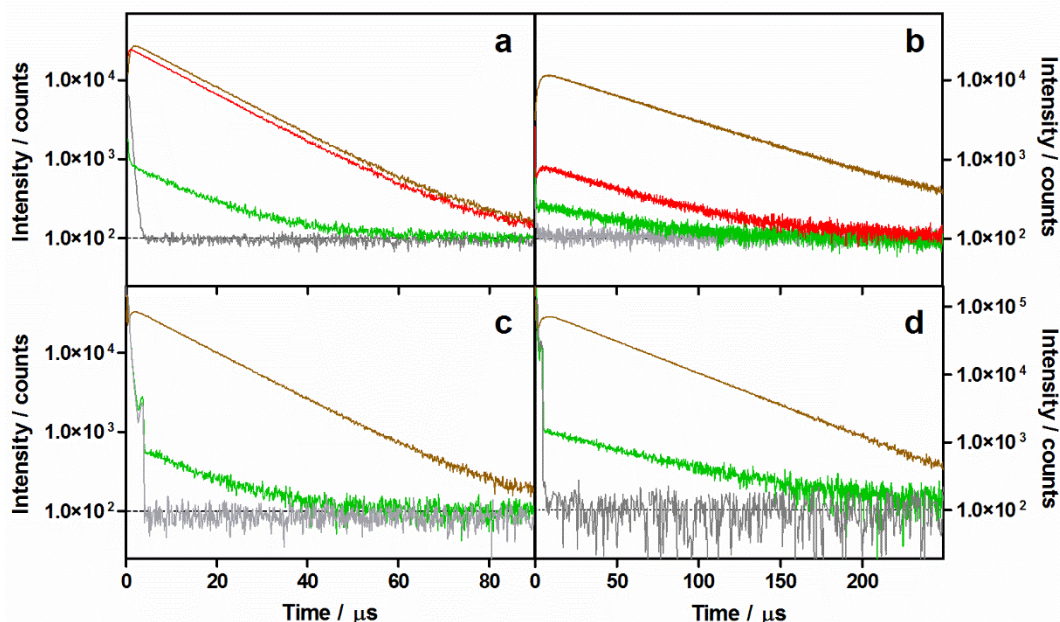


Figure 3.45 ¹O₂ phosphorescence kinetics in EtOH (a,c) and D₂O (b,d) solutions of Doxo (green), PhA (red) and reference PSs (brown). The signals completely disappeared in the presence of 25 mM NaN₃ (grey). Rose bengal in EtOH (Φ_{Δ} = 0.75⁵⁰⁶) and flavin mononucleotide in D₂O (Φ_{Δ} = 0.56^{263,264}) were used as references. λ_{exc} was 532 nm for panels a,b and 473 nm for panels c,d.

Doxo is well known to localize in the nucleus where it binds to DNA.⁵²⁶ Spectral and photophysical consequences of DNA binding are shown in Figure 3.46: (i) the absorption spectrum appears more structured (Figure 3.46a), (ii) the fluorescence is strongly

quenched (Figure 3.46b), (iii) the amount of $^1\text{O}_2$ produced is strongly reduced (Figure 3.46c), and (iv) τ_T is extended, as demonstrated by the slower rise of the $^1\text{O}_2$ phosphorescence signal; whilst τ_A remains similar, which indicates that the $^1\text{O}_2$ generated is able to escape from DNA structure. On the other hand, the fluorescence lifetime does not change (Figure 3.46d). These observations are consistent with strong static quenching of the Doxo excited states and shielding from $^3\text{O}_2$ upon binding to DNA.

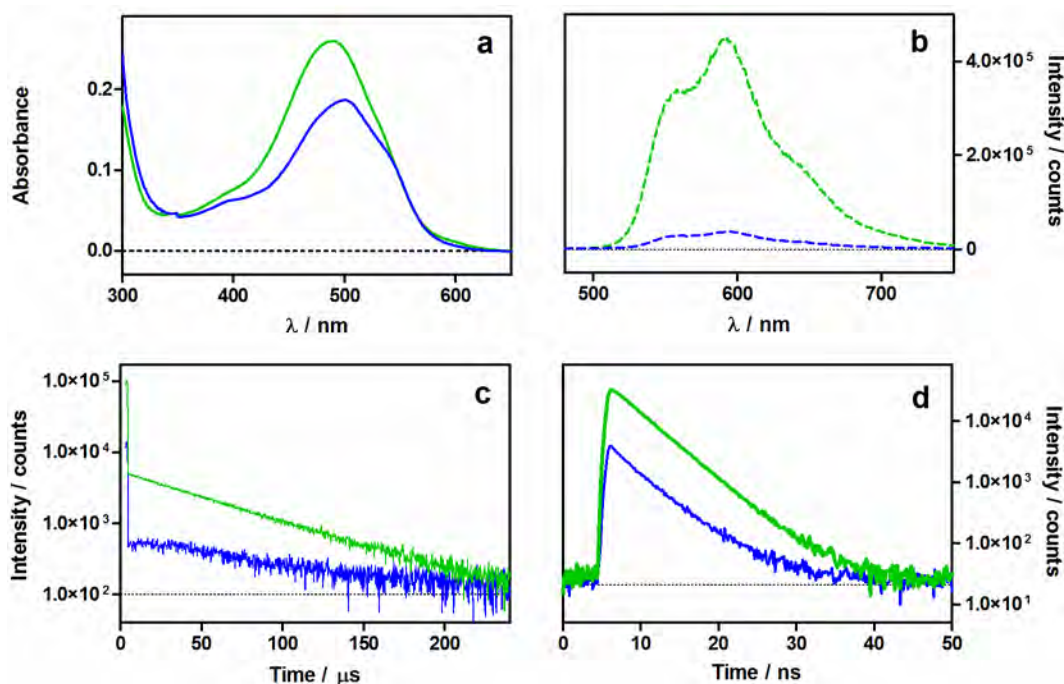


Figure 3.46 Spectroscopic and photophysical properties of Doxo in D_2O solutions in the absence (green traces) and presence (blue traces) of $60 \mu\text{g/mL}$ DNA: (a) absorption spectra, (b) fluorescence emission spectra, (c) $^1\text{O}_2$ phosphorescence kinetics ($\lambda_{\text{exc}} 473 \text{ nm}$), (d) time-resolved fluorescence decay ($\lambda_{\text{exc}} 504 \text{ nm}$; $\lambda_{\text{obs}} 660 \text{ nm}$).

Given the ability of Doxo to produce $^1\text{O}_2$ upon exposure to light, we assessed whether it could be used as a dual agent, namely cytotoxic and photocytotoxic. Thus, in separate experiments, cells were pre-incubated with $0.2 \mu\text{M}$ and $0.4 \mu\text{M}$ Doxo and irradiated with green light. No decrease in the cell viability could be observed relative to the non-irradiated controls.

Our collaborators in the Universidad Autonoma de Madrid performed photoinactivation studies combining Doxo and PhA with HeLa cells. The timing of the chemo- and photo-therapeutic events is expected to play a major role in the outcome of the combined treatments. To identify the best synchronization conditions, the drug and the PS were administered according to three different protocols:

- In the first protocol (PhA-Doxo), cells were incubated with PhA for 4 h, washed to remove any unbound PhA, irradiated with red light ($634 \pm 8 \text{ nm}$; 6.4 J/cm^2), and then further incubated with Doxo for a period of 24 h.
- In the second protocol (Doxo-PhA), cells were first treated with Doxo for 24 h, washed, incubated with PhA for 4 h, washed again, and finally irradiated with red light ($634 \pm 8 \text{ nm}$; 6.4 J/cm^2).

- In the third protocol (Doxo+PhA), cells were incubated with Doxo for 20 h, washed, co-incubated with PhA and Doxo for 4 h, washed again, and finally irradiated with red light (634 ± 8 nm; 6.4 J/cm²).

At the end of the three protocols, HeLa cells have been incubated with Doxo for 24 h, with PhA for 4 h, and the same light fluence has been delivered (Figure 3.47). For PhA-Doxo there was no appreciable difference in cell viability between the dark- and light experiments. For Doxo-PhA, the expected additive effect was observed. Remarkably, the Doxo+PhA treatment resulted in a survival fraction of 18%, which indicates that a synergistic effect can indeed be achieved under the proper conditions.^w

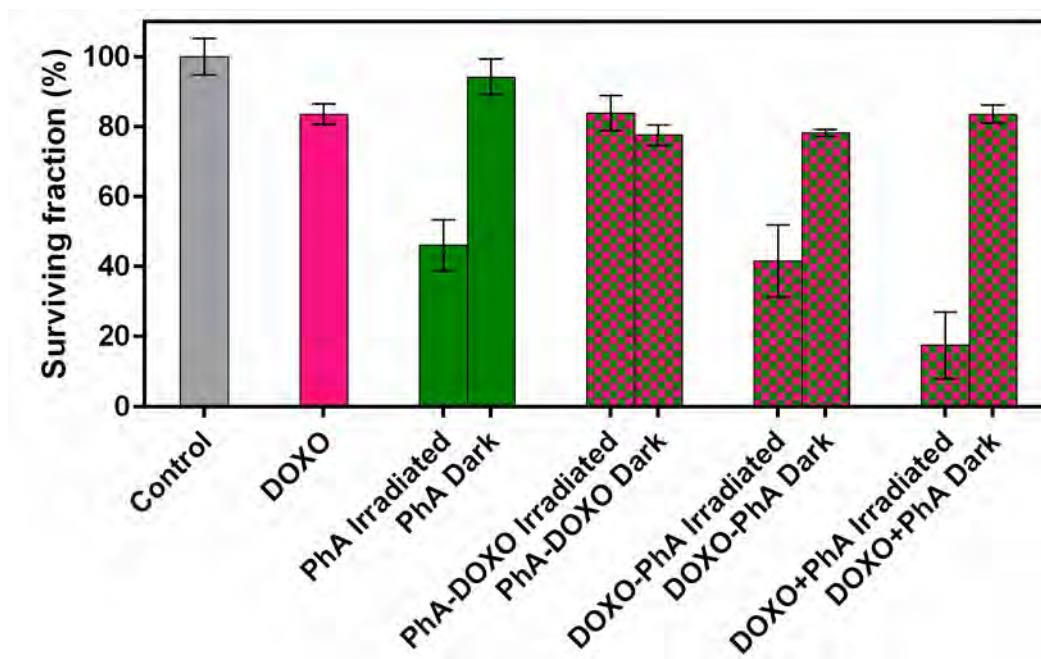


Figure 3.47 Viability of HeLa cells treated with 0.2 μ M Doxo, 2 μ M PhA or a combination of the two drugs according to three different protocols described above. The standard deviation presented in this figure is the average of at least 3 independent experiments. This data has been obtained by Ms. Paula Milán, Dr. Angeles Villanueva and Dr. Magdalena Cañete in the Universidad Autonoma de Madrid (Madrid, Spain).

From these experiments, it has been observed that the order in which the chemotherapeutic and the photodynamic treatments are delivered plays a key role in the outcome of Doxo and “PhA+light” combined treatments. It seems that the best performing treatment is in first step to do a chemical damage by conventional antitumoral treatment and once the HeLa cell is not healthy then PDT treatment seems to be more efficient.

^w The outcome of the combined treatments was evaluated according to the method described by Valeriote and Lin,⁷⁵⁴ which compares the efficacy of the individual drugs (ϵ_A , ϵ_B) with that of its combination (ϵ_{A+B}). The treatment is:

$$\begin{aligned}
 &\text{synergic if } \epsilon_{A+B} < (\epsilon_A \times \epsilon_B)/100 \\
 &\text{additive if } \epsilon_{A+B} = (\epsilon_A \times \epsilon_B)/100 \\
 &\text{sub-additive if } (\epsilon_A \times \epsilon_B)/100 < \epsilon_{A+B} < \epsilon_A, \text{ provided } \epsilon_A < \epsilon_B \\
 &\text{interference if } \epsilon_A < \epsilon_{A+B} < \epsilon_B, \text{ when } \epsilon_A < \epsilon_B \\
 &\text{antagonic if } \epsilon_B < \epsilon_{A+B}, \text{ when } \epsilon_A < \epsilon_B.
 \end{aligned}$$

3.6. Reactive oxygen species mediated activation of a dormant singlet oxygen photosensitizer in HeLa cells

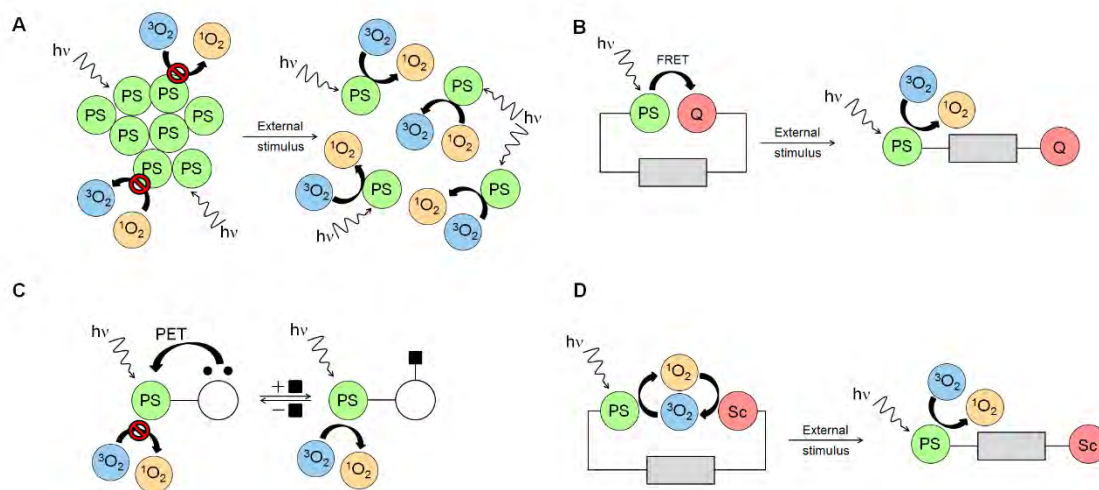
The results reported in this section have been carried out in the McGill university (Montreal, Canada).

3.6.1. Activatable photosensitizers

(Adapted from: **R. Bresolí-Obach**, C. Hally and S. Nonell; Chapter 8: Activatable Photosensitizers; in Singlet oxygen: Applications in biosciences and nanosciences Volume 1, RSC Publishing, 2016.)

Conventional $^1\text{O}_2$ photogeneration is a tri-stimulus process that requires the simultaneous combination of a PS, light, and $^3\text{O}_2$. Activatable photosensitizers (aPSs) are a special type of PSs whose activity can be turned on by a wide variety of molecular stimuli. This allows a more precise control on $^1\text{O}_2$ generation, thereby improving the selectivity and safety during photosensitisation processes.^{214,243,527} Their general principle of action is that an aPS is maintained in a quenched state until a molecular activation step takes place that relieves its ability to photosensitize $^1\text{O}_2$. As such, aPSs can be considered to be examples of 3rd generation PSs.⁵²⁸ This chapter reviews the known aPSs, the reported mechanisms of activation, and the main stimuli used to control singlet oxygen generation.

As explained in detail in section 1.1, effective photosensitisation of $^1\text{O}_2$ requires absorption of light by the PS, formation of a long-lived excited state, energy transfer to molecular oxygen, and release of the caged $^1\text{O}_2$ from the PS vicinity to the external bulk media.⁵²⁹ Each of these steps are amenable to quenching, therefore rendering the aPS inactive. To achieve $^1\text{O}_2$ quenching effect different activation mechanism have been used (Scheme 3.28).



Scheme 3.28 The different activation mechanisms presented. (A): Self-Quenching (SQ). (B): Förster Resonance Energy Transfer (FRET). (C): Photoinduced Electron Transfer (PET). (D): $^1\text{O}_2$ Scavenging.

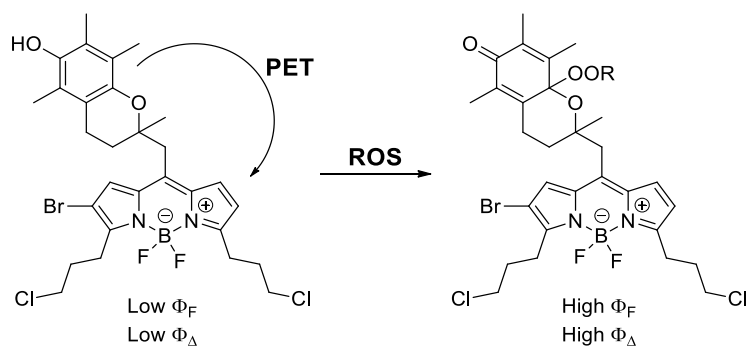
The first mechanism, is the self-quenching phenomena that refers to the scavenging of aPSs* by interaction with a ground-state PS. In most cases, this requires close vicinity between PS molecules, and therefore, the relief mechanism is due to an increase of the distance between these (Scheme 3.28A).^{530,531} The second one is based in Förster resonance energy transfer (FRET). The PS and a suitable energy-transfer acceptor (Q) are held together in an initial conformation, thereby enabling

efficient deactivation of the PS* through non-radiative dipole–dipole coupling.⁵³² Since FRET efficiency is proportional to the reciprocal sixth power of the distance between donor and acceptor, an external stimulus which changes the donor-acceptor distance will have a large impact on FRET efficiency (Scheme 3.28B). The third one is based in photoinduced electron transfer (PET), which can effectively quench the PS*, thereby shutting down ¹O₂ production.^{533,534} In contrast, ¹O₂ generation would occur if this electron transfer were blocked by external stimuli (Scheme 3.28C). Usually, this electron transfer occurs from a non-bonding electron lone pair, like an amine, ethers or alcohols. Finally, all the previous strategies try to avoid ¹O₂ generation. However, ¹O₂ scavenging strategy attempts to quench ¹O₂ (either physically or chemically) before it exits the system. When the system is activated by external stimuli, PS and scavenger are separated, reducing ¹O₂ scavenging effectivity (Scheme 3.28D).

The activation of an aPS must be carried out by a specific external stimulus. These stimuli can be either from a molecular recognition, by means of coupling of small molecules, such as protons, or by media properties, like oxidative stress or viscosity. This can be visualized as a molecular “Trojan horse” system. These types of molecules can quickly change into an aggressive form, able to kill cells (both tumorous and microbial).

Among the different studied stimuli, we are interested in the activation the PS by ROS. The basal level of ROS production between cancerous and non-cancerous cells is different. Cancer cells due to its accelerated metabolism produce much more ROS than non-cancerous. This difference could be taken in advantage for designing a selective PS among them.

In this approach the photosensitizing properties of a Br-bodipy are quenched by photoinduced electron transfer from the chromanol moiety. The chromanol acts as an antioxidant and only when the chromanol is oxidized, the photosensitizing properties of the Br-bodipy are fully restored. Moreover, we chosed a Br-bodipy as PS instead of a Br₂-bodipy or I₂-bodipy because we wanted a theragnostic agent. Spin-orbit coupling of Br-bodipy is not so intense compared with di-bromo or di-iodo and then we expect an acceptable Φ_{Δ} for killing and Φ_F for imaging.

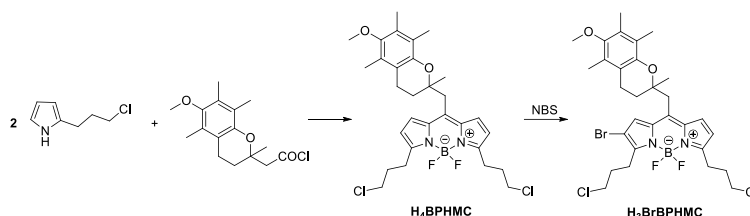


Scheme 3.29 Proposed off/on sensing mechanism of the new aPS H₃BrBPHMC, relying on PET.

3.6.2. Experimental

3.6.2.1. Synthesis of H₄BPHMC and H₃BrBPHMC

The compounds used in this section have been synthesized in the group of Dr. G. Cosa (McGill University, Montreal, Canada) by Ms. Julia McCain. The synthetic routes for 8-((6-Hydroxy-2,5,7,8-tetramethylchroman-2-yl)-methyl)-1,5-di(3-chloropropyl)-pyrromethene fluoroborate (H₄BPHMC) and 8-((6-Hydroxy-2,5,7,8-tetramethylchroman-2-yl)-methyl)-2-chloro-1,5-di(3-chloropropyl)-pyrromethene fluoroborate (H₃BrBPHMC) are described in Scheme 3.30.



Scheme 3.30 Synthesis of H₄BPHMC and H₃BrBPHMC.

3.6.2.2. Microscopy used

Differential interference contrast (DIC) imaging of HeLa cells were performed using either a wide-field objective-based total internal reflection fluorescence (TIRF) microscopy setup equipped with an oil-immersion objective (Nikon CFI SR Apochromat TIRF 100 \times , NA = 1.49) or a lower magnification widefield microscopy setup equipped with an air objective (Nikon CFI Plan Apo VC 20 \times objective, NA = 0.75) consisting of an inverted microscope (Nikon Eclipse Ti) equipped with a Perfect Focus System (PFS). A stage-top incubator (Tokai Hit) was used to maintain the cells at 37 °C (5% CO₂) in a humidified atmosphere. The excitation laser was 488 nm with powers of 0.10 mW (for x20) and variable (for x100) measured out of the objectives where the beam was coupled into the microscope objective using a multiband beam splitter (ZT488/640rpc, Chroma Technology). The emission was spectrally filtered with an emission filter (ZET488/640m). For multichannel imaging between the 488 channel and DIC, a motorized filter block turret was used. The fluorescence emission was collected through the same objective and captured on a back illuminated electron multiplying charge coupled device (EM-CCD) camera (Andor iXon Ultra DU-897).

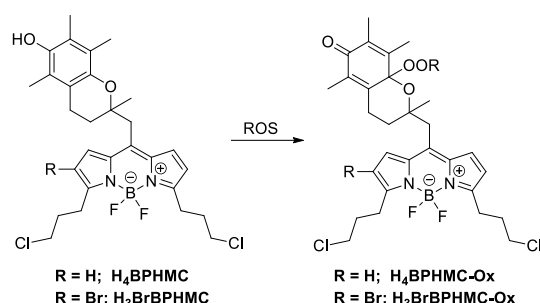
3.6.2.3. Cell Imaging of H₄BPHMC and H₃BrBPHMC

Twenty-four hours prior to day of imaging, cells were plated on an 8-well ibidi-Treat μ -slide (for x20) or 35 mm glass imaging dishes (for x100; World Precision Instruments, Inc.) precoated with fibronectin (1 μ g/cm²), in DMEM containing growth factors.

After 24 h, cells were then washed twice with incubation LCS buffer, followed by the addition of 1 mL of fresh incubation buffer. Cells were stained by the addition of 500 μ L of the dye (300 nM) to give a final concentration of 100 nM in dye. The solution of dye was prepared from the addition of 5 μ L of a 30 μ M stock solution in DMSO. This overall 300-fold dilution was to ensure the percentage of DMSO in media was 0.33% (v/v). Then the dye was incubated during 30 minutes followed by two washes with incubation LCS. The different experiments were realized immediately after.

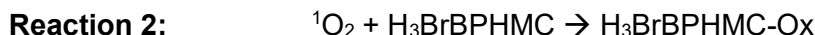
3.6.3. Results

We studied the photophysical, photochemical and phototherapeutical properties of H₃BrBPHMC against HeLa cancer cells (Scheme 3.31). H₃BrBPHMC in its reduced state has low Φ_F and Φ_{Δ} values because the chromanol moiety quenches the singlet state of the PS (Br-Bodipy) thorough PET. Chromanol act an antioxidant and can react with ROS to generate H₃BrBPHMC-Ox. In this state, the oxidised-chromanol cannot quench the singlet state of Br-Bodipy anymore and consequently H₃BrBPHMC-Ox photophysical and photochemical properties are recovered.



Scheme 3.31 Proposed mechanism for the ROS-mediated activation of H₃BrBPHMC / H₄BPHMC.

H₃BrBPHMC-Ox is a good PS and under green light irradiation is capable to produce ¹O₂, which can further oxidize other H₃BrBPHMC molecules. This ¹O₂-mediated pathway offers an alternative to the dark-oxidation of H₃BrBPHMC by endogenous-generated ROS. This kinetic pathway should be autocatalytic accordingly to presented reactions:



In a first experiment, we determined the fluorescence enhancement of H₃BrBPHMC upon oxidation with a radical initiator (2,2-azobis(4-methoxy-2,4-dimethyl valeronitrile)).^{535;x} Moreover we decided to study H₃BrBPHMC oxidation inside liposomes as a simplified model of cellular membrane (Figure 3.48). Under these conditions, we observed a fluorescence enhancement higher than 200-fold.

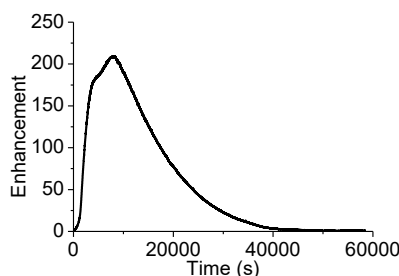
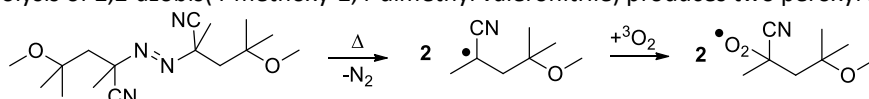


Figure 3.48 Fluorescence enhancement of H₃BrBPHMC upon reaction with the radical initiator (2,2-azobis(4-methoxy-2,4-dimethyl valeronitrile)).

^x The thermolysis of 2,2-azobis(4-methoxy-2,4-dimethyl valeronitrile) produces two peroxy radicals.



Once the reactivity of H₃BrBPHMC towards ROS is studied in solution, we further studied its behaviour inside HeLa cancer cells. For the cellular studies, we used H₄BPHMC, which is an analogue of H₃BrBPHMC without Br atom, as control. In figure 3.49, is observed how the H₃BrBPHMC fluorescence increases upon blue light irradiation, whilst the control (H₄BPHMC) do not present such increase.

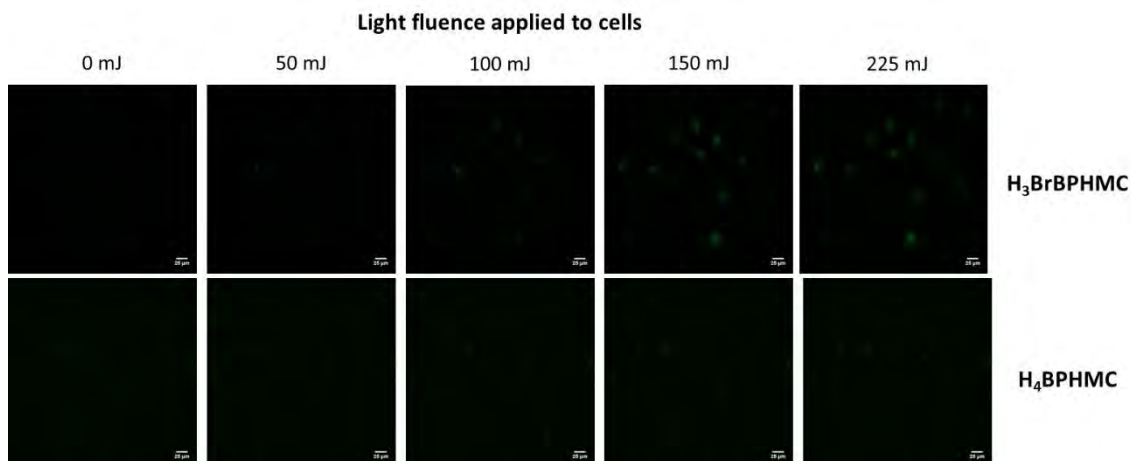


Figure 3.49 HeLa cells images acquired after blue light irradiation (0 to 225 mJ; $\lambda_{exc} = 488$ nm) incubated with 100 nM of H₃BrBPHMC (top) or H₄BPHMC (bottom).

Figure 3.50 depicts the numerical analysis of H₃BrBPHMC and H₄BPHMC fluorescence kinetics traces. For H₃BrBPHMC, the fluorescence enhancement presents a sigmoidal profile, which is typical from autocatalytic kinetics. In the high fluence range, only photobleaching of H₃BrBPHMC is observed. Such behaviour is not detected for H₄BPHMC in where only a slight fluorescence enhancement is observed. We can take advantage of the autocatalytic behaviour of H₃BrBPHMC to activate it only in the cellular regions where ROS concentration is high.

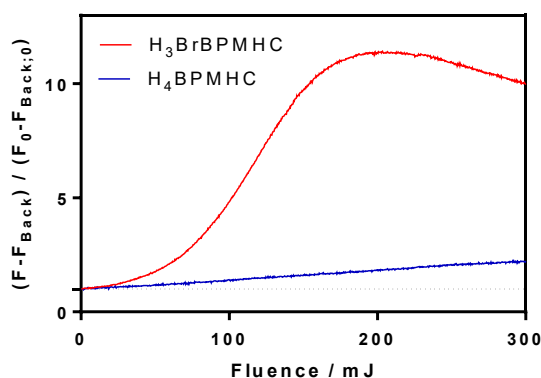


Figure 3.50 Fluorescence enhancement of 100 nM H₃BrBPHMC (red line) and H₄BPHMC (blue line) incubated in HeLa cells.

The next step was to study the effect of endogenous generated ROS in the activation of H₃BrBPHMC and H₄BPHMC in dark conditions. The two compounds present roughly the same oxidation kinetics. Moreover, both compounds do not present dark toxicity in the range of concentrations tested.

Once, the two key parameters (light fluence and incubation time) in the oxidation of H₃BrBPHMC have been studied independently, we decided to study them together. We

chose two different incubation times (0 and 180 minutes). For 0 minutes, H₃BrBPHMC was almost no oxidized, whilst for 180 minutes H₃BrBPHMC was partially oxidized. In figure 3.51, we observed that fluorescence enhancement kinetics as well as its photo-toxicity is dependent on the initial incubation time. This is coherent, because as more incubation time, more H₃BrBPHMC-Ox will be present and more ¹O₂ will be generated. For the control H₄BPHMC only a slight fluorescence enhancement is observed.

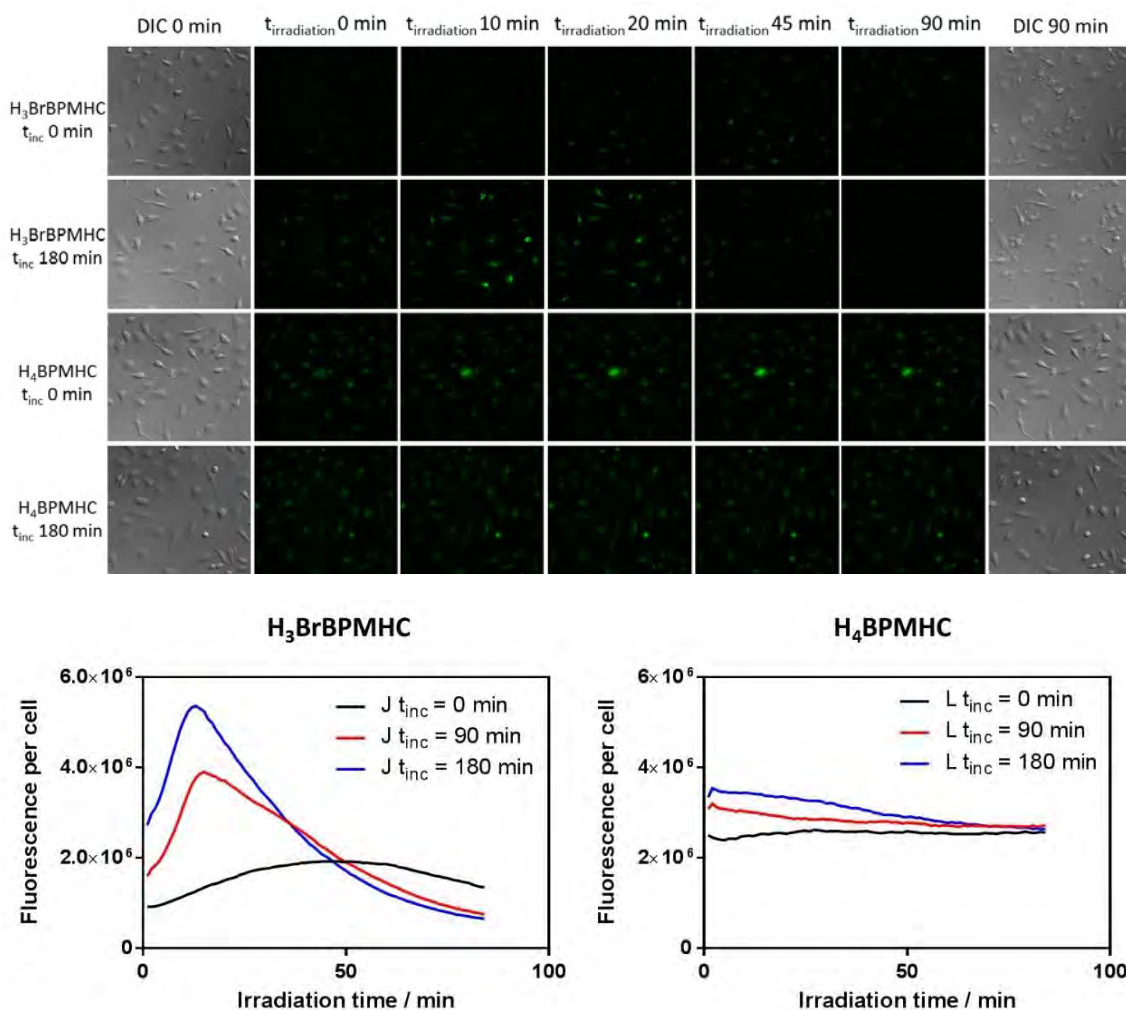


Figure 3.51 Top: HeLa cells photographs acquired at different light fluences and dye incubation time. Bottom: Fluorescence enhancement kinetics analysis for the previous fluorescence images. Left: H₃BrBPMHC. Right: H₄BPMHC. The concentration of dyes tested was 100 nM.

In another series of experiments, the intracellular behaviour of H₃BrBPHMC was studied. Like the previous experiments we irradiated H₃BrBPHMC with blue light and collected images in regular intervals. In figure 3.52/3.53 is observed that the fluorescence enhancement kinetics for H₃BrBPHMC is dependent of the subcellular localization. The control H₄BPHMC under these conditions presents a similar behaviour but with higher light fluence values (approximately a ten-fold higher). The observed activation order for H₃BrBPHMC was:

Lipids vesicles or peroxisomes > mitochondria > endoplasmic reticulum > nucleus

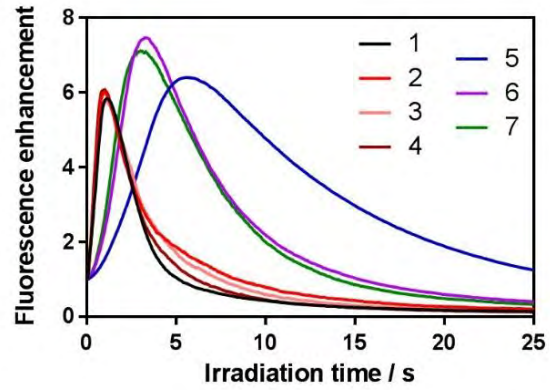
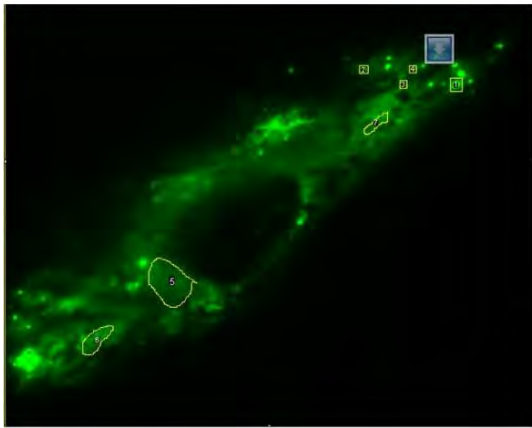


Figure 3.52 Left: HeLa cell fluorescence image with the different subcellular regions analysed. Right: Fluorescence enhancement kinetics analysis. 1-4 lipids vesicles or peroxisomes, 5 endoplasmic reticulum and 6-7 mitochondria.

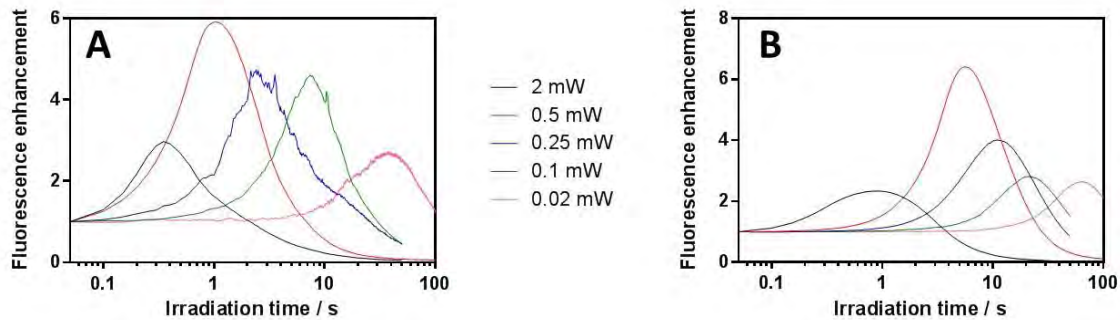


Figure 3.53 Fluorescence enhancement kinetics for 100 nM H₃BrBPHMC for different-used laser powers. Left: Lipids vesicles. Right: endoplasmic reticulum.

Taking into account that the activation of H₃BrBPHMC/H₄BPHMC is subcellular-localization dependent, we decide to study the behaviour of HeLa cells upon punctual ¹O₂ generation. Under that purpose, several cycles of blue light irradiation (1.25 mJ) followed for 20 minutes of dark-relaxation (Figure 3.54). A first observation, is that the fluorescence enhancement of H₃BrBPHMC is minor when the cell is non-stressed (cycle 1) in comparison when the cell is stressed (cycle 2-5). Moreover, it has been observed the release of vesicles after the first cycle of irradiation for H₃BrBPHMC, whilst for H₄BPHMC such behaviour is not observed. Third, for the case of non-stressed cells H₃BrBPHMC fluorescence is quenched during the 20 minutes dark-relaxation, whilst for stressed cells this fluorescence is enhanced. This clearly indicates that when cell produces more ROS than a limit, then the cell goes out of control and produces a high concentration of ROS, which can kill the cell. This effect also is more remarkable in subcellular regions where ROS concentration is higher. These observations have not been detected for controls experiments.

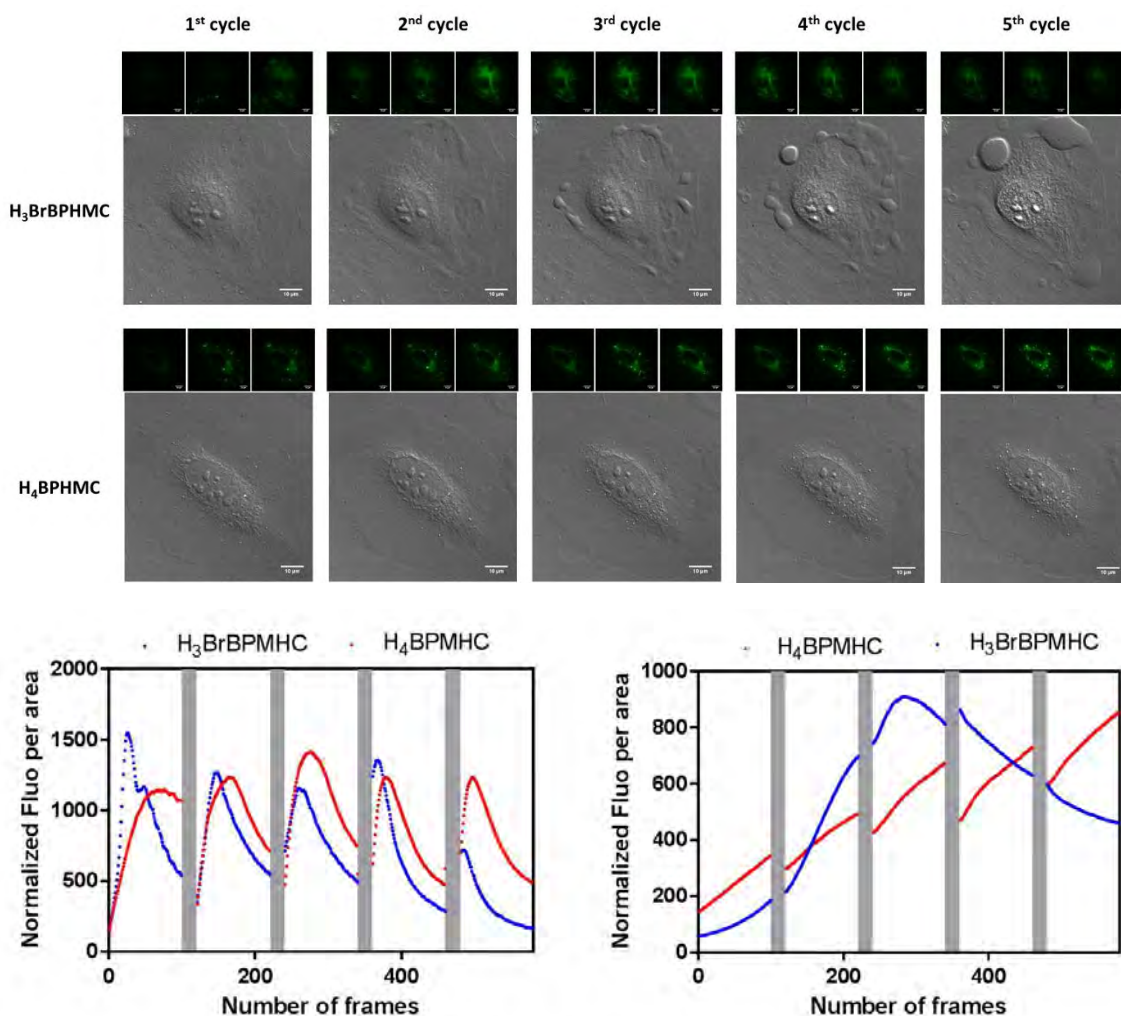


Figure 3.54 Top: HeLa cells photographs acquired at different cycles (light fluence per cycle 1.25 mJ). The three fluorescence images are the first, 50st and the last frame per cycle. Bottom: Fluorescence enhancement kinetics. Left: endoplasmic reticulum. Right: lipid vesicles and peroxisomes.

Finally, we irradiated the HeLa cells with blue light (fluences of 1.25 and 12.5 mJ) co-incubated with H₃BrBPHMC or H₄BPHMC. In figure 3.55 is observed that the endogenous ROS generation due to cellular stress perturbation by light is produced mainly in the first minutes after the irradiation. The fluorescence maxima enhancement is observed after 20 minutes of the irradiation. Afterwards, seems that ROS production returns to its basal level. This increment in ROS endogenous production is not observed for the control (H₄BPHMC).

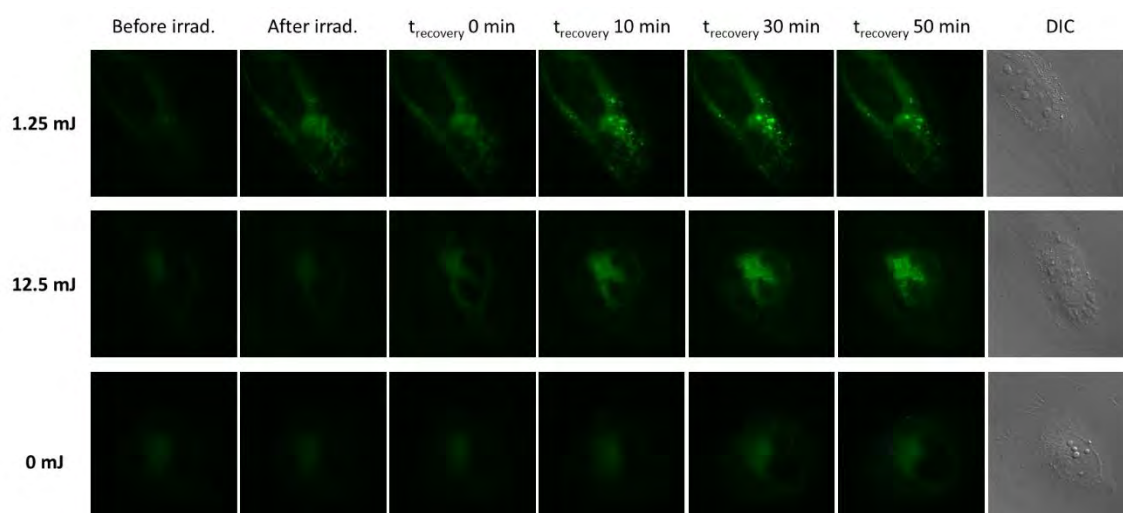


Figure 3.55 HeLa cells photographs acquired before and after the blue light irradiation. The fluorophore used is 100 nM H₃BrBPHMC.

Chapter IV

Novel strategies for $^1\text{O}_2$ and other ROS detection in biological systems

*Ens en sortirem,
malgrat que semblà que, de fet, ningú ens entén.
Mentre quedi algú dempeus que hi confii cegament,
m'has de creure si et dic que ens en sortirem.*

[...]

*L'esperança dins dels ulls
per saltar tots els escullés,
quan la causa és noble cal salvar l'orgull.
I per fi ens vam alçar,
els que hi vam ser hi tornàrem
mil vegades per tornar-los a guanyar.*

Arnau Tordera – Obeses

4.1. When can be $^1\text{O}_2$ traps an alternative to near-infrared phosphorescence to detect $^1\text{O}_2$?

As discussed in section 1.2, $^1\text{O}_2$ can be monitored directly through its near-infrared phosphorescence at 1275 nm or by trapping it with a chemical scavenger. Although ideally the best methodology to monitor $^1\text{O}_2$ should be recording its phosphorescence due to its specificity; that methodology presents the main drawback that the $^1\text{O}_2$ phosphorescence quantum yield (Φ_P) is extremely low (Figure 4.1). For the best cases, such as in CCl_4 or CS_2 it has a Φ_P equal or lower to 0.05.^{59,83,536,537} In the commonly used solvents like acetonitrile, benzene or methanol its $\Phi_P < 1 \times 10^{-4}$ ^{59,83} and this even is worst for water where is estimated to be around 3×10^{-6} .⁵³⁸⁻⁵⁴⁰ Under these conditions, for every 1.000.000 of $^1\text{O}_2$ molecules generated only they will emit in average 3 photons.

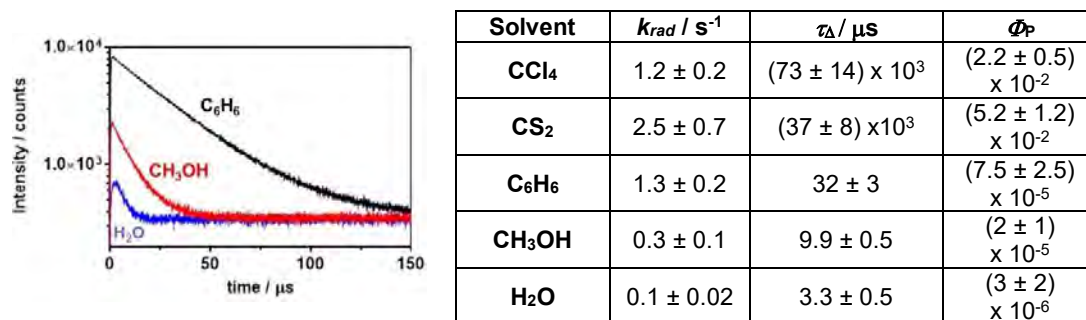


Figure 4.1 Left: Effect of the radiative decay rate constant (and consequently in the phosphorescence quantum yield) on the $^1\text{O}_2$ phosphorescence intensity in selected solvents (benzene, methanol and water; black, red and blue lines respectively). For the three solvents, the PS used is 10 μM phenalenone and the acquisition conditions are the same, in order to obtain comparable $^1\text{O}_2$ phosphorescence signals. Reproduced from reference ⁷⁸. Right: Table with $^1\text{O}_2$ radiative decay rate constant (k_{rad}), $^1\text{O}_2$ lifetime (τ_{Δ}) and $^1\text{O}_2$ phosphorescence quantum yield (Φ_P) for selected solvents.^{59,83,536-540}

Biological environments are mainly composed from water, so it can be expected k_{rad} and τ_{Δ} similar to water. However, the presence of multiple $^1\text{O}_2$ quenchers (i.e. antioxidants, proteins, nucleic acids among others) can reduce its τ_{Δ} which consequently it reduces Φ_P , making even more difficult its detection.⁸⁰ Recently, some authors have described plasmon-enhanced $^1\text{O}_2$ phosphorescence signal either in solid state and in solution.^{468,541,542} However these alternative tricks are in a preliminary investigation stage, and they will not be implemented soon for $^1\text{O}_2$ detection as routine.

Once the highly-improbable $^1\text{O}_2$ phosphorescence photon is emitted, then is necessary to be able to detect it. Detection of near-infrared photon has lower quantum efficiency than in the ultraviolet or visible region (Figure 4.2). The near-infrared photomultiplier (H9170-45, Hamamatsu Photonics) used for this thesis has a quantum efficiency of 0.01 in the region 1000-1350 nm.⁵⁴³

In addition, not each $^1\text{O}_2$ -phosphorescence photon that is emitted from the sample will arrive to the detector. Moreover, the sample can emit other photons in the near infrared region (i.e. scattered photons from the sample), which can contaminate the signal and should be eliminated through the use of filters or monochromators (See figure 2.2). For each "obstacle", there will be an inevitable loss of photons.

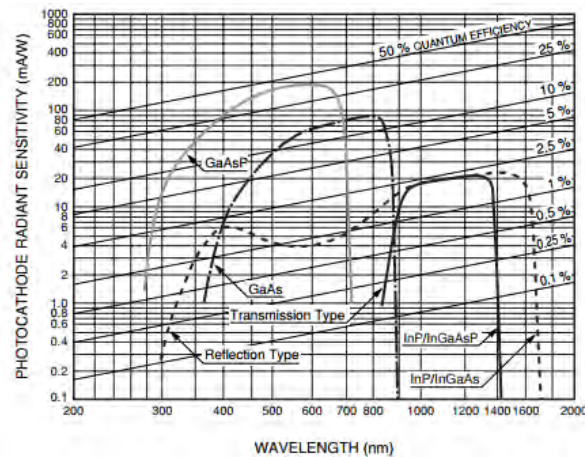


Figure 4.2 Photocathode radiant sensitivity and quantum efficiency characteristics of semiconductor crystal photomultipliers. Reproduced from reference ⁵⁴³.

In brief, in biological systems –where it is important to detect efficiently $^1\text{O}_2$ in order to study its cytotoxic effects in depth- the probability to detect one $^1\text{O}_2$ -phosphorescence photon is in the order of 10^{-10} or less,⁷⁸ which is 70 fold less probable than winning the first prize of Euromillions.⁵⁴⁴

These approximate numbers show the difficulty of $^1\text{O}_2$ detection via its intrinsic phosphorescence. In addition, it is necessary to have specialized instrumentation (i.e. high sensitivity near-infrared photomultiplier), which is typically expensive, and optimize the system up to the limit in order to gain as many photons as possible. Therefore, indirect methods that typically rely on a $^1\text{O}_2$ trap have been developed and are extensively used.

$^1\text{O}_2$ chemical trapping played a central role in early studies on $^1\text{O}_2$ chemistry, particularly before the development and growth of electronics, which allowed detecting $^1\text{O}_2$ phosphorescence in 1979 for first time.⁷⁵ Nowadays, several $^1\text{O}_2$ traps are used (see section 1.2). The chemical trapping can be easily followed using common instrumentation found in research laboratories (i.e. spectrophotometer, spectrofluorometer or liquid/gas chromatography).⁹⁹

Furthermore, there are even less laboratories that have a microscope with a near-infrared camera able to detect $^1\text{O}_2$ phosphorescence.⁵⁴⁵ Alternatives such as $^1\text{O}_2$ -sensitized delayed fluorescence (SOSDF) of the PS also give information about $^1\text{O}_2$ generation with spatial resolution in a time-resolved fluorescence imaging experiment.^{91,546} Notwithstanding, it is easier for a non-specialized laboratory the use of $^1\text{O}_2$ fluorescent probes for $^1\text{O}_2$ imaging in biological media. Under that purpose this chapter will focus to solve (or at least improve) some drawbacks of $^1\text{O}_2$ traps.

4.2. Small particles, big improvement: the use of nanoprobess for reactive oxygen species detection in biological media

4.2.1. Nanoparticles protect the fluorescent probes

A large number of fluorescent molecular probes have been synthesized and used, either in solution or in biological medium, for the detection of a variety of analytes.⁵⁴⁷ One of the drawbacks of several fluorescent probes is the interferences with other compounds. This can be due to a lack of specificity or by complexation with proteins presents in the culture medium or inside cells.^{105,107} Furthermore, other possible drawbacks are their phototoxicity due to ROS generation, oxidation of the probe by several oxidants, lack of solubility in water or cell impermeability.⁵⁴⁸ These drawbacks can result in false positives or negatives which can lead to misunderstanding data.

In order to solve, or at least minimize, these drawbacks, some authors have proposed the use of NPs to protect the fluorescence probes (known as nanoprobess).^{549,550} The nanoparticle scaffold shields the fluorescence probe from interaction with medium or large-size macromolecules (e.g., proteins) due to steric hindrance.^{551,552} Figure 4.3 shows the size comparison of a typical globular protein such as bovine serum albumin with a 10-nm size nanoparticle.⁵⁵³

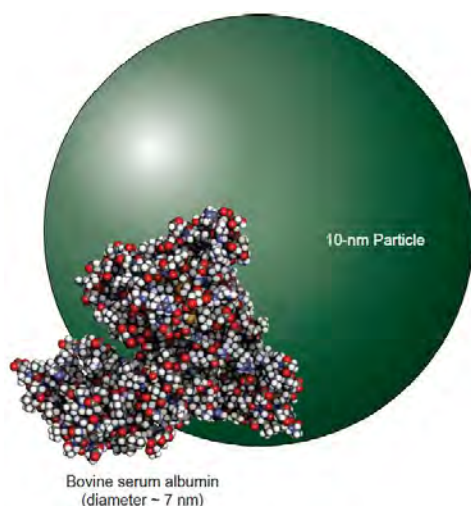


Figure 4.3 Comparison of the relative size of a 10 nm particle and the diameter of a typical protein, bovine serum albumin (BSA), at about 7 nm across its largest axis. Reproduced from reference ⁵⁵³.

Pioneering works in this field were realized by Kopelman and collaborators.⁵⁵⁴ They named them as PEBBLES (Photonic Explorer for Biomedical use with Biologically Localized Embedding). Advances in nanotechnology have made many types of NPs available as platforms, as well as parts of the sensing components, for the construction of PEBBLE sensors in order to overcome the specific drawbacks of each fluorescent probe. The nanosensors have been developed for measurements of ions (H^+ , Ca^{2+} , Cu^+ , Cu^{2+} , Fe^{3+} , Mg^{2+} , K^+ , Na^+ , Pb^{2+} , Zn^{2+} , Cl^-), small molecules (3O_2 , 1O_2 , H_2O_2 , $\bullet OH$) enzymatic intracellular processes (i.e. apoptosis) and physical properties (temperature, electric field). For the case of 1O_2 , only a proof of concept has been described.⁵⁵⁵ Dimethyl-anthracene was embedded inside organically modified silicate. In that study, they proved that nanoprobe was capable to detect 1O_2 generated in solution, however no intracellular 1O_2 detection was explored.

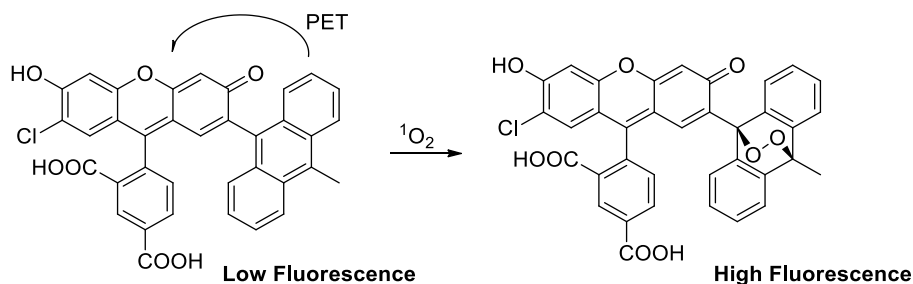
4.2.2. NanoSOSG: a nanostructured fluorescent probe for the detection of intracellular $^1\text{O}_2$

(Adapted from: R. Ruiz-González, ⁺ **R. Bresolí-Obach**, ⁺ Ò. Gulías, M. Agut, H. Savoie, R. W. Boyle, S. Nonell and F. Giuntini, NanoSOSG: A Nanostructured Fluorescent Probe for the Detection of Intracellular Singlet Oxygen, *Angew. Chem. Int. Ed.* **2017**, *56*, 2885.; ⁺These authors contributed equally to this work.)

The results reported in this section have been carried out in collaboration with the University of Hull (United Kingdom) and the Liverpool John Moores University (United Kingdom).

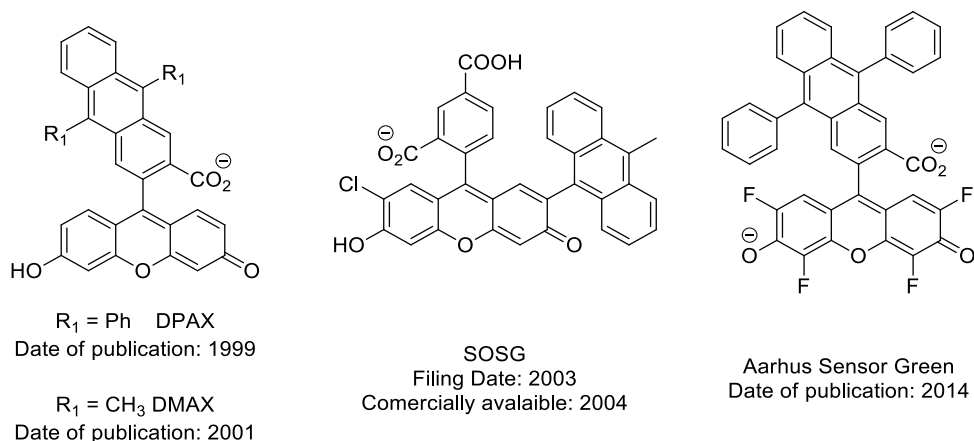
4.2.2.1 Singlet Oxygen Sensor Green[®]

Singlet Oxygen Sensor Green[®] (SOSG) is a dyad composed by a fluorescein moiety whose fluorescence is quenched by photoinduced intramolecular electron transfer (PET) due to the presence of a proximal, covalently bound, anthracene moiety.^{104,105} Upon anthracene endoperoxidation in the presence of $^1\text{O}_2$, the electron transfer is blocked restoring the fluorescein's intrinsic fluorescence (see scheme 4.1).¹⁰⁵ Moreover, according to manufacturer: "SOSG does not show any appreciable response to $\cdot\text{OH}$ or $\text{O}_2^{\cdot-}$ ".⁵⁵⁶



Scheme 4.1 SOSG chemical structure before and after oxidation by $^1\text{O}_2$ as described in manufacturer patent⁵⁵⁷ and by Gollmer *et al.*¹⁰⁵

SOSG is the natural-evolution from the original $^1\text{O}_2$ fluorogenic probes DMAX and DPAX designed, synthesized and characterized by Nagano *et al* (Scheme 4.2).^{103,558} In one of the first works that used SOSG as $^1\text{O}_2$ fluorescent probe, Flors *et al* used it in order to detect the $^1\text{O}_2$ generation in plant leaves.⁹⁵ Since then, the scientific community has widely used SOSG[®] in different biological situations.



Scheme 4.2 DPAX (9-[2-(3-carboxy-9,10-diphenyl)anthryl]-6-hydroxy-3H-xanthen-3-one), DMAX (9-[2-(3-carboxy-9,10-dimethyl)anthryl]-6-hydroxy-3H-xanthen-3-one), SOSG and Aarhus Sensor Green chemical structures.^{103,105,558,559}

In that moment, SOSG structure was trade secret and its mechanism of activation was unknown. So, different works have been published in order to elucidate its structure and unravel its photochemistry.^{104,105,560} The more-important elucidated characteristics:

i) SOSG is able to produce $^1\text{O}_2$ under exposure to UV or visible radiation (Φ_{Δ} of 0.03 and 0.009 for λ_{exc} 355 and 532 nm respectively in methanol). This self-sensitization is enough for the appearance of green fluorescence upon exposure of SOSG to either UV or visible radiation, even in the absence of external PS.¹⁰⁴ Recently, computational studies that UV-A irradiation opens the way to a possible intersystem crossing pathways leading to fluorescein triplet population.⁵⁶¹

ii) UV irradiation leads to its photobleaching due to the formation of radical species by electron transfer from fluorescein excited state to anthracene.^{104,560}

iii) SOSG fluorescent endoperoxide, is itself an efficient sensitizer of $^1\text{O}_2$ (Φ_{Δ} of 0.18 for λ_{exc} 420 nm).¹⁰⁵

iv) The fast PET (as the intramolecular fluorescence quenching of the fluorescein singlet excited state by anthracene to obtain anthracene radical cation) has a $k_{\text{PET}} = 9.7 \times 10^{11} \text{ s}^{-1}$ and the subsequent back electron transfer has a $k_{\text{CR}} = 2.0 \times 10^{11} \text{ s}^{-1}$.⁵⁶⁰

v) SOSG is capable to form complexes with globular proteins (such as BSA), hindering the interpretation of the results in complex biological media as explained below.¹⁰⁵

vi) SOSG can be used in quantitative studies of $^1\text{O}_2$. As example, Lin *et al* obtained Φ_{Δ} of a porphyrin-based photosensitizer in PBS by using SOSG in good agreement with the value that independently determined by using direct $^1\text{O}_2$ phosphorescence.⁵⁶²

Nowadays, is so widely-used SOSG, that some authors synthesize SOSG analogues such as Aarhus Sensor Green to solve some the previous explained drawbacks, such as self- $^1\text{O}_2$ generation.⁵⁵⁹ Other authors take advantage of the dyad concept, but they use other fluorophores and/or $^1\text{O}_2$ traps to improve the performance of SOSG as turn-on $^1\text{O}_2$ fluorescent probe (i.e. the $^1\text{O}_2$ fluorescent probe used in section 4.2.4. is one example).

With all the previous considerations in mind, we envisaged a polyacrylamide NP scaffold that might be able to fulfill the requirements for a good intracellular $^1\text{O}_2$ nanoprobe and circumvent many of the reported drawbacks of SOSG (such as protein interaction or cell-internalization). In this section it is reported the photochemical behavior and performance of polyacrylamide-based SOSG nanoprobes.

4.2.2.2. Experimental section

4.2.2.2.1. Synthesis of the NPs

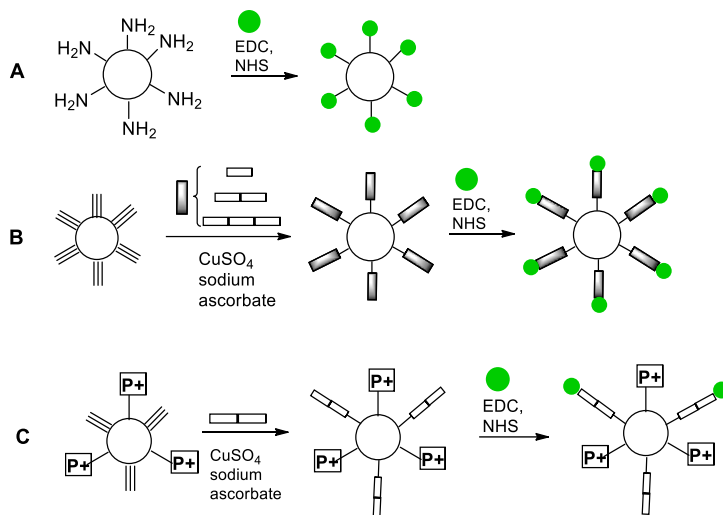
All the NPs of this section were synthesized by Dr. Rubén Ruiz-González.

4.2.2.2.2. Photodynamic inactivation protocol

Photodynamic inactivation experiments of *E. coli* (ATCC 35218) and *E. coli* DH5 α expressing miniSOG were carried out. Cell cultures in exponential growing phase were induced with 0.1% arabinose for 20 min. After replacing the growth medium with PBS, cells were transferred to an optical non-treated sterile glass chamber and irradiated through the top of the chamber by means of blue fluorescent lamps (LZC-420; λ_{irr} 420 \pm 20 nm; 13 mW/cm²). For CFU determination, irradiated/control sample aliquots was serially diluted, streaked on nutrient agar, and incubated in the dark for 18 h at 37 °C.

4.2.2.3 Assessment and optimization of the nanoprobess

As a primary approach to produce a versatile NP scaffold for attaching a fluorescent probe, we developed the simplest scenario in which a $^1\text{O}_2$ chemical trap is readily attached to the polyacrylamide NPs, as depicted in Scheme 4.3, panel A. Amino-derivatized NPs were covalently bound to SOSG. SOSG has a carboxylic group that under suitable activation can react with amino groups on the NPs.



Scheme 4.3 Conjugation of SOSG to functionalized polyacrylamide NPs, in the absence (A) and in the presence (B) of a spacer, and with positively-charged trimethylphosphonium groups (C; nanoSOSG).

Aqueous solutions containing 2 mg/mL of these NPs and 1 μM of new methylene blue (NMB) as PS were irradiated and the probe fluorescence changes observed over time. The response of the nanoprobess was poor when compared to the free probes, i.e. a modest 10% fluorescence increase for SOSG-NPs after 10 min irradiation (Figure 4.5). Even in D_2O , where the $^1\text{O}_2$ lifetime is 20-fold longer than in H_2O and is thus more available for reaction,^{55,214,529} the fluorescence enhancement was below 40%.

We ascribed the poorer nanoprobe performance (compared to free SOSG) to nonspecific interactions occurring between the probe and the polyacrylamide matrix, leading to decreased reactivity of the SOSG molecule bound to the polymer network. In this context, it is relevant that the initial fluorescence on SOSG-NPs was substantially higher than that of free SOSG, which suggests that the microenvironment of SOSG in the nanoprobe precludes efficient electron-transfer quenching.

Thus, spacers of different lengths were introduced to separate the polyacrylamide scaffold and the probe. To this end, the polyacrylamide matrix was synthesized presenting alkyne groups on the outer surface so that the linkers could be coupled via copper-catalyzed azide-alkyne cycloaddition chemistry.⁵⁶³ Moreover, all the linkers displayed a free terminal amino group, which could be conjugated to SOSG via amide bond formation.

New nanoprobess including linkers of three different lengths S, M and L were synthesized, characterized and tested in solution, as summarized in Scheme 4.3 (panel B). For both types of probe, absorption and emission spectra corresponded to that of the free probe (Figure 4.4) even if, in the case of absorption, a tail in the base line could be seen due to NP scattering. Inclusion of a linker improved the performance of the nanoprobess, although none of them could outperform their free molecular counterparts. The

nanoprobe in which a medium-size (M, 7.1 Å) linker was used provided the best $^1\text{O}_2$ trapping efficiency: SOSG enhanced its fluorescence up to 3.2-fold in D_2O after 50 min irradiation. This nanoprobe (henceforth called NanoSOSG) was selected for further experiments. Its surface was further functionalized with cationic groups to facilitate cellular uptake (Scheme 4.3C).

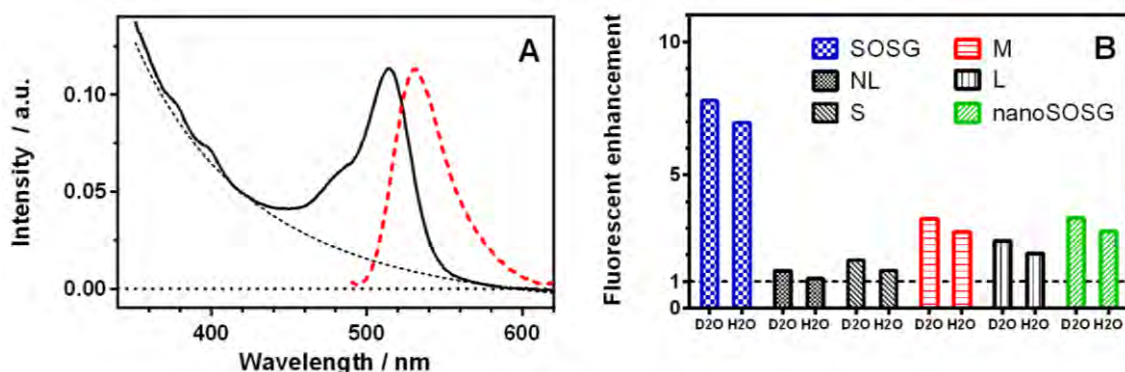


Figure 4.4 (A): Absorption and emission spectra SOSG bound to the NPs through the M spacer. (B): SOSG (and their nanoparticulates derivatives) fluorescence enhancement after 50 min irradiation in H_2O or D_2O . The concentration of the probes was 1 mg/mL. $^1\text{O}_2$ was generated by irradiation of 1 μM NMB with red light. Results for the corresponding molecular probes are given for comparison.

SOSG is described as cell-impermeant,⁵⁵⁶ which would detract from its usefulness as $^1\text{O}_2$ probe in biological media. Gollmer *et al.* concluded that this was actually due to binding to proteins in the culture medium and showed that SOSG could in fact be internalized by HeLa cells if cultured in protein-free media.¹⁰⁵ Additional effects of protein binding were reported such as a red-shifted fluorescence spectrum and a lower rate of fluorescence increase in the presence of bovine serum albumin (BSA), which the authors attributed to the protein kinetically competing with SOSG for $^1\text{O}_2$ molecules. Moreover, intracellular SOSG showed an additional number of problems for use as $^1\text{O}_2$ reporter: its fluorescence spectrum was also red-shifted relative to that observed in aqueous solutions, intense fluorescence could be observed even before exposing it to $^1\text{O}_2$, and it was difficult to obtain systematic and reproducible results upon irradiation.¹⁰⁵ In view of these negative reports we set out to assess whether nanoSOSG suffered from the same drawbacks.

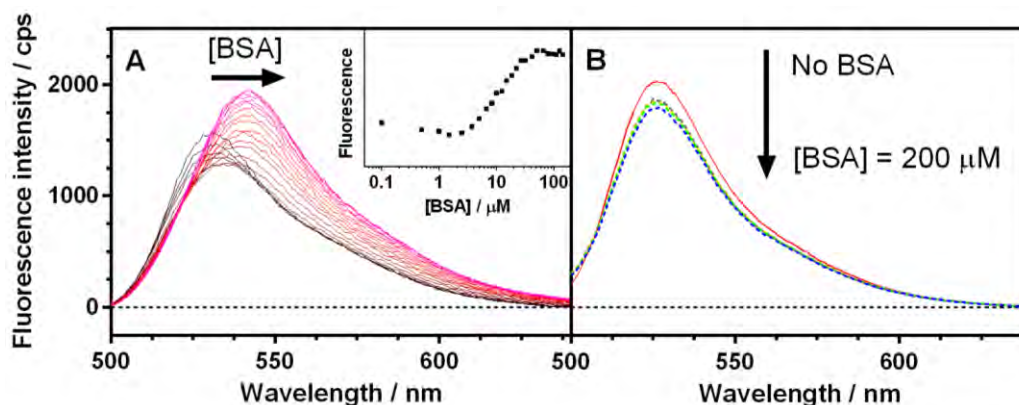


Figure 4.5 Changes in the (A) SOSG and (B) nanoSOSG fluorescence spectra upon addition of BSA (0-200 μM). $\lambda_{\text{exc}} = 485 \text{ nm}$. Inset: Fluorescence intensity at 541 nm as a function of BSA concentration.

Figure 4.5 shows the fluorescence spectra of SOSG and nanoSOSG in PBS in the presence of increasing amounts of BSA up to 200 μM . In the case of SOSG the spectrum shifted to the red and the fluorescence intensity changed biphasically, indicating that the probe associates to the protein.⁵⁶⁴ Similar situations are likely to occur in protein-rich environments as in cells. In contrast, no such effects were observed for nanoSOSG except for a slight fluorescence quenching at the highest BSA concentration, indicating that the interactions of the nanoprobe with the protein are essentially prevented by the NP scaffold. Thus, nanoSOSG seems more suited than SOSG as a fluorescent probe for $^1\text{O}_2$ in biological media.

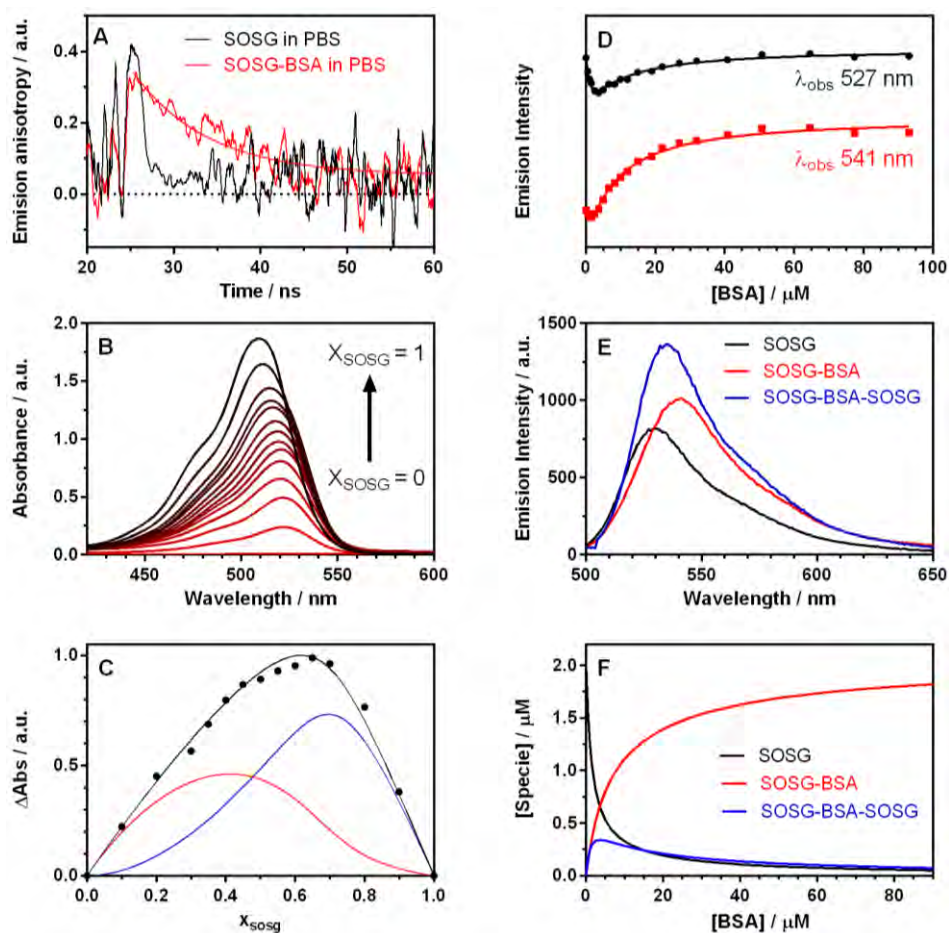


Figure 4.6 (A): Time-resolved anisotropy of SOSG (black) and a mixture of 2 μM SOSG and 150 μM BSA in PBS (red). $\lambda_{\text{exc}} = 502$ nm; $\lambda_{\text{obs}} = 540$ nm. (B) Absorption spectra of SOSG-BSA mixtures in which the sum of concentrations is kept constant ($[\text{SOSG}] + [\text{BSA}] = 30$ μM). (C) Job plot of the data in panel B. The solid line is a simulation of a model that assumes the formation of 1:1 and 2:1 complexes, whose individual contribution is given by the red and blue lines, respectively. (D) Examples for two particular wavelengths of the global fit of the association model to the fluorescence spectra in Figure 4.5. (E) Decomposition of the fluorescence spectra of the SOSG-BSA mixtures into its individual components. (F) Calculated concentrations of SOSG and the 1:1 and 2:1 complexes as a function of the BSA concentration.

Due to importance of SOSG as the mainly used $^1\text{O}_2$ fluorescent probe, we decided to study further the association of SOSG to BSA by absorption and fluorescence spectroscopies (Figure 4.6). Time-resolved fluorescence anisotropy of a mixture 2 μM SOSG and 150 μM BSA in PBS was measured and compared to that of free SOSG (Figure 4.6A).^{565–567} The anisotropy decay for free SOSG was faster than the time resolution of our system (0.1 ns), in agreement with free rotation in PBS. In contrast, the

anisotropy decay in the presence of BSA showed a much slower decay that could be fitted with a single rotational correlation time of 8.6 ns, indicating that SOSG rotation was restricted, consistent with its association to BSA. The stoichiometry of the complex(es) was(were) characterized by a Job plot analysis.⁵⁶⁸ Thus, the absorption spectra of a series of SOSG-BSA solutions were measured keeping their sum concentration constant ($[SOSG] + [BSA] = 30 \mu\text{M}$; Figure 4.6B). The Job plot maximum at SOSG molar fraction 0.66 indicates that a 2:1 complex is formed (Figure 4.6C). However, closer inspection of the plot suggests that the 1:1 complex is formed as well, albeit with a lower association constant. The fluorescence data in Figure 4.5 was analysed by a spectral deconvolution software (Specfit/32) assuming the formation of 1:1 and 2:1 complexes with association constants β_1 and β_2 . Data analysis yielded the two association constants, $\beta_1 = 3.8 \times 10^5 \text{ M}^{-1}$ and $\beta_2 = 3.0 \times 10^{11} \text{ M}^{-2}$, the spectra of the two complexes, the concentration of the two species at each BSA concentration and the fitted fluorescence intensity profiles (Figure 4.6D-F).

At last step, in order to assess the ability of the nanoprobe to respond to the presence of $^1\text{O}_2$ inside cells, a series of assays were conducted on wild type *E. coli* (wt) and on a genetically-modified *E. coli* strain expressing miniSOG, a flavin-binding fluorescent protein with strong capacity to sensitize $^1\text{O}_2$ production inside cells.^{286–288} Figure 4.7 presents the behavior of SOSG/nanoSOSG in both types of cells.

Figure 4.7A shows that the fluorescence spectrum of SOSG in the presence of *E. coli* cells matches that in PBS, indicating that it is not bound to a protein. The effects of irradiation at $420 \pm 20 \text{ nm}$ are shown in Figure 4.7B and 4.7C. In wt cells the fluorescence of SOSG increases linearly as a result of its self-sensitized photooxidation.⁵⁶⁹ In miniSOG-expressing cells, the rate of fluorescence increase shows two distinct regions: up to 15 min irradiation, the fluorescence increases at a rate similar to that observed in wt cells, whereas after that the rate increases approximately by 2.5-fold. The viability of wt cells is not compromised by irradiation of SOSG whereas cells expressing miniSOG are killed very effectively, with more than 90% being killed after just 15 min (Figure 4.7C). Taken together, these results indicate that SOSG and miniSOG are not in close proximity at the early stages of irradiation, i.e., SOSG is not internalized by *E. coli* cells. The fluorescence increase observed in both cells at these early times is due solely to SOSG self-sensitized $^1\text{O}_2$ produced in the outer aqueous media and it is therefore independent of intracellular $^1\text{O}_2$. In miniSOG-expressing cells, intracellular $^1\text{O}_2$ damages the cell from the inside^{570,571} and eventually miniSOG is released to the external medium where it enhances the rate of SOSG photooxidation. An alternative explanation such as photochemical internalization of SOSG⁵⁷² can be ruled out because no spectral changes are observed after irradiation.

As expected, nanoSOSG does not interact with cell proteins neither before nor after extensive irradiation (Figure 4.7D). The rate of fluorescence increase in wt and miniSOG-expressing cells is different already at early irradiation stages (Figure 4.7E), indicating that nanoSOSG is close to miniSOG from the onset, i.e., nanoSOSG has been internalized by *E. coli* cells. This is confirmed by the results of cell photoinactivation studies, which show cell mortality in wt bacteria (Figure 4.7F) due to intracellular $^1\text{O}_2$ photosensitized by nanoSOSG. In miniSOG-expressing cells, both a higher fluorescence increase and an enhanced cell photokilling can be observed, consistent with a higher rate of intracellular $^1\text{O}_2$ production due to miniSOG. Of note, nanoSOSG is devoid of any

measurable dark toxicity (Figure 4.7F). NanoSOSG-sensitized photoinactivation of bacteria should be of lesser importance in imaging experiments because the light doses used are typically at least one order of magnitude lower than those used in this section.⁵⁷³ Moreover, it can be totally avoided in photosensitisation experiments by using an excitation wavelength where SOSG does not absorb.

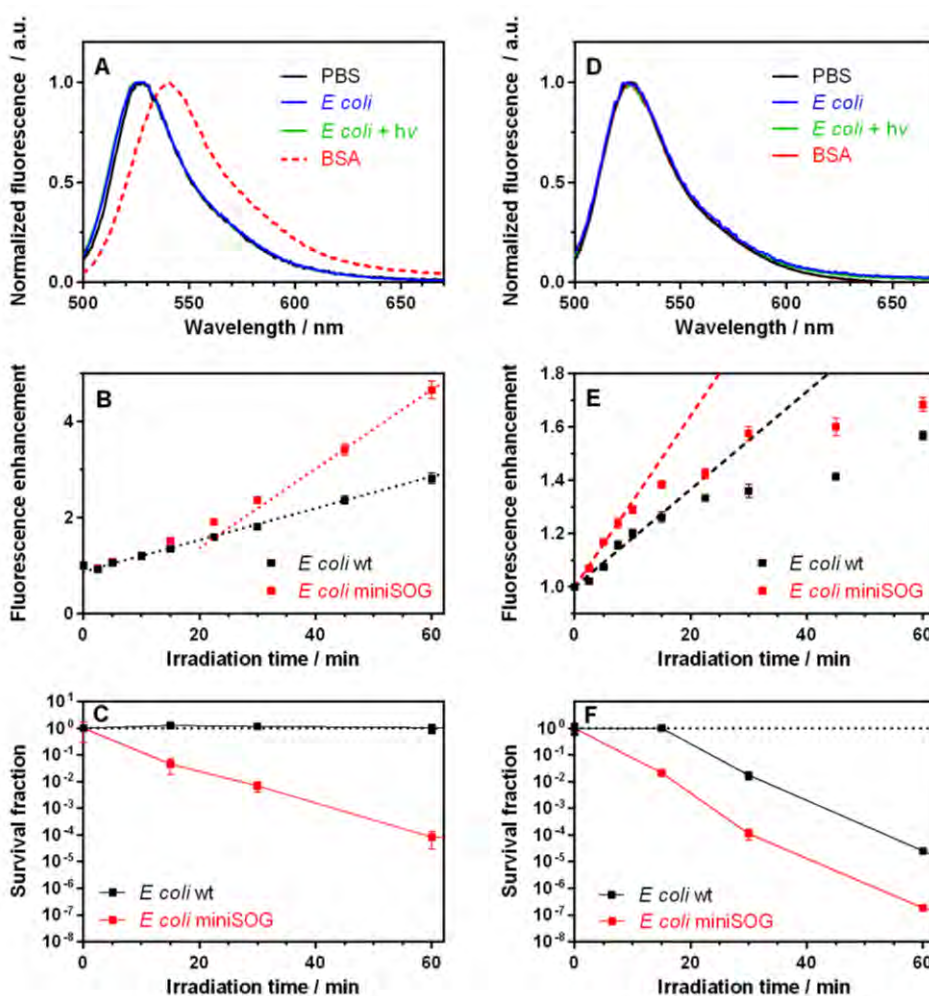


Figure 4.7 Comparison of SOSG (left panels) and NanoSOSG (right panels). (A) Fluorescence spectra of SOSG in PBS, in *E. coli* before and after irradiation, and in the presence of 200 μ M BSA. (B) Fluorescence enhancement of SOSG in wt (black) and miniSOG-expressing (red) *E. coli* cells as a function of the irradiation time ($\lambda_{exc} = 420 \pm 20$ nm). (C) Photoinactivation of wt (black) and miniSOG-expressing (red) *E. coli* cells pre-incubated with SOSG as a function of the irradiation time ($\lambda_{exc} = 420 \pm 20$ nm). (D) Fluorescence spectra of NanoSOSG in PBS, in *E. coli* before and after irradiation, and in the presence of 200 μ M BSA. (E) Fluorescence enhancement of NanoSOSG in wt (black) and miniSOG-expressing (red) *E. coli* cells as a function of the irradiation time ($\lambda_{exc} = 420 \pm 20$ nm). (F) Photoinactivation of wt (black) and miniSOG-expressing (red) *E. coli* cells pre-incubated with SOSG as a function of the irradiation time.

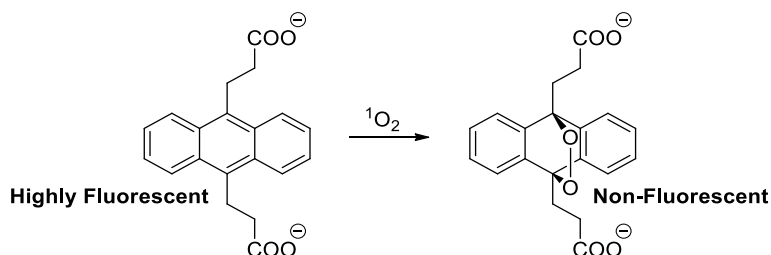
4.2.3. NanoADPA: a nanostructured fluorescent probe for the detection of intracellular $^1\text{O}_2$

(Adapted from: **R. Bresolí-Obach**, J. Nos, M. Mora, M.L. Sagristà, R. Ruiz-González and S. Nonell, Anthracene-based fluorescent nanoprobe for singlet oxygen detection in biological media, *Methods*. **2016**, 109, 64)

The results reported in this section have been carried out in collaboration with the Universitat de Barcelona (Barcelona, Spain).

4.2.3.1 Anthracene dipropionate

Polycyclic aromatic hydrocarbons such as anthracenes or rubrene are commonly used as $^1\text{O}_2$ traps.¹¹¹ Among them, anthracene dipropionic acid (ADPA), which can be monitored by both absorption and/or fluorescence spectroscopies,^{286,506,574,575} is highly reactive against $^1\text{O}_2$ (reactive rate constant, $k_r = 8 \times 10^7 \text{ M}^{-1}\text{s}^{-1}$ in D_2O).⁵⁷⁶ ADPA shows structured absorption and fluorescence spectra with maximums around 380 and 430 nm respectively. Upon reaction with $^1\text{O}_2$, its characteristic absorption/fluorescence is bleached concomitant with the formation of an endoperoxide adduct (Scheme 4.4).⁵⁷⁶



Scheme 4.4 ADPA chemical structure before and after oxidation by $^1\text{O}_2$.

A main problem from molecular $^1\text{O}_2$ fluorescent traps is complex-formation with proteins (see section 4.2.2) which affects their response to $^1\text{O}_2$ and often prevents their uptake by cells.^{105,287} Novel anthracene derivatives have been developed that aim at alleviating these problems.^{577,578} Although that, these drawbacks have not been fully solved and its synthetic complexity is highly increased.

In this section, we prove that the “nano” approach for polyacrylamide NPs can also be expanded to other types of NPs (i.e. mesoporous and compact silica NPs) which our group have a better know-how for its synthesis and derivatization. NanoADPA has been internalized by HeLa cells, thus being capable of detecting intracellularly $^1\text{O}_2$.

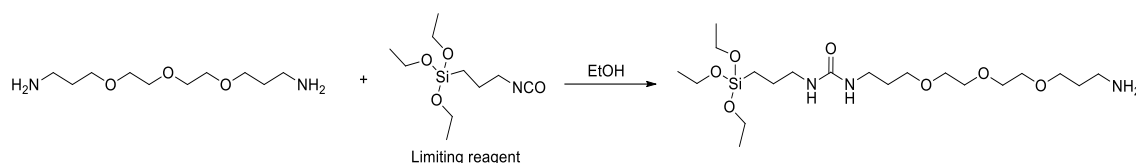
4.2.3.2. Experimental section

4.2.3.2.1. Synthesis of N-(4,7,10-trioxa-13-tridecaneamine)-N'-(3-(triethoxysilyl)-propyl)-urea ((OEt)₃-Si-L-NH₂)

220 μ L (1.00 mmol) 4,7,10-trioxa-1,13-tridecanediamine and 83 μ L (0.34 mmol) 3-(triethoxysilyl)propyl isocyanate were mixed in 2 mL of EtOH and kept reacting 24 h at room temperature. The crude was diluted with 3 mL of EtOH and used without further purification (Scheme 4.5).

¹H-NMR (CDCl₃): 3.79 (6H, q, 7.0 Hz), 3.63-3.54 (12H, m), 3.27 (2H, m), 3.11 (2H, m), 2.88 (2H, m), 2.61 (4H, s, deuterable signal), 1.75 (4H, m), 1.57 (2H, m), 1.20 (9H, t, 7.0 Hz) and 0.60 (2H, m). ¹³C-NMR (CDCl₃): 158.7 (1C, urea carbon), 70.4 (1C), 70.3 (2C), 69.9 (1C), 69.8 (1C), 69.6 (1C), 58.3 (3C), 42.9 (1C), 39.5 (1C), 38.4 (1C), 32.5 (1C), 29.3 (1C), 23.8 (1C), 18.3 (3C) and 7.6 (1C) ppm. No signals were observed in the region 130-120 ppm that could be attributed to N=C=O.

IR (KBr disk): 3450 (t N-H), 2945 (t C-H), 1654 (t C=O; urea bridge), 1402 and 1085 cm⁻¹. No bands could be observed in the region 2400 to 2200 cm⁻¹ that could be attributed to N=C=O tension.



Scheme 4.5 Synthesis of (OEt)₃-Si-L-NH₂.

4.2.3.2.2 Silica Nanoparticles synthesis

Synthesis of MSNP. 200 μ L of ammonia solution (30 % w/w; 3.2 mmol) were added to a solution of water (65 mL), EtOH (12 mL), and CTAC (10.5 mL; 7.9 mmol). The mixture was heated at 80 °C and stirred at 1200 rpm for 1 hour. Then, 7.5 mL of TEOS (33.6 mmol) were added dropwise and the reaction was stirred for 12 minutes at 80 °C. The crude was centrifuged at 6000 rpm for 5 min in order to remove any microparticles synthesized. After removing the solid, the supernatant was further centrifuged at 12000 rpm for 20 min and resuspended in EtOH. The MSNPs were washed two more times with EtOH. Afterwards, 100 mL of HCl (37% w/w) were added under stirring and kept at reflux for 17 h. MSNPs were obtained after centrifugation at 12000 rpm for 20 minutes and were resuspended in water. Afterwards, MSNPs were washed twice with water and later twice with EtOH. The final NPs were stored suspended in EtOH (10 mg/mL).

Synthesis of CSNP. The method has been adapted from ref.⁵⁷⁹ Briefly, 5 mL of TEOS (23 mmol) were added to a solution of water (2.5 mL), 2-propanol (94 mL) and ammonia solution (300 μ L; 4.8 mmol). The reaction was left stirring at room temperature for 3 days. The crude was centrifuged at 6000 rpm for 5 min in order to remove the microparticles synthesized. The solid was removed and the supernatant was centrifuged at 12000 rpm for 20 min and resuspended in EtOH. Afterwards, CSNP were washed twice with EtOH and stored suspended in EtOH (10 mg/mL).

Synthesis of SMSNP/SCSNP. 200 μL of APTES (0.77 mmol) were added to 50 mL of MSNP/CSNP solution (10 mg/mL). The reaction was left stirring at 40 °C for 24 hours. Afterwards, the mixture was washed 3 times with EtOH by centrifugation at 12000 rpm for 20 minutes. The final SMSNP/SCSNP were stored suspended in EtOH (5 mg/mL).

Synthesis of LMSNP/LCSNP. 1.5 mL of the $(\text{OEt})_3\text{-Si-L-NH}_2$ solution (0.10 mmol) were added to 10 mL of MSNP/CSNP solution (10 mg/mL). The reaction was left stirring at 40 °C for 24 hours. Afterwards, the mixture was washed 3 times with EtOH after centrifugation at 12000 rpm for 20 minutes. The final SMSNP/SCSNP were stored suspended in EtOH (5 mg/mL).

Conjugation of ADPA onto the functionalized NPs. 14.7 mg (77 μmol) of EDC, 14.5 mg (126 μmol) of NHS and 4.0 mg (11 μmol) of ADPA were dissolved in 2 mL of dry CH_2Cl_2 . The mixture was left under stirring at room temperature for 2 h. The activated ADPA mixture was added dropwise to a stirred solution of SNPs in acetonitrile (10 mg/mL). The reaction crude was kept reacting at room temperature for 72 h. Afterwards, the SNPs were isolated and washed through repeated centrifugations (20 min at 12000 rpm) in EtOH.

4.2.3.2.3 Cellular techniques

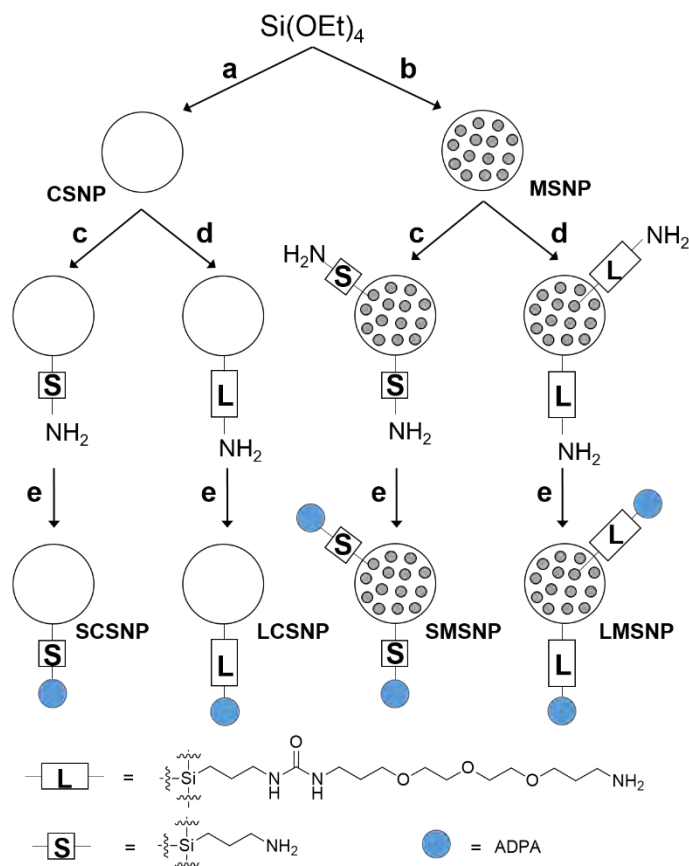
Cell Culture. Human carcinoma HeLa cells were grown as monolayer cultures in DMEM supplemented with 10% (v/v) FBS, 1% (v/v) penicillin-streptomycin solution and 1% (v/v) L-Glutamine. Cells were cultured in an incubator with 5% CO_2 plus 95% air at 37 °C. Cells were seeded in 25 cm^2 flask and subconfluent cell cultures were used.

Cell preparation for confocal microscopy. Main cell culture was trypsinized and 5×10^4 HeLa cells/well were added to 8-wells plates. The cells were incubated at 37 °C for 24 h. Then the cell culture medium was removed and 2 μM nanoADPA was added and left under incubation at 37 °C for 24 h. The cell culture was washed 6 times with PBS in order to discard the non-internalized suspended NPs. Then, CMFDA (CellTracker™ Green; 2.5 μM) was added and incubated at 37 °C for 30 min. The cells were washed twice with PBS. When RB was needed, cells were incubated for 60 minutes with supplemented DMEM and 10 μM of RB. Otherwise cells were incubated with supplemented DMEM for 60 minutes. Afterwards, they were washed twice with PBS. Finally, DMEM (without phenol red) with Hepes buffer were added.

Microscopical analysis. All confocal images were taken with minimum exposure using a TCSP SP2 Leica Confocal Microscope (Leica Microsystems CMS, Wetzlar, Germany) and were collected with 2 channels. The first one was used for monitoring nanoADPA (Ar-UV laser, λ_{exc} 364 nm, λ_{obs} 381-477 nm) and the second for CMFDA (Ar laser, λ_{exc} 488 nm, λ_{obs} 500-550 nm). The RB samples were irradiated at 561 nm (DPSS laser) in order to generate $^1\text{O}_2$. All photographs were processed and analysed using the Fiji J software (Adobe Systems, San Jose, CA).^{580,581}

4.2.3.3. Assessment and optimization of the nanoADPA

In a first step, we developed a simple nanoconjugate in which ADPA is directly attached covalently to the pre-formed SNPs, as depicted in Scheme 4.6. Two different types of SNP were synthesized: compact (CSNP)⁵⁷⁹ and mesoporous (MSNP).⁴⁶⁹ Each type was functionalized with short (S) and long (L) linkers with terminal amino groups and finally ADPA was covalently linked by Steglich amidation.⁵⁸²



Scheme 4.6 Synthesis, derivatization and ADPA conjugation. Reagents and conditions: a) CTAC, EtOH, H_2O , NH_3 , 80 °C, 12 min, then HCl (37%), reflux, 24 h. b) 2-Propanol, EtOH, H_2O , NH_3 , room temperature (rt). 72 h. c) APTES, EtOH, rt, 24 h. d) Si-Linker, EtOH, rt, 24 h. e) ADPA, EDC, NHS, Na_2CO_3 , $\text{CH}_3\text{CN}:\text{CH}_2\text{Cl}_2$ (1:1), rt, 24 h.

All synthesized SNPs were characterized by their size and ζ -potential (Table 4.1) as well as by infrared spectroscopy. Dynamic light scattering shows that the starting CSNP and MSNP rendered a hydrodynamic diameter of 100 and 140 nm, respectively, and a ζ -potential of -30 and -41 mV, respectively. After surface functionalization and ADPA conjugation, the diameter of the NPs increased up to 30 nm and the ζ -potential became less negative and even turned positive when the external amines were protonated (Table 4.1). ADPA concentration was quantified for these NPs, ranging from 0.02 to 0.18 μmol per mg of silica. MSNP showed the highest loading capacity.

Table 4.1 Size, ζ -potential, free amino concentration, and ADPA conjugated concentration of the NP synthesized. ADPA concentration is calculated by UV-Vis spectroscopy (a) and elemental organic analysis (b).

SNPs	Size / nm	ζ -potential in H ₂ O /mV	ζ -potential in 100 mM AcOH /mV	[Terminal NH ₂] / mmol/mg SNP	[ADPA] / mmol/mg SNP
MSNP	144 ± 56	-40.9 ± 3.7	-40.9 ± 3.7	---	---
SMSNP	136 ± 40	-4.4 ± 5.5	55.0 ± 4.3	0.77 ± 0.08	---
SMSNP@ADPA	173 ± 32	-12.1 ± 4.8	43.4 ± 4.4	0.59 ± 0.06	0.18 ± 0.01 ^a 0.16 ± 0.01 ^b
LMSNP	132 ± 32	-4.6 ± 5.2	32.5 ± 5.2	0.35 ± 0.03	---
LMSNP@ADPA	127 ± 32	-13.3 ± 4.3	15.5 ± 3.9	0.32 ± 0.02	0.034 ± 0.004 ^a 0.037 ± 0.004 ^b
CSNP	99 ± 29	-30.4 ± 6.0	-30.4 ± 6.0	---	---
SCSNP	97 ± 24	-8.7 ± 3.1	50.2 ± 5.1	0.14 ± 0.02	---
SCSNP@ADPA	138 ± 38	-12.4 ± 3.4	30.3 ± 3.4	0.12 ± 0.01	0.022 ± 0.004 ^a 0.018 ± 0.004 ^b
LCSNP	145 ± 42	-11.5 ± 4.3	25.3 ± 3.8	0.24 ± 0.02	---
LCSNP@ADPA	148 ± 49	-14.5 ± 4.1	11.5 ± 3.5	0.21 ± 0.02	0.028 ± 0.004 ^a 0.029 ± 0.004 ^b

To evaluate the ¹O₂ detection capacity, ethanolic solutions containing 6 μM ADPA conjugated with SNPs and 6 μM MB as PS ($\Phi_{\Delta} = 0.52$)⁵⁸³ were irradiated at 656 nm. The fluorescence of ADPA was then monitored as photooxidation proceeded. Figure 4.8 shows that MSNPs (squares) enhance ADPA photooxidation compared to the CSNP (circles) counterparts. Figure 4.8 also shows that the length of the linker between the NP surface and ADPA has a pronounced effect of the photooxidation rate (cf. empty versus filled symbols, respectively). Specifically, a long linker facilitates ADPA photooxidation, probably because it is further away from the NP surface (1.9 versus 0.7 nm respectively) where ¹O₂ quenching by surface silanols takes place.⁵⁰³ We therefore selected MSNPs with long linkers as the best scaffold for ADPA to maximise its response to ¹O₂ (hereafter nanoADPA).

It is noteworthy that, for the same overall ADPA concentration, nanoADPA loses its fluorescence faster than free molecular ADPA. This effect is due to the increased generation of ¹O₂ as scattering extends the pathway of light in the MSNPs suspension. This interpretation was confirmed in an experiment in which empty MSNPs were added to a molecular ADPA solution. Under these conditions, ADPA bleached faster than nanoADPA (Figure 4.8B).

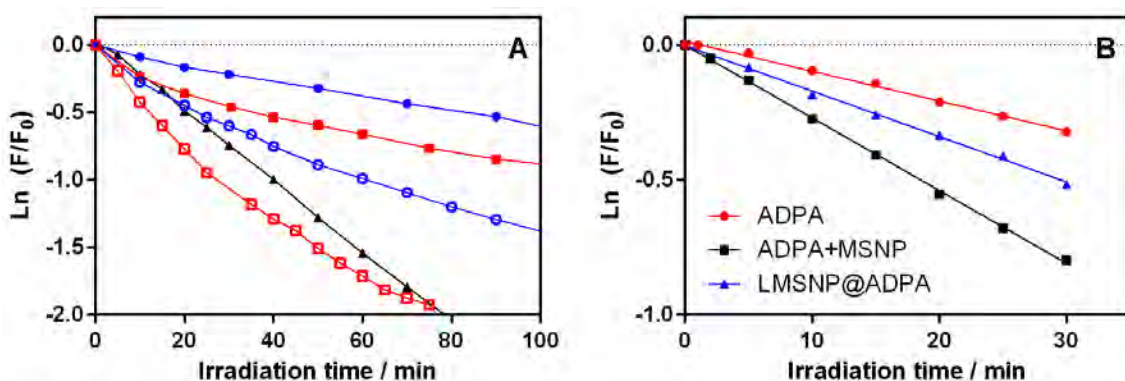


Figure 4.8 ADPA bleaching upon $^1\text{O}_2$ generation by an exogenous photosensitizer (6 μM MB; λ_{exc} 656 nm) in ethanol. (A): Black triangle free ADPA. Blue circles and red squares ADPA-CSNP and ADPA-MSNP respectively. Closed for short linker and open for large linker. (B): Black square is free ADPA with empty MSNP in order to simulate the scattering effect. Blue triangles is LMSNP and red circles is free ADPA without empty MSNP.

An alternative explanation could be that MB binds to the silica surface and engage in specific photochemistry with the probe. We have previously shown that MB can indeed adsorb on MSNPs and that binding shifts its fluorescence spectrum to the blue (Section 3.4.2.1). However, we did not see such shift when nanoADPA was added to ethanol solutions of MB, therefore we rule out binding of MB to nanoADPA. On the other hand, after 90% decrease of ADPA fluorescence we observe a mere 7% loss of MB fluorescence. Moreover, the photooxidation rate (v_{ADPA}) is faster in deuterated phosphate buffer saline (dPBS) than in PBS (Figure 4.9A), which is consistent with a longer lifetime of $^1\text{O}_2$ in D_2O than in H_2O (68 μs versus 3.3 μs , respectively).^{584,585} Taken together, the results above indicate that $^1\text{O}_2$ is the oxidizing species, other oxidation mechanisms playing a minor role, if any, in the photobleaching of nanoADPA.

In order to further characterize nanoADPA, its response to $^1\text{O}_2$ was tested also using three PSs with different electrical charge and solvents of different polarity. The chosen PSs were the neutral tetraphenylporphyrin (TPP), its tetracationic N-methylpyridyl counterpart (TMPyP) and its tetraanionic sulfonatophenyl analogue (TPPS₄), which have almost identical Φ_{Δ} values.^{436,586} Likewise, the chosen solvents were EtOH, acetonitrile and PBS. As shown in Figure 4.9B, v_{ADPA} was the same for all three PSs irrespective of the solvent, indication of insensitivity of the probe to neither PS charge nor solvent polarity. On the other hand, v_{ADPA} was faster in acetonitrile than in ethanol, which, in turn, was faster than in PBS.

This observation is consistent with the known variation of $^1\text{O}_2$ lifetime with the solvent, namely 83 μs in acetonitrile, 15.5 μs in ethanol and 3.3 μs in PBS,⁵⁸⁵ indicating that $^1\text{O}_2$ decay is controlled by solvent interactions (Eq. 4.1):

$$v_{\text{ADPA}} \approx v_{\Delta} \cdot k_r \cdot \tau_{\Delta}^0 \cdot [\text{ADPA}] \quad \text{Eq. 4.1}$$

where v_{Δ} is the rate of $^1\text{O}_2$ production, k_r corresponds to the endoperoxidation rate constant and τ_{Δ}^0 stands for the lifetime of $^1\text{O}_2$ in the neat solvent. It can thus be concluded that nanoADPA photooxidation by $^1\text{O}_2$ is independent of the PS charge and solvent polarity.

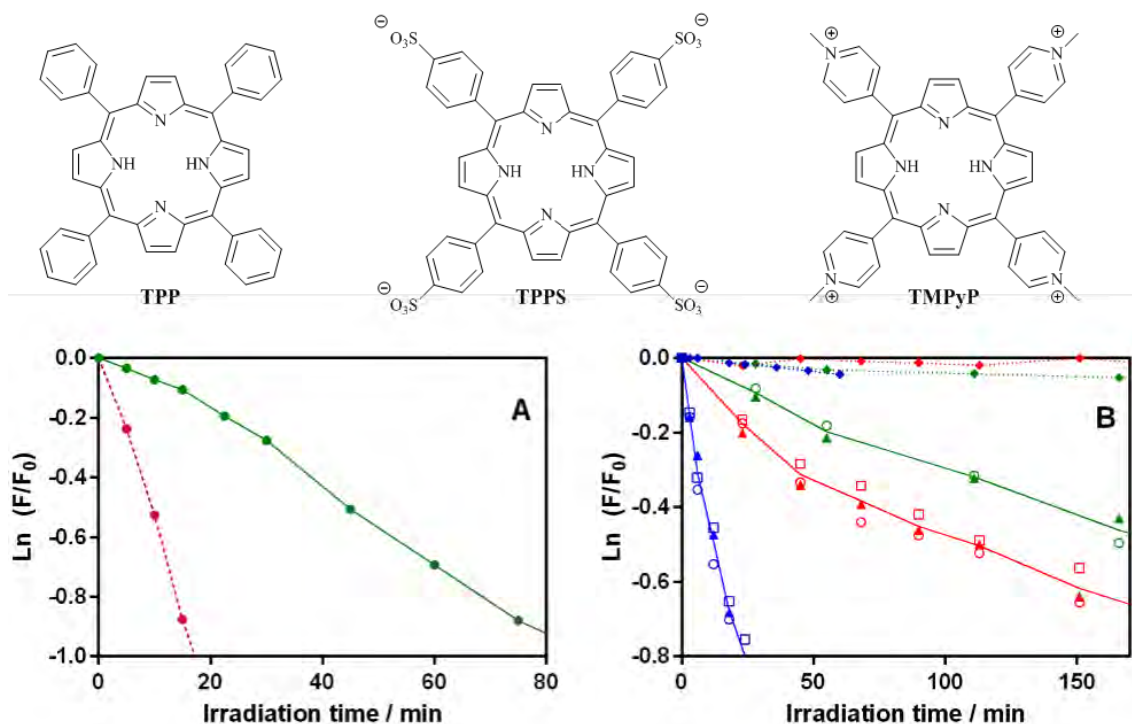


Figure 4.9 Top: chemical structures for: meso-tetraphenylporphyrin (TPP), meso-tetra(4-sulfonatophenyl)-porphine tetrasodium salt (TPPS₄) and meso-Tetra(N-methyl-4-pyridyl)porphine tetratosylate salt (TMPyP). Bottom: solvent and PS effects on nanoADPA photobleaching. (A) MB 6 μM in PBS (green solid line) and dPBS (magenta dashed line), $\lambda_{exc} = 640$ nm. (B) TPP, TMPyP and TPPS₄ (open squares, open circles and closed triangles, respectively) 3 μM in acetonitrile (blue), ethanol (red) and PBS (green). $\lambda_{exc} = 420$ nm. The dashed lines correspond to irradiation in the absence of PS.

In section 4.2.2.4, we studied the interaction between SOSG and BSA. For ADPA, it can be expected that some type of interaction between ADPA and BSA. Firstly, time-resolved fluorescence anisotropy of ADPA in the presence and absence of 170 μM BSA was measured. Whilst the anisotropy decay for free ADPA was faster than the resolution time of our system (0.1 ns), the anisotropy decay in the presence of BSA was significantly slower, 16 ns (Figure 4.10A). This is consistent with complex formation between ADPA and BSA. ADPA fluorescence spectra were then measured in the presence of increasing amounts of BSA (Figure 4.11 left). A clear fluorescence intensity decrease could be observed along with a bathochromic shift of the spectrum. From the change in fluorescence intensity, the value of the binding equilibrium constant (K_a) was estimated as 0.03 μM⁻¹ by a Benesi-Hildebrand plot assuming the formation of a 1:1 complex (Figure 4.10B).⁵⁸⁷ Time-resolved fluorescence experiments showed that ADPA fluorescence quenching by BSA is mainly due to static quenching (Figure 4.10C).

The results for nanoADPA were strikingly different (Figure 4.11 right). Neither a spectral shift nor a fluorescence intensity decrease could be detected even at BSA concentrations as high as 170 μM. This indicates that the NP scaffold protects ADPA from complex formation with BSA.

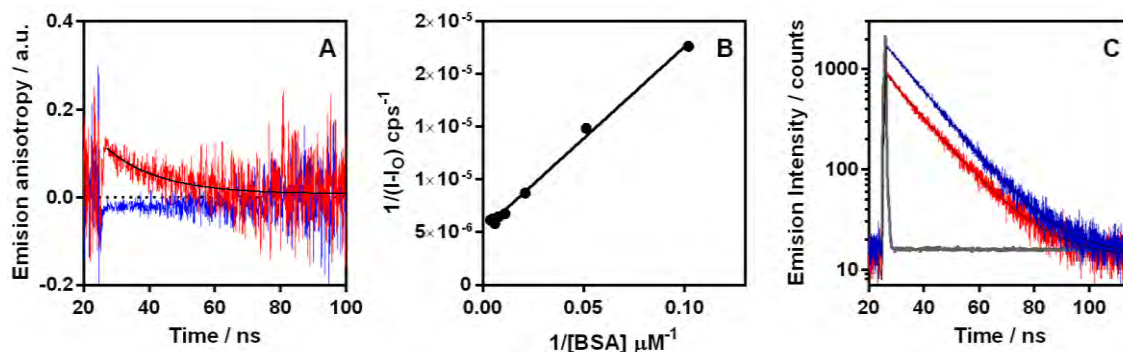


Figure 4.10 (A): Time-resolved fluorescence anisotropy for free ADPA and ADPA:BSA complex (6 μM ADPA and 170 μM BSA). λ_{exc} 375 nm, λ_{obs} 428 nm. (B): Benesi–Hildebrand plot for the determination of the equilibrium constant K_a of ADPA-BSA complexation. (C): Fluorescence emission decay of ADPA (6 μM) in PBS in the presence (red line) and absence (blue line) of BSA (170 μM). λ_{exc} 375 nm, λ_{obs} 428 nm. The grey line is the instrument's response function.

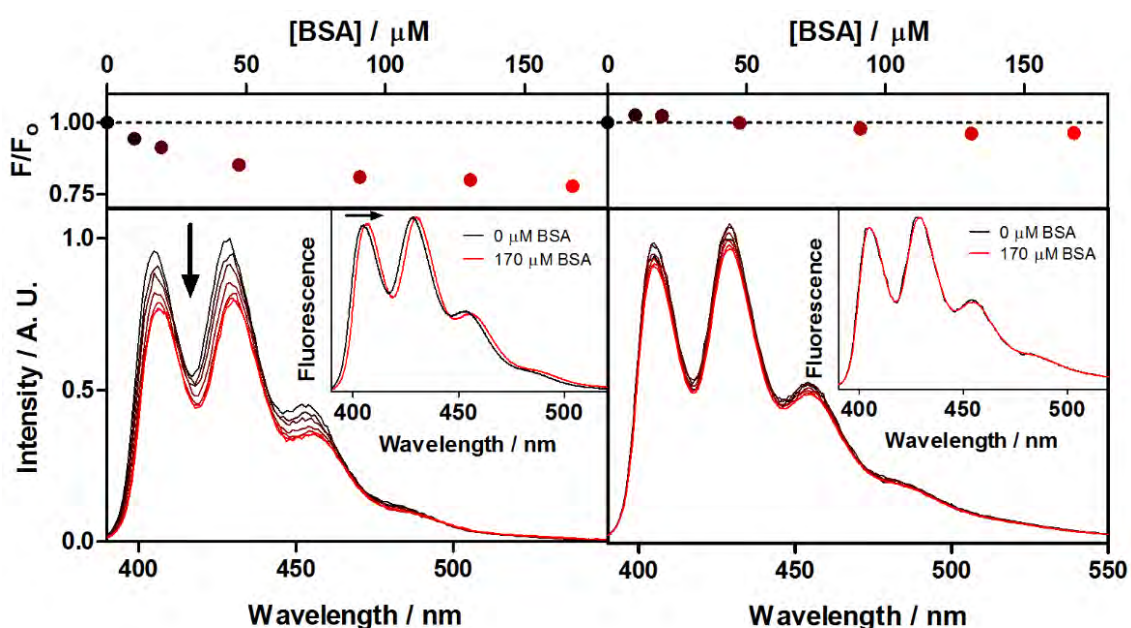


Figure 4.11 ADPA (left) and nanoADPA (right) fluorescence spectra upon different BSA concentration (0–170 μM). λ_{exc} = 380 nm. Top changes in total fluorescence area. Inset: fluorescence spectra shift from 0 to 170 μM BSA concentration.

In order to assess the $^1\text{O}_2$ detection capacity in more complex media, it is decided to measure the $^1\text{O}_2$ generated from a genetically-encodable protein, called miniSOG. It is an engineered flavin mononucleotide-binding protein derived from phototropin 2.²⁸⁶ Initially, the Φ_{Δ} of miniSOG had been reported as 0.47 ± 0.05 , using ADPA as fluorescence probe.²⁸⁶ Two independent research groups have revised that Φ_{Δ} value and it was determined as 0.03 ± 0.01 by two independent methods (one direct ($^1\text{O}_2$ phosphorescence emission) and one indirect (uric acid as $^1\text{O}_2$ trap)).^{287,588}

That value was approximately 15-fold lower than the obtained using ADPA as $^1\text{O}_2$ trap, which indicates that a secondary and non-desirable non-mediated $^1\text{O}_2$ photooxidation also occurs.¹⁶ Indeed, it has been reported that anthracenes can be oxidized by electron-transfer processes.⁵⁸⁹ Furthermore, it is also well-known that flavins are able to undergo electron transfer reactions with suitable electron donors.^{590,591} As final piece of evidence,

it was observed that the fluorescence of miniSOG was partially quenched and the spectrum lost its vibrational structure in the presence of ADPA. This suggests that ADPA interacts to miniSOG which facilitates the electron-transfer process.²⁸⁷ As Figure 4.12 shows, if nanoADPA is used instead, the correct Φ_{Δ} value is arrived at.

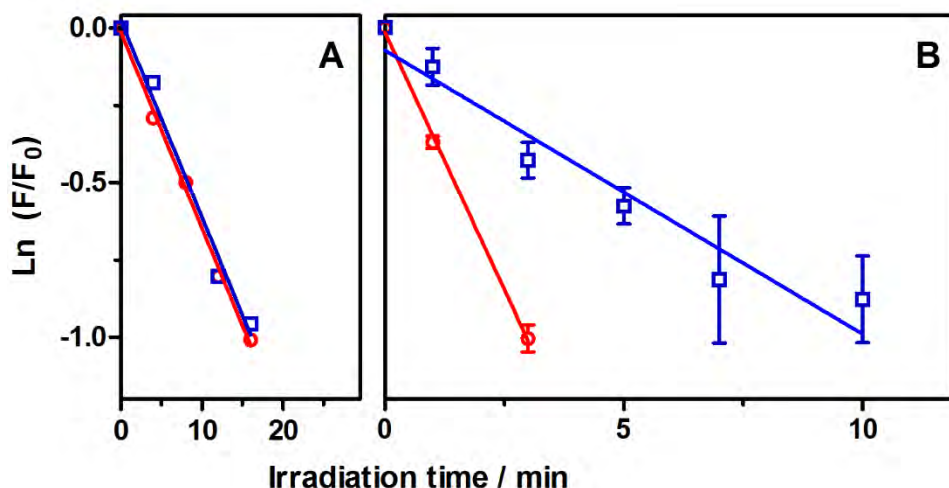


Figure 4.12 (A) ADPA fluorescence bleaching photosensitized by flavin mononucleotide (FMN, $\Phi_{\Delta} = 0.51$,⁵⁹² red) and miniSOG (blue). (B) The same experiment using nanoADPA. λ_{irr} 473 nm.

Having established that nanoADPA does not interact with proteins, it is studied whether it could be internalized by HeLa cells and sense intracellular 1O_2 . We first determined its dark toxicity and found it to be negligible below 4 μ M. Confocal fluorescence microscopy showed that cells incubated with 2 μ M nanoADPA for 24 h display its characteristic blue emission overlapping that of the CellTracker Green CMFDA Dye (Figure 4.13A). This confirms that nanoADPA is localized inside the cells, where it forms fluorescent aggregates up to 1.5 μ m diameter. A 3D stack image shows that nanoADPA is well distributed throughout the cytoplasm. Figure 4.13B shows a 3D cell reconstruction.

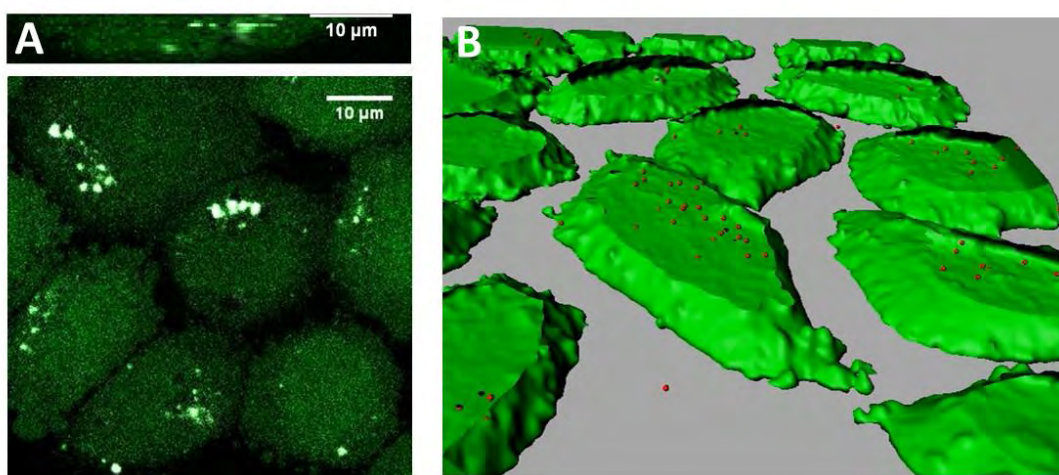


Figure 4.13 (A) Confocal fluorescence images of HeLa cells co-incubated with nanoADPA (white) and CellTracker Green CMFDA (green). Top: Perpendicular plane. Bottom: Transversal plane. (B) 3D cell reconstruction. The green volume is the cytoplasm and the red dots represent the nanoADPA aggregates.

In a second series of experiments, HeLa cells were co-incubated with nanoADPA and RB, which is cell-permeable, can be selectively excited where ADPA does not absorb (561 nm) and shows very low absorption where ADPA emits.^{593,594} Moreover, we could find no evidence for interaction between nanoADPA and RB in PBS or in DMEM. Figure 4.14 shows that the intracellular fluorescence of nanoADPA decreased to 1/3rd of its original value when the cells were irradiated at 561 nm for 10 minutes, while no fluorescence decrease could be observed in the absence of RB. These results confirm the ability of nanoADPA to sense ¹O₂ inside HeLa cells.

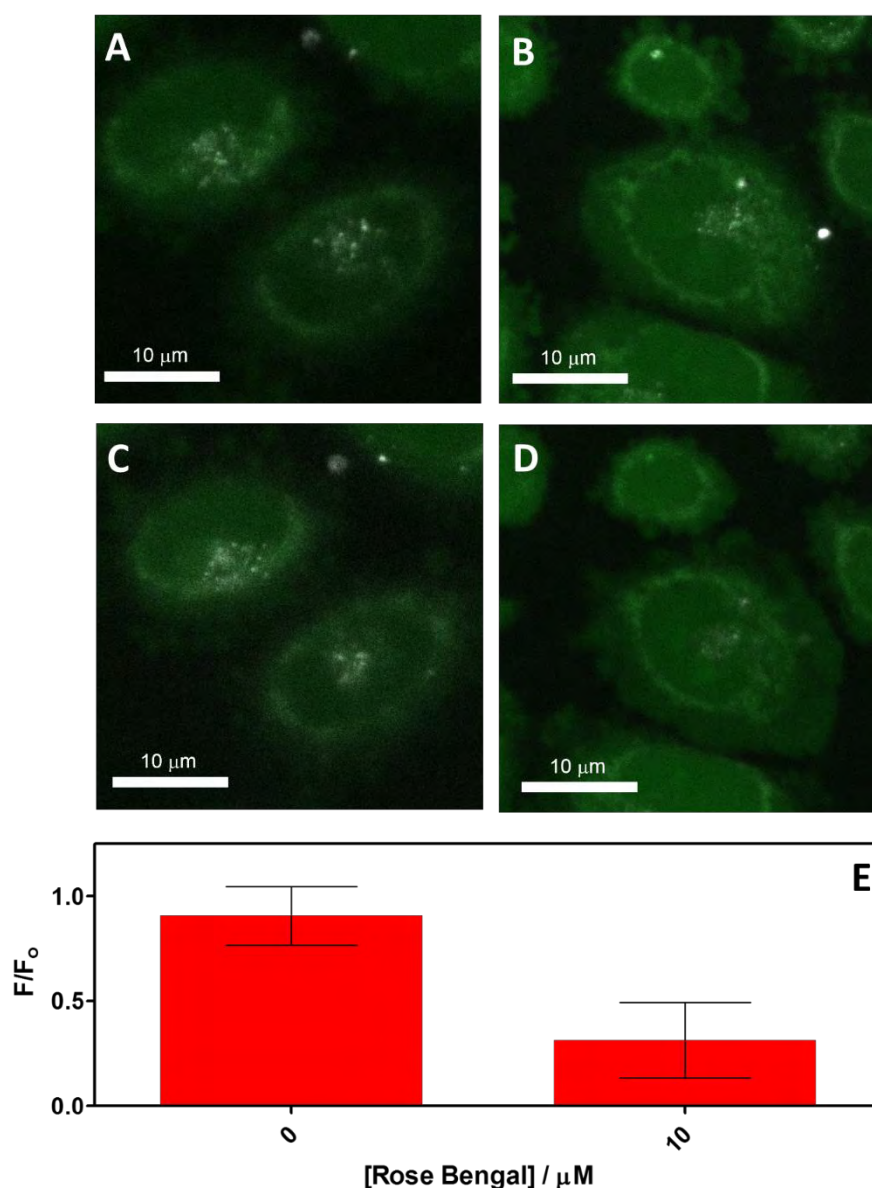


Figure 4.14 Fluorescence images of HeLa cells incubated with 2 μM nanoADPA . (A) no RB, no light. (B) 10 μM RB, no light. (C) no RB, 10 min laser irradiation at 561 nm. (D) 10 μM RB and 10 min laser irradiation at 561 nm. (E) nanoADPA fluorescence decrease after 10 minutes irradiation in the presence and absence of RB. Open bars represent the mean SD for seven independent NPs systems where only the mean pixel intensity of the images is considered.

4.2.4. NanoNOX: A turn-on fluorescence nanoprobe for $^1\text{O}_2$ detection

(Adapted from: **R. Bresolí-Obach**,⁺ R.P. Zanocco,⁺ R. Ruiz-González, F. Nájera, E. Pérez-Inestrosa, A.L. Zanocco, E. Lemp and S. Nonell, In preparation; ⁺These authors contributed equally to this work.)

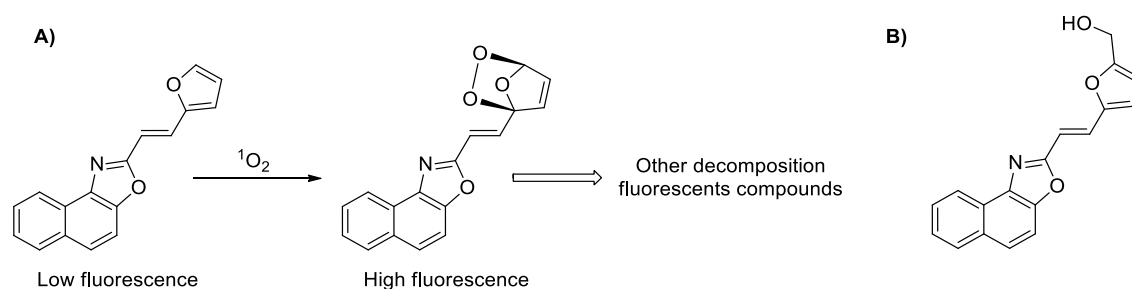
The results reported in this section have been carried out in collaboration with the Universidad de Chile (Santiago de Chile, Chile) and the Universidad de Málaga (Málaga, Spain). Some experiments of this section have been realized by myself as visiting student in Universidad de Málaga (18th february to 18th march of 2016).

4.2.4.1. Furyl–vinyl-naphthoxazole: “Click-ON” dyads to detect $^1\text{O}_2$

Furan derivatives such as 2,5-diphenyl-3,4-isobenzofuran (DPBF) or 2,5-dimethylfuran, have been widely used as a $^1\text{O}_2$ scavengers since 70s.^{595,596} These derivatives are advantageous $^1\text{O}_2$ chemical traps because:

- i) They can be easily followed by using routine analytical techniques such as absorption spectroscopy, fluorescence or gas chromatography.
- ii) Furan reactivity towards $^1\text{O}_2$ produces mainly endoperoxides, with a minimal or null contribution of physical quenching.⁵⁹⁷
- iii) $^1\text{O}_2$ is capable to react with furan derivatives with high k_R ; even for some derivatives such as DPBF is diffusionally controlled ($k_R = 1.3 \times 10^9 \text{ M}^{-1}\text{s}^{-1}$ in CH_3OH).⁵⁹⁸
- iv) Furan k_R shows a very modest solvent effect, making them almost solvent insensitive.^{88,599}

So, considering potentialities of furan derivatives as $^1\text{O}_2$ traps, Nonell and Zanocco groups designed, synthesized and studied the photochemical behavior of new “click-on” compounds to assess its potentiality as $^1\text{O}_2$ probes (Scheme 4.7).¹⁰⁹



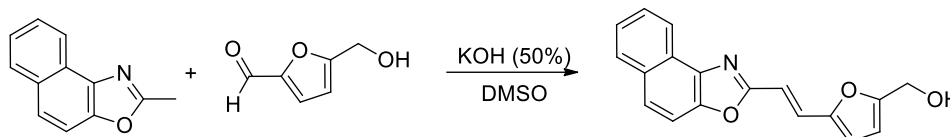
Scheme 4.7 (A): Furyl–vinyl-naphthoxazole dyad reactivity towards $^1\text{O}_2$ described in reference ¹⁰⁹. (B): Furyl–vinyl-naphthoxazole ((E)-5-(2-(naphtho[1,2-d]oxazol-2-yl)vinyl)furan-2-yl)methanol; NOX) chemical structure used in this section.

These molecules are dyads composed by a naphthoxazole fluorescent moiety linked to a furan trap through an unsaturated bond to the oxazole ring. In the native state, the inherent naphthoxazole fluorescence is quenched, possibly through intramolecular charge transfer process from the furan ring to the naphthoxazole moiety. Furan moiety will form an endoperoxide after reacting with $^1\text{O}_2$, which disrupts the extended π -conjugation and the intramolecular deactivation process is no longer operational. It affords a new chemical entity whose fluorescence is two orders of magnitude higher than that of the initial compound, at the optimal selected wavelength. Moreover, these dyads have Φ_A smaller than the most used $^1\text{O}_2$ fluorescent probes such as SOSG.¹⁰⁹

4.2.4.2. Experimental section

4.2.4.2.1. Synthesis of (E)-(5-(2-(naphtho[1,2-d]oxazol-2-yl)vinyl)furan-2-yl)methanol (NOX)

(E)-(5-(2-(naphtho[1,2-d]oxazol-2-yl)vinyl)furan-2-yl)methanol (NOX) used in this section has been synthesized by Dr. R.P. Zanocco in Institut Químic de Sarrià as visiting student. Its synthetic route is described in Scheme 4.8.



Scheme 4.8 Synthesis of (E)-(5-(2-(naphtho[1,2-d]oxazol-2-yl)vinyl)furan-2-yl)methanol (NOX).

4.2.4.2.2. Synthesis of the NPs

The MSNP, long linker silane, RB-Silane and MSNP-RB have been synthesized as described in the previous sections.

Synthesis of MSNP-L-NH₂ / RB-MSNP-L-NH₂. 200 mg of (OEt)₃-Si-L-NH₂ (430 μmols) were added to 12 mL of MSNP/MSNP-RB solution (33 mg/mL). The solution was left stirring at room temperature during 24 hours. Afterwards, the NPs were recovered by centrifugation (15000g x 20 min). The MSNP were washed twice with ethanol and once with CH₃CN. The final MSNP-L-NH₂/RB-MSNP-L-NH₂ were stored suspended in CH₃CN (10 mg/mL).

Synthesis of MSNP-L-NH-CO-CH₂-CH₂-COOH / RB-MSNP-L-NH-CO-CH₂-CH₂-COOH. 100 mg of succinic anhydride (1000 μmols) were added to 12 mL of MSNP-L-NH₂/RB-MSNP-L-NH₂ solution (33 mg/mL). The solution was left stirring at room temperature during 24 hours. Afterwards, the NPs were recovered by centrifugation (15000g x 20 min). The MSNP were washed thrice with CH₃CN. The final MSNP-L-NH-CO-CH₂-CH₂-COOH / RB-MSNP-L-NH-CO-CH₂-CH₂-COOH were stored suspended in CH₃CN (10 mg/mL).

Synthesis of MSNP-L-NH-CO-CH₂-CH₂-CO-O-NOX (nano1) / RB-MSNP-L-NH-CO-CH₂-CH₂-CO-O-NOX (nanoNOX). 350 mg (2.3 mmols) of EDC, 350 mg of NHS (3.3 mmols) and 300 mg (2.5 mmols) of DMAP were directly dissolved into the 12 mL of MSNP-L-NH-CO-CH₂-CH₂-COOH / RB-MSNP-L-NH-CO-CH₂-CH₂-COOH solution (CH₃CN, 33 mg/mL). The solution was left stirring at room temperature during 2 hours. Then, 100 mg (3.4 mmols) of NOX was added and it was left stirring for 72 hours more. Afterwards, the NPs were recovered by centrifugation (15000g x 20 min). The NPs were washed twice with CH₃CN and twice with CH₃OH. The final MSNP-L-NH-CO-CH₂-CH₂-CO-O-NOX (nano1) / RB-MSNP-L-NH-CO-CH₂-CH₂-CO-O-NOX (nano2) were stored suspended in CH₃OH (5 mg/mL).

4.2.4.3. Behaviour of furyl-vinyl naphthoxazole as a $^1\text{O}_2$ fluorescent probe

The molecular probe NOX is a modification of the furyl naphthoxazole previously studied in the group,¹⁰⁹ in which the hydrogen in position C-5 of the furan has been replaced by a hydroxymethyl group. This improves the furan's reactivity towards $^1\text{O}_2$ and allows its conjugation to nanoparticles via a Steglich esterification (Figure 4.15a). NOX has been synthesized by a one-pot, two-step reaction in which the attack of methylnaphthoxazole anion to furaldehyde is followed by a dehydration step (Scheme 4.8).

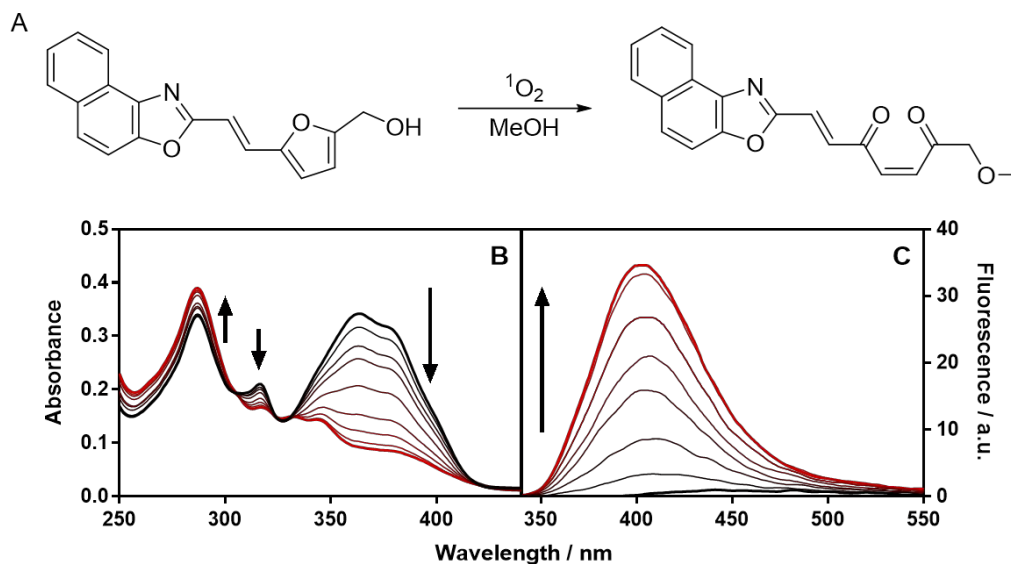


Figure 4.15. a) Oxidation of NOX with $^1\text{O}_2$. b) Absorbance changes upon reaction of NOX with $^1\text{O}_2$. c) Fluorescence changes upon reaction of NOX with $^1\text{O}_2$. The photosensitizer used to generate $^1\text{O}_2$ was new methylene blue $5 \mu\text{M}$, the irradiation wavelength was $640 \pm 10 \text{ nm}$ and the experiments were carried out in aerated methanol. The fluorescence was excited at 335 nm .

The absorption spectrum of NOX in methanol shows a maximum at 363 nm and a second peak at 290 nm (Figure 4.15), while the fluorescence spectra shows a maximum at 439 nm (Figure 4.15). The absorption and fluorescence spectra are practically solvent independent and the Φ_F is very small in all solvents, indicating efficient quenching of the naphthoxazole singlet excited state by the furan (Table 4.2).

Table 4.2 Photophysical properties of NOX

	$\lambda_{\text{abs}} / \text{nm}$ ($\epsilon / \text{M}^{-1}\text{cm}^{-1}$)	$\lambda_{\text{flu}} / \text{nm}$	Φ_F	τ_S / ns	$k_q / \text{M}^{-1}\text{s}^{-1}$
Benzene	365 (3.9×10^4)	436	0.035	5.5	---
Acetonitrile	362 (4.4×10^4)	436	0.055	4.0	1.4×10^7
N,N'- dimethylformamide	365 (4.3×10^4)	441	0.005	5.8	---
Methanol	363 (4.3×10^4)	439	0.005	6.2	3.0×10^7

The reactivity of NOX towards $^1\text{O}_2$ was studied noting changes in its absorption and emission spectra upon photosensitized oxidation. Thus, a strong absorbance decrease was observed (Figure 4.15B), consistent with furan oxidation leading to a shortening of

the conjugated path and hence to a blue shift of the absorption spectrum. As shown in figure 4.15C, the fluorescence showed concomitantly a remarkable 180-fold enhancement.

The rate constant for overall $^1\text{O}_2$ quenching was determined using time-resolved $^1\text{O}_2$ phosphorescence spectroscopy and found to be $3.0 \times 10^7 \text{ M}^{-1}\text{s}^{-1}$ (Figure 4.16), 32-fold larger than for unsubstituted furyl naphthoxazoles.⁶⁰⁰ The rate constant for reaction, determined by comparing the rate of photooxidation with that of dimethylantracene,⁶⁰¹ is $1.7 \times 10^7 \text{ M}^{-1}\text{s}^{-1}$ (Figure 4.16). Oxidation generates a single product, as demonstrated by HPLC and consistent with the observation of isosbestic points in the absorption spectra. The selectivity of NOX towards $^1\text{O}_2$ was assessed by testing its reactivity towards other ROS and it was found that it does not react with superoxide or hydrogen peroxide. Moreover, it shows a negligible Φ_{Δ} (0.003 and 0.007 in methanol and acetonitrile, respectively); for comparison, SOSG has Φ_{Δ} of 0.03 at 355 nm and 0.009 at 532 nm in methanol.¹⁰⁴ Taken together, these results indicate that NOX is an excellent probe for $^1\text{O}_2$ detection.

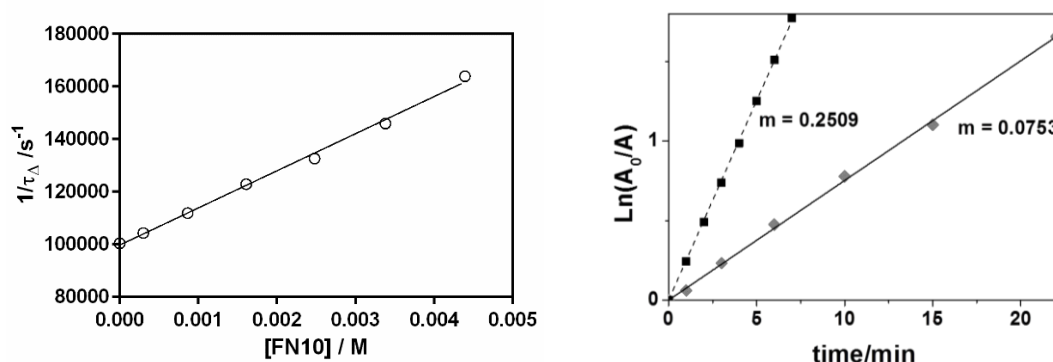


Figure 4.16 Left: Determination of k_q for NOX with $^1\text{O}_2$. Right: Determination of k_r for reaction of NOX with $^1\text{O}_2$ (dashed black line) using 9,10-dimethylantracene as reference (solid grey line; DMA; $k_r(\text{DMA}) = (6.3 \pm 0.4) \times 10^7 \text{ M}^{-1}\text{s}^{-1}$).⁶⁰¹ Solvent: CH_3OH , PS: NMB.

Given the promising results for NOX, we synthesized a simple nanosensor attaching NOX to the surface of preformed MSNP through a long linker (nanoNOX), which facilitates the reaction with $^1\text{O}_2$. We then suspended the nanoprobe in methanol, added new methylene blue and irradiated it with red light to generate $^1\text{O}_2$. As expected, a 10-fold fluorescence enhancement could be observed together with a blue-shift in the absorption spectrum of the oxidized nanoprobe (Figure 4.17).

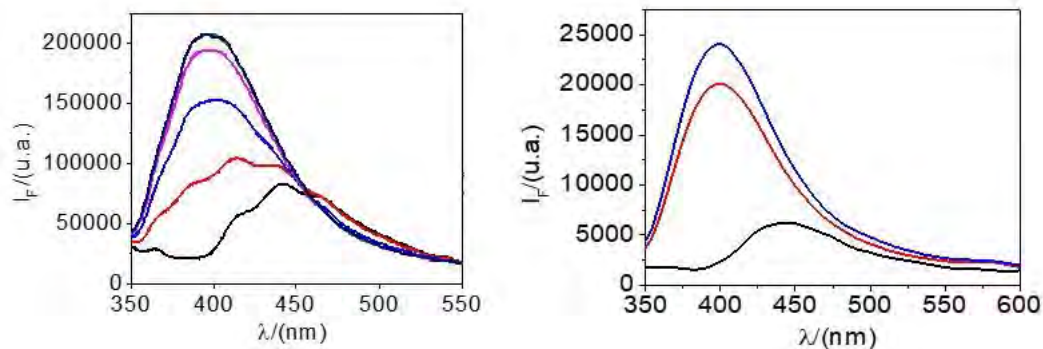


Figure 4.17 Fluorescence enhancements for nanoNOX (left) and nanoNOX-RB (right). The photosensitizer used to generate $^1\text{O}_2$ was new methylene blue $5 \mu\text{M}$, the irradiation wavelength was $640 \pm 10 \text{ nm}$ and the experiments were carried out in aerated methanol. The fluorescence was excited at 335 nm .

Having established that the nanoprobe reacts with $^1\text{O}_2$, we further modified it by attaching a $^1\text{O}_2$ photosensitizer (Rose Bengal) to its surface in order to ensure that $^1\text{O}_2$ would be generated in close vicinity of the sensor in the cellular experiments. The resulting bifunctional nanoprobe (termed nanoNOX-RB) showed a 14-fold fluorescence enhancement together with a blue shift in the absorption spectrum when irradiated with green light. No fluorescence enhancement could be observed when the nanoprobe contained no Rose Bengal (nanoNOX).

4.2.5. NanoDCFH-DA: a silica-based nanostructured unspecific fluorescent probe for the detection of reactive oxygen species in biology

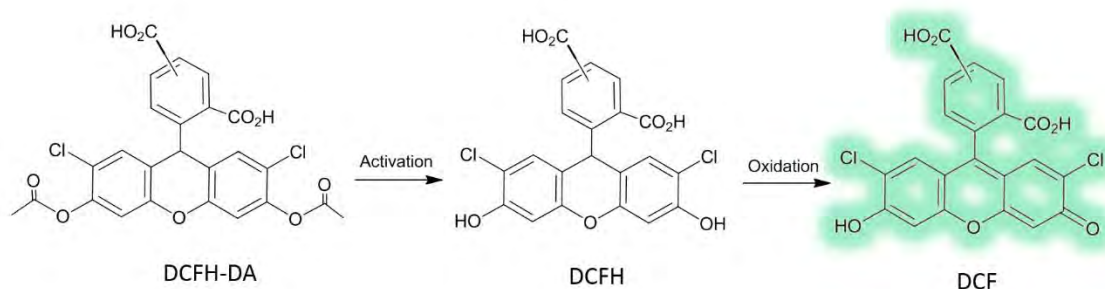
(Adapted from: **R. Bresolí-Obach**,⁺ L. Busto,⁺ C. Muller, M. Reina and S. Nonell, NanoDCFH-DA: a silica-based nanostructured unspecific fluorescent probe for the detection of reactive oxygen species in biology, submitted (intended for Photochem. Photobiol.; ⁺These authors contributed equally to this work.)

The results reported in this section have been carried out in collaboration with the Universitat de Barcelona (Barcelona, Spain).

4.2.5.1. Introduction

Direct, real-time detection of ROS can be done only in a few cases and requires the use of highly-sophisticated equipment available only in specialized laboratories.^{224,602} An alternative and simpler strategy is to detect them by chemical trapping methods.⁶⁰³ Among them, the use of molecular fluorescent probes that change their emission properties upon reaction with ROS is becoming highly popular in connection with the increased use of fluorescence imaging techniques.^{604,605} Thus, a number of fluorescent probes have been developed that either show specificity for a given ROS, e.g., SOSG for $^1\text{O}_2$,⁹⁵ dihydroethidium for $\text{O}_2^{\bullet-}$ ⁶⁰⁶ or hydroxyphenyl fluorescein for $\bullet\text{OH}$,⁶⁰⁷ or are non-specific and can therefore be used to assess oxidative stress.^{608,609}

2',7'-Dichlorodihydrofluorescein diacetate (DCFH-DA) is arguably the most-widely used non-specific ROS probe. Its reduced form absorbs in the UV region only and is not fluorescent. Upon entering a cell, DCFH-DA is hydrolyzed by esterases to the non-fluorescent 2',7'-dichlorodihydrofluorescein (DCFH), which is oxidized by a variety of ROS to dichlorofluorescein (DCF), a highly conjugated product that absorbs in the visible range and shows intense green fluorescence (Scheme 4.9).



Scheme 4.9 Oxidation of DCFH-DA by ROS.

Molecular probes in general and fluorescein derivatives in particular interact with proteins, which affects their cell uptake and response to ROS.^{105,107,610} In order to prevent this problem, encapsulation within nanoparticles or covalent binding to their surface have been proposed and successfully demonstrated.⁶¹¹⁻⁶¹³ In addition, redox ROS probes such as DCFH-DA are slowly oxidized by dissolved $^3\text{O}_2$, which may lead to unwanted background signals and eventually false positives.^{614,615}

In this subchapter, a biocompatible silica-based fluorescent nanoprobe for detection of ROS in biological systems has been designed, synthesized, and characterized, circumventing some of the limitations of the molecular probe DCFH-DA, such as protein complexation and self-oxidation by air. The nanoprobe reactivity has been successfully tested both in phosphate buffer saline solution and inside HeLa cells.

4.2.5.2. Experimental section

4.2.5.2.1 Synthesis of nanoDCFH-DA

The MSNP, (EtO)₃-Si-L-NH₂ and MSNP-L-NH₂ have been synthesized as described in the previous sections.

Conjugation of DCFH-DA onto MSNP-L-NH₂: DCFH-DA conjugation to MSNP-L-NH₂ was performed through Steglich amidation adapting the procedure proposed by Steglich *et al.*⁵⁸² Briefly, 4.0 mg (7.5 μmol) of DCFH-DA were previously activated by mixing them for 2 hours with 14.7 mg of EDC (77 μmol) and 14.5 mg (126 μmol) of NHS in 2 mL of dry CH₂Cl₂. The mixture was then added dropwise to 14 mL of a stirred solution of MSNP-L-NH₂ in acetonitrile (7 mg/mL) and the crude was kept reacting for 72 h in darkness and at room temperature. Simultaneously, 0.5 g (5 mmol) of anhydrous Na₂CO₃ were added in order to deprotonate linker's amino terminal groups, since the amidation is not favorable with the protonated form. Afterwards, nanoDCFH-DA was centrifuged and washed 6 times with ethanol (20 min at 13000 rpm).

The concentration of amino groups (C_{NH₂}) in MSNP-L-NH₂ was determined as the amount of nitrogen in the NPs divided by 3 on account that each linker unit contains 3 nitrogen atoms. Since DCFH-DA contains no nitrogen, comparison the carbon/nitrogen ratio in nanoDCFH-DA relative to MSNP-L-NH₂ allowed to calculate the fraction of amino groups functionalized by the probe and therefore the concentration of DCFH-DA on the nanoparticles.

4.2.5.2.2. Fluorescence measurements

The fluorescence of the nano- and molecular probes was studied in PBS at the DCFH-DA concentration of 1.5 μM using a Fluoromax-4 spectrofluorometer (Horiba Jobin-Yvon, Edison, USA). Samples were exposed to known amounts of the different ROS after deacetylation by NaOH treatment and subsequent neutralization with sulfuric acid (20 mM).

4.2.5.2.3. Sources of ROS

ClO⁻ and H₂O₂ were added from stock solutions. O₂^{•-} was added as a KO₂ suspension in anhydrous CCl₃CN (140 mM). •OH was generated by UV-A irradiation (353 ± 20 nm; 6.3 mW/cm²) of a NaNO₂ solution (1 mM).⁶¹⁶ The reactive rate constant was determined by a comparative method using terephthalic acid as reference (5.3 μM, rate constant 4.4 × 10⁹ M⁻¹s⁻¹).⁶¹⁷ ¹O₂ was generated by irradiation of a 8.7 μM MB solution with red light (634 ± 8 nm; 7.8 mW/cm²).⁴³⁶ The reactive rate constant was determined by the comparative method using ADPA as reference (1.5 μM, rate constant 8.7 × 10⁷ M⁻¹s⁻¹).⁵⁷⁶ Oxidation by ³O₂ was assessed by periodically recording the fluorescence of air-equilibrated solutions kept in the dark.

4.2.5.2.4. Cellular techniques

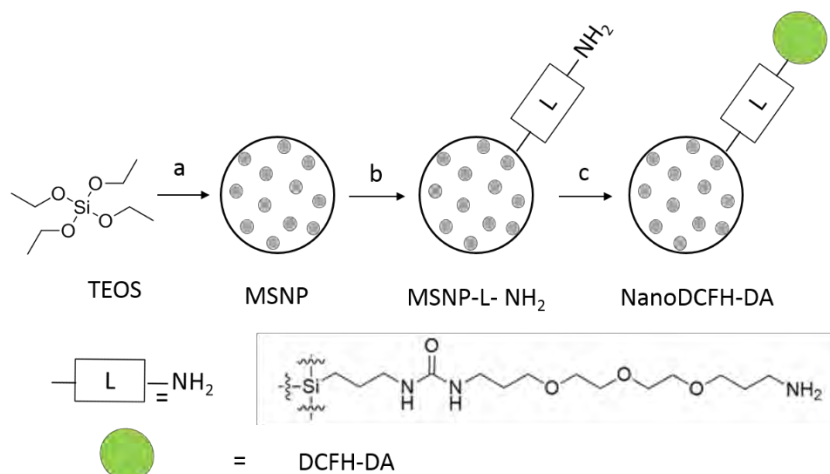
HeLa cells culture. Human carcinoma HeLa cells were grown as monolayer cultures in DMEM supplemented with 10% (v/v) FBS, 1% (v/v) penicillin-streptomycin solution and 1% (v/v) l-Glutamine. Cells were cultured in an incubator with 5% CO₂ plus 95% air at 37 °C. Cells were seeded in 75 cm² flask and subconfluent cell cultures were used.

Cell preparation procedure for microscopical analysis. Main cell culture was trypsinized and 5×10⁴ HeLa cells/well were added to 8-wells plates. The cells were incubated at 37 °C for 24 h. Then the cell culture medium was removed and 250 µL/well 2 µM nanoDCFH-DA diluted in HBSS⁺ with and without 10 µM Hyp were added and left under incubation at 37 °C for 2h. The cell culture was washed 3 times with 200 µL/well HBSS⁺ in order to discard the non-internalized suspended nanoDCHF-DA. Finally, 250 µL/well HBSS⁺ were added before the microscopical analysis.

Microscopical analysis. All confocal images were taken using a TCSP SP2 Leica Confocal Microscope (Leica Microsystems CMS, Wetzlar, Germany). Images before and after irradiation were collected using Ar laser (λ_{exc} 488 nm; λ_{obs} 500–550 nm) and 561 nm (DPSS laser) using 3 different photomultiplier configurations (transmitted light (for widefield), λ_{obs} 500-550 nm (for DCF) and λ_{obs} 570-620 nm (for Hyp)). The samples were irradiated at 561 nm for 2 min in order to generate ROS and during this time, sequential images were collected. All photographs and videos construction were processed and analyzed using ImageJ1.x software.^{580,581}

4.2.5.3. Assessment and optimization of the nanoDCFH-DA

In the previous chapters, we had identified the structural features of a silica based $^1\text{O}_2$ fluorescence nanosensor to optimize its response.⁶¹³ It was concluded that MSNP were superior to compact ones and that covalent grafting of the probe should be through a sufficiently long PEG linker (MSNP-L-NH₂) optimum performance. The same structural conditions have now been adopted for the preparation of a DCFH-DA-based silica nanoprobe (nanoDCFH-DA) as shown in Scheme 4.10.



Scheme 4.10 NanoDCFH-DA synthesis. Reagents and conditions (a): CTAC, EtOH, H₂O, NH₃, 80 °C, 12 min, then HCl (37%), reflux, 24 h. (b): N-(4,7,10-trioxa-13-tridecaneamine)-N'-(3-(triethoxysilyl)propyl)-urea, EtOH, rt, 24 h. (c): DCFH-DA, EDC, NHS, dry CH₂Cl₂, rt, 2h; then addition of the activated DCFH-DA to MSNP-L-NH₂ in CH₃CN, rt, 72h.

All intermediates obtained in each synthetic step, ranging from MSNP to nanoDCFH-DA, were characterized by their hydrodynamic diameter and ζ -potential by dynamic light scattering techniques (Table 4.3). ζ -potential was measured under both neutral and acidic conditions to assess the presence of free amino groups at the surface of the MSNPs after each preparation step, since protonation of the amino groups in acidic media results in a more positive ζ -potential. The number of free amino groups was then determined by organic elemental analysis.

Table 4.3 Size, ζ -potential, free amino concentration and conjugated DCFH-DA concentration of the different nanosystems synthesized. The estimated error is 10% for each analysis.

	MSNP	MSNP-L	nanoDADCFH ₂
Size / nm	108	209	300
ζ -potential (H ₂ O) / mV	-32	-21	-21
ζ -potential (H ₂ O; pH 7.4) / mV	---	---	+9.2
ζ -potential (H ₂ SO ₄ 0.1 M) / mV	-30	+19	+7.8
ζ -potential (NaOH 0.1 M) / mV	---	---	-40
[-NH ₂] / $\mu\text{mol/mg}$	---	0.30	0.27
[DCFH-DA] / $\mu\text{mol/mg}$	---	---	0.03
Molecules of DCFH-DA per NP	---	---	4080
Organic elemental analysis / %	0.23 %C 0.00 %N	5.88 %C 1.24 %N	4.53 %C 0.78 %N

Inspection of Table 4.3 shows that the NP size increases after each preparation step. The final size (300 nm), is appropriate for internalization by mammalian cells such as HeLa.^{618,619} Regarding the ζ - potential, the changes observed for MSNP-L-NH₂ upon acidification of the solvent confirm MSNP functionalization with the linker. The observation that the changes are smaller for nanoDCFH-FA indicate that a substantial fraction of the amino groups have successfully reacted with DCFH-DA to form the amide bond. This was further confirmed by infrared spectroscopy: in the 1500-1800 cm⁻¹ region, the MSNP spectra show only a band corresponding to adsorbed water bending (1630 cm⁻¹), whereas nanoDCFH-DA shows, in addition, C=O stretching due to the urea moiety (1653 cm⁻¹) and C=C stretching due to DCFH-DA (1560 cm⁻¹) can be observed.

From organic elemental analysis we conclude that the yield of MSNP functionalization with the linker is 0.3 μ mol/mg MSNP, a value similar to the one previously obtained. Likewise, we estimate that 10% of the amino groups are finally functionalized with the probe in nanoDCFH-DA. The average distance between DCFH-DA and the silica surface is estimated to be 1.7 nm. This separation should prevent DCFH-DA from interacting with large biomolecules such as proteins, while at the same time allowing efficient reaction with small species such as ROS.

As depicted in Scheme 4.9, the two diacetyl moieties in DCFH should be hydrolyzed in order to efficiently detect ROS. Such activation is performed by estereases in biological environments⁶²⁰ and can also be achieved in simple solution by basic hydrolysis, e.g., with NaOH, followed by neutralization. This is the procedure followed in our solution experiments. The optimal NaOH concentration and activation time were determined by measuring the increase of fluorescence in nanoDCFH-DA samples upon exposure to ClO⁻. Samples prepared under the same conditions without the oxidant were used as references. Table 4.4 shows the fluorescence ratio between the oxidant-exposed and non-exposed samples. Optimal activation conditions were 1 mM NaOH and 15 minutes contact time before neutralization, under which a maximum fluorescence enhancement of 10.5 was obtained. Detachment of the DCFH-DA or DCFH from the probe by dissolution of the silica matrix during the NaOH treatment was ruled out since the supernatant obtained by centrifugation of the nanoparticles did not show any fluorescence after exposure to oxidants.

Table 4.4 Fluorescence ratio between the ClO⁻ oxidized sample and its non-oxidized counterpart, activated in the same conditions regarding NaOH concentration and hydrolysis time.

[NaOH] / mM	Activation time / min								
	0	7.5	15	22.5	30	60	90	120	180
1	3.0	9.6	10.5	10.4	9.0	---	---	---	---
3		8.1	9.2	8.5	8.3	6.0	4.6	4.9	1.2
10		---	4.0	---	3.9	3.0	2.4	2.7	2.9
30		---	3.3	---	1.0	1.9	2.8	3.0	2.3

One problem associated with redox-based probes is oxidation by atmospheric or intracellular ³O₂.^{614,615} This can be especially important in long-lasting experiments such as cellular incubations. Figure 4.18 shows that the fluorescence of DCFH-DA and nanoDCFH-DA indeed increase over time when their solutions are exposed to oxygen in air-equilibrated samples kept in the dark. It can be clearly observed that covalent grafting

of the probe to the surface of MSNPs protects it from oxygen. The rate constants for oxidation, deduced from the initial slopes of the plots, were $1.4 \times 10^{-7} \text{ M}^{-1}\text{s}^{-1}$ for nanoDCFH-DA and $2.0 \times 10^{-6} \text{ M}^{-1}\text{s}^{-1}$ for DCFH-DA, i.e., the nanoprobe is 14-fold less reactive than its molecular counterpart.

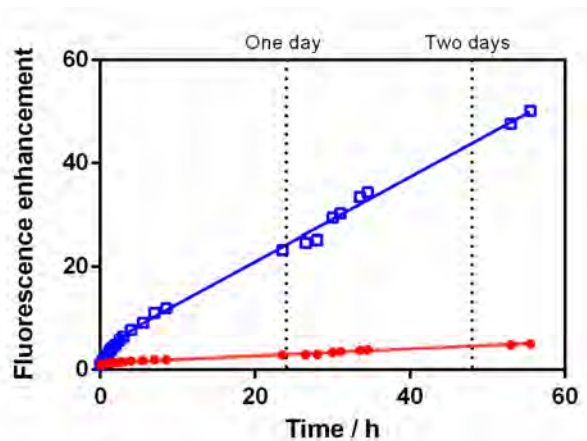


Figure 4.18 Fluorescence enhancement of DCFH-DA (blue) and nanoDCFH-DA (red) upon oxidation by $^3\text{O}_2$ in air-equilibrated PBS ($\lambda_{\text{exc}} 490 \text{ nm}$; $\lambda_{\text{obs}} 530 \text{ nm}$).

Since nanoDCFH-DA and DCFH-DA are used as fluorescent probes, it is important to ascertain if exposure to light of the deacetylated probes can affect the rate of fluorescence growth. This has been tested by irradiating air-equilibrated samples of the activated probes with green light ($524 \pm 17 \text{ nm}$; 7.5 mW/cm^2) in PBS solution. The results (Figure 4.19) show that the fluorescence of the probes increases upon exposure to light in a non-linear fashion. This was probably to be expected since this is essentially an autocatalytic process: Thus, trace amounts of the oxidized form of the probes, produced previously by thermal oxidation (Figure 4.18), may photosensitize the production of ROS, propagating the oxidation and rapidly leading to a dramatic increase in the fluorescence. The process shows saturation, indicating that the originally-reduced probe has been consumed. Figure 4.19 also shows that the nanoprobe is approximately 10-fold more photostable than its molecular counterpart. It is worth highlighting that typical light doses in microscopy imaging experiments are less than 1 J/cm^2 at which the nanoprobe has barely been photoconverted.⁵⁷³

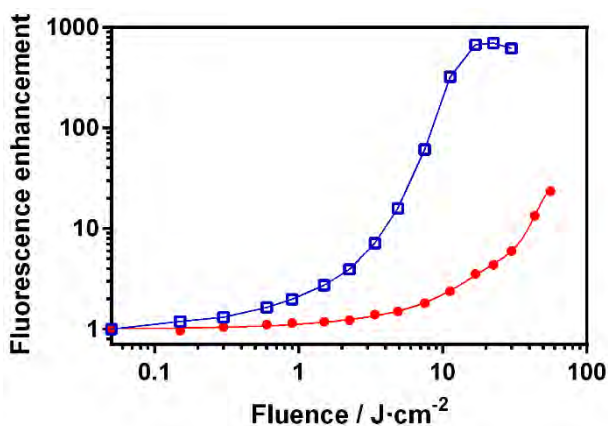


Figure 4.19 Fluorescence enhancement of DCFH-DA (blue) and nanoDCFH-DA (red) upon green light irradiation ($524 \pm 17 \text{ nm}$) in air-equilibrated PBS ($\lambda_{\text{exc}} 490 \text{ nm}$; $\lambda_{\text{obs}} 530 \text{ nm}$).

The reactivity of nanoDCFH-DA and DCFH-DA towards ROS was assessed by exposing them to defined amounts of these species (Figure 4.20).

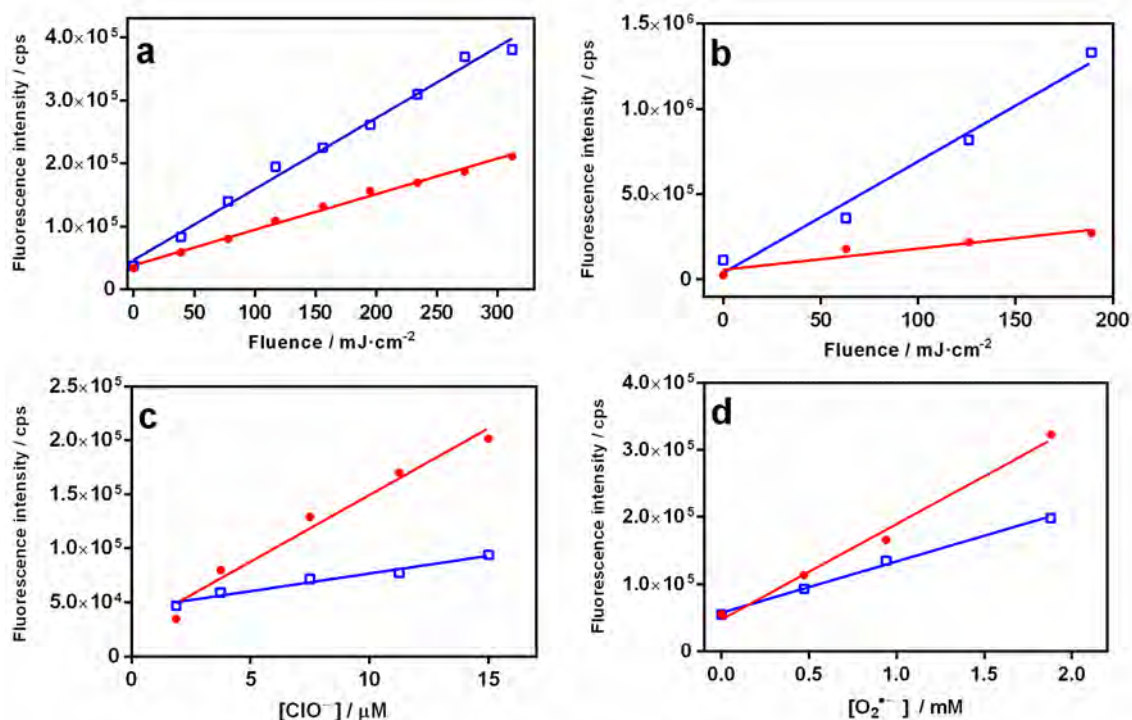


Figure 4.20 a: NanoDCFH-DA (red) and DCFH-DA (blue) fluorescence intensity after irradiation with red light in presence of MB. b: NanoDCFH-DA (red) and DCFH-DA (blue) fluorescence intensity after irradiation with UV-A light in presence of NaNO₂. c: NanoDCFH-DA (red) and DCFH-DA (blue) initial rates at each ClO⁻ concentration. d: NanoDCFH-DA (red) and DCFH-DA (blue) fluorescence intensity with O₂^{•-} addition.

Both nanoDCFH-DA and DCFH-DA react readily with ¹O₂, •OH, ClO⁻ and to a lesser extent with O₂^{•-}, when added at concentrations comparable to those found in biological systems. However, they show different reactivity against each particular ROS (Table 4.5). Thus, nanoDCFH-DA is less reactive than DCFH-DA against the neutral species ¹O₂ and •OH, but more reactive against the anionic ROS. The case of H₂O₂ deserves a specific comment since the fluorescence of both nanoDCFH-DA and DCFH-DA increased with the same rate constant. Control experiments showed that DCFH-DA was detached from the MSNP surface in the presence of H₂O₂.

Table 4.5 Reactive rate constants for DCFH-DA (k_{mol}^x) and nanoDCFH-DA (k_{nano}^x) towards ROS and ³O₂ (k^{O_2}).

ROS (X)	$k_{\text{nano}}^x / \text{M}^{-1}\text{s}^{-1}$	$k_{\text{mol}}^x / \text{M}^{-1}\text{s}^{-1}$	$k_{\text{nano}}^x / k_{\text{mol}}^x$	$(k^x/k^{\text{O}_2})_{\text{nano}}$	$(k^x/k^{\text{O}_2})_{\text{mol}}$	$(k^x/k^{\text{O}_2})_{\text{nano}} / (k^x/k^{\text{O}_2})_{\text{nano}}$
³ O ₂	1.4×10^{-7}	2.0×10^{-6}	0.35	1	1	1
ClO ⁻	140	10.5	13	1.0×10^9	5.3×10^6	189
O ₂ ^{•-}	0.31	0.17	1.9	2.2×10^6	8.5×10^4	26
•OH	5.2×10^7	2.7×10^8	0.19	3.7×10^{14}	1.4×10^{14}	2.6
¹ O ₂	2.2×10^6	4.3×10^6	0.50	1.6×10^{13}	2.2×10^{12}	7.3
H ₂ O ₂	1.2×10^{-5}	1.2×10^{-5}	1	6.0	6.0	1

It has been reported that the interaction of different fluorescent probes with proteins detracts from their performance in biological systems, either because it interferes with cell uptake or leads to fluorescence quenching.^{105,107,610} Figure 4.21 shows that this is the case for DCFH-DA in the presence of bovine serum albumin (BSA). The fluorescence of its active (oxidized) form shows a clear spectrum shift and is quenched by more than 85% at 150 μM BSA. In contrast, nanoDCFH-DA shows only a slight broadening of the fluorescence spectrum and with a 25% loss of intensity. This indicates that the MSNP protect the probe from interaction with BSA. Using Benesi-Hildebrand plots, the equilibrium constants for BSA binding were calculated as $18 \times 10^4 \text{ M}^{-1}$ for DCFH-DA and $2.8 \times 10^4 \text{ M}^{-1}$ for nanoDCFH-DA, 6.4-fold smaller.

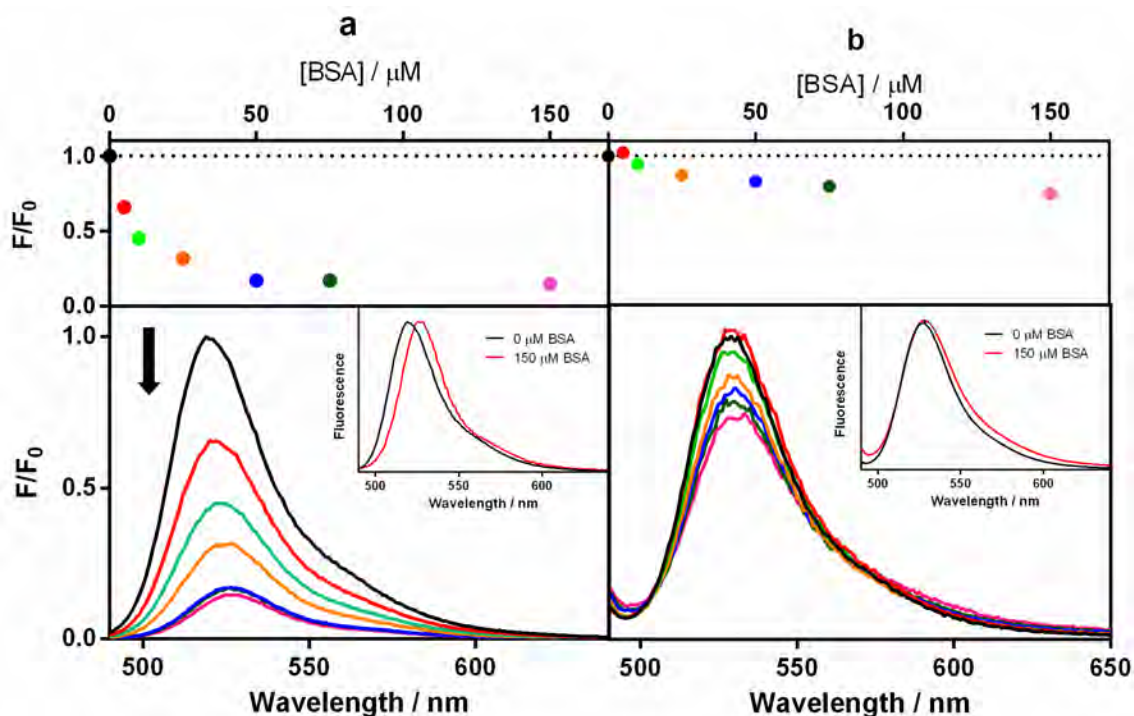


Figure 4.21 Top: DCFH-DA (a) and nanoDCFH-DA (b) changes in fluorescence maximum intensity. Bottom: DCFH-DA (a) and nanoDCFH-DA (b) fluorescence spectra with increasing BSA concentration (0-150 μM). $\lambda_{\text{exc}} = 490 \text{ nm}$. Inset: fluorescence spectra shift from 0 to 150 μM BSA.

Finally, we studied whether nanoDCFH-DA could be internalized by HeLa cancer cells and detect intracellular ROS. We used hypericin (Hyp) as PS, since it is known to be cell permeant and to generate a variety of ROS upon photoexcitation.⁶²¹ Moreover, Hyp can be selectively excited at wavelengths where DCFH-DA does not absorb (e.g., 561 nm) and shows very low absorption where DCF emits, which reduces the risk of inner-filter effects.

First, we assessed the dark toxicity of nanoDCFH-DA and found it to be negligible below 2 μM even after 24 h of incubation. Cells were then incubated for 2 hours with pre-activated 2 μM nanoDCFH-DA and 10 μM Hyp and were observed by confocal microscopy before and after photoexcitation of Hyp at 561 nm. While no green fluorescence could be observed in the absence of Hyp or before irradiation, a large increase, almost 10-fold, was recorded after exposing Hyp to light (Figure 4.22). The images show that nanoDCFH-DA is indeed internalized by HeLa cells after 2h

incubation, although a fraction remains bound to the cell membrane. Likewise, the presence of Hyp inside HeLa cells was confirmed by imaging its red fluorescence.

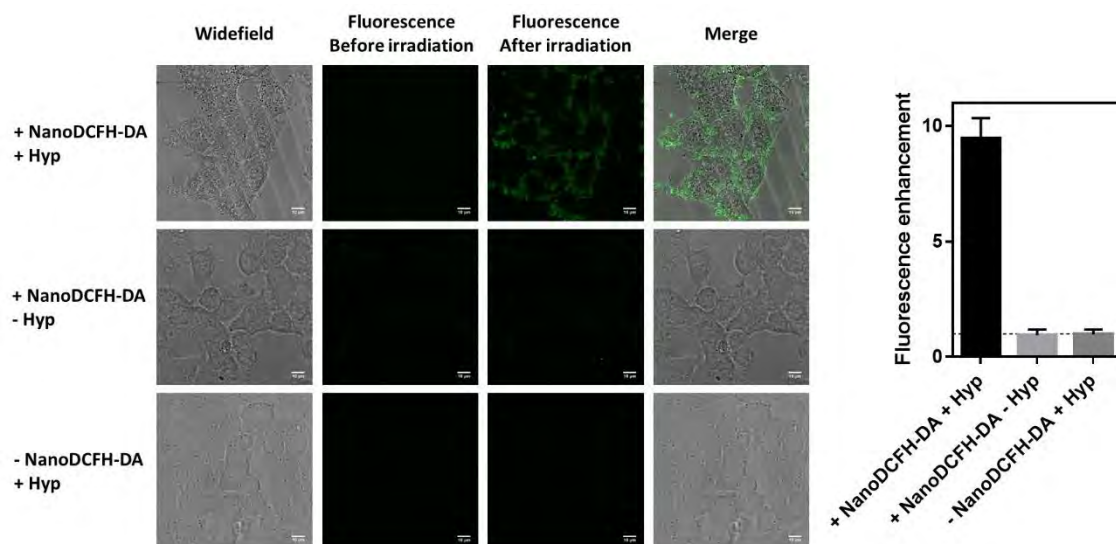


Figure 4.22 Images of HeLa cells incubated with 2 μM nanoDCFH-DA and 10 μM Hyp (top), 2 μM NanoDCFH-DA (middle) and 10 μM Hyp (bottom). Widefield, nanoDCDH-DA fluorescence before irradiation and nanoDCFH-DA fluorescence enhancement after 2 min of irradiation ($\lambda_{\text{irr}} = 561 \text{ nm}$) are displayed for each condition. Open bars represent the mean and the standard deviation for thirteen independent cells where only the mean pixel intensity of the images is considered.

4.3. Unravelling CellROX[®] Deep Red: a nonspecific reactive oxygen species fluorescent probe

(Adapted from: **R. Bresoli-Obach**, J. Torra, C. Flors, M. Agut, X. Shu, R. Ruiz-González and S. Nonell, Unravelling CellROX[®] Deep Red: a nonspecific Reactive Oxygen Species fluorescent probe, *in preparation*)

The results reported in this section have been carried out in collaboration with the University of California San Francisco (United States) and the IMDEA Nanociencia (Madrid, Spain).

4.3.1. CellROX[®] a novel ROS fluorescent probe

We have recently recalled our attention to a family of commercially available probes that are cell-permeant, wide range of absorption and with the capacity to increase their fluorescence upon reactivity to ROS.⁶²² Exactly, according to the manufacturer CellROX[™]'s ROS-sensitive fluorescent dyes are:

“CellROX[™] Oxidative Stress Reagents are fluorogenic probes designed to reliably measure reactive oxygen species (ROS) in live cells. The cell-permeable reagents are non-fluorescent or very weakly fluorescent while in a reduced state and upon oxidation exhibit strong fluorogenic signal. [...]. The fluorescence resulting from CellROX[™] Oxidative Stress Reagents can be measured using traditional fluorescence microscopy, high-content imaging and analysis, microplate fluorometry, or flow cytometry.”⁶²²

The manufacturer sells three different types of CellROX[™] fluorescent dyes: i) CellROX[™] Deep Red Reagent (λ_{exc} 640 nm; λ_{obs} 665 nm), ii) CellROX[™] Orange Reagent (λ_{exc} 545 nm; λ_{obs} 565 nm) and iii) CellROX[™] Green Reagent (λ_{exc} 485 nm; λ_{obs} 520 nm). These compounds have been widely and successfully used by several independent groups in order to detect ROS in live-cell confocal imaging or in flow-cytometry experiments (see different examples in refs.^{623–627}). In counter-position with DCFH-DA, CellROX fluorescent probes can be applied to cells directly in complete growth medium and it retains their fluorescence signal after formaldehyde fixation, allowing for assay flexibility and improved workflows.⁶²² Moreover according to manufacturer, CellROX[™] Reagents are sensitive to exposure to light and air, but no more information is described. Among them, CellROX[™] Deep Red Reagent (hereafter as CellROX) is the most used due to its excitation in the far-red region.

As explained above: nowadays, CellROX is a widely-used ROS fluorescent probe. To the best of our knowledge, neither the chemical structure of CellROX nor its selectivity towards different ROS is available. In this sense, we set up a study to elucidate the possible structure of the dye, assess its behaviour against different ROS/RNS and finally challenge it with different miniSOG derivatives expressed inside *E. coli* bacterial cells.

4.3.2. Experimental section

4.3.2.1. Structural elucidation

¹H-NMR spectra was recorded on a Varian 400 spectrometer (400 MHz) using residual solvent ($\delta(\text{CD}_3\text{SOCD}_3) = 2.50$) as internal standard.²³¹

Mass spectra was recorded on LTQ-FT Ultra mass spectrometer (Thermo Scientific). CellROX was directly infused for MS analysis. Elemental compositions from experimental exact mass monoisotopic values were obtained with a dedicated algorithm integrated in Xcalibur software.

Sample introduction: Direct infusion (Automated Nanoelectrospray). The NanoMate (Advion BioSciences, Ithaca, NY, USA) aspirated the samples from a 384-well plate (protein Lobind) with disposable, conductive pipette tips, and infused the samples through the nanoESI Chip (which consists of 400 nozzles in a 20 x20 array) towards the mass spectrometer. Spray voltage was 1.70 kV and delivery pressure was 0.50 psi.

Ionization: NanoESI, positive ionization

Spray voltage: 1.70 kV

Capillary Temperature: 200°C

Capillary Voltage: 35V

Tube Lens: 100 V

m/z range: 150-2000 a.m.u.

Infrared spectra supported onto diamond ATR top-plate was recorded in Nicolet Magna 560 FTIR spectrophotometer.

4.3.2.2. Computational calculations

The calculations of this section were performed using the Gaussian09 suite of programs.³⁹⁷ CellROX and Cy5 core energy minima were fully optimized at the density functional theorem (DFT) B3LYP/6-31G(d)³⁹⁸ level of theory. A frequency analysis was done to ensure convergence to a minimum in the potential energy surface. Time-dependent-DFT (TD-DFT) B3LYP/6-31G(d) was used to estimate the energy of the singlet excited state.⁶²⁸ The influence of water solvation on singlet state energies was calculated by performing Polarizable Continuum Model (PCM)³⁹⁹ single point energy calculations at the TD-DFT-B3LYP/6-31G(d) level of theory, based on gas-phase DFT-B3LYP/6-31G(d) geometries.

4.3.2.3. Generation of ROS and RNS

Various ROS and RNS were prepared according to the protocols below. All these species were generated at 1 mM concentration. CellROX and Cy5 concentration was 2.5 μ M.

Superoxide anion radical ($O_2^{\cdot-}$) was added as solid KO_2 .

Hydrogen peroxide (H_2O_2) was diluted from the commercial source (H_2O_2 at 30% in water).

Hydroxyl radical ($\cdot OH$) was generated by Fenton reaction.⁶²⁹ Briefly, Mohr salt ($(NH_4)_2SO_4 \cdot 6H_2O$) was dissolved in PBS. That solution (0.2 mM) was added to a solution with the fluorescent probe and H_2O_2 (1 mM).

Singlet oxygen (1O_2) was generated by irradiation of Rose Bengal (a well-known 1O_2 photosensitizer)⁵⁹³ with green light (520 ± 18 nm).

Sodium hypochlorite ($NaOCl$) was diluted from the commercial source (50 g/L of $NaClO$ in water).

Nitric oxide (NO) was generated from the decomposition of an aqueous solution of 1 M Sodium nitroprusside ($Na_2[Fe(CN)_5NO]$).⁶³⁰

Peroxynitrite anion ($ONOO^-$) was generated as described in ref.⁶³¹ Briefly, 1.5 M $NaOH$ (aq) was added in a mixture of 0.6 M $NaNO_2$, 0.7 M H_2O_2 and 0.6 M HCl . The $ONOO^-$ solution was readily used after its preparation.

Nitrogen dioxide (NO_2) was generated from the decomposition of sodium nitrite ($NaNO_2$).⁶³² Briefly, 1 M $NaNO_2$ solution is added to H_2SO_4 (96%) and the generated brownish gas is collected.

4.3.2.4 Cell cultures

E. coli cells (DH10 β , Invitrogen) were transformed with the expression vector encoding the fluorescent proteins miniSOG wt, miniSOG Q103L and miniSOG Q103V. Cells were grown from single colonies to OD_{600} of 0.3 at 37°C in LB medium supplemented with 100 μ g/mL ampicillin. Untransformed (blank) cells were grown in LB without ampicillin. Protein expression was induced by addition of 0.2% (w/v) L-arabinose. Cells were harvested by centrifugation after 3 hours and washed three times with PBS (pH 7.4). Cell density was matched to $OD_{600} = 1 \pm 0.1$ for all samples. All experiments were performed in triplicate.

4.3.3. Results

In a first approach, CellROX's absorbance and emission spectra were studied. In its original (reduced) form it shows an absorbance maximum at 367 nm and it is weakly fluorescent at 400 nm (Figure 4.23, left panel and Table 4.6). After oxidation with ROS/RNS, a highly fluorescent species is formed, with an absorption and emission maxima at 642 and 658 nm, respectively (Figure 4.23, right panel and Table 4.6) which matches that of a cyanine chromophore (i.e. cyanine 5 dye, Cy5, Table 4.6).

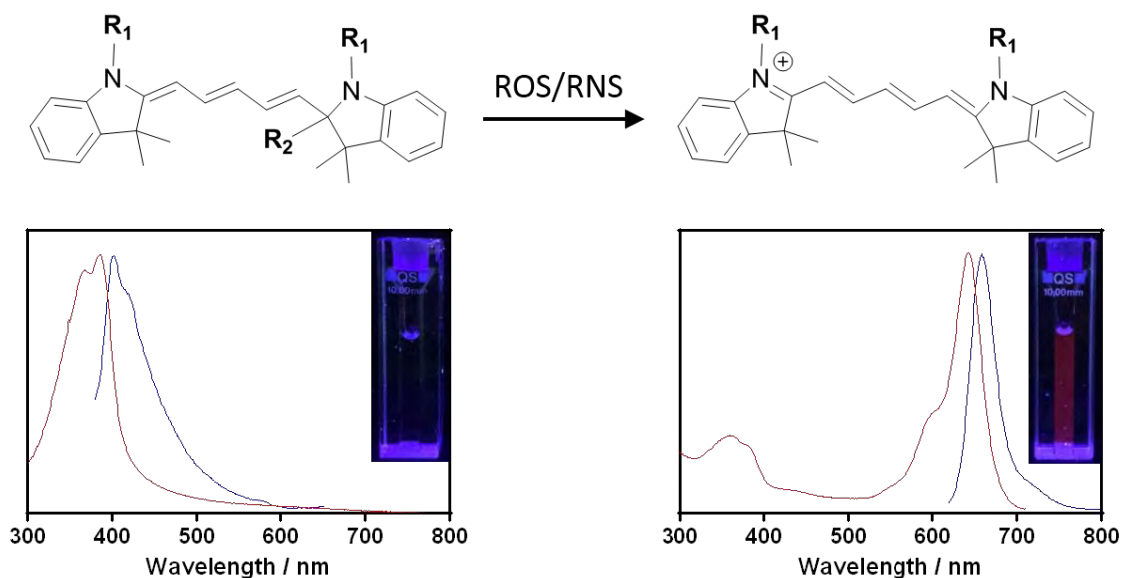


Figure 4.23 Absorption and fluorescence spectra for original (a) and oxidized-CellROX (b). Hydrogen peroxide (H_2O_2) was used as oxidant. Elucidated structures on top. λ_{exc} 370 and 610 nm, respectively.

Table 4.6 Photophysical properties of CellROX, oxidized-CellROX and Cy5 chromophore in PBS

	$\lambda_{\text{abs}} / \text{nm}$	$\lambda_{\text{fluo}} / \text{nm}$	Φ_{F}	$\tau_{\text{F}} / \text{ns}$
CellROX	367	400	< 0.001	5.0
Oxidized-CellROX	642	659	0.29	0.6
Cy5	637	655	0.28	0.5

Density functional theory (DFT) calculations³⁹⁸ revealed the loss of planarity in hydrocyanine 5, the reduced form of Cy5, which is recovered upon oxidation concomitant with a reduction of the LOMO-HUMO energy gap. This is in excellent agreement with the bathochromic shift experimentally observed upon CellROX oxidation. Furthermore, time-dependent DFT computational calculations have been carried out in order to simulate its absorption spectrum, which is in concordance to the non-oxidized CellROX spectrum (Figure 4.24). As a result, we hypothesize that other commercial CellROX derivatives could indeed be analogues of other hydrocyanine dyes (i.e. CellROXTM Orange and CellROXTM Green could correspond to hydrocyanines 3 and 2, respectively). Its synthetic viability has been demonstrated by Kundu *et al.* which efficiently obtained different hydrocyanines using sodium borohydride as reducing agent.⁶¹⁴

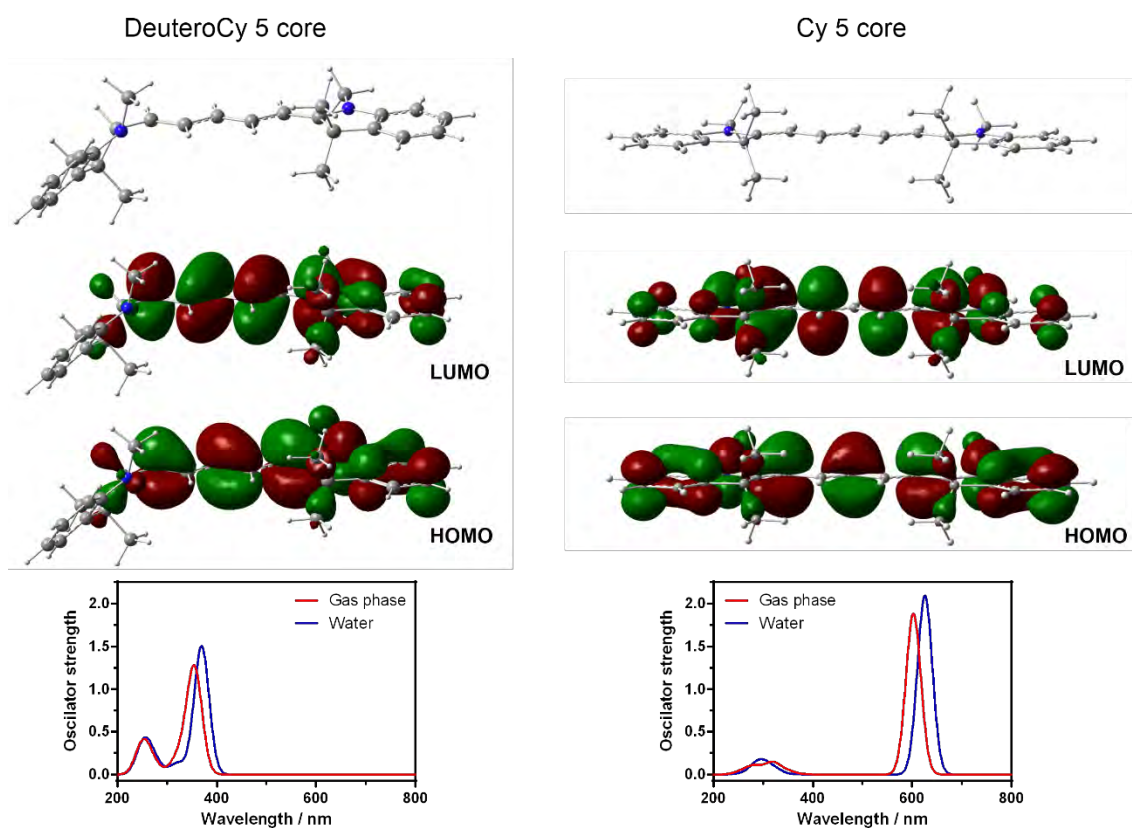


Figure 4.24 Top: Ground state optimized structure for DeuteroCy5 and Cy5 core (left and right, respectively) at DFT-B3LYP (Basis set: 6-31G(d)) level of theory. Middle: LUMO and HOMO orbitals for each species. Bottom: Calculated absorption spectra at TD-DFT-B3LYP (Basis set: 6-31G(d)) level of theory for each specie in gas phase (red line). The influence of water solvation on the absorption spectrum (blue line) was investigated by performing Polarizable Continuum Model (PCM) single point energy calculations at the TD-DFT B3LYP/6-31G(d) level of theory, based on gas-phase DFT B3LYP/6-31G(d) geometries.

CellROX structures are protected under trade secret. Thus, the molecule shown in Figure 4.23 represents a Markush structure of a molecule presented in the company's patent.⁶³³ In order to further ascertain the most accurate CellROX Deep Red structure, several experiments have been carried out:

- i) From steady state spectroscopy, only a 4-5 nm red-shift difference is encountered between the oxidized-CellROX and the Cy5 core which can be reasonably attributed to the nature of R₁ substituents. Furthermore, the fluorescence quantum yield (Φ_F) for both species is roughly the same (Table 4.6).
- ii) Time-resolved fluorescence decays for the oxidized-CellROX and for Cy5 core have the same singlet state lifetime (Table 4.6).
- iii) ¹H-NMR spectroscopy shows 13 aromatic hydrogens, which is consistent with the proposed structure of the fluorophore core. Moreover, 26 aliphatic hydrogens are also observed, which is in line with the proposed structure obtained from the patent (R₁=(CH₂)₃-COO-Et).⁶³³
- iv) From high resolution mass spectrometry, a molecular weight of 585.36931 Da is obtained, in agreement with a M⁺ of C₃₇H₄₇DN₂O₄. In addition, it can also be detected the M-2 signal. show M-17 and M-32 fragmentations, which could indicate the loss of a deuterium atom and one or two methyl groups, respectively.

v) From IR spectrum, a key band is observed at 2160 cm^{-1} , which matches that of the C-D stretching. The C-D band is in concordance with the deuterio-Cy5 core simulated using DFT calculations (2140 cm^{-1}), thus indicating that $R_2=D$.

Firstly, the substitution of a hydrogen by a deuterium atom in R_2 . The goal of this substitution, as stated in the manufacturer's patent, is to improve the stability of the reduced form in solution. It is reported that the C-D bond is stronger than the C-H analogue, which should reduce its reactivity towards $^3\text{O}_2$ dissolved in the medium. If the key step of this reaction is the deuterium bond breaking, primary hydrogen kinetic isotope effect should be observed reducing its reactivity by a minimum factor of 6.^{309,634,635} In Figure 4.25 we determine the reactive constant of CellROX towards $^3\text{O}_2$ resulting in a constant rate of $0.13\text{ M}^{-1}\text{s}^{-1}$ at $25\text{ }^\circ\text{C}$ in PBS. Secondly, the presence of ethyl acetate groups: As reported for other fluorescent probes, once internalized, cell esterases can break these ester bonds to carboxylate moieties, which facilitate its accumulation inside the cell due to their negative charges.⁶³⁶⁻⁶³⁸

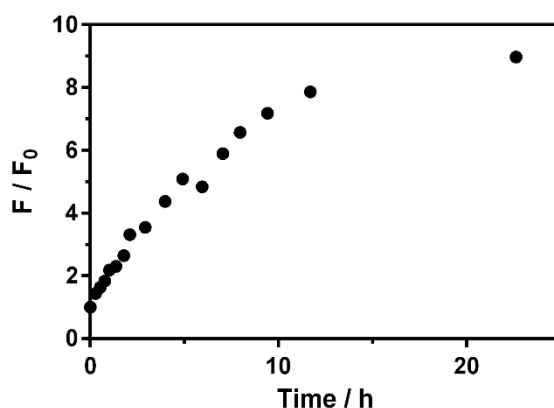


Figure 4.25 CellROX fluorescence enhancement due to its oxidation by $^3\text{O}_2$ in air-saturated PBS at $25\text{ }^\circ\text{C}$ (λ_{exc} 630 nm; λ_{obs} 640-800 nm).

In counterpart, CellROX does generate ROS by itself under irradiation that can lead to self-generation of the oxidized form. When illuminated in presence of d-mannitol and sodium azide ($^{\bullet}\text{OH}$ and $^1\text{O}_2$ quenchers, respectively)^{639,640} no difference is observed (Figure 4.26A). However, in the presence of Tiron (a $\text{O}_2^{\bullet-}$ and $^{\bullet}\text{OH}$ quencher)⁴⁵² CellROX photooxidation kinetics become slower (Figure 4.26A). In addition, when CellROX is illuminated under hyperoxic conditions, the photo-oxidation rate is faster, while under hypoxic conditions it is slower (Figure 4.26B). Taken together, these results point out that CellROX photooxidation is mainly due to the generation of $\text{O}_2^{\bullet-}$ by self-photosensitization.

Since stability of the oxidized product is a key parameter for its use as fluorescence tag in microscopy, we have further studied this light-driven effect. Figure 4.26C shows that Cy5's fluorescence is halved when 6 J/cm^2 red light have been delivered. This value is over one-order of magnitude larger than that used in conventional live-cell confocal microscopy experiments.⁵⁷³ Provided that oxidized-CellROX could be exposed to other wavelengths when combined with other fluorescent tags, Cy5 was also irradiated with violet, blue and green light. The observed fluorescence decrease was below 20% after fluences as high as 50 J/cm^2 in all the cases.

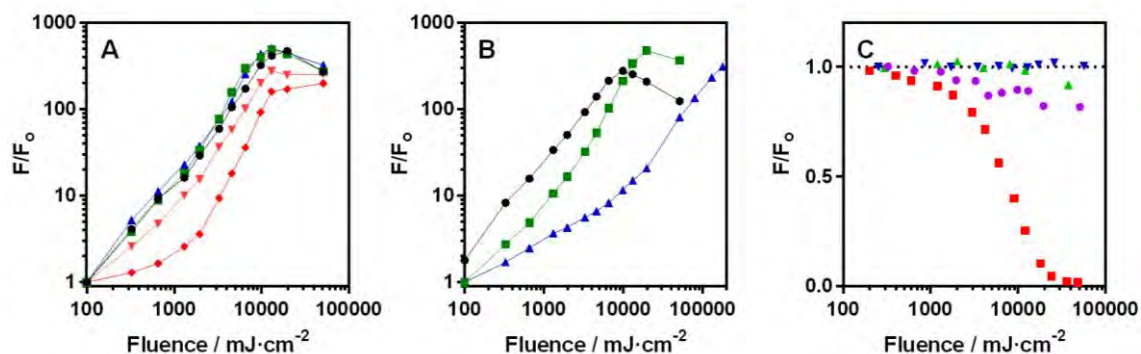


Figure 4.26 CellROX deep red fluorescence enhancement by irradiation under violet light. (A): in absence (black line) or in presence of ROS scavengers (NaN_3 ($^1\text{O}_2$ scavenger; 25 mM; green line); D-mannitol ($^{\bullet}\text{OH}$ scavenger; 60 mM; blue line); Tiron ($\text{O}_2^{\bullet-}$ and $^{\bullet}\text{OH}$ scavenger; 25 and 250 mM; pink and red line respectively)). (B): in hyperoxic (O_2 -saturated PBS; black line), air-saturated PBS (green line) and hypoxic (Argon-saturated PBS; blue line) conditions. (C): Photostability of Cy5 under violet, blue, green and red light irradiation.

The next step was to study CellROX and Cy5 performance towards oxidation mediated by different ROS and RNS (Figure 4.27). For equal oxidant concentrations, the highest CellROX fluorescent enhancement (filled bars) was achieved for $^{\bullet}\text{OH}$, followed by $\text{O}_2^{\bullet-}$ and H_2O_2 . Figure 4.27 demonstrates that CellROX is highly reactive and unselective towards different ROS/RNS except for $^1\text{O}_2$. For this latest species, reactivity towards CellROX resulted in a fluorescence decrease. This observation can be justified by the results obtained when CellROX is irradiated in the presence or absence of a PS. Figure 4.27 (striped bars) also shows the reactivity of the Cy5 core towards the same ROS/RNS, pointing out that Cy5 is readily oxidized by ClO^- , $^{\bullet}\text{OH}$, NO_2 and $^1\text{O}_2$.

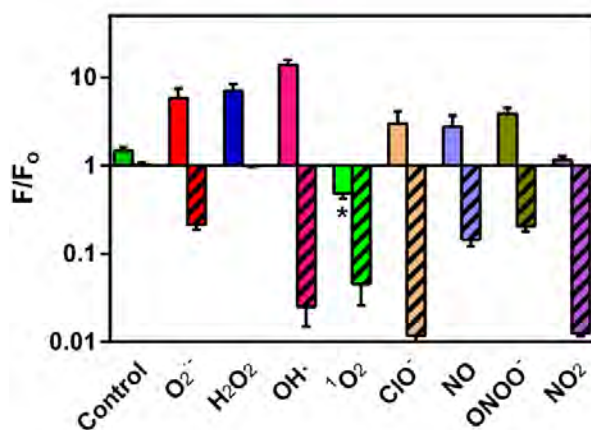


Figure 4.27 Oxidation of 2.5 μM CellROX Deep Red (filled bars) and Cy5 core (striped bars) towards different ROS/RNS at 1 mM concentration: $\text{O}_2^{\bullet-}$ (as KO_2), H_2O_2 , $^{\bullet}\text{OH}$ (generated by Fenton reaction), ClO^- (as NaClO), $^1\text{O}_2$ (generated by irradiation of Rose Bengal at 520 ± 18 nm), NO (generated by sodium nitroprusside decomposition), ONOO^- (generated by reaction of NO with $\text{O}_2^{\bullet-}$) and NO_2 (generated by sodium nitrite decomposition in acidic media).

Despite being unselective, CellROX can still be used to ascertain which type of photo-generated ROS/RNS is the main responsible for the fluorescent change. On the one hand, Type I ROS, which involve species such as $\text{O}_2^{\bullet-}$, H_2O_2 , $^{\bullet}\text{OH}$ and RNS, leads to an increase in the probe's fluorescence signal. This enhancement could be partially reduced in the presence of specific Type I ROS quenchers. On the other hand, Type II ROS,

which involves $^1\text{O}_2$, reduces CellROX's fluorescence signal, which could be reversed with an appropriate $^1\text{O}_2$ quencher such as sodium azide.

Finally, we have assessed CellROX performance when challenged to *E. coli* cells expressing different flavin-binding proteins with the capacity to photosensitize ROS. On the one hand, CellROX incubated with non-recombinant *E. coli* presented a non-negligible fluorescence enhancement (Figure 4.28) probably due to the sole effect of blue-light illumination as observed previously in PBS. On the other hand, CellROX incubated with *E. coli* expressing different flavin-binding proteins presents larger fluorescence enhancement values. This increase can be partially suppressed by the addition of different type I ROS quenchers (i.e. Tiron or d-mannitol). Conversely, in presence of NaN_3 the fluorescence enhancement becomes larger. When comparing the different proteins, the trend in fluorescence enhancement (miniSOG Q103V > miniSOG Q103L >> miniSOG) correlates with the overall capacity of these flavoproteins to sensitize ROS.⁶⁴¹

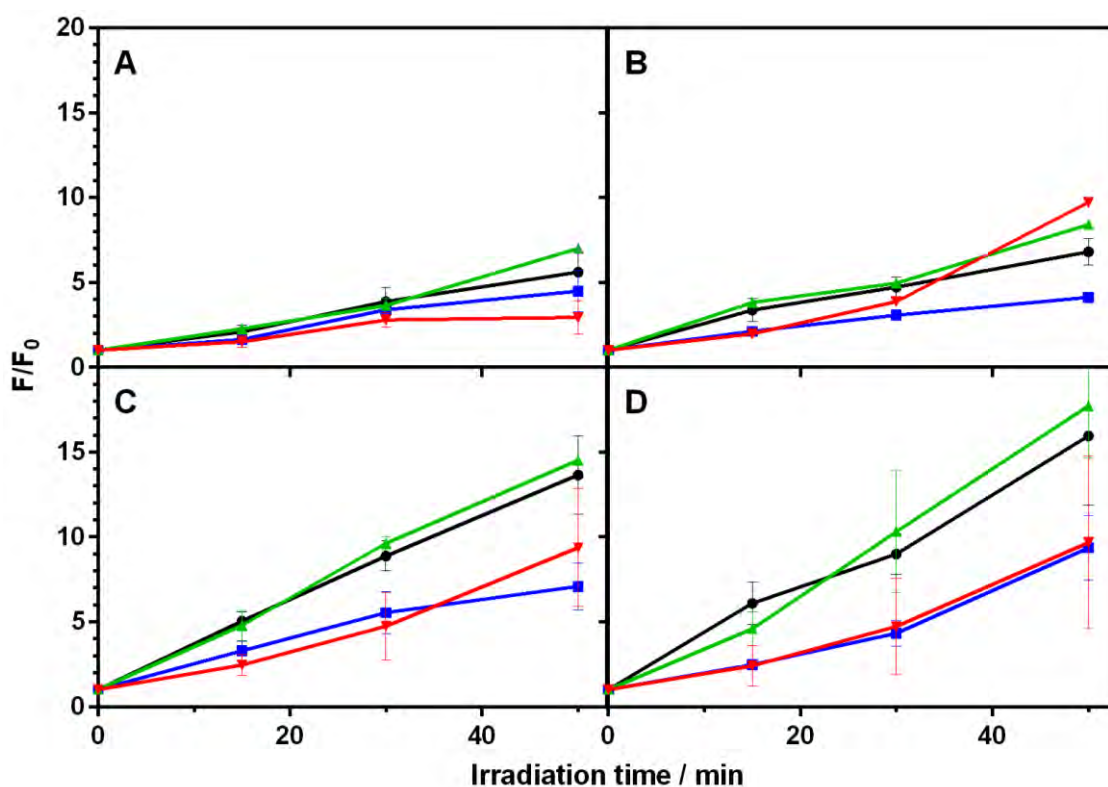


Figure 4.28 Fluorescence enhancement of CellROX in wt *E. coli* (A), and *E. coli* expressing miniSOG (B), miniSOG Q103L (C) and miniSOG Q103V (D) as a function of the irradiation time ($\lambda_{\text{exc}} = 463 \pm 11$ nm). The experiments have been performed in the absence (black line) and in the presence of different ROS quenchers, namely 10 mM NaN_3 (green), 10 mM Tiron (red) and 60 mM d-mannitol (blue).

4.4. Tetramethylbenzidine: a photoacoustic probe for reactive oxygen species detection

(Adapted from: **R. Bresolí-Obach**, M. Frattini, M. Agut, S. Abruzetti, C. Viapianni and S. Nonell, Tetramethylbenzidine: a photoacoustic probe for reactive oxygen species detection, *in preparation*)

The results reported in this section have been carried out in collaboration with the Università degli Studi di Parma (Italy).

4.4.1. Introduction to photoacoustic techniques

Photoacoustics, also known as optoacoustics, were pioneered by A.G. Bell, more than a century ago (1880).^{642,643} The experiments were difficult to perform and quantitate since the detector was the investigator's ear.



“We find that when a vibratory beam of light falls upon these substances^y they emit sounds, the pitch of which depends upon the frequency of the vibratory change in the light. We find farther, that when we control the form or character of the light, vibrations on selenium (and probably on the other substances), we control the quality of the sound, and obtain all varieties of articulate speech.”

*On the Production and Reproduction of Sound by Light
- Alexander Graham Bell*

Photoacoustics, had been revived by Harshbarger and Robin and Rosencwaig in 70s.^{644–646} The first optoacoustics experiments were performed in gas phase.⁶⁴⁷ Some years after, Patel *et al* have demonstrated a highly sensitive pulsed optoacoustic spectroscopy technique, involving the use of pulsed lasers, a piezoelectric transducer in direct contact with the liquid sample, and gated detection.⁶⁴⁸ This was the first example of optoacoustics experiments in condensed-phase. Since then photoacoustic techniques have been extensively developed because they are extremely sensitive, allowing to monitor absorptivity as low as 10^{-7} - 10^{-8} cm^{-1} ,^{649,650} and absorbance changes smaller than 10^{-4} units.⁶⁵¹

Photoacoustic techniques relies on the detection of thermal relaxation of excess energy associated with photoexcitation of the sample. Among all the photothermal techniques, the most used is the so-called Laser-induced optoacoustic spectroscopy (LIOAS), which monitors the pressure changes induced in a liquid sample after excitation with a pulsed laser.^{92,230}

Briefly, the pressure waves in the excited sample arise from the volume changes produced by radiationless relaxation (ΔV_{th}) and/or structural rearrangements at the molecular level (ΔV_r) (Figure 4.29). Relaxation contributions originates either from nonradiative decay of excited states or heat release (enthalpy change) in photoinitiated

^y Gold, silver, platinum, iron, steel, brass, copper, zinc, lead, antimony, german-silver, Jenkin's metal, Babbitt's metal, ivory, celluloid, gutta-percha, hard rubber, soft vulcanized rubber, paper, parchment, wood, mica, and silvered glass; and the only substances from which we have not obtained results, are carbon and thin microscope glass.

reactions. The structural volume changes reflect movements of the photoexcited molecules and/or the surrounding solvent.⁶⁵²⁻⁶⁵⁵

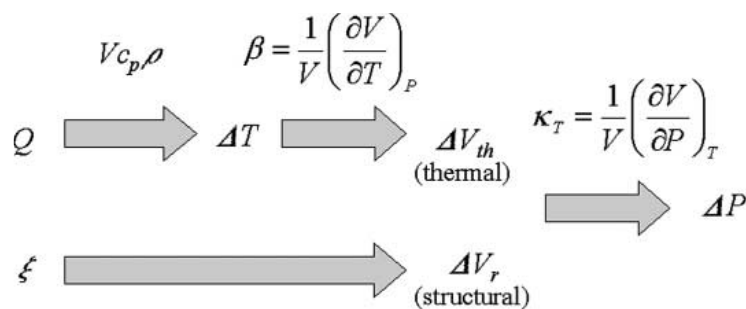
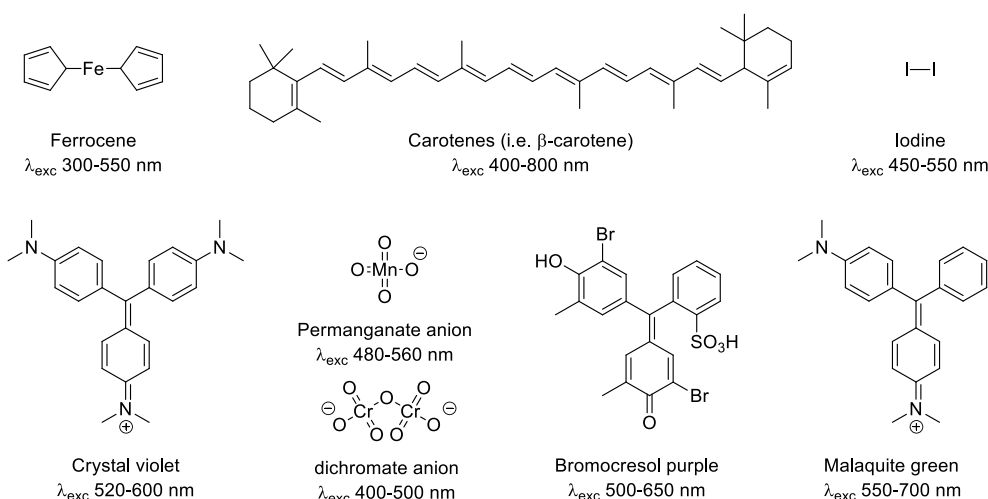


Figure 4.29 Heat release (nonradiative decays or enthalpic changes; Q) are converted to changes in temperature through the heat capacity ($VC_{p,\rho}$), and to volume changes of the solution (ΔV_{th}) through the isobaric expansion coefficient (β). ξ stands for all molecular, atomic, and electronic rearrangements of solute and solvent molecules leading to a structural volume change (ΔV_r). The pressure changes arising from volumetric variations are mediated by the isothermal compressibility (κ_T). Reproduced from reference ²³⁰.

For small-molecules, the contribution of ΔV_r normally is small.^{656,657} Therefore, the pressure changes are mainly derived from heat release. Approximately, a 1 mK temperature rise results in an 800 Pa pressure rise, which is above the noise level of a typical ultrasonic transducer. So, it is interesting to study the relationship between the various forms of dissipation of energy by the excited species. Thus, after the absorption of energy in the form of radiation (E_a), a simple energy balance considerations is depicted in equation 4.1.

$$1 - 10^{-A} \alpha E_A = \phi_F E_F + \phi_{ST} E_{ST} + \alpha E_A \quad \text{Eq. 4.1}$$

Where, E_A is the absorbed molar energy, which depends on the number of photons absorbed and the energy of these photons. The right hand of the equation is the sum of three terms. The first term is the energy dissipated in the form of fluorescence (radiative decay). The second term is the energy stored by species living longer than the heat-integration time of the system (i.e. long-lived triplet states or photochemical intermediates). The third term is the fraction of energy released in the medium as heat as a result of rapid vibrational relaxation including relaxation to the first singlet excited state. Furthermore, if a photochemical reaction can take place, to this released energy is necessary to sum the ΔH of that reaction.^{92,230}



Scheme 4.11 Widely-used photoacoustic labels and references.^{92,230}

A good photoacoustic reference should be a molecule that absorbs light efficiently and release all the absorbed energy as heat in a fast time scale (in the range of nanoseconds). Typical photoacoustic probes are depicted in Scheme 4.11. Recently, some genetically encoded photoacoustic probes have also been engineered.⁶⁵⁸

LIOAS has been used to study different systems such as electron transfer in photosynthetic reaction centers,⁶⁵⁹ volumes changes in excited states,⁶⁶⁰ Φ_T and Φ_A calculations⁶⁶¹ or proteins motions (i.e. biological photoreceptors⁶⁶² or protein folding⁶⁶³) among others. Recently, photoacoustic techniques have gained popularity thanks to photoacoustic imaging, which is an emerging hybrid imaging modality that can provide three-dimensional images with real-time correlation, clinically relevant depths and relatively high spatial resolution using nonionizing radiation.^{664–667}

As explained before, fluorescence imaging of tissue offers potential advantages in distinguishing different structures according to their chemical composition. However, tissue is a highly scattering medium for visible light (less for near-infrared light), so it provides fine resolution but with a low imaging depth in tissue up to few millimeters.⁶⁶⁸ Photoacoustic imaging can penetrate further inside tissue due to the low acoustic scattering of tissue (approximately 1,000 times less than optical scattering).⁶⁶⁹ Figure 4.30 depicts a typical optoacoustic microscope and an example of a photoacoustic image of the microvasculature in a mouse ear.⁶⁵⁸ For that reason, recently different optoacoustics probes have been developed in counterposition to fluorescent probes.⁶⁶⁴

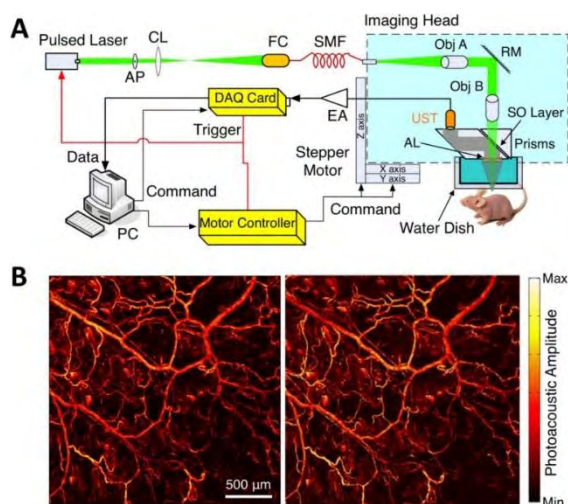
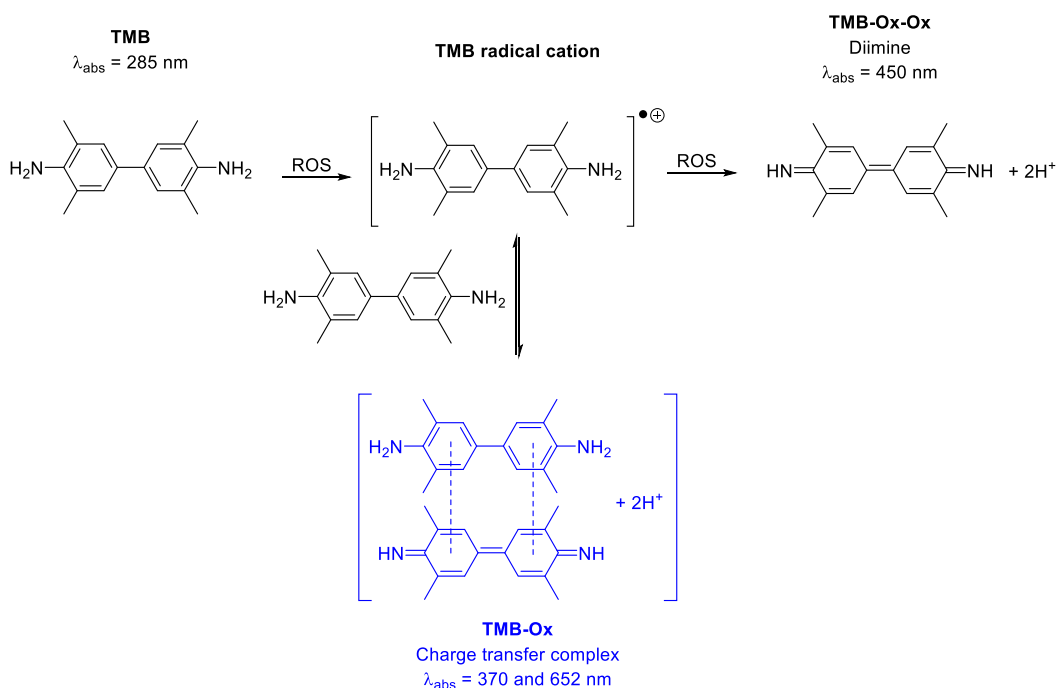


Figure 4.30 Photoacoustic imaging of microvasculature in a mouse ear imaged *in vivo*. (A) Schematic diagram of the photoacoustic microscopy system. (B) Photoacoustic images of the microvasculature in a mouse ear. Left: raw data; right: after blind deconvolution². Reproduced from reference ⁶⁵⁸.

² In image processing, blind deconvolution is a deconvolution technique that permits recovery of the target scene from a single or set of "blurred" images in the presence of a poorly determined or unknown point spread function.

4.4.2. Reactivity of tetramethylbenzidine

Ideally, a photoacoustic probe should have high molar extinction coefficient, should release all the absorbed energy as heat as fast as possible and it should have high photobleaching resistance.⁶⁵⁸ Under these objective, we did a bibliographic research in order to reprofile some dyes that are highly reactive against ROS and present these previous exposed properties. 3,3',5,5'-Tetramethylbenzidine (TMB) is a non-coloured and non-carcinogenic compound that can react with some ROS in order to generate a blue oxidized compound.^{670,671} TMB has been extensively used as visualising reagent upon its reaction with hydrogen peroxide in presence of horseradish peroxidase in ELISA assays.⁶⁷²



Scheme 4.12 TMB reactivity towards oxidant agents.

Scheme 4.12 shows the reactivity of TMB towards ROS. In a first step, TMB reacts to form a radical cation, which in presence of free TMB it generates one-electron charge transfer complex (TMB-Ox) and it exhibits a blue colour ($\lambda_{\text{abs}} = 652 \text{ nm}$). In a second step, the reaction will be complete and form a diimine product (TMB-Ox-Ox), which presents a yellow colour ($\lambda_{\text{abs}} = 450 \text{ nm}$). Finally, with an excess of oxidant it generates other non-coloured molecules.⁶⁷³

To our best knowledge there isn't any $^1\text{O}_2$ photoacoustic probe already described and only few works to detect some ROS (i.e. sodium hypochlorite or hydrogen peroxide).^{674,675} Under that purpose we tried to develop a $^1\text{O}_2$ sensitive photoacoustic probe, taking in advantage the oxidation of non-coloured tetramethylbenzidine to blue coloured oxidation-compounds.⁶⁷⁶

4.4.3. Experimental part

4.4.3.1. Statistical analysis

The limit of detection (LOD) and the limit of quantification (LOQ) are assumed to be 3- and 10-fold the standard deviation of the blank interpolated to the linearity fitting for analyte calibration curve with a security of 99%.

4.4.3.2. ROS and RNS generation

The different ROS and RNS used in this work were prepared according to the protocols below. Sodium hypochlorite (NaOCl) was diluted from the commercial source (50 g/L of NaClO in water). Superoxide anion radical ($O_2^{\bullet-}$) was added as solid KO_2 . Hydrogen peroxide (H_2O_2) was diluted from the commercial source (H_2O_2 at 30% in water). Hydroxyl radical ($\bullet OH$) was generation by irradiation of 1 mM $NaNO_2$ solution with UV-A light (354 ± 20 nm).⁶⁷⁷ $\bullet OH$ generation was further verified by scavenging it with terephthalic acid.⁶⁷⁸ Singlet oxygen (1O_2) was generated by irradiation of RB with green light (520 ± 18 nm). Sodium peroxide (Na_2O_2) was added as solid Na_2O_2 . Nitric oxide (NO) was generated from the decomposition of an aqueous solution of 1 M Sodium nitroprusside ($Na_2[Fe(CN)_5NO]$).⁶³⁰ Peroxynitrite anion ($ONOO^-$) was generated as described in reference ⁶³¹. Briefly, 1.5 M NaOH (aq) was added in a mixture of 0.6 M $NaNO_2$, 0.7 M H_2O_2 and 0.6 M HCl. The $ONOO^-$ solution was readily used after its preparation. Nitrogen dioxide (NO_2) was generated from the decomposition of sodium nitrite ($NaNO_2$).⁶³² Briefly, 1 M $NaNO_2$ solution is added to H_2SO_4 (96%) and the generated brownish gas is collected. Nitrite (NO_2^-) was diluted from a 1M sodium nitrite solution. 2,2,6,6-Tetramethylpiperidin-1-yl)oxyl (TEMPO) was added as solid.

4.4.3.3. 1O_2 detection in *E. coli* cells using miniSOGs as photosensitizer

E. coli cells (DH10 β , Invitrogen, CA, USA) were transformed with the expression vector encoding the fluorescent proteins miniSOG wt, miniSOG Q103L and miniSOG Q103V. Cells were grown aerobically from a single colony to an $OD_{600} = 0.3$ at 37°C in LB medium supplemented with 100 $\mu g/mL$ ampicillin. Untransformed DH10 β cells were grown in LB without ampicillin. Protein expression was induced by addition of 0.2% (w/v) L-arabinose. Cells were harvested by centrifugation after 3 hours and washed three times with PBS.

4.4.3.4. 1O_2 detection in *E. coli* cells using MDPyTMPyP as photosensitizer

E. coli cells (ATCC 25922, Manassas, VA, USA) were grown aerobically from a single colony to an $OD_{600} = 0.3$ cm^{-1} at 37 °C in LB medium. Afterwards, cells were harvested by centrifugation and washed three times with PBS (pH 7.4). Cells were incubated with MDPyTMPyP (10 μM) and NaN_3 (if it was necessary; 25 mM) during 20 minutes and after were washed three times with PBS.

4.4.4. TMB assessment as ROS optoacoustic probe

The absorption spectra of TMB, TMB-Ox and TMB-Ox-Ox were recorded in PBS (pH = 7.4; Figure 4.31A). The formation of TMB-Ox, which presents absorption maxima at 280, 370 and 650 nm, is observed by low concentrations of NaClO. When a soft-excess of NaClO is added TMB-Ox further oxidates to generate the yellow TMB-Ox-Ox product, which presents absorption maxima at 450 nm. Further addition of NaClO oxidizes even more TMB-Ox-Ox to other uncoloured dyes, which its characterization is not the scope of this work.

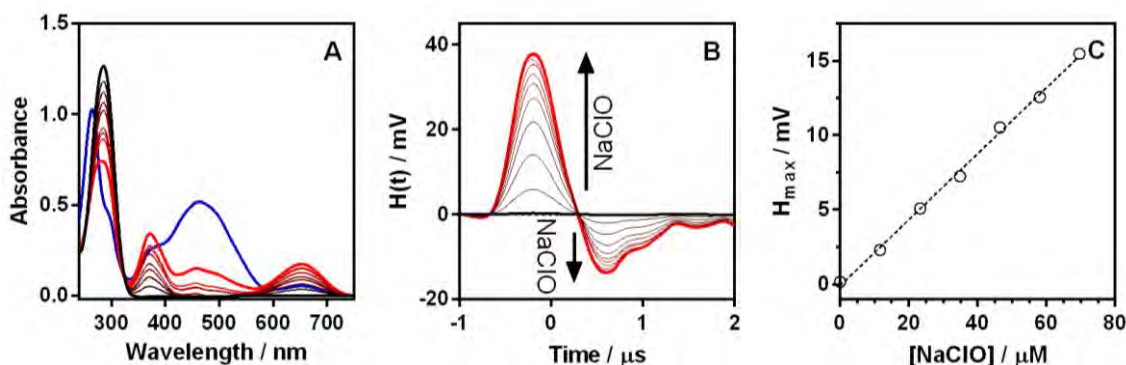


Figure 4.31 A: Absorption spectra of TMB (black line) upon successive NaClO additions. The red and blue line are expected to be TMB-Ox and TMB-Ox-Ox absorption spectra in PBS. B: TMB photoacoustic waveforms enhancement upon successive NaClO additions in PBS ([TMB] = 200 μM; [NaClO] = 0-1500 μM; λ_{exc} = 652 nm). C: Photoacoustic maximum amplitude vs concentration of NaClO added in PBS. [TMB] = 200 μM; λ_{exc} = 652 nm.

The formation of TMB-Ox is further studied by LIOAS techniques (Figure 4.31B), where up to 150 fold optoacoustic signal enhancement is achieved upon reaction with NaClO (λ_{exc} = 562 nm). After reaching a maximum, the photoacoustic signals decrease due to further oxidation to TMB-Ox-Ox. The next step was to determine the fraction of absorbed energy that is released as heat (α). By comparison with a suitable pure photocalorimetric reference (Bromocresol purple) is obtained an α value of 0.95 for TMB-Ox. Furthermore, temporal-deconvolution analysis of photoacoustic signal revealed that its heating release rate (in this case internal conversion) is less than the temporal-resolution of the system ($\tau_s < 20$ ns). The lack of fluorescence of TMB-Ox precluded the measurement of a reliable τ_s by time-resolved fluorescence methods.

Other photophysical parameters that have been studied are: i) TMB-ox optoacoustic signal linearity upon increasing excitation laser fluences in order to rule out multiphoton processes that could interfere in system response (Figure 4.32A), ii) TMB-ox under these experimental conditions is fairly photostable. TMB-Ox photoacoustic signal is reduced to half after 8500 laser shots (Figure 4.32B) and iii) it is known that LIOAS obtained signals have a big deviation between independent prepared samples with equal concentration. Under these conditions, the standard deviation between different 10 independent prepared samples but with same TMB concentration is 19% (Figure 4.32C).

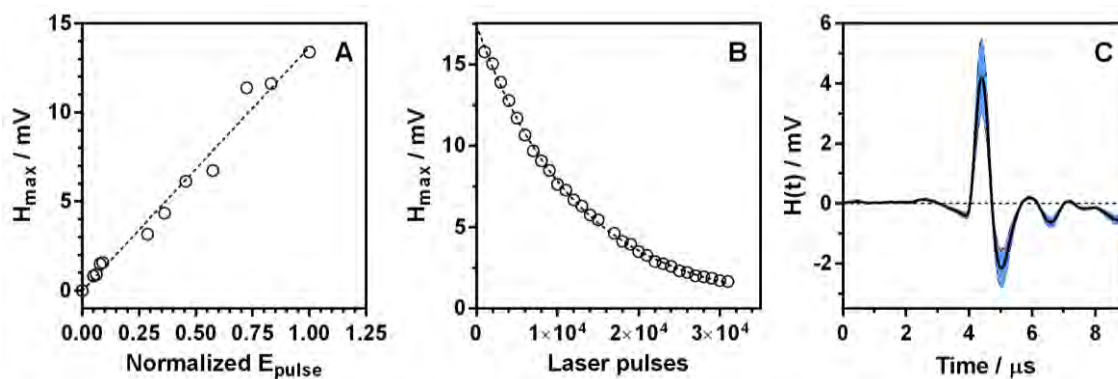


Figure 4.32 A: Laser energy dependence of optoacoustic maximum amplitude for TMB-Ox. B: Photostability of TMB-Ox upon laser pulsed-irradiation ($E_{\text{pulse}} = 1 \text{ mJ}$). C: Precision study of ten photoacoustic waves for one sample, but prepared independently. $[\text{TMB}] = 200 \text{ } \mu\text{M}$; $[\text{NaClO}] = 11 \text{ } \mu\text{M}$. $\lambda_{\text{exc}} = 652 \text{ nm}$.

Afterwards, we have optimized the concentration of TMB in order to maximize the obtained signal. At low TMB concentrations it is observed a linear signal increase up to approximately $30 \text{ } \mu\text{M}$, whilst for higher concentrations it gets saturated reaching the maximum signal value at $200 \text{ } \mu\text{M}$. This saturation mainly is due to photoacoustic signal do not depend linearly with absorbance, if not with absorption factor ($1-10^{-A}$), and with a possible inner filter effect. From these experiments, the chosen TMB concentration for upcoming experiments will be $200 \text{ } \mu\text{M}$ because is the minima concentration that allows to reach the maxima photoacoustic signals.

We studied the photoacoustic system linearity to a fix concentration of TMB with increasing concentration of NaClO, which is linear up to a concentration of $100 \text{ } \mu\text{M}$ (Figure 4.31C). From the standard deviation of the blank it was able to calculate the limit of detection (LOD) and quantification (LOQ) as 1 and $4 \text{ } \mu\text{M}$ respectively.

TMB-Ox-Ox photoacoustic properties has also been studied in order to be able to detect NaClO in a higher concentration range exciting it at 450 nm . It has a lower photoacoustic response due to its smaller absorbance, but its linearity range is increased up to $500 \text{ } \mu\text{M}$ NaClO. TMB-Ox-Ox photostability decreases (from 8500 to 5500 laser shots), its precision is reduced (19% to 25%) and its LOD and LOQ is increased (1 and 4 to 10 and $35 \text{ } \mu\text{M}$ respectively).

The following step was studying TMB reactivity towards different ROS and RNS (Figure 4.33). Under that purpose TMB was co-incubated with different concentrations ranging from 0.05 to various equivalents of the different ROS/RNS studied and afterwards its photoacoustic response is recorded. Additionally, it is added $200 \text{ } \mu\text{M}$ of ClO^- for ensure if there have been another reaction between ROS/RNS added and TMB, in the case that no photoacoustic signal enhancement is detected.

From experimental data three different casuistry is observed: i) ROS/RNS react with TMB for obtaining TMB-Ox (ClO^- , H_2O_2 , $^1\text{O}_2$ and NO_2); ii) ROS/RNS react with TMB, but it is obtained uncoloured-compounds (O_2^+ , Na_2O_2 , NO , ONOO^-) or iii) ROS/RNS do not react with TMB ($^{\bullet}\text{OH}$, TEMPO, NaNO_2).

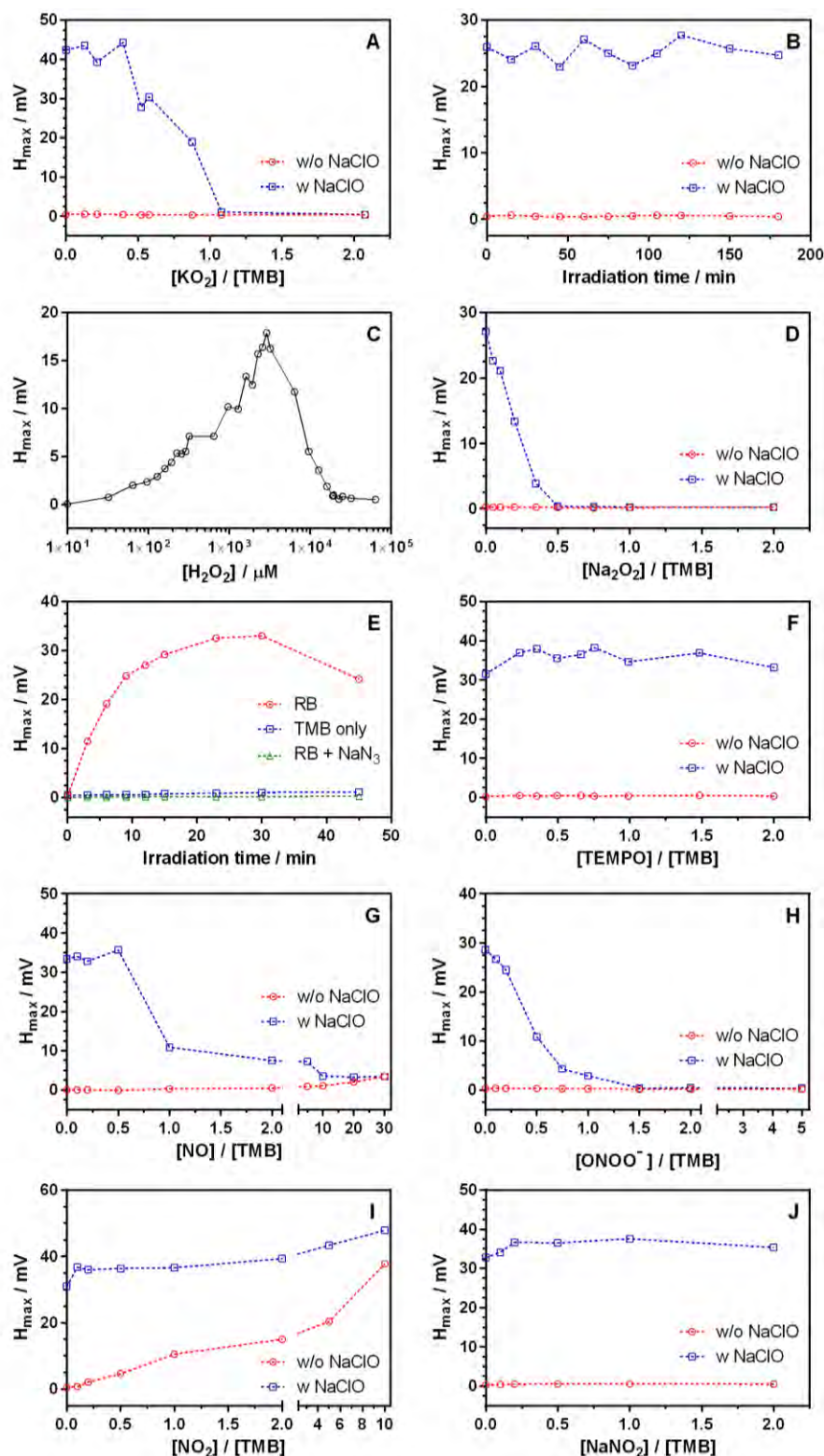


Figure 4.33 Photoacoustic maximum amplitude of TMB after reacting with different ROS and RNS. A): Superoxide radical anion ($O_2^{\cdot-}$). B): Hydroxyl radical ($\cdot OH$) generated via sodium nitrite photolysis in water ($\lambda_{exc} = 354 \pm 20$ nm). C): Hydrogen peroxide (H_2O_2). D): Sodium peroxide (Na_2O_2). E): Singlet oxygen (1O_2) generated via Rose Bengal irradiation ($\lambda_{exc} = 520 \pm 18$ nm). F): (2,2,6,6-Tetramethylpiperidin-1-yl)oxyl (TEMPO). G): Nitric oxide (NO) generated via sodium nitroprusside decomposition. H): Peroxynitrite ($ONOO^-$). I): Nitrogen dioxide (NO_2) generated via sodium nitrite acid decomposition. J): Sodium nitrite. For A, B, D, F, G, H, I and J the same experiment is repeated and afterwards NaClO up to an $200 \mu M$ was added (red and blue line respectively).

Moreover, LOD and LOQ are determined for those ROS/RNS that react with TMB to form TMB-ox, which are around micromolar range. For $^1\text{O}_2$, LOD and LOQ have not been measured due to the difficulty of quantifying the exact amount of $^1\text{O}_2$ generated. The obtained LOD and LOQ are in the range of interest from these ROS/RNS in live cells systems.

Once the reactivity towards different ROS/RNS is known, the next step was to detect ROS (i.e. $^1\text{O}_2$) in a more biological relevant media. In a first approach, the ability of TMB to respond to intracellular ROS was assessed comparing the optoacoustic maximum amplitude enhancement between wild-type *E. coli* and three different genetically modified *E. coli* that expresses three different miniSOG proteins (miniSOG, miniSOG Q103L and miniSOG Q103V; Figure 4.34A).

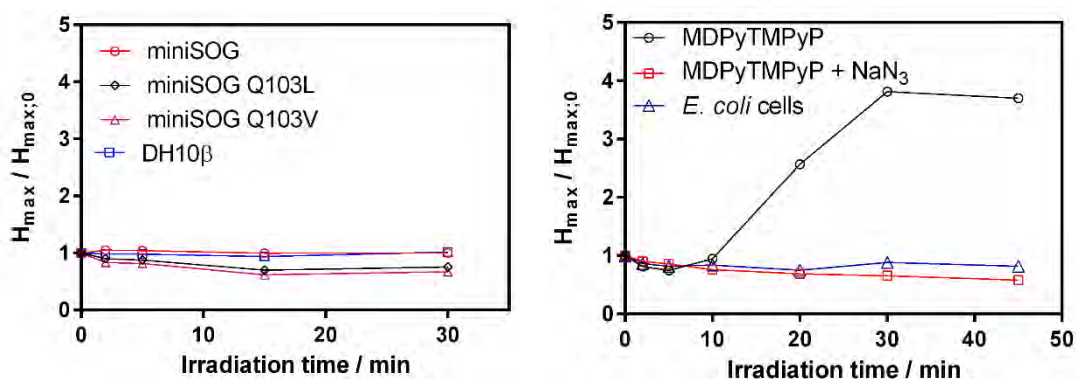
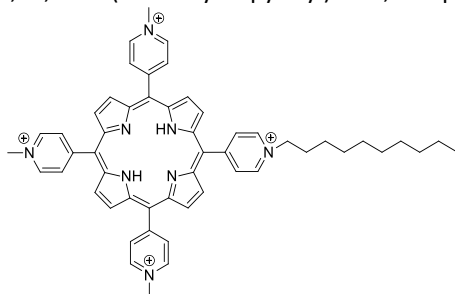


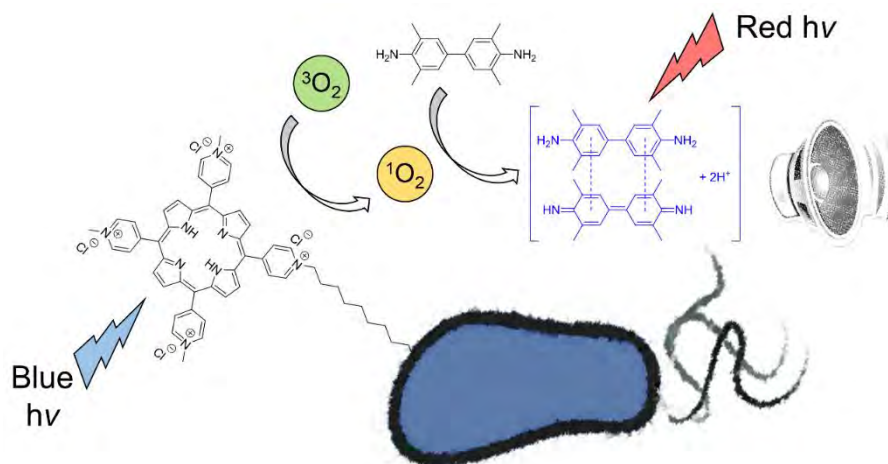
Figure 4.34 Photoacoustic maximum amplitude enhancement of TMB. Left: in untransformed DH10 β (blue squares) and miniSOG-expressing (red circles, black rhombuses and magenta triangles for miniSOG, miniSOG Q103L and miniSOG Q103V respectively) *E. coli* cells as a function of the irradiation time ($\lambda_{\text{irr}} = 459 \pm 10$ nm). Right: in presence (10 μM ; black circles) and absence (blue triangles) of MDPyTMPyP as a function of the irradiation time ($\lambda_{\text{irr}} = 420 \pm 20$ nm). Control experiment was realized coincubating MDPyTMPyP with 25 mM NaN₃ (red squares).

No significant TMB photoacoustic response differences are detected between the three genetically modified and the untransformed DH10 β *E. coli* cells. In this situation, TMB is not able to react with the generated ROS, indicating that TMB is far away from the PS. Therefore, under these conditions, TMB is not cell internalized and it should be localized in the outer part of bacterial cell-wall or free in the supernatant.

In a second approach, instead of using flavin-binding proteins as PS, will be used a tetracationic porphyrin with an unsaturated lipophilic tail, called MDPyTMPyP^{aa} (Scheme 4.13). The lipophilic tail would preclude MDPyTMPyP penetration into the cytosol of *E. coli* cells, so $^1\text{O}_2$ will be generated in the outer region of the cell wall.⁶⁷⁹

^{aa} 5-mono(N-decyl-4-pyridyl)-10,15,20-tri(N-methyl-4-pyridyl)-21H,23H-porphine tetrachloride.





Scheme 4.13 Experiment proposed for detecting $^1\text{O}_2$ generated in *E. coli* cell-wall.

A photoacoustic amplitude enhancement for TMB was recorded after co-incubation of TMB and MDPyTMPyP with *E. coli* cells followed by three washing steps and irradiated with blue light (Figure 4.34B). This enhancement is reversed when in the biological media there is 25 mM of NaN_3 or in absence of TMB. This observation clearly indicates that $^1\text{O}_2$ is generated nearby TMB, so it would be adsorbed also in the outer-cell wall. This is further confirmed because when the *E. coli* cells were separated by centrifugation, photoacoustic signal was observed in the re-suspended pellet but not in the supernatant.

Deeper TMB photoacoustic enhancement kinetics analysis, relates that only after some “lag” time the signal begins to enhance although some $^1\text{O}_2$ have been generated previously. This time is also observed when fluorescent probes are used in biological media and mainly are due to a competitive process between TMB and the endogenous antioxidants of *E. coli* for scavenging $^1\text{O}_2$. Initially, *E. coli* have a higher concentration of antioxidants than TMB, so $^1\text{O}_2$ will interact preferentially with them. After some time, local antioxidant concentration decreases and then TMB is able to compete to scavenge $^1\text{O}_2$ to generate TMB-Ox (and consequently the photoacoustic signal).

Moreover, TMB oxidation by H_2O_2 catalysed by Horseradish peroxidase is one of the most used reactions in ELISA analysis. Depending on the analysis conditions used, when the ELISA analysis is positive TMB is oxidized to TMB-Ox or TMB-Ox-Ox and its formation typically is detected by an absorption spectrum. Taking into account the results of this work, an alternative should be TMB-Ox/TMB-Ox-Ox detection by LIOAS, which is more sensible than conventional absorption spectroscopy.

Chapter V

A self-reporting nanophotosensitizer

*Ara mateix enfilo aquesta agulla
amb el fil d'un propòsit que no dic
i em poso a apedaçar. Cap dels prodigis
que anunciaven taumaturgs insignes
no s'ha complert, i els anys passen de pressa.
De res a poc, i sempre amb vent de cara,
quin llarg camí d'angoixa i de silencis.
I som on som; més val saber-ho i dir-ho
i assentar els peus en terra i proclamar-nos
hereus d'un temps de dubtes i renúncies
en què els sorolls ofeguen les paraules
i amb molts miralls mig estrafem la vida.
De res no ens val l'enyor o la complanta,
ni el toc de displicent malenconia
que ens posem per jersei o per corbata
quan sortim al carrer. Tenim a penes
el que tenim i prou: l'espai d'història
concreta que ens pertoca, i un minúscul
territori per viure-la. Posem-nos
dempeus altra vegada i que se senti
la veu de tots solemnement i clara.
Cridem qui som i que tothom ho escolti.
I en acabat, que cadascú es vesteixi
com bonament li plagui, i via fora!,
que tot està per fer i tot és possible*

Miquel Martí i Pol

5.1 $^1\text{O}_2$ dosimetry

(Adapted from: C. Hally, B. Rodríguez-Amigo, **R. Bresolí-Obach**, O. Planas, J. Nos, E. Boix-Garriga, R. Ruiz-González and S. Nonell; Chapter 4: Photodynamic Therapy; in *Theranostics and Image Guided Drug Delivery*, RSC Publishing, 2018.)

A real-time assessment of the amount of ROS generated during PDT is essential to remove the malignant entity, whilst minimising the harm done to healthy tissues.^{680–682} Explicit conventional dosimetry only takes into consideration the amount of light irradiated and the local concentration of PS and O_2 . This is a simple approximation to dosimetry, but in many cases is insufficient. Dosimetry can be greatly improved by taking advantage of the theranostic properties of the PS (Figure 5.1).⁶⁸³ For example, fluorescence can be used to obtain quality information on the amount of $^1\text{O}_2$ generated.

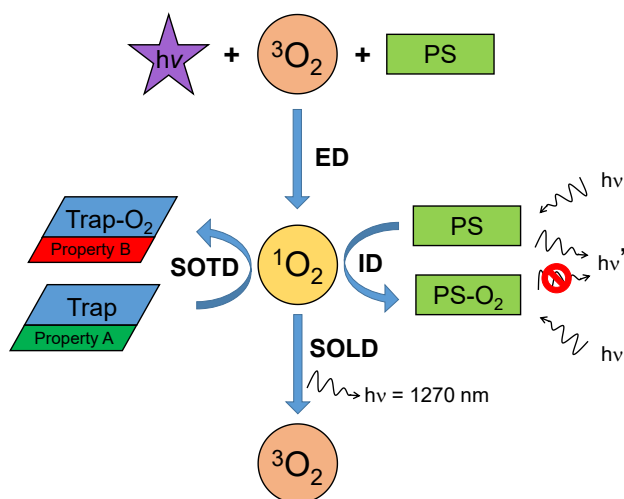


Figure 5.1 Scheme of the four types of PDT dosimetry. ED: Explicit dosimetry, where the concentration of O_2 , PS and the irradiated light are used to calculate the $^1\text{O}_2$ dose. ID: Implicit dosimetry, where the PS photobleaching is measured in order to calculate the $^1\text{O}_2$ dose. SOLD: Singlet oxygen luminescence dosimetry, where the $^1\text{O}_2$ dose is calculated directly from $^1\text{O}_2$ phosphorescence at 1270 nm. SOTD: Singlet oxygen trapping dosimetry where the $^1\text{O}_2$ dose is calculated from the evolution of a $^1\text{O}_2$ trapping moiety.

Implicit dosimetry (ID) monitors PDT by measuring the extent of photodegradation of the PS or the formation of photo-byproducts. Fluorescence is usually the property chosen to assess dosimetry. Implicit methods deliver combined information on the three parameters which affect PDT. Then, PS photobleaching has been correlated by means of biophysical methods with the amount of $^1\text{O}_2$ generated.^{684,685} These models have enabled the definition of “PDT dose” as: the total cumulative $^1\text{O}_2$ produced during the treatment time.

Despite its promising applications, implicit dosimetry methods present some drawbacks: i) Cell and tissue autofluorescence can partially mask photobleaching fluorescence;⁶⁸⁶ ii) certain PSs and physiological conditions, such as hypoxia ($<5 \text{ O}_2 \mu\text{M}$), present negligible $^1\text{O}_2$ -mediated photobleaching, being non- $^1\text{O}_2$ -mediated photobleaching the dominant phenomenon. In these cases, implicit measurements no longer deliver a reliable dose metric;⁶⁸⁷ iii) formation of photo-byproducts with different photophysical properties which could hinder PDT efficiency.⁶⁸⁸

Singlet oxygen luminescence dosimetry (SOLD) can be used to directly monitor the extent and evolution of PDT, because $^1\text{O}_2$ phosphorescence intensity will be proportional

to the $^1\text{O}_2$ generated.⁶⁸⁹ SOLD only began to be a feasible option in $^1\text{O}_2$ quantification 15 years ago due to the difficulty in measuring its emission in biologic media. Hirano *et al.* reported the detection of $^1\text{O}_2$ phosphorescence generated using Photofrin[®] from murine tumours cells suspended in non-deuterated.⁶⁹⁰ In the same year, Niedre *et al.* proved correlation between the integrated intensity of $^1\text{O}_2$ phosphorescence and leukaemia cell mortality (OCI-AML5) *in vitro*.^{691,692} They also demonstrated that the correlation is not affected by the dose of light nor the concentration of PS and $^3\text{O}_2$.⁶⁹²

ID and SOLD techniques are able to monitor and even predict cell viability in the majority of studied conditions. SOLD has had difficulties entering clinical studies due to its cost, technological complexity and low signal to noise ratio. On the other hand, ID presents a more practical, cheap and simpler monitoring system, which has enabled this methodology to already be used in clinical studies.

To circumvent the ID and SOLD limitations, an alternative would be the use of chemical compounds which selectively react with $^1\text{O}_2$ and also have a “*singular property*” which is measured. In singlet oxygen trapping dosimetry (SOTD), two major strategies have been pursued: the self-reporting PSs and the use of $^1\text{O}_2$ detection probes.

Self-reporting PSs are supramolecular entities with three embedded functionalities: a PS responsible for $^1\text{O}_2$ generation, a scissile linker that breaks when $^1\text{O}_2$ is formed, and a fluorophore ($^1\text{O}_2$ reporter) whose fluorescence is quenched by the PS. Once $^1\text{O}_2$ is generated, it cleaves the linker and releases the fluorophore, which then recovers its inherent fluorescence.^{693,694} Thus, fluorescence evolution is used to monitor $^1\text{O}_2$ production. A variation of this strategy is to use a reporter whose fluorescence increases upon reacting with $^1\text{O}_2$.⁶⁹⁵

Molecular probes are another option in order to detect intracellular $^1\text{O}_2$. A popular approach is to use $^1\text{O}_2$ chemiluminescent probes, such as fluoresceinyl cypridina luciferin analogues (FCLA).⁶⁹⁶ When FCLA probes react with $^1\text{O}_2$, an excited photoproduct is generated that decays emitting light. *In vitro* and *in vivo* PDT studies have reported good correlations between cell viability and cumulative chemiluminescence.^{696–698} Likewise, $^1\text{O}_2$ fluorescent probes are based on the fluorescent change of the probe after reacting with $^1\text{O}_2$ as explained at section 1.2.

5.2 Aim of the study

In one hand, nanotechnology has become a promising path in order to protect the probe against protein complexation and facilitate cellular internalisation (Chapter 4.2). In the other hand, we have been able to synthesize MSNP with RB attached covalently and this system is capable to produce $^1\text{O}_2$ efficiently (Chapter 3.4.4).

What would be the behaviour of a nanosystem containing simultaneously a $^1\text{O}_2$ fluorescent probe (ADPA) and a PS (RB)?

We expect that under green irradiation RB would be capable to photosensitize $^1\text{O}_2$. Then, a fraction of this $^1\text{O}_2$ generated will react with ADPA, allowing to follow its generation by SOTD. The other fraction will escape from the nanoparticle scaffold and it will be able to induce photodamage to bacterial and/or mammalian cells. As prove of concept, this nanoprobe (so called ADPA-MSNP-RB) has been used for *S. aureus* photoinactivation in which a correlation was observed between fluorescent change of ADPA and bacterial cellular death.

5.3. Experimental section

5.3.1. Synthesis of ADPA-MSNP-RB

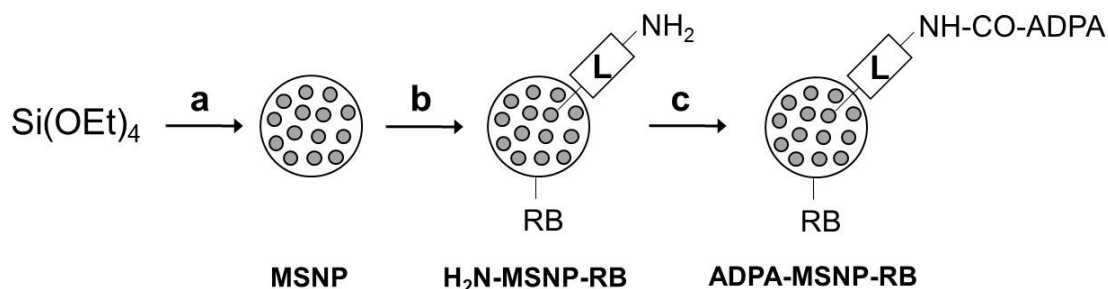
MSNP, $(\text{OEt})_3\text{-Si-L-NH}_2$ and $(\text{OEt})_3\text{-Si-RB}$ have been synthesized as described in the previous sections.

200 mg of $(\text{OEt})_3\text{-Si-L-NH}_2$ (430 μmol) and 1 mL of the $(\text{OEt})_3\text{-Si-RB}$ solution (53 μmol) were added to 12 mL of MSNP ethanolic solution (33 mg/mL). The solution was left stirring at room temperature during 24 hours. Afterwards, the NPs were recovered by centrifugation (15000g x 20 min). The $\text{H}_2\text{N-L-MSNP-RB}$ were washed twice with EtOH, once with CH_3CN and they were stored suspended in CH_3CN (10 mg/mL).

14.7 mg (77 μmol) of EDC, 14.5 mg (126 μmol) of NHS and 4.0 mg (11 μmol) of ADPA were dissolved in 2 mL of dry CH_2Cl_2 . The mixture was left under stirring at room temperature for 2 h. The activated ADPA mixture was added dropwise to a stirred solution of $\text{H}_2\text{N-L-MSNP-RB}$ in acetonitrile (30 mL; 10 mg/mL). The reaction crude was kept reacting at room temperature for 72 h. Afterwards, the ADPA-MSNP-RB were isolated and washed through repeated centrifugations (20 min at 12000 rpm) in EtOH and they were stored suspended in EtOH (5 mg/mL).

5.4 Assessment of ADPA-MSNP-RB as a self-reporter nanophotosensitizer

For this prove of concept, it is developed a simple nanoconjugate in which ADPA is directly attached covalently by a long linker to the pre-formed SNPs and RB also is directly attached as depicted in Scheme 5.1.



Scheme 5.1 Synthesis of ADPA-MSNP-RB. Reagents and conditions: a): CTAC, EtOH, H₂O, NH₃, 80 °C, 12 min, then HCl (37%), reflux, 24 h. b): (OEt)₃-Si-L-NH₂, (OMe)₃-Si-RB, EtOH, rt, 24 h. c): ADPA, EDC, NHS, Na₂CO₃, CH₃CN:CH₂Cl₂, rt, 72 h.

ADPA-MSNP-RB was characterized by its size (173 ± 52 nm) in ethanol and ζ -potential (-20 ± 5 mV) in water. In presence of 100 mM AcOH, the external amines were protonated and the ζ -potential turned positive ($+11 \pm 4$ mV), which is ideal for its interaction with bacterial cells.

ADPA and RB concentration was quantified for ADPA-MSNP-RB by absorption spectroscopy (Figure 5.2A). The MSNP loading is 0.114 and 0.099 μmol per mg of silica for ADPA and RB respectively. Moreover, ADPA and RB can be followed independently by fluorescence in function of the excitation wavelength (λ_{exc} 370 and 530 nm for ADPA and RB respectively).

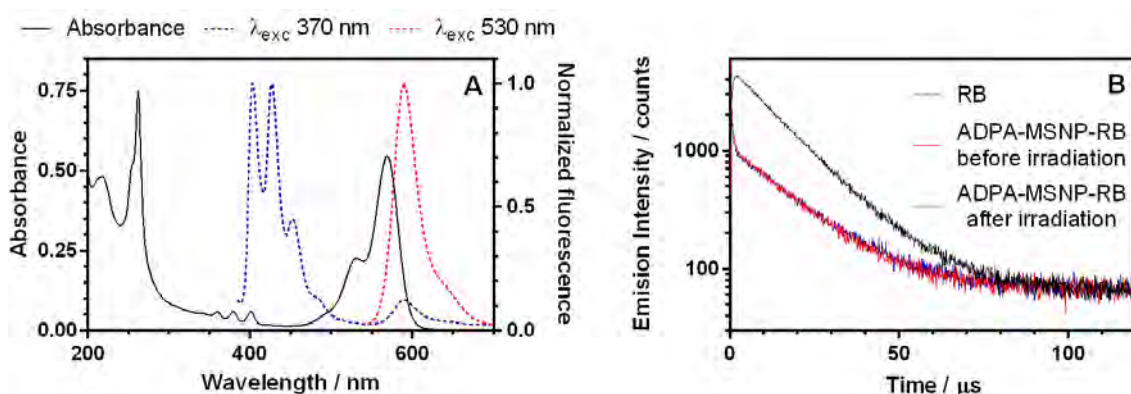


Figure 5.2 (A): Absorption (black line) and normalized fluorescence spectra of ADPA-MSNP-RB exciting at 370 nm and 530 nm, where mainly absorb ADPA and RB respectively (blue and red dashed lines respectively). (B): Time-resolved ¹O₂ phosphorescence of optically matched solutions of RB (black line) and ADPA-MSNP-RB before and after irradiation (red and blue lines respectively) at 532 nm in EtOH.

Pulsed-laser irradiation of ADPA and ADPA-MSNP-RB suspended in ethanol produced clear time-resolved ¹O₂ phosphorescence signals (Figure 5.2B). The ¹O₂ kinetics for all samples could be fitted with a biexponential rise-and-decay function. For RB, the time constants for rise and decay were 0.5 μs and 14.3 μs , respectively. The corresponding

values for ADPA-MSNP-RB were 0.6 μs and 16.6 μs and increased to 0.6 μs and 17.5 μs after irradiation with green light. The differences between τ_{Δ} before and after green irradiation is due to the $^1\text{O}_2$ quenching by ADPA, which is estimated as $\approx 5\%$.

For ADPA-MSNP-RB, Φ_{Δ} was determined by comparing the intensity of the $^1\text{O}_2$ phosphorescence decay sensitized by RB and ADPA-MSNP-RB. A value of 0.16 is obtained, which is roughly 5-fold smaller than free RB due to the oxygen shielding effect of the MSNP.

In order to further characterize ADPA-MSNP-RB, its response to $^1\text{O}_2$ was tested in two different solvents (Figure 5.3). $V_{\text{-ADPA}}$ was faster in EtOH than in PBS, which is consistent with the known variation of τ_{Δ} with the solvent,⁶⁹⁹ indicating that $^1\text{O}_2$ decay is controlled by solvent interactions.

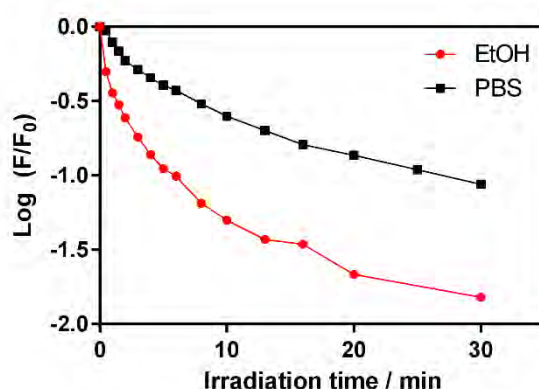


Figure 5.3 ADPA-MSNP-RB fluorescence bleaching (λ_{exc} 370 nm) upon $^1\text{O}_2$ generation by RB upon irradiation with green light (λ_{irr} 520 \pm 18 nm; 6.7 mW/cm²) in EtOH and PBS (red and black lines respectively).

Finally, it is assessed ADPA-MSNP-RB potential to photoinactivate *S. aureus* cells. Under that purpose, ADPA-MSNP-RB is co-incubated with *S. aureus* during 30 minutes and after successively irradiated with green light (λ_{irr} 520 \pm 18 nm; 6.7 mW/cm²). For each irradiation time, ADPA fluorescence bleaching and *S. aureus* survival rate is measured (Figure 5.4). It is observed a linear dependence between ADPA fluorescence bleaching and $\text{Log}_{10}(\textit{S. aureus}$ viability reduction). No dark toxicity is observed for ADPA-MSNP-RB for the experimental conditions tested.

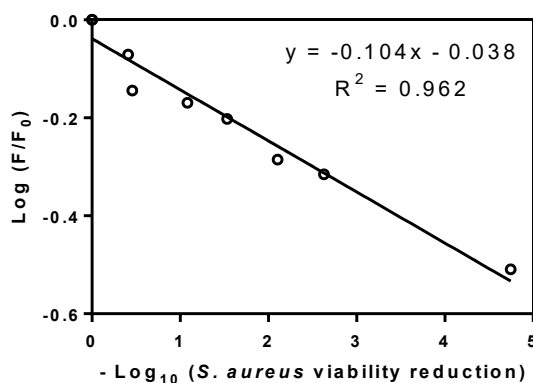


Figure 5.4 *S. aureus* survival response towards ADPA-MSNP-RB fluorescence bleaching (λ_{exc} = 370 nm), which should be related to the amount of $^1\text{O}_2$ generated.

Chapter VI

General discussion and outlook

*Hegoak ebaki banizkio
nerea izango zen,
ez zuen aldegingo
Bainan, honela
ez zen gehiago txoria izango
eta nik...
txoria nuen maite.*

Mikel Laboa

*Si li hagués tallat les ales
hauria estat meu,
no s'hauria escapat.
Però així,
hauria deixat de ser ocell.
I jo...
Jo el que estimava era l'ocell.*

Some months ago, the putative title of this PhD thesis was “**Life and miracles of singlet oxygen: A battle to improve its generation and its detection**”, however science does not believe in miracles, science tries to answer questions using whether the reason and empirical observations as proposed by Immanuel Kant. Moreover, “life and miracles” can be translated in catalan to “vida i miracles” which is an idiom typically used for explaining the most important life experiences of a person.

In this context, the results presented in the previous chapters deal with the generation and detection of $^1\text{O}_2$ (or other ROS). Specifically, we have tried to answer several questions related with $^1\text{O}_2$, specially related to its use in PDT.

Our first question was: Which is the effect of triphenylphosphonium cation as a targeting group in antimicrobial PDT? Under that purpose we studied the photophysical and photo-antimicrobials properties of two different triphenyl-phosphonium derivatized PS. These derivatives have photo-antimicrobial effect against Gram-positive bacteria while they do not kill Gram-negative bacteria. Control experiments with the same PS skeleton but neutral or anionic do not present any photoantimicrobial effect. Similar nitrogen-based cationic PS present photo-antimicrobial properties against Gram-positive and negative bacteria.^{265–267}

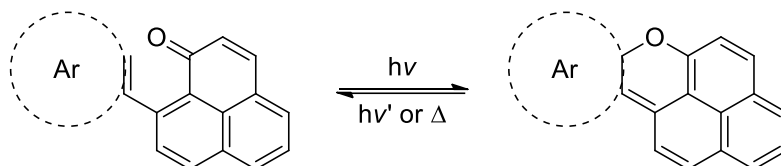
It is known that the double lipid bilayer of Gram-negative bacteria has a low degree of permeability for lipophilic molecules.⁷⁰⁰ The three phenyl groups partially shield the positive charge, then increasing their lipophilic character.²⁴⁸ So, when the triphenylphosphonium derivatives PS cannot pass through the polysaccharide barrier, whose environment is highly hydrophilic (consistent with the $^1\text{O}_2$ kinetics decays), resulting in no killing effect. This is in concordance with the anti-microbial activity of other triphenyl-phosphonium antimicrobial derivatives such as phenothiazines or indolylalkyl.^{259,260}

Nature has always been a source of inspiration for several academic disciplines, from arts to mathematics. In pharmacy, several natural-occurring compounds have been used as drugs.⁷⁰¹ Among them, we are interested in phenalenones which phototoxicity was already reported in Charles Darwin “On the Origin of Species”. Unsubstituted PN is an excellent $^1\text{O}_2$ PS (Φ_Δ around 1 in several solvents from cyclohexane to water).^{262,306,307} Surprisingly, for 9-substituted PNs the Φ_Δ drops more than one order of magnitude.³³⁰ The proposed explanation to this experimental fact is that excited states of 9-phenyl phenalenones can undergo thorough a $6-\pi$ electrocyclic intramolecular photocyclisation, so-called β -phenyl quenching. This photocyclisation generates a 6aH-naphtho[2,1,8-mna]xanthene which lives few microseconds reverting to the original 9-phenylphenalenone.^{309,348}

The obtained data shows that BPQ is not restricted to triplet ketones but applies to their singlet excited states as well, effectively competing with intersystem crossing and therefore with $^1\text{O}_2$ production.³³² Moreover, the observation of preferential ortho-attack in 9-phenylphenalenones is partially due to the rigidity of the PN skeleton. Also of importance is probably a stereoelectronic effect: the two π -systems, PN and phenyl, are orthogonal ($\psi = 180^\circ$) in the transition state of ipso-BPQ of PN1, whereas the corresponding dihedral is $\psi = 120^\circ$ in ortho-BPQ. X-Ray data have revealed that the

actual dihedral angle is $\psi = 180^\circ$ ⁷⁰² thus ortho attacks appear more likely. Thus, phenalenone offers a unique scaffold for the control of the BPQ reactivity.

Moreover, the BPQ reactivity observed for 9-phenylphenalenones can be expanded for 9-substituted aryl PNs (Scheme 6.1). In function of the electronic density of the aryl moiety the lifetime of naphthoxanthene generated is modulated. The stability of the naphthoxanthene is reduced up to picosecond range when the phenyl group is substituted by a pyridinium cation. In counter position, its stability is increased up to microsecond range when the phenyl group is substituted by a furyl or thienyl group. However, this substitution strongly reduces their photostability.

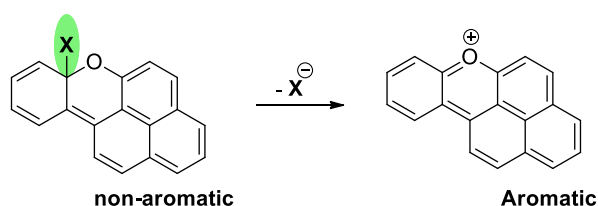


Scheme 6.1 β -phenyl quenching reaction for 9-arylphenalenones.

The wide range on the lifetimes of the different substituted naphthoxanthenes opens the door for its use as photochromic compounds.⁷⁰³ Ultrafast photochromic compounds nowadays are extremely useful compounds due to their applications in data transmission.³⁷⁸ Moreover, the decyclization of naphthoxanthene can also be a photochemical reaction. While “slow” photochromic compounds are now widely used, for example in photopharmacology they are used for activating prodrugs with light.^{704,705}

Comparing naphthoxanthenes with other photochromic compounds, a chemical similarity can be observed with chromenes compounds.^{372,385–387} As exposed in section 3.3.4., we propose that 9-aryl-phenalenones can be considered as inverse chromene compounds. For chromenes the thermodynamic stable isomer is the cyclic compound, whilst for 9-aryl-phenalenones the stable one is the non-cyclic compound. Considering that phenyl substitution for smaller and electronic rich heteroaryl groups (i.e. furyl or thienyl) increases the stability of naphthoxanthene, we further propose for 9-vinyl-phenalenone the cyclic and non-cyclic isomer should have similar stability.

On the other hand, aromaticity in the naphthoxanthene is disrupted by a $C(sp^3)$ atom (Scheme 6.2). The $C(sp^3)$ -H bond in the different naphthoxanthenes is extremely weak, as example the bond dissociation energy (BDE) for PN1 is predicted to be only 28.8 kcal/mol.³⁰⁹ It is significantly weaker than the corresponding C-H BDE of phenalene itself, which has been determined to be 64 kcal/mol and to our best knowledge the weakest C-H bond.⁷⁰⁶ Typical BDE values for $C(sp^3)$ -H bonds are around 100 kcal/mol.⁷⁰⁷

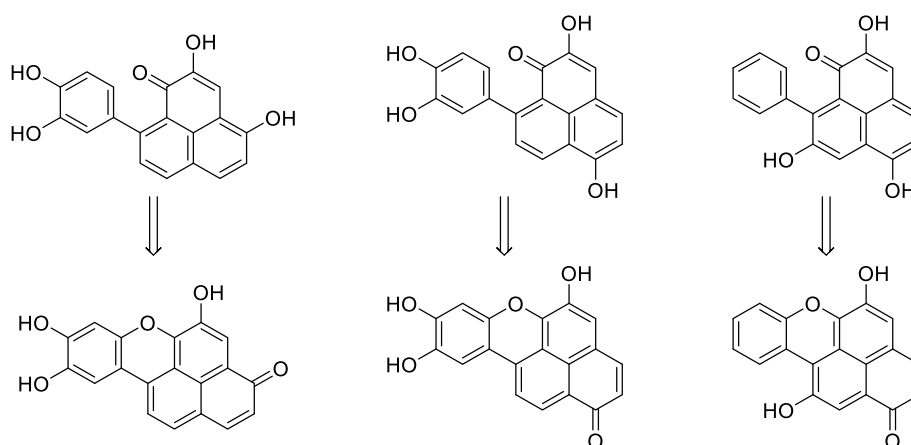


Scheme 6.2 Structure of the naphthoxanthene generated with the $C(sp^3)$ -X bond highlighted.

The driving force for this reaction is the recovery of aromaticity after hydrogen and/or hydride abstraction. This driving force also could be used for photouncaging purposes.

For that and as proof of concept, we studied the photoreleasing properties of 9-(o-nitrophenyl)-phenalenone. Under blue light irradiation, PN-NO₂ releases NO₂ or NO₂⁻ in apolar or polar media respectively via homolytic or heterolytic C-NO₂ rupture of the naphthoxanthene. This photouncaging properties probably can be expanded to other good leaving groups.

It is interesting to note that cyclisation products closely related to those described in this thesis have been isolated from plants (Scheme 6.3). Indeed, the synthesis of natural naphthoxanthenones (flurones) from 9-phenylphenalenones, recently proposed to occur by a radical-initiated reaction,^{708,709} could also stem from an excited-state cyclisation reaction as described in this report, which suggests a light-mediated metabolic pathway.^{305,314,320} Unravelling the metabolic pathways of phenylphenalenones upon fungal infection of banana plants has recently become of special interest for enhancing their disease resistance to pathogen infection due to the worldwide drop in crops.⁷¹⁰



Scheme 6.3 Possible excited-state pathways for the production of fluorone pigments in plants.

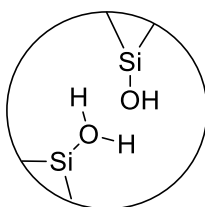
In addition, the PN skeleton, due to its excellent photosensitizing properties, can be further derivatized as a ¹O₂ label. Like other labels, 6-isothiocyanate-phenalenone can be used for its conjugation to several biomolecules (i.e. antibodies or antimicrobial peptides)^{427,711} resulting to the thiourea derivative, which red-shift its absorbance spectrum without a spectacular Φ_{Δ} decrease.^{431,712} The drawback is the poor thermal stability of the generated thiourea, which evolves to several products within few days. This lack of stability difficults its use for targeted-PDT.

As opposed to PN which is mainly a pure type II PS^{bb},^{262,306,307} other naturally-occurring PS can proceed either type I and/or II (i.e. anthraquinones).⁴⁴³ Under that purpose we studied which is the main phototoxic specie for Rubiadin and its methylated derivative. It is known that different aromatic ketones as anthraquinones can produce ¹O₂ or O₂^{-•} (via electron transfer from precursor AQ^{-•}).⁷¹³ Indeed, we were capable to detect either the ¹O₂ phosphorescence and the precursor AQ^{-•} by transient absorption. Additional experiments with selective ¹O₂ (NaN₃) or O₂^{-•} / •OH (Tiron) quenchers allow to proclaim that O₂^{-•} is the main responsible for the phototoxicity of AQs in *C. tropicalis* biofilms.

^{bb} PN in some conditions it can accept one electron from tryptophan generating PN radical anion. PN^{-•} can transfer this electron to ³O₂ for generate O₂^{-•} via type I photosensitization.⁷⁵⁵

Other alternatives for improving the PDT treatments are the use of NPs as drug delivery systems.⁶¹⁸ We synthesized two different nanosystems in order to study them. In the first case, MB is adsorbed onto the surface of MSNP,⁴⁶⁹ which is further derivatized with amines or mannose. In the second case, RB is covalently attached onto the MSNP surface.

MSNP hampers $^3\text{O}_2$ diffusion thorough the NP, which lengthens MB τ_T . For covalently attached-PS, the lengthening of τ_T is smaller because the PS is in the external layer of the NP and $^3\text{O}_2$ is more accessible.⁷¹⁴ This also happens with other NPs-PS combinations such as nanoADPA.⁶¹³ On the other hand, when $^1\text{O}_2$ is generated inside the NP, it can be quenched by the silanols groups present in the MSNP surface or pores (Scheme 6.4).^{503,504}



Scheme 6.4 Possible $^1\text{O}_2$ quenchers in bare MSNP.

These nanosystems present lower photo-antimicrobial efficacy than the PS free in solution due to their lower $^1\text{O}_2$ generation capacity. However, these nanosystems could incorporate targeting moieties more easily than their molecular counterparts, which should increase the photokilling properties of $^1\text{O}_2$ generated.^{715,716}

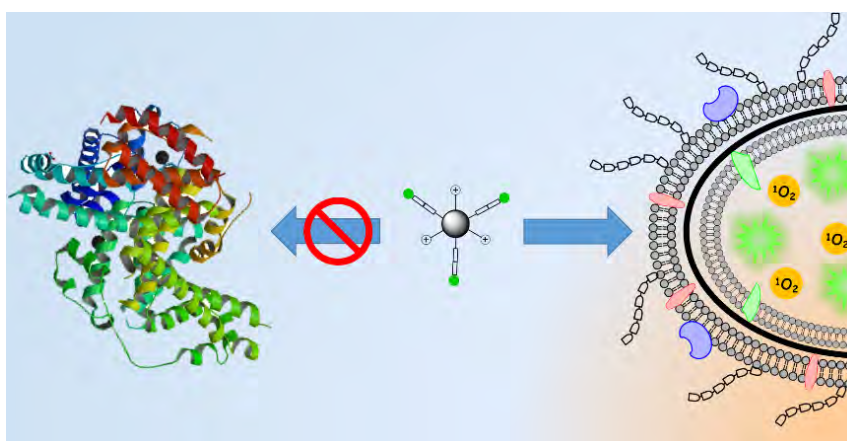
Finally, some drugs can absorb light and like dyes they can produce ROS with different efficiency.⁷¹⁷ Among them, the vast majority of drugs only have chromophores capable to absorb UV light (i.e. Camptothecin⁷¹⁸ or Fenofibric acid⁷¹⁹). Only few of them, like doxorubicin, can absorb visible light. For that we decided to study the photosensitizing properties of Doxo free in solution as well as complexed with DNA.

We observed that complexation of Doxo with DNA increases the non-radiative rate constants, whilst it reduces its capacity to fluorescence and produce $^1\text{O}_2$. Moreover, the presence of DNA difficult the $^3\text{O}_2$ diffusion nearby Doxo, lengthening its τ_T . HeLa cells incubated with 0.2 μM and 0.4 μM DOXO and irradiated with green light did not show any increased toxicity compared to the non-irradiated samples.⁷²⁰

It was hypothesized that the combined use of drugs with different cellular localizations could increase their cytotoxic capacity and could hence be a valuable strategy to reduce their concentrations and thus their side effects.⁷²¹ The combination of PhA with Doxo seemed suitable, as damage would occur in the lysosomal compartment and the nucleus, respectively. In this sense, in vitro combinations of Doxo with different PSs and cell lines have already been explored aiming at enhancing the final cell-killing effect.^{519,722–725} Moreover, combination implies sequencing of the active agents, and thus, the order is a significant factor. Indeed, it has been reported that synergic interaction between PDT and chemotherapy is dependent not only on the nature of the PS and the chemotherapeutical agent, as well as on the irradiance dose, but also on the treatment sequence. Using 0.2 μM of Doxo, we found that PhA-Doxo was now borderline between interference and antagonistic; Doxo-PhA was additive; and PhA+Doxo was synergic.

Regarding to reactive oxygen species detection, we have studied the use of chemical trapping for detecting them, in counter position to direct detection which is not so sensitive and requires specialized equipment. In a first step, we have nanovehiculized different $^1\text{O}_2$ fluorescent probes to overcome some problems of their molecular counterpart. Under that purpose we have nanoparticulated three different $^1\text{O}_2$ fluorescent probes: one turn-off (ADPA),⁶¹³ one turn-on (SOSG)⁶¹² and one fluorogenic (NOX).

In a first approach and in collaboration with the University of Hull, we have designed the nanoparticulated version of SOSG (the so-called nanoSOSG; Scheme 6.5). We chose SOSG because nowadays is the most used commercial $^1\text{O}_2$ fluorescent probe.^{95,104,105} We synthesized different polyacrylamide NPs and further functionalized with different linkers where SOSG was covalent attached via Steglich amidation. In a second step we synthesized different types of silica nanoparticles (compact and mesoporous) functionalized with a short or long linker where ADPA is attached via Steglich amidation.



Scheme 6.5 When bound to NPs (gray sphere), the cell-impermeable fluorescent probe SOSG (green circles) escapes protein sequestration, readily undergoes cell uptake, and efficiently reports on intracellular variations in intracellular singlet oxygen levels.

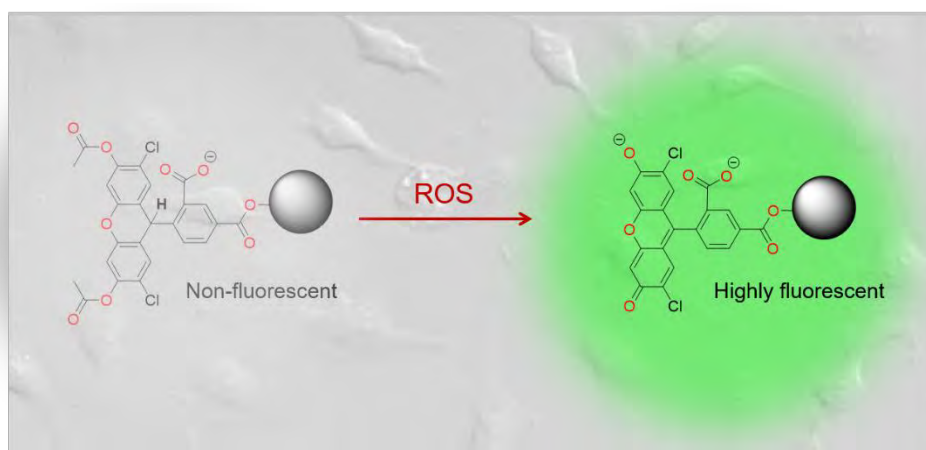
The length of the linkers⁷²⁶ had a critical role in SOSG reactivity towards $^1\text{O}_2$. A short linker places SOSG nearby NP surface hampering its reaction with $^1\text{O}_2$. The reactivity of all nanoparticulated forms towards $^1\text{O}_2$ is smaller than the free-molecular form. Similar reactivity results were obtained for the nanoparticulated version of ADPA (the so-called nanoADPA). In the case for nanoADPA, MSNP scaffold enhances ADPA endoperoxidation compared to the CSNP counterpart because MSNP have a higher surface which should enhance ADPA loading per NP. This higher ADPA concentration per NP should favor its macroscopic reactivity towards $^1\text{O}_2$.

It is known that both SOSG and ADPA interacts with different proteins such as bovine serum albumin (BSA).¹⁰⁵ These interactions with proteins can produce false positives or negatives as well as difficult their cell internalization. The nanoparticulate version of these probes do not present any significant interaction with BSA, because the NP scaffold is at least one order of magnitude bigger than proteins and itself produces notable steric hindrance hampering the interaction of the probe with the protein.⁷²⁷

This lack of interaction allows to overcome some specific drawbacks of their molecular counterparts: i) SOSG is defined by the manufacturer as cell-impermeant⁵⁵⁶ and only can be uptaken by cells in a protein free medium.¹⁰⁵ We prove that SOSG is not internalized by *E. coli* cells even in protein free media, whilst nanoSOSG is internalized under these

conditions. Moreover, we were able to detect $^1\text{O}_2$ generated inside such *E. coli* cells by the genetically-encoded flavin-binding protein miniSOG. ii) When ADPA is used as $^1\text{O}_2$ fluorescent probe for measuring the Φ_Δ of miniSOG,²⁹ a fifteen-fold higher Φ_Δ value ($\Phi_\Delta = 0.47$) was obtained than the correct one ($\Phi_\Delta = 0.03$; measured by $^1\text{O}_2$ phosphorescence as well as using acid uric as $^1\text{O}_2$ trap).⁷²⁸ The correct Φ_Δ value was obtained when nanoADPA was used. iii) nanoADPA is readily internalized by HeLa cancer cells, non-cytotoxic up to 4 μM and is able to efficiently detect intracellular generated $^1\text{O}_2$.

Once $^1\text{O}_2$ behavior against nanoprobe is well assessed, we expanded the nanoprobe concept to other ROS (Scheme 6.6). As a proof of concept, a “nano” version of the widely-used generic ROS probe DCFH-DA⁶²⁰ has been prepared and its reactivity against a variety of ROS has been assessed and compared to that of its molecular counterpart. The first remarkable result is that nanoDCFH-DA is more resistant against $^3\text{O}_2$ oxidation, which is advantageous for its use in biological systems as the likelihood of false positives is strongly diminished. The same results are observed for neutral ROS such as $^1\text{O}_2$ and $\cdot\text{OH}$, while anionic ROS such as ClO^- and $\text{O}_2^{\cdot-}$ show higher reactivity against nanoDCFH-DA than against its molecular counterpart.



Scheme 6.6 Expansion of the concept from $^1\text{O}_2$ fluorescent nanoprobe to non-specific ROS fluorescent nanoprobe using DCFH-DA as fluorescent ROS probe.

These observations are consistent with the surface properties of the nanoprobe. Thus, the water layer adsorbed onto the surface of the nanoparticles is highly structured owing to the presence of silanols,⁴⁵⁷ making it difficult to diffuse through it. On the other hand, the presence of cationic ammonium groups on the surface at pH 7.4 favors electrostatic attraction of anionic ROS, whereas repulsion dominates in the negatively-charged molecular probe. The last column in Table 4.5 shows that the combination of reactivity and resistance to $^3\text{O}_2$ oxidation makes nanoDCFH-DA better fluorescent probe than molecular DCFH-DA. In addition, nanoDCFH-DA is also 10-fold more resistant to self-sensitized photooxidation. Finally, a further advantage is its lower affinity for proteins, as binding results in severe quenching of the fluorescence.

The case of H_2O_2 is special in that exposure to this ROS cleaves the amide bond between probe and nanoparticle,⁷²⁹ releasing it into the external medium. Indeed, the rate constants observed for the nano- and molecular probe are undistinguishable. Fortunately, the very low H_2O_2 physiological concentrations found in cells⁷³⁰ make this

process very slow. The performance of the probe in cells has been tested using HeLa cancer cells. Microscopy imaging shows that the probe is readily internalized by the cells and accumulates in the cytoplasm, where it reacts with ROS generated by irradiation of hypericin increasing its fluorescence. Contrast values up to 10-fold have been observed.

All the previous used probes use changes in fluorescence to detect the respective ROS.⁶⁰⁵ However, it can be monitored other properties to follow ROS. Recently, optoacoustic techniques has become a trending topic due to the capacity of sound to pass through the tissues.⁷³¹ Under that purpose, it has been assessed the properties of tetramethylbenzidine (TMB) as optoacoustic probe against different ROS.⁶⁷³

TMB is a non-colored compound which can be oxidized by some ROS to a blue-colored charge transfer complex (TMB-Ox). TMB-Ox is non-fluorescent and almost releases all the absorbed light energy as heat ($\alpha = 0.95$) in a fast time scale, which makes it an excellent photoacoustic sensor.^{cc} With an excess of oxidant TMB-Ox can be further oxidized to yellow-colored diimine derivative.

TMB reactivity towards ROS/RNS presents three different casuistic (Scheme 6.7): i) ROS/RNS react with TMB for obtaining TMB-Ox (ClO^- , H_2O_2 , $^1\text{O}_2$ and NO_2); ii) ROS/RNS react with TMB, but it is obtained uncoloured-compounds ($\text{O}_2^{\bullet-}$, Na_2O_2 , NO , ONOO^-) or iii) ROS/RNS do not react with TMB ($\bullet\text{OH}$, TEMPO, NaNO_2). The pair TMB/TMB-Ox and TMB/TMB-Ox-Ox have a reduction potential of +0.553 and +0.665 V respectively ($[\text{TMB}] = 0.3 \text{ mM}$, $\text{pH} = 5$).⁷³² So, TMB oxidation should be thermodynamically favourable for the tested ROS/RNS, however above presented results seems indicate that TMB oxidation by some ROS/RNS (i.e. $\bullet\text{OH}$) should be hampered by low kinetics rate. In the other hand, other ROS/RNS reacts with TMB, but they not change significantly its absorption spectrum.

	A	B	C
$^1\text{O}_2$	X		
ClO^-	X		
H_2O_2	X		
$\bullet\text{OH}$		X	
$\text{O}_2^{\bullet-}$			X
TEMPO		X	
NO_2	X		
NO			X
ONOO^-			X
Na_2O_2			X

Scheme 6.7 Reactivity of TMB towards different ROS/RNS.

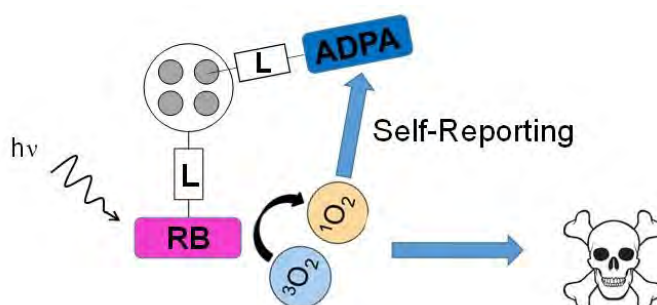
^{cc} A good turn-on fluorescence probe should have a high Φ_F value in the presence of the analyte, whilst in absence should be “ideally” non-fluorescent. For a good turn-on optoacoustic probe, instead of releasing the absorbed energy as light it should be release as heat. So, a good fluorophore will never be a good sonochrome and vice versa. For a fluorescent probe is interesting a high k_F , whilst for an optoacoustic probe is interesting a high k_{IC} .

Under the experimental conditions used, TMB is not internalized by *E. coli* because it does not react with the ROS produced by genetically-encoded flavin-binding proteins (miniSOG and its derivatives Q103L and Q103V)⁷³³. A feasible explanation could be because TMB's amines will be protonated in physiological pH and then it is adsorbed by the negatively charged bacterial surface.

Then for proving the ability of TMB to react with $^1\text{O}_2$ in a biological environment, we change the strategy and we incubated *E. coli* cells with a cationic but lipophilic porphyrin (MDPyTMPyP) for attaching it on the bacterial surface.⁶⁷⁹ Under these conditions TMB is able to react with the $^1\text{O}_2$ generated by the bacteria observing 4-fold optoacoustic signal enhancement. In that experiment is not observed a linear enhancement of TMB-ox photoacoustic signal. In the first 10 minutes of irradiation, only a slight increase is observed, whilst afterwards a much-marked enhancement is detected. For the first irradiation times, bacterial surface has a high concentration of biomolecules capable to physical quench or react with the generated $^1\text{O}_2$.⁷³⁴ They efficiently compete with TMB to react with $^1\text{O}_2$. With longer irradiation times, they get depleted and the competition with TMB is not there anymore.

TMB probably will not be the most useful optoacoustic probe for ROS/RNS detection, however, as a proof of concept is useful to prove that new generation of optoacoustic probes can be used to monitor ROS, and specially $^1\text{O}_2$. They offer an alternative to widely used fluorescent probes, especially for deeply tissues where light cannot reach and escape easily, whilst sound does.⁷³⁵

Finally, but not least important and as the last proof of concept, we designed and synthesized a self-reporter nanophotosensitizer combining what we have learnt from sections 3.4.4. and 4.2.3. (Scheme 6.8). RB (as PS) and ADPA (as $^1\text{O}_2$ fluorescent probe) are covalently attached to the same MSNP. The vast majority of the $^1\text{O}_2$ generated can escape from the NP whilst a small fraction (5%) reacts with ADPA which can be used to estimate the amount of $^1\text{O}_2$ produced by SOTD. This nanostructure has been used to correlate the amount of $^1\text{O}_2$ generation with the *S. aureus* photoinactivation properties.



Scheme 6.8 Self-reporter nanophotosensitizer.

So, this “nano” self-reporting PS has thus proven useful to extend the utility of an existing $^1\text{O}_2$ fluorescent probe and a widely-used PS to theragnostic, which is based on the combination of a diagnose imaging agent with a therapeutic drug on the same multifunctional platform.^{418,736} Therefore, ADPA-MSNP-RB is ideally suited for theragnostic purposes, since following the ADPA fluorescence bleaching can give rise

to SOTD and could aid surgical resections as well as monitoring of the treatment response.

More than 85 years latter of the $^1\text{O}_2$ discovery by Kautsky and Bruijn, several questions about $^1\text{O}_2$ remains unclear.⁵¹ Initially, the physical and chemical properties of $^1\text{O}_2$ in homogenous mediums were unknown and nowadays they are well established: first in “long-lived” $^1\text{O}_2$ solvents (i.e. CCl_4 or CS_2), afterwards in C-H solvents (i.e. C_6H_6 , CH_3CN or CH_3OH) and finally in water (H_2O).⁷³⁷

In the last years, understanding $^1\text{O}_2$ in heterogenous media (specially in live biological environments) has become a trending topic in this community. As example, until approximately 2-3 years ago it was widely established that τ_{Δ} inside a cell was <100 ns, so $^1\text{O}_2$ diffusion thorough the cell was unlikely, but more recent studies probe that this statement is no longer true and $^1\text{O}_2$ can diffuse thorough a cell.⁷³⁸ Like this there will be other examples in the next few years and the next generation of photochemists/photobiologists will be able to answer such questions and improving the actual $^1\text{O}_2$ paradigm.

Chapter VII

General conclusions

I, a vegades, ens en sortim
I, a vegades, ens en sortim
I, a vegades, una tonteria de sobte ens indica que ens en sortim
I, a vegades, una carambola de sobte ens demostra que ens en sortim

I, a vegades, ens en sortim
I, a vegades, ens en sortim
I, a vegades, una tonteria de sobte ens indica que ens en sortim
I, a vegades, se'ns baixa la verge i de sobte ens revela que ens en sortim
I, a vegades, contra tot pronòstic una gran bestiesa capgira allò que creiem lògic,
Tot fent evident,
Que per un moment,
Ens en sortim.

Manel

The following conclusions have been arrived at, as a result of the presented thesis:

- From studies on two different triphenylphosphonium photosensitizers, namely a new cationic phenalenone and a new perylene derivative, with opposite photophysical profiles, it has been concluded that cationic triphenylphosphonium photosensitisers should be considered as photoantimicrobials in situations where selective killing of Gram-positive bacteria in the presence of Gram-negative species could be of therapeutic value.
- Excitation of 9-phenylphenalenones results in the formation of highly reactive naphthoxanthenes by β -phenyl quenching via addition to the ortho position of the 9-phenyl substituent. Naphthoxanthene is highly reactive, undergoing facile electrocyclic ring opening to revert to original 9-phenylphenalenone in the ground state. It is also an exceedingly potent hydrogen donor, reacting with TCNE to yield the highly-stable naphthoxanthenyl free radical and/or the highly-coloured naphthoxanthenium cation. The scope of the BPQ reaction for 9-phenylphenalenones has been extended to other 9-heteroaryl-phenalenones varying the naphthoxanthene lifetime from picoseconds to milliseconds, which suggest a potential use as photoswitches. Moreover 9-phenylphenalenone can be used as photouncaging scaffold due to the low stability of the naphthoxanthene generated.
- The photoantimicrobial properties of the assayed natural AQs, Rubiadin and Rubiadin-1-methyl ether, was mediated mainly by $O_2^{\bullet-}$ generation after exposure to light (Type-I photodynamic mechanism) for *C. tropicalis* biofilms. Production of 1O_2 was observed in biofilm incubated with deuterated PBS, however its participation in the photo-induced biofilm reduction seems negligible.
- Methylene Blue adsorbed on amino- or mannose-functionalized mesoporous silica nanoparticles is capable of efficiently inactivating *E. coli* and *P. aeruginosa* bacteria upon exposure to red light. The photodynamic activity is similar to that of free MB but, in the case of *E. coli*, the dark toxicity is improved. In the case of *P. aeruginosa*, mannose is a better targeting agent than free amino groups on the surface of the nanoparticle. Time-resolved spectroscopic studies reveal the existence of two different populations of MB in the nanoparticles, the major one being adsorbed on the mesopores' walls and the minor on the external surface of the nanoparticle. Strong quenching of 1O_2 in the pores of the nanoparticle is observed. Similar results have been observed for the other nanosystem studied: Rose Bengal covalently bonded to MSNP.
- Photophysical studies of the compounds alone and in combination have revealed that doxorubicin quenches the excited states of Pheophorbide a, detracting from its photosensitizing ability. On the other hand, while doxorubicin can itself photosensitize the production of 1O_2 , this is largely suppressed by aggregation and by binding to DNA. The order of drug and light delivery plays a crucial role in the final outcome of the treatments, ranging from antagonistic to synergic for the same concentrations. Thus, while combined photodynamic and chemotherapeutic treatments show strong potential to decrease the dose of the

toxic chemotherapeutic agent and therefore its side effects, the delivery protocols must be very finely tuned to achieve this desired outcome.

- An activatable photosensitizer (composed by a brominated bodipy dye and a chromanol) shows a sigmoidal fluorescence enhancement upon exposure to light in HeLa cells and can efficiently kill such cancer cells at submicromolar concentration (100 nM). The results of these studies pave the way to enhance the selectivity of photodynamic treatments by the use of autocatalytic photosensitization processes.
- A number of nanoprobe for $^1\text{O}_2$ detection in biological systems have been developed, namely a polyacrylamide-based biocompatible fluorescent nanoprobe (nanoSOSG), the mesoporous silica-bound Anthracene DiPropionic Acid (nanoADPA) and dichloro-dihydro-fluorescein diacetate (nanoDCFH-DA). The reactivity against $^1\text{O}_2$ has been optimized by choosing appropriate linkers, a protective effect against protein interactions has been demonstrated, internalization by HeLa cancer cells has been observed and intracellular singlet oxygen and other ROS sensing has been demonstrated as well. Higher resistance to oxidation by air and to self-sensitized photooxidation, as well as lower affinity for interaction with proteins, make these nanoprobe safer and more reliable fluorescence markers for ROS in cells. This “nano” approach has thus proven useful to extend the utility of existing and valuable fluorescent probe to complex biological systems.
- The structure and chemical properties of the commercial fluorescent probe CellROX[®] Deep Red have been elucidated. The fluorophore has a reduced Cy5 core and the presence of a deuterium atom which is meant to play a key role on its stability. CellROX is reactive towards different ROS/RNS both in solution and in *E. coli* cells expressing photosensitizing flavoproteins as a model of its use in biological media. The results are in line with the reported ROS capacity of miniSOG and their derivatives (Q103L and Q103V). However, the probe suffers from auto-oxidation induced by $^3\text{O}_2$ as well as by low light doses at different wavelengths.
- 3,3',5,5'-Tetramethylbenzidine oxidation by different ROS/RNS (ClO^- , H_2O_2 , $^1\text{O}_2$ and NO_2) can be followed by laser induced optoacoustic spectroscopy using red and/or blue light excitation. LIOAS circumvents many of the limitations of the widely used fluorescent probe, such as poor tissue penetration. TMB is not internalized by *E. coli* cells, however it gets adsorbed in their outer-cell wall and correctly detects the $^1\text{O}_2$ generated in that region. Optoacoustic probe may be an alternative to fluorescent probe for ROS imaging in biological systems.
- A self-reporter nanophotosensitizer has been designed and synthesized by attaching a PS (Rose Bengal) and a $^1\text{O}_2$ fluorescent probe (anthracene dipropionate) to the same mesoporous silica scaffold. It has been successfully proved that the decrease of fluorescence correlates with the photoantimicrobial activity against *S. aureus*, thereby paving the way to the development of molecular dosimeters for light-based therapeutics.

Chapter VIII

Bibliography

*Ve la fi de tota cosa:
malaurat el que se'n tem.
La corrandà se l'emporta
una mena de gemec,
la mirada, un punt de fosca,
la besada, un poc de fred;
la mirada, un punt de fosca
i l'amor, un fil de vent.*

Josep Carner

- 1 M. D. Daniell and J. S. Hill, *Aust. N. Z. J. Surg.*, 1991, **61**, 340–348.
- 2 M.H. Abdel-kader, The Journey of PDT Throughout History: PDT from Pharos to Present, in *Photodynamic Medicine: From Bench to Clinic*, Ed. H. Kostron and T. Hasan, 2016, 1-21.
- 3 T. Patrice, J. Moan and Q. Peng, An outline of the history of PDT, in *Photodynamic Therapy*, Ed. T. Patrice, 2003, 1–18.
- 4 A. F. McDonagh, *J. Perinatol.*, 2001, **21**, S7–S12.
- 5 E. Snellman, J. Lauharanta, A. Reunanen, C. T. Jansen, T. J. Pakkasvirta, M. Kallio, J. Luoma, A. Aromaa and J. Waal, *Br. J. Dermatol.*, 1993, **128**, 172–177.
- 6 A. A. Krasnovsky, *Biofizika*, 1993, **38**, 904–918.
- 7 M. F. Holick, *Arch. Dermatol.*, 1987, **123**, 1677.
- 8 S. L. Murov, I. Carmichael and G. L. Hug, *Handbook of Photochemistry, Second Edition*, CRC Press, 1993, vol. 2.
- 9 C. N. Yang and R. L. Mills, *Phys. Rev.*, 1954, **96**, 191–195.
- 10 J. R. Lakowicz, *Principles of Fluorescence Spectroscopy*, Springer, Maryland, USA, Third Edit., 2006.
- 11 M. Kasha, *Discuss. Faraday Soc.*, 1950, **9**, 14.
- 12 G. N. Lewis and M. Kasha, *J. Am. Chem. Soc.*, 1944, **66**, 2100–2116.
- 13 M. A. El-Sayed, *Acc. Chem. Res.*, 1968, **1**, 8–16.
- 14 J. C. Koziar and D. O. Cowan, *Acc. Chem. Res.*, 1978, **11**, 334–341.
- 15 N. J. Turro, P. Ramamurthy and J. C. Scaiano, *Modern molecular photochemistry of organic molecules*, University Science Books, California, 2nd ed., 2010.
- 16 C. S. Foote, *Photochem. Photobiol.*, 1991, **54**, 659.
- 17 L. Huang, Y. Xuan, Y. Koide, T. Zhiyentayev, M. Tanaka and M. R. Hamblin, *Lasers Surg. Med.*, 2012, **44**, 490–499.
- 18 K. M. Scherer, R. H. Bisby, S. W. Botchway and A. W. Parker, *Anticancer. Agents Med. Chem.*, 2017, **17**, 171–189.
- 19 A. B. Ormond and H. S. Freeman, *Materials*, 2013, **6**, 817–840.
- 20 R. Bonnett, *J. Heterocycl. Chem.*, 2002, **39**, 455–470.
- 21 R. Pottier and T. G. Truscott, *Int. J. Radiat. Biol. Relat. Stud. Physics*, 1986, **50**, 421–452.
- 22 R. Bonnett, *Chem. Soc. Rev.*, 1995, **24**, 19.
- 23 R.R. Allison, G.H. Downie, R. Cuenca, X.H. Hu, C.J. Childs and C. H. Sibata, *Photodiagnosis Photodyn. Ther.*, 2004, **1**, 27–42.
- 24 L. B. Josefsen and R. W. Boyle, *Br. J. Pharmacol.*, 2008, **154**, 1–3.
- 25 H. Kataoka, H. Nishie, N. Hayashi, M. Tanaka, A. Nomoto, S. Yano and T. Joh, *Ann. Transl. Med.*, 2017, **5**, 183–183.
- 26 J. Zhang, C. Jiang, J.P. Figueiró Longo, R.B. Azevedo, H. Zhang and L. A. Muehlmann, *Acta Pharm. Sin. B*, 2018, **8**, 137–146.
- 27 M.E. Bulina, K.A. Lukyanov, O.V. Britanova, D. Onichtchouk, S. Lukyanov and D.M. Chudakov, *Nat. Protoc.*, 2006, **1**, 947–953.
- 28 S. Pletnev, N. G. Gurskaya, N.V. Pletneva, K. A. Lukyanov, D.M. Chudakov, V.I. Martynov, V.O. Popov, M.V. Kovalchuk, A. Wlodawer, Z. Dauter and V. Pletnev, *J. Biol. Chem.*, 2009, **284**, 32028–32039.
- 29 X. Shu, V. Lev-Ram, T.J. Deerinck, Y. Qi, E.B. Ramko, M. W. Davidson, Y. Jin, M. H. Ellisman and R. Y. Tsien, *PLoS Biol.*, 2011, **9**, e1001041.
- 30 L. M. Uusitalo and N. Hempel, *Int. J. Mol. Sci.*, 2012, **13**, 10660–10679.
- 31 K. Krumova and G. Cosa, Overview of Reactive Oxygen Species, in *Singlet Oxygen: Applications in Biosciences and Nanosciences*, Volume 1, Ed. S. Nonell and C. Flors, 2016, 1–21.
- 32 K. Apel and H. Hirt, *Annu. Rev. Plant Biol.*, 2004, **55**, 373–399.
- 33 K. Plaetzer, T. Kiesslich, C.B. Oberdanner and B. Krammer, *Curr. Pharm. Des.*, 2005, **11**, 1151–1165.
- 34 P. T. Schumacker, *Cancer Cell*, 2006, **10**, 175–176.
- 35 S. S. Gill and N. Tuteja, *Plant Physiol. Biochem.*, 2010, **48**, 909–930.
- 36 E. Birben, U. M. Sahiner, C. Sackesen, S. Erzurum and O. Kalayci, *World Allergy Organ. J.*, 2012, **5**, 9–19.

- 37 V. Afonso, R. Champy, D. Mitrovic, P. Collin and A. Lomri, *Jt. Bone Spine*, 2007, **74**, 324–329.
- 38 B. Poljsak, D. Šuput and I. Milisav, *Oxid. Med. Cell. Longev.*, 2013, **2013**, 1–11.
- 39 T. Finkel and N. J. Holbrook, *Nature*, 2000, **408**, 239–247.
- 40 C. Harris and J. M. Hansen, 2012, pp. 325–346.
- 41 L. Mignolet-Spruyt, E. Xu, N. Idänheimo, F. A. Hoerberichts, P. Mühlenbock, M. Brosché, F. Van Breusegem and J. Kangasjärvi, *J. Exp. Bot.*, 2016, **67**, 3831–3844.
- 42 R. Mittler, *Trends Plant Sci.*, 2017, **22**, 11–19.
- 43 P. D. Ray, B.-W. Huang and Y. Tsuji, *Cell. Signal.*, 2012, **24**, 981–990.
- 44 M. C. Martínez and R. Andriantsitohaina, *Antioxid. Redox Signal.*, 2009, **11**, 669–702.
- 45 R.P. Patel, J. McAndrew, H. Sellak, C. R. White, H. Jo, B.A. Freeman and V.M. Darley-Usmar, *Biochim. Biophys. Acta - Bioenerg.*, 1999, **1411**, 385–400.
- 46 P. Klatt and S. Lamas, *Eur. J. Biochem.*, 2000, **267**, 4928–4944.
- 47 S.S. Beevi, M.H. Rasheed and A. Geetha, *Clin. Chim. Acta*, 2007, **375**, 119–123.
- 48 Y.I. Chirino and J. Pedraza-Chaverri, *Exp. Toxicol. Pathol.*, 2009, **61**, 223–242.
- 49 B. Leonard and M. Maes, *Neurosci. Biobehav. Rev.*, 2012, **36**, 764–785.
- 50 D.D. Thomas, L.A. Ridnour, J.S. Isenberg, W. Flores-Santana, C.H. Switzer, S. Donzelli, P. Hussain, C. Vecoli, N. Paolocci, S. Ambs, C.A. Colton, C.C. Harris, D.D. Roberts and D.A. Wink, *Free Radic. Biol. Med.*, 2008, **45**, 18–31.
- 51 H. Kautsky and H.S. de Bruijn, *Naturwissenschaften*, 1931, **19**, 1043.
- 52 H. Kautsky, *Trans. Faraday Soc.*, 1939, **35**, 216–218.
- 53 D. R. Kearns, *Chem.Rev.*, 1971, **71**, 395–427.
- 54 M. C. DeRosa and R. J. Crutchley, *Coord. Chem. Rev.*, 2002, **233–234**, 351–371.
- 55 P. R. Ogilby, *Chem. Soc. Rev.*, 2010, **39**, 3181–3209.
- 56 E. Boix-Garriga, B. Rodríguez-Amigo, O. Planas and S. Nonell, Properties of Singlet Oxygen, in *Singlet Oxygen: Applications in Biosciences and Nanosciences*, Ed. S. Nonell and C. Flors, 2016, 23–46.
- 57 F. Wilkinson, W. P. Helman and A. B. Ross, *J. Phys. Chem. Ref. Data*, 1995, **24**, 663–677.
- 58 L. Manring and C. Foote, *J. Phys. Chem.*, 1982, 1257–1259.
- 59 A. Darmany, W.S. Jenks and P. Jardon, *J. Phys. Chem. A*, 1998, **102**, 7420–7426.
- 60 D. Sawyer and J. Valentine, *Acc. Chem. Res.*, 1981, **14**, 393–400.
- 61 R. Schmidt and M. Bodesheim, *J. Phys. Chem.*, 1994, **98**, 2874–2876.
- 62 M. Bodesheim and R. Schmidt, *J. Phys. Chem. A*, 1997, **101**, 5672–5677.
- 63 N. I. Krinsky, *Trends Biochem. Sci.*, 1977, **30**, 35–38.
- 64 O. L. Gijzeman, F. Kaufman and G. Porter, *J. Chem. Soc. Trans. II*, 1973, **69**, 721–726.
- 65 F. Wilkinson, D.J. McGarvey and A.F. Olea, *J. Phys. Chem.*, 1994, **98**, 3762–3769.
- 66 C. Grewer and H.D. Brauer, *J. Phys. Chem.*, 1994, **98**, 4230–4235.
- 67 R. Schmidt, *Photochem. Photobiol.*, 2006, **82**, 1161.
- 68 O.L.J. Gijzeman, F. Kaufman and G. Porter, *J. Chem. Soc. Faraday Trans. 2*, 1973, **69**, 708.
- 69 R. Bresolí-Obach, C. Hally and S. Nonell, Activatable Photosensitizers, in *Singlet Oxygen: Applications in Biosciences and Nanosciences, Volume 1*, Ed. S. Nonell and C. Flors, 2016, pp. 163–181.
- 70 F. Wilkinson, D. McGarvey, J.A.F. Olea and D.J. McGarvey, *J. Am. Chem. Soc.*, 1993, **115**, 12144–12151.
- 71 K.C. Wu and A.M. Trozzolo, *J. Phys. Chem.*, 1979, **83**, 2823–2826.
- 72 K.C. Wu and A.M. Trozzolo, *J. Phys. Chem.*, 1979, **83**, 3180–3183.
- 73 R.C. Kanner and C.S. Foote, *J. Am. Chem. Soc.*, 1992, **114**, 678–681.
- 74 C.K. Duncan and D.R. Kearns, *J. Chem. Phys.*, 1971, **55**, 5822–5823.
- 75 K.I. Salokhiddinov, I.M. Byteva and B.M. Dzhagarov, *Opt. I Spektrosk.*, 1979, **47**, 881–886.

- 76 S. Nonell and S.E. Braslavsky, *Methods Enzymol.*, 2000, **319**, 37–49.
- 77 J. Baier, T. Fuß, C. Pöllmann, C. Wiesmann, K. Pindl, R. Engl, D. Baumer, M. Maier, M. Landthaler and W. Bäumlner, *J. Photochem. Photobiol. B Biol.*, 2007, **87**, 163–173.
- 78 S. Nonell and C. Flors, Steady-State and Time-Resolved Singlet Oxygen Phosphorescence Detection in the Near-IR, in *Singlet Oxygen: Applications in Biosciences and Nanosciences Volume 2*, Ed. S. Nonell and C. Flors, 2016, 7–26.
- 79 E. Skovsen, J. W. Snyder, J.D.C. Lambert and P.R. Ogilby, *J. Phys. Chem. B*, 2005, **109**, 8570–8573.
- 80 J.W. Snyder, E. Skovsen, J.D.C. Lambert and P.R. Ogilby, *J. Am. Chem. Soc.*, 2005, **127**, 14558–14559.
- 81 W. Tian, L. Deng, S. Jin, H. Yang, R. Cui, Q. Zhang, W. Shi, C. Zhang, X. Yuan and G. Sha, *J. Phys. Chem. A*, 2015, **119**, 3393–3399.
- 82 R. Schmidt, K. Seikel and H. D. Brauer, *J. Phys. Chem.*, 1989, **93**, 4507–4511.
- 83 N. Hasebe, K. Suzuki, H. Horiuchi, H. Suzuki, T. Yoshihara, T. Okutsu and S. Tobita, *Anal. Chem.*, 2015, **87**, 2360–2366.
- 84 R.M. Badger, A. C. Wright and R. F. Whitlock, *J. Chem. Phys.*, 1965, **43**, 4345.
- 85 P.R. Ogilby, R.D. Scurlock, *J. Phys. Chem.*, 1987, **91**, 4599–4602.
- 86 M.A.J. Rodgers, *J. Am. Chem. Soc.*, 1983, **105**, 6201–6205.
- 87 P.R. Ogilby and C.S. Foote, *J. Am. Chem. Soc.*, 1981, **103**, 1219–1221.
- 88 M. Okamoto, F. Tanaka and H. Teranishi, *J. Phys. Chem.*, 1990, **94**, 669–672.
- 89 E.W. Gray and E.A. Ogryzlo, *Chem. Phys. Lett.*, 1969, **3**, 658–660.
- 90 P.M. Borrell, P. Borrel and K. R. Grant, *J. Chem. Soc. Faraday Trans. 2*, 1980, **76**, 1442.
- 91 M. Scholz, R. Dëdic, J. Valenta, T. Breitenbach and J. Hála, *Photochem. Photobiol. Sci.*, 2014, **13**, 1203–12.
- 92 S.E. Braslavsky and G.E. Heibel, *Chem. Rev.*, 1992, **92**, 1381–1410.
- 93 R.W. Redmond and S.E. Braslavsky, *Chem. Phys. Lett.*, 1988, **148**, 523–529.
- 94 B.R. Rabello, A.P. Gerola, D.S. Pellosi, A.L. Tessaro, J.L. Aparício, W. Caetano and N. Hioka, *J. Photochem. Photobiol. A Chem.*, 2012, **238**, 53–62.
- 95 C. Flors, M. J. Fryer, J. Waring, B. Reeder, U. Bechtold, P. M. Mullineaux, S. Nonell, M. T. Wilson and N. R. Baker, *J. Exp. Bot.*, 2006, **57**, 1725–1734.
- 96 A. Thompson, H. H. Seliger and G. H. Posner, *Methods Enzymol.*, 1986, **187**, 569–584.
- 97 N. Hananya, O. Green, R. Blau, R. Satchi-Fainaro and D. Shabat, *Angew. Chemie Int. Ed.*, 2017, **56**, 11793–11796.
- 98 E. Hideg, C. Spetea and I. Vass, *Photosynth. Res.*, 1994, **39**, 191–199.
- 99 R. Ruiz-González and A. L. Zanocco, Singlet Oxygen Fluorescent Probes, in *Singlet Oxygen: Applications in Biosciences and Nanosciences, Volume 2*, Ed. S. Nonell and C. Flors, 2016, pp. 103–120.
- 100 E.J. Corey and W.C. Taylor, *J. Am. Chem. Soc.*, 1964, **86**, 3881–3882.
- 101 T. Wilson, *J. Am. Chem. Soc.*, 1969, **91**, 2387–2388.
- 102 P.B. Merkel and D.R. Kearns, *J. Am. Chem. Soc.*, 1975, **97**, 462–463.
- 103 N. Umezawa, K. Tanaka, Y. Urano, K. Kikuchi, T. Higuchi and T. Nagano, *Angew. Chemie*, 1999, **38**, 2899–2901.
- 104 X. Ragàs, A. Jiménez-Banzo, D. Sanchez-Garcia, X. Batllori and S. Nonell, *Chem. Commun.*, 2009, **20**, 2920–2922.
- 105 A. Gollmer, J. Arnbjerg, F.H. Blaikie, B.W. Pedersen, T. Breitenbach, K. Daasbjerg, M. Glasius and P.R. Ogilby, *Photochem. Photobiol.*, 2011, **87**, 671–679.
- 106 K. Xu, L. Wang, M. Qiang, L. Wang, P. Li and B. Tang, *Chem. Commun.*, 2011, **47**, 7386–7388.
- 107 L.E. Greene, R. Lincoln and G. Cosa, *J. Am. Chem. Soc.*, 2017, **139**, 15801–15811.
- 108 H.W. Liu, S. Xu, P. Wang, X.X. Hu, J. Zhang, L. Yuan, X.B. Zhang and W. Tan, *Chem. Commun.*, 2016, **52**, 12330–12333.
- 109 R. Ruiz-González, R. Zanocco, Y. Gidi, A. L. Zanocco, S. Nonell and E. Lemp, *Photochem. Photobiol.*, 2013, **89**, 1427–1432.
- 110 D. Song, S. Cho, Y. Han, Y. You and W. Nam, *Org. Lett.*, 2013, **15**, 3582–3585.
- 111 C. S. Foote, *Acc. Chem. Res.*, 1968, **1**, 104–110.

- 112 G.O. Schenck, *Naturwissenschaften*, 1948, **35**, 28–29.
- 113 E.L. Clennan, *Tetrahedron*, 2000, **56**, 9151–9179.
- 114 E.L. Clennan and A. Pace, *Tetrahedron*, 2005, **61**, 6665–6691.
- 115 E.L. Clennan, *Acc. Chem. Res.*, 2001, **34**, 875–884.
- 116 R. Gao, D. G. Ho, T. Dong, D. Khuu, N. Franco, O. Sezer and M. Selke, *Org. Lett.*, 2001, **3**, 3719–3722.
- 117 E.L. Clennan, L.J. Noe, T. Wen and E. Szneler, *J. Org. Chem.*, 1989, **54**, 3581–3584.
- 118 E.L. Clennan, L.J. Noe, E. Szneler and T. Wen, *J. Am. Chem. Soc.*, 1990, **112**, 5080–5085.
- 119 M. Selke, C.S. Foote and W.L. Karney, *Inorg. Chem.*, 1993, **32**, 5425–5426.
- 120 A.A. Frimer, *Chem. Rev.*, 1979, **79**, 359–387.
- 121 N.J. Turro and M.F. Chow, *J. Am. Chem. Soc.*, 1979, **101**, 3701–3703.
- 122 W. Fudickar and T. Linker, *Chem. Commun.*, 2008, 1771–1773.
- 123 P.D. Bartlett and A.P. Schaap, *J. Am. Chem. Soc.*, 1970, **92**, 3223–3225.
- 124 W. Adam, S.G. Bosio and N.J. Turro, *J. Am. Chem. Soc.*, 2002, **124**, 8814–8815.
- 125 R.G.O. Thomas and B.A. Thrush, *Proc. R. Soc. A Math. Phys. Eng. Sci.*, 1977, **356**, 287–294.
- 126 R.G.O. Thomas and B. A. Thrush, *Proc. R. Soc. A Math. Phys. Eng. Sci.*, 1977, **356**, 295–306.
- 127 C.S. Foote and R.W. Denny, *J. Am. Chem. Soc.*, 1968, **90**, 6233–6235.
- 128 C. Ouannes and T. Wilson, *J. Am. Chem. Soc.*, 1968, **90**, 6527–6528.
- 129 R.D. Hall and C.F. Chignell, *Photochem. Photobiol.*, 1987, **45**, 459–464.
- 130 D.J. Carlsson, T. Suprunchuk and D.M. Wiles, *Can. J. Chem.*, 1974, **52**, 3728–3737.
- 131 P. Agostinis, K. Berg, K.A. Cengel, T.H. Foster, A.W. Girotti, S.O. Gollnick, S.M. Hahn, M.R. Hamblin, A. Juzeniene, D. Kessel, M. Korbelik, J. Moan, P. Mroz, D. Nowis, J. Piette, B.C. Wilson and J. Golab, *CA. Cancer J. Clin.*, 2011, **61**, 250–281.
- 132 C. Kim, R. Meskauskiene, K. Apel and C. Laloi, *EMBO Rep.*, 2008, **9**, 435–439.
- 133 D. Kopetzki, F. Lévesque and P. H. Seeberger, *Chem. Eur. J.*, 2013, **19**, 5450–5456.
- 134 D. B. Min and J. M. Boff, *Compr. Rev. Food Sci. Food Saf.*, 2002, **1**, 58–72.
- 135 T. Demidova and M. Hamblin, *Int. J. Immunopathol. Pharmacol.*, 2004, **17**, 245–254.
- 136 G.O. Schenck and K. Ziegler, *Naturwissenschaften*, 1954, **32**, 157.
- 137 J.E. Barbarow, A.K. Miller and D. Trauner, *Org. Lett.*, 2005, **7**, 2901–2903.
- 138 N. Sofikiti, M. Tofi, T. Montagnon, G. Vassilikogiannakis and M. Stratakis, *Org. Lett.*, 2005, **7**, 2357–2359.
- 139 Z. Amara, J.F.B. Bellamy, R. Horvath, S.J. Miller, A. Beeby, A. Burgard, K. Rossen, M. Poliakoff and M. W. George, *Nat. Chem.*, 2015, **7**, 489–495.
- 140 S. Triemer, K. Gilmore, G. T. Vu, P. H. Seeberger and A. Seidel-Morgenstern, *Angew. Chemie Int. Ed.*, 2018, **57**, 5525–5528.
- 141 E. Choe and D.B. Min, *Crit. Rev. Food Sci. Nutr.*, 2006, **46**, 1–22.
- 142 F.H. Doleiden, S.R. Fahrenholtz, A.A. Lamola and A. M. Trozzolo, *Photochem. Photobiol.*, 1974, **20**, 519–521.
- 143 T. Sano, M. Iwahashi, J. Imagi, T. Sato, T. Yamashita, E. Fukusaki and T. Bamba, *J. Oleo Sci.*, 2016, **65**, 447–450.
- 144 M.Y. Jung, S.H. Yoon, H.O. Lee and D.B. Min, *J. Food Sci.*, 1998, **63**, 408–412.
- 145 J.M. King and D.B. Min, *J. Food Sci.*, 1998, **63**, 31–34.
- 146 O.W. Parks and C. Allen, *J. Dairy Sci.*, 1977, **60**, 1038–1041.
- 147 K. Whang and I.C. Peng, *J. Food Sci.*, 1988, **53**, 1863–1865.
- 148 R.G.W. Norrish and C.H. Bamford, *Nature*, 1937, **140**, 195–196.
- 149 H. Kaneda, Y. Kano, T. Osawa, N. Ramarathnam, S. Kawakishi and K. Kamada, *J. Food Sci.*, 1988, **53**, 885–888.
- 150 C.W. Bamforth and R. Parsons, *J. Am. Soc. Brew. Chem.*, 1985, **43**, 197–203.
- 151 O. Raab, *Z. Biol.*, 1900, **39**, 524.
- 152 H. von Tappeiner and O. Raab, *Munch. Med. Wochenschr.*, 1900, **47**, 5.
- 153 J. D. Spikes, *Photochem. Photobiol.*, 1997, **65**, 142–147.
- 154 N. R. Finsen, Niels Ryberg Finsen - Nobel Prize Banquet Speech, 1903.

- 155 H. von Tappeiner and A. Jesionek, *Munch. Med. Wochenschr.*, 1903, **50**, 2042–2044.
- 156 H. von Tappeiner and A. Jodlbauer, *Arch. Klin. Med.*, 1904, **80**, 427–487.
- 157 Z. Meyer-Betz, *Dtsch. Arch. Klin. Med.*, 1913, **112**, 476–503.
- 158 M.R. Hamblin and T. Hasan, *Photochem. Photobiol. Sci.*, 2004, **3**, 436–450.
- 159 M. Wainwright, T. Maisch, S. Nonell, K. Plaetzer, A. Almeida, G.P. Tegos and M.R. Hamblin, *Lancet Infect. Dis.*, 2017, **17**, 49–55.
- 160 H. Abrahamse and M.R. Hamblin, *Biochem. J.*, 2016, **473**, 347–364.
- 161 J.M.C. Gutteridge, *Clin. Chem.*, 1995, **41**, 1819–1828.
- 162 M.J. Davies, *Photochem. Photobiol. Sci.*, 2004, **3**, 17–25.
- 163 F.R. Hallett, B.P. Hallett and W. Snipes, *Biophys. J.*, 1970, **10**, 305–315.
- 164 E. Dumont, R. Grüber, E. Bignon, C. Morell, Y. Moreau, A. Monari and J.-L. Ravanat, *Nucleic Acids Res.*, 2016, **44**, 56–62.
- 165 F.J. Schmitt, G. Renger, T. Friedrich, V.D. Kreslavski, S.K. Zharmukhamedov, D.A. Los, V.V. Kuznetsov and S.I. Allakhverdiev, *Biochim. Biophys. Acta - Bioenerg.*, 2014, **1837**, 835–848.
- 166 J.M. Chalker, G.J.L. Bernardes, Y. Lin and B.G. Davis, *Chem. Asian J.*, 2009, **4**, 630–40.
- 167 [Http://www.cancer.gov/about-cancer/understanding/what-is-cancer](http://www.cancer.gov/about-cancer/understanding/what-is-cancer), Visited on: 27th February 2018.
- 168 [Http://www.who.int/mediacentre/factsheets/fs297/en/](http://www.who.int/mediacentre/factsheets/fs297/en/), Visited on: 27th February 2018.
- 169 J. Ferlay, I. Soerjomataram I, R. Dikshit, S. Eser, C. Mathers, M. Rebelo, D.M. Parkin, D. Forman and F. Bray, *Int. J. Cancer*, 2014, **136**, 359–86.
- 170 R. Airley, *Cancer chemotherapy*, Wiley-Blackwell, 2009.
- 171 [Http://www.medicalnewstoday.com/articles/158401.php](http://www.medicalnewstoday.com/articles/158401.php), Visited on: 27th February 2018.
- 172 A.P. Castano, T.N. Demidova and M.R. Hamblin, *Photodiagnosis Photodyn. Ther.*, 2004, **1**, 279–293.
- 173 A.P. Castano, T.N. Demidova and M.R. Hamblin, *Photodiagnosis Photodyn. Ther.*, 2005, **2**, 1–23.
- 174 A.P. Castano, T.N. Demidova and M.R. Hamblin, *Photodiagnosis Photodyn. Ther.*, 2005, **2**, 91–106.
- 175 G. Rodighiero, L. Musajo, F. Dall'acqua, S. Marciani, G. Caporale and L. Ciavatta, *Biochim. Biophys. Acta - Nucleic Acids Protein Synth.*, 1970, **217**, 40–49.
- 176 A. R. Kamuhabwa, R. Roelandts and P.A. de Witte, *J. Photochem. Photobiol. B Biol.*, 1999, **53**, 110–114.
- 177 E. Panzarini, B. Tenuzzo, F. Palazzo, A. Chionna and L. Dini, *J. Photochem. Photobiol. B.*, 2006, **83**, 39–47.
- 178 L. Liu, Z. Zhang and D. Xing, *Free Radic. Biol. Med.*, 2011, **51**, 53–68.
- 179 A.D. Garg, D. Nowis, J. Golab and P. Agostinis, *Apoptosis*, 2010, **15**, 1050–1071.
- 180 A.D. Garg, D. Nowis, J. Golab, P. Vandenamee, D. V Krysko and P. Agostinis, *Biochim. Biophys. Acta*, 2010, **1805**, 53–71.
- 181 J. A. Parrish, *J. Invest. Dermatol.*, 1981, **77**, 45–50.
- 182 A. Martella and M. Raichi, *Dermatology Reports*, 2017, **9**, 7116.
- 183 C.S. Oliveira, R. Turchiello, A.J. Kowaltowski, G.L. Indig and M.S. Baptista, *Free Radic. Biol. Med.*, 2011, **51**, 824–833.
- 184 Q. Peng, J. Moan and J.M. Nesland, *Ultrastruct. Pathol.*, 1996, **20**, 109–129.
- 185 D. Kessel, Y. Luo, Y. Deng and C. K. Chang, *Photochem. Photobiol.*, 1997, **65**, 422–426.
- 186 A. Fleming, *Bull World Heal. Organ.*, 1929, **46**, 780–790.
- 187 [Http://www.who.int/mediacentre/factsheets/antibiotic-resistance/en/](http://www.who.int/mediacentre/factsheets/antibiotic-resistance/en/), Visited on: 27th February 2018.
- 188 C. L. Ventola, *P&T*, 2015, **40**, 277–83.
- 189 C. L. Ventola, *P&T*, 2015, **40**, 344–52.
- 190 G. Jori and O. Coppellotti, *Antiinfect. Agents Med. Chem.*, 2007, **6**, 119–131.
- 191 L.A. Pedigo, A.J. Gibbs, R.J. Scott and C.N. Street, *Proc. Vol.*, 2009, **7380**, 73803H.
- 192 F.M. Lauro, P. Pretto, L. Covolo, G. Jori and G. Bertoloni, *Photochem. Photobiol. Sci.*, 2002, **1**, 468–470.
- 193 [Https://www.nobelprize.org/nobel_prizes/medicine/laureates/1908/ehrl ich-bio.html](https://www.nobelprize.org/nobel_prizes/medicine/laureates/1908/ehrl ich-bio.html), Visited on: 27th February 2018.

- 194 M.R.J. Salton, *Biochim. Biophys. Acta*, 1953, **10**, 512–523.
- 195 M. Merchat, G. Bertolini, P. Giacomini, A. Villanueva and G. Jori, *J. Photochem. Photobiol. B.*, 1996, **32**, 153–157.
- 196 F.F. Sperandio, Y.Y. Huang and M.R. Hamblin, *Recent Pat. Antiinfect. Drug Discov.*, 2013, **8**, 108–120.
- 197 Z. Malik, H. Ladan and Y. Nitzan, *J. Photochem. Photobiol. B Biol.*, 1992, **14**, 262–6.
- 198 E. Alves, L. Costa, C.M.B. Carvalho, J.P.C. Tomé, M.A. Faustino, M.G. Neves, A.C. Tomé, J.A. Cavaleiro, A. Cunha and A. Almeida, *BMC Microbiol.*, 2009, **9**, 1–13.
- 199 [Http://nptel.ac.in/courses/102103012/module1/lec1/3.html](http://nptel.ac.in/courses/102103012/module1/lec1/3.html), Visited on: 27th February 2018.
- 200 M. Wainwright, D.A. Phoenix, J. Marland, D. R. Wareing and F.J. Bolton, *FEMS Immunol. Med. Microbiol.*, 1997, **19**, 75–80.
- 201 M. Wainwright and K.B. Crossley, *J. Chemother.*, 2002, **14**, 431–443.
- 202 X. Ragàs, D. Sánchez-García, R. Ruiz-González, T. Dai, M. Agut, M.R. Hamblin and S. Nonell, *J. Med. Chem.*, 2010, **53**, 7796–7803.
- 203 D. Vecchio, T. Dai, L. Huang, L. Fantetti, G. Roncucci and M.R. Hamblin, *J. Biophotonics*, 2013, **6**, 733–742.
- 204 E. Anaya-Plaza, E. van de Winkel, J. Mikkilä, J.-M. Malho, O. Ikkala, O. Gulías, R. Bresolí-Obach, M. Agut, S. Nonell, T. Torres, M. A. Kostianen and A. de la Escosura, *Chem. Eur. J.*, 2017, **23**, 4320–4326.
- 205 B. Hager, W.S.L. Strauss and H. Falk, *Photochem. Photobiol.*, 2009, **85**, 1201–1206.
- 206 F. Cieplik, A. Späth, J. Regensburger, A. Gollmer, L. Tabenski, K.A. Hiller, W. Bäuml, T. Maisch and G. Schmalz, *Free Radic. Biol. Med.*, 2013, **65**, 477–87.
- 207 A. Späth, C. Leibl, F. Cieplik, K. Lehner, J. Regensburger, K.A. Hiller, W. Bäuml, G. Schmalz and T. Maisch, *J. Med. Chem.*, 2014, **57**, 5157–5168.
- 208 I. Tabenski, F. Cieplik, L. Tabenski, J. Regensburger, K.-A. Hiller, W. Buchalla, T. Maisch and A. Späth, *Photochem. Photobiol. Sci.*, 2016, **15**, 57–68.
- 209 A. Spaeth, A. Graeler, T. Maisch and K. Plaetzer, *Eur. J. Med. Chem.*, 2018, DOI:10.1016/j.ejmech.2017.09.072.
- 210 G.P. Tegos, T.N. Demidova, D. Arcila-Lopez, H. Lee, T. Wharton, H. Gali and M.R. Hamblin, *Chem. Biol.*, 2005, **12**, 1127–1135.
- 211 T.N. Demidova and M.R. Hamblin, *Antimicrob. Agents Chemother.*, 2005, **49**, 2329–2335.
- 212 D.K. Chatterjee, L.S. Fong and Y. Zhang, *Adv. Drug Deliv. Rev.*, 2008, **60**, 1627–37.
- 213 S.S. Lucky, K.C. Soo and Y. Zhang, *Chem. Rev.*, 2015, **115**, 1990–2042.
- 214 O. Planas, E. Boix-Garriga, B. Rodríguez-Amigo, J. Torra, R. Bresolí-Obach, C. Flors, C. Viappiani, M. Agut, R. Ruiz-González and S. Nonell, Newest approaches to singlet oxygen photosensitisation in biological media, in *Photochemistry Volume 42*, Ed. E. Fasani and A. Albini, 2015, 233–278.
- 215 I. Khan, K. Saeed and I. Khan, *Arab. J. Chem.*, 2018, DOI:10.1016/j.arabjc.2017.05.011.
- 216 S. Nonell, M. González and F. R. Trull, *Afinidad*, 1993, **44**, 445–450.
- 217 W. Becker, A. Bergmann, M.A. Hink, K. König, K. Benndorf and C. Biskup, *Microsc. Res. Tech.*, 2004, **63**, 58–66.
- 218 W. Becker, A. Bergmann, G. Biscotti and A. Rück, *BMC Microbiol.*, 2004, **5340**, 1–9.
- 219 W. Becker, *J. Microsc.*, 2012, **247**, 119–136.
- 220 C. G. Morgan, A. C. Mitchell and J. G. Murray, *TrAC Trends Anal. Chem.*, 1992, **11**, 32–41.
- 221 W. Becker, *Advanced Time-Correlated Single Photon Counting Techniques*, Springer Berlin Heidelberg, Berlin, Heidelberg, 2005, vol. 81.
- 222 M.G. Badea and L. Brand, *Chem. Rev.*, 1979, **85**, 378–425.
- 223 A.J. Cross and G.R. Fleming, *Biophys. J.*, 1984, **46**, 45–56.
- 224 A. Jiménez-Banzo, X. Ragàs, P. Kapusta and S. Nonell, *Photochem. Photobiol. Sci.*, 2008, **7**, 1003–1010.
- 225 L. Lindqvist, *Hebd. Seances Acad. Sci.*, 1966, **263**, 852.
- 226 J. C. Scaiano, Nanosecond Laser Flash Photolysis: A Tool for Physical Organic Chemistry, in *Reactive Intermediate Chemistry*, Ed. R.A. Moss, M.S. Platz, M. Jones, 2005, 847–871.

- 227 M. Eigen, *Angew. Chemie*, 1968, **80**, 892–906.
- 228 R.G.W. Norrish, *Angew. Chemie*, 1968, **80**, 868–881.
- 229 G. Porter, *Angew. Chemie*, 1968, **80**, 882–891.
- 230 T. Gensch and C. Viappiani, *Photochem. Photobiol. Sci.*, 2003, **2**, 699.
- 231 G.R. Fulmer, A.J.M. Miller, N.H. Sherden, H. E. Gottlieb, A. Nudelman, B.M. Stoltz, J.E. Bercau and K.I. Goldberg, *Organometallics*, 2010, **29**, 2176–2179.
- 232 A. Juzeniene, Q. Peng and J. Moan, *Photochem. Photobiol. Sci.*, 2007, **6**, 1234–1245.
- 233 S. Sabbahi, L. Ben Ayed and A. Boudabbous, *J. Water Health*, 2013, **11**, 590.
- 234 A. Coates, Y. Hu, R. Bax and C. Page, *Nat. Rev. Drug Discov.*, 2002, **1**, 895–910.
- 235 D.M. Shlaes and B. Spellberg, *Curr. Opin. Pharmacol.*, 2012, **12**, 522–526.
- 236 A. Villanueva, J.C. Stockert, M. Cañete and P. Acedo, *Photochem. Photobiol. Sci.*, 2010, **9**, 295–297.
- 237 P. Acedo, J.C. Stockert, M. Cañete and A. Villanueva, *Cell Death Dis.*, 2014, **5**, e1122.
- 238 E.B. Gyenge, D. Lüscher, P. Forny, M. Antoniol, G. Geisberger, H. Walt, G. Patzke and C. Maake, *Photochem. Photobiol.*, 2013, **89**, 150–162.
- 239 I. Rizvi, J.P. Celli, C.L. Evans, A.O. Abu-Yousif, A. Muzikansky, B.W. Pogue, D. Finkelstein and T. Hasan, *Cancer Res.*, 2010, **70**, 9319–9328.
- 240 W. Cao, Y. Gu, M. Meineck and H. Xu, *Chem. - An Asian J.*, 2014, **9**, 48–57.
- 241 J.A. McCubrey, N.M. Davis, S.L. Abrams, G. Montalto, M. Cervello, M. Libra, F. Nicoletti, A. B. D'Assoro, L. Cocco, A.M. Martelli and L. S. Steelman, *Adv. Biol. Regul.*, 2014, **56**, 81–107.
- 242 G. Jori, *J. Photochem. Photobiol. B.*, 1996, **36**, 87–93.
- 243 J.F. Lovell, T.W.B. Liu, J. Chen and G. Zheng, *Chem. Rev.*, 2010, **110**, 2839–57.
- 244 E.A. Liberman, V.P. Topaly, L.M. Tsofina, A.A. Jasaitis and V.P. Skulachev, *Nature*, 1969, **222**, 1076–1078.
- 245 M.F. Ross, G.F. Kelso, F.H. Blaikie, A.M. James, H.M. Cochemé, A. Filipovska, T. Da Ros, T.R. Hurd, R.A.J. Smith and M.P. Murphy, *Biochem.*, 2005, **70**, 222–230.
- 246 J. Zielonka, J. Joseph, A. Sikora, M. Hardy, O. Ouari, J. Vasquez-Vivar, G. Cheng, M. Lopez and B. Kalyanaraman, *Chem. Rev.*, 2017, **117**, 10043–10120.
- 247 R.A.J. Smith, C. M. Porteous, A.M. Gane and M.P. Murphy, *Proc. Natl. Acad. Sci.*, 2003, **100**, 5407–5412.
- 248 M.P. Murphy, *Biochim. Biophys.*, 2008, **1777**, 1028–1031.
- 249 G.F. Azzone, D. Pietrobon and M. Zoratti, *Curr. Top. Bioenerg.*, 1984, **13**, 1–77.
- 250 M.P. Murphy, *Trends Biotechnol.*, 1997, **15**, 326–330.
- 251 R.J. Burns, R.A.J. Smith and M.P. Murphy, *Arch. Biochem. Biophys.*, 1995, **322**, 60–68.
- 252 R.J. Burns and M.P. Murphy, *Arch. Biochem. Biophys.*, 1997, **339**, 33–39.
- 253 R.A.J. Smith, C.M. Porteous, C.V. Coulter and M.P. Murphy, *Eur. J. Biochem.*, 1999, **263**, 709–716.
- 254 <https://www.microscopyu.com/references/cellular-phototoxicity>, Visited on: 8th March 2018.
- 255 W. Lv, Z. Zhang, K.Y. Zhang, H. Yang, S. Liu, A. Xu, S. Guo, Q. Zhao and W. Huang, *Angew. Chemie Int. Ed.*, 2016, **55**, 9947–9951.
- 256 W. Lei, J. Xie, Y. Hou, G. Jiang, H. Zhang, P. Wang, X. Wang and B. Zhang, *J. Photochem. Photobiol. B Biol.*, 2010, **98**, 167–171.
- 257 K.M. Robinson, M.S. Janes, M. Pehar, J.S. Monette, M.F. Ross, T.M. Hagen, M.P. Murphy and J.S. Beckman, *Proc. Natl. Acad. Sci.*, 2006, **103**, 15038–15043.
- 258 W.F. Martin and M. Mentel, *Nat. Educ.*, 2010, **3**, 58.
- 259 E.A. Dunn, M. Roxburgh, L. Larsen, R.A.J. Smith, A.D. McLellan, A. Heikal, M. P. Murphy and G. M. Cook, *Bioorg. Med. Chem.*, 2014, **22**, 5320–5328.
- 260 M. Li, S.A. Nyantakyi, P. Gopal, D. Binte-Aziz, T. Dick and M.L. Go, *ACS Med. Chem. Lett.*, 2017, **8**, 1165–1170.
- 261 N. Soh and T. Ueda, *Talanta*, 2011, **85**, 1233–1237.
- 262 C. Martí, O. Jürgens, O. Cuenca, M. Casals and S. Nonell, *J. Photochem. Photobiol. A Chem.*, 1996, **97**, 11–18.

- 263 P. Drössler, W. Holzer, A. Penzkofer and P. Hegemann, *Chem. Phys.*, 2003, **286**, 409–420.
- 264 M. Wingen, J. Potzkei, S. Endres, G. Casini, C. Rupprecht, C. Fahlke, U. Krauss, K.E. Jaeger, T. Drepper and T. Gensch, *Photochem. Photobiol. Sci.*, 2014, **13**, 875–883.
- 265 I. Tabenski, F. Cieplik, L. Tabenski, J. Regensburger, K.A. Hiller, W. Buchalla, T. Maisch and A. Späth, *Photochem. Photobiol. Sci.*, 2016, **15**, 57.
- 266 A. Späth, C. Leibl, F. Cieplik, K. Lehner, J. Regensburger, K. A. Hiller, W. Bäuml, G. Schmalz and T. Maisch, *J. Med. Chem.*, 2014, **57**, 5157–5168.
- 267 F. Cieplik, A. Späth, J. Regensburger, A. Gollmer, L. Tabenski, K.A. Hiller, W. Bäuml, T. Maisch and G. Schmalz, *Free Radic. Biol. Med.*, 2013, **65**, 477–487.
- 268 N. Hirota, S. Matsuura, N. Mochizuki, N. Mutoh and Y. Imae, *J. Bacteriol.*, 1981, **148**, 399–405.
- 269 J. K. Borchardt, *Drug News Perspect.*, 2002, **15**, 187.
- 270 K. C. Huang, *The pharmacology of chinese herbs*, Taylor & Francis, Second Edition, 1998.
- 271 G.M. Cragg and D.J. Newman, *Biochim. Biophys. Acta*, 2013, **1830**, 3670–3695.
- 272 D.J. Newman and G.M. Cragg, *J. Nat. Prod.*, 2016, **79**, 629–661.
- 273 G.H.N. Towers, J.E. Page and J.B. Hudson, *Curr. Org. Chem.*, 1997, **1**, 395–414.
- 274 C. Flors and S. Nonell, *Acc. Chem. Res.*, 2006, **39**, 293–300.
- 275 R. Dai, R. Shoemaker, D. Farrens, M.J. Han, C.S. Kim and P.S. Song, *J. Nat. Prod.*, 1992, **55**, 1241–1251.
- 276 P.M.K. Tang, X.Z. Liu, D.M. Zhang, W.P. Fong and K.P. Fung, *Cancer Biol. Ther.*, 2009, **8**, 533–539.
- 277 X. Sun and W.N. Leung, *Photochem. Photobiol.*, 2002, **75**, 644–651.
- 278 W. Holzer, J. Shirdel, P. Zirak, A. Penzkofer, P. Hegemann, R. Deutzmann and E. Hochmuth, *Chem. Phys.*, 2005, **308**, 69–78.
- 279 M. Insińska-Rak and M. Sikorski, *Chem. Eur. J.*, 2014, **20**, 15280–15291.
- 280 H. Görner and H. Go, *J. Photochem. Photobiol. B.*, 2007, **87**, 73–80.
- 281 V. Massey, *J. Biol. Chem.*, 1994, **269**, 22459–22462.
- 282 I. Ahmad and F. H. M. Vaid, *Flavins photochemistry and photobiology, Comprehensive series in photochemical and photobiological sciences*, RSC Publishing, 2006.
- 283 W.A. Massad, S. Bertolotti and N.A. Garcia, *Photochem. Photobiol.*, 2004, **79**, 428–433.
- 284 C. Castillo, S. Criado, M. Diaz and N.A. Garcia, *Dye. Pigment.*, 2007, **72**, 178–184.
- 285 C. Lu, W. Lin, W. Wang, Z. Han, Z. Zheng and S. Yao, *Radiat. Phys. Chem.*, 2000, **59**, 61–66.
- 286 X. Shu, V. Lev-Ram, T.J. Deerinck, Y. Qi, E.B. Ramko, M.W. Davidson, Y. Jin, M.H. Ellisman and R.Y. Tsien, *PLoS Biol.*, 2011, **9**, e1001041.
- 287 R. Ruiz-González, A.L. Cortajarena, S.H. Mejias, M. Agut, S. Nonell and C. Flors, *J. Am. Chem. Soc.*, 2013, **135**, 9564–9567.
- 288 F.M. Pimenta, R.L. Jensen, T. Breitenbach, M. Etzerodt and P.R. Ogilby, *Photochem. Photobiol.*, 2013, **89**, 1116–1126.
- 289 A.S. Mishin, V.V. Belousov, K.M. Solntsev and K.A. Lukyanov, *Curr. Opin. Chem. Biol.*, 2015, **27**, 1–9.
- 290 A. Mukherjee and C. M. Schroeder, *Curr. Opin. Biotechnol.*, 2015, **31**, 16–23.
- 291 A.M. Buckley, J. Petersen, A.J. Roe, G.R. Douce and J.M. Christie, *Curr. Opin. Chem. Biol.*, 2015, **27**, 39–45.
- 292 A.P. Ryumina, E.O. Serebrovskaya, M.V. Shirmanova, L.B. Snopova, M.M. Kuznetsova, I.V. Turchin, N.I. Ignatova, N.V. Klementieva, A.F. Fradkov, B.E. Shakhov, E.V. Zagaynova, K.A. Lukyanov and S.A. Lukyanov, *Biochim. Biophys. Acta*, 2013, **1830**, 5059–67.
- 293 Y. B. Qi, E. J. Garren, X. Shu, R.Y. Tsien and Y. Jin, *Proc. Natl. Acad. Sci. U. S. A.*, 2012, **109**, 7499–504.
- 294 J.Y. Lin, S.B. Sann, K. Zhou, S. Nabavi, C.D. Proulx, R. Malinow, Y. Jin and R.Y. Tsien, *Neuron*, 2013, **79**, 241–253.
- 295 J. Torra, A. Burgos-Caminal, S. Endres, M. Wingen, T. Drepper, T. Gensch, R. Ruiz-González and S. Nonell, *Photochem. Photobiol. Sci.*, 2015, **14**, 280–287.
- 296 M. Westberg, L. Holmegaard, F. M. Pimenta, M. Etzerodt and P.R. Ogilby, *J. Am. Chem. Soc.*, 2015, **137**, 1632–1642.
- 297 A. M. Romo, *Les plantes medicinals dels paisos catalans*, Centre excursionista de Barcelona, 1997.

- 298 A. C. Giese, *Photochem. Photobiol. Rev.*, 1980, **5**, 229–255.
- 299 P. López-Chicón, M.P. Paz-Cristobal, A. Rezusta, C. Aspiroz, M. Royo-Cañas, E. Andres-Ciriano, Y. Gilaberte, M. Agut and S. Nonell, *Photochem. Photobiol. Sci.*, 2012, **11**, 1099–1107.
- 300 M. Zeisser-Labouèbe, N. Lange, R. Gurny and F. Delie, *Int. J. Pharm.*, 2006, **326**, 174–181.
- 301 J. Comas-Barceló, B. Rodríguez-Amigo, S. Abbruzzetti, P. del Rey-Puech, M. Agut, S. Nonell and C. Viappiani, *RSC Adv.*, 2013, **3**, 17874–17879.
- 302 B. Rodríguez-Amigo, P. Delcanale, G. Rotger, J. Juárez-Jiménez, S. Abbruzzetti, A. Summer, M. Agut, F. J. Luque, S. Nonell and C. Viappiani, *J. Dairy Sci.*, 2015, **98**, 89–94.
- 303 K. R. Downum and J. Wen, *ACS Symposium Ser. Light-Activated Pest Control*, 1995, **616**, 135–143.
- 304 C. Darwin, *The origin of species*, Encyclopedia Britannica, 1952.
- 305 J.M.M. Edwards and U. Weiss, *Phytochemistry*, 1974, **13**, 1597–1602.
- 306 E. Oliveros, P. Suardi-Murasecco, T. Aminian-Saghafi, A. M. Braun, H. Hanseu and H.J. Hansen, *Helv. Chim. Acta*, 1991, **74**, 79–90.
- 307 R. Schmidt, C. Tanielian, R. Dunsbach, C. Wolff and C. Womb, *J. Photochem. Photobiol. A Chem.*, 1994, **79**, 11–17.
- 308 M.F. Elsebai, M. Saleem, M. V Tejesvi, M. Kajula, S. Mattila, M. Mehiri, A. Turpeinen and A.M. Pirttilä, *Nat. Prod. Rep.*, 2014, **31**, 628–45.
- 309 G. Bucher, R. Bresolí-Obach, C. Brosa, C. Flors, J. G. Luis, T.A. Grillo and S. Nonell, *Phys. Chem. Chem. Phys.*, 2014, **16**, 18813–18820.
- 310 D. Hölscher and B. Schneider, *Phytochemistry*, 1997, **45**, 87–91.
- 311 F. Otálvaro, J. Nanclares, L. E. Vásquez, W. Quiñones, F. Echeverri, R. Arango and B. Schneider, *J. Nat. Prod.*, 2007, **70**, 887–890.
- 312 F. Echeverri, F. Torres, W. Quiñones, G. Escobar and R. Archbold, *Phytochem. Rev.*, 2010, **11**, 1–12.
- 313 T. Kamo, N. Kato, N. Hirai, M. Tsuda, D. Fujioka and H. Ohigashi, *Biosci. Biotechnol. Biochem.*, 1998, **62**, 95–101.
- 314 R. Cooke and R. Thomas, *Aust. J. Chem.*, 1975, **28**, 1053.
- 315 J. G. Luis, W. Quiñones, F. Echeverri, T. A. Grillo, M. P. Kishi, F. Garcia-Garcia, F. Torres and G. Cardona, *Phytochemistry*, 1996, **41**, 753–757.
- 316 D. Hölscher and B. Schneider, *Phytochemistry*, 1999, **50**, 155–161.
- 317 G. Dora, J. Edwards and W. Campbell, *Planta Med.*, 1990, **56**, 569–569.
- 318 J. Fang, C. Paetz, D. Hölscher, T. Munde and B. Schneider, *Phytochem. Lett.*, 2011, **4**, 203–208.
- 319 R. Brkljača and S. Urban, *J. Nat. Prod.*, 2015, **78**, 1600–1608.
- 320 S. Opitz, D. Hölscher, N.J. Oldham, S. Bartram and B. Schneider, *J. Nat. Prod.*, 2002, **65**, 1122–1130.
- 321 J.M.M. Edwards and U. Weiss, *Phytochemistry*, 1974, **13**, 1597–1602.
- 322 G. Dora, X.Q. Xie and J.M. Edwards, *J. Nat. Prod.*, 1993, **56**, 2029–2033.
- 323 S. Urban, M.A. Timmers, R. Brkljača and J.M. White, *Phytochemistry*, 2013, **95**, 351–359.
- 324 R. Thomas, *J. Chem. Soc. D Chem. Commun.*, 1971, **153**, 739–740.
- 325 D.A. Dias, D.J. Goble, C.A. Silva and S. Urban, *J. Nat. Prod.*, 2009, **72**, 1075–1080.
- 326 M. DellaGreca, L. Previtiera and A. Zarrelli, *Tetrahedron*, 2009, **65**, 8206–8208.
- 327 J.M. Edwards, M. Mangion, J.B. Anderson, M. Rapposch and G. Hite, *Tetrahedron Lett.*, 1979, **20**, 4453–4456.
- 328 F. Otálvaro, H. Görls, D. Hölscher, B. Schmitt, F. Echeverri, W. Quiñones and B. Schneider, *Phytochemistry*, 2002, **60**, 61–6.
- 329 K.R. Downum, *New Phytol.*, 1992, **122**, 401–420.
- 330 A. Lazzaro, M. Corominas, C. Martí, C. Flors, L.R. Izquierdo, T.A. Grillo, J.G. Luis and S. Nonell, *Photochem. Photobiol. Sci.*, 2004, **3**, 706–710.
- 331 C. Flors, C. Prat, R. Suau, F. Najera and S. Nonell, *Photochem. Photobiol.*, 2005, **81**, 120–124.
- 332 C. Flors, P.R. Ogilby, J.G. Luis, T.A. Grillo, L.R. Izquierdo, P.L. Gentili, L. Bussotti and S. Nonell, *Photochem. Photobiol.*, 2006, **82**, 95–103.
- 333 R. Bresolí-Obach, Master Thesis: Fotociclació de 9-fenilfenalenones, Universitat Ramon Llull, 2014.

- 334 R. Bresolí-Obach and S. Nonell, *Afinidad*, 2016, **574**, 90–95.
- 335 D.G. Whitten and W.E. Punch, *Mol. Photochem.*, 1970, **2**, 77.
- 336 P.J. Wagner, P.A. Kelso, A.E. Kemppainen, A. Haug and D.R. Graber, *Mol. Photochem.*, 1970, **2**, 81–85.
- 337 F.R. Stermitz, D.E. Nicodem, V.P. Muralidharan and C.M. O'Donnell, *Mol. Photochem.*, 1970, **2**, 87.
- 338 P.J. Wagner and A.E. Kemppainen, *J. Am. Chem. Soc.*, 1968, **90**, 5898–5899.
- 339 J.C. Scaiano, M.J. Perkins, J.W. Sheppard, M. S. Platz and R.L. Barcus, *J. Photochem.*, 1983, **21**, 137–147.
- 340 T. Wismontski-Knittel and T. Kilp, *J. Phys. Chem.*, 1984, **88**, 110–115.
- 341 J.C. Netto-Ferreira, W. J. Leigh and J. C. Scaiano, *J. Am. Chem. Soc.*, 1985, **107**, 2617–2622.
- 342 G. Bucher, *J. Phys. Chem. A*, 2008, **112**, 5411–5417.
- 343 W.J. Leigh, J.A.H. Banisch and M.S. Workentin, *J. Chem. Soc. Chem. Commun.*, 1993, 988–990.
- 344 J.N. Moorthy, W.S. Patterson and C. Bohne, *J. Am. Chem. Soc.*, 1997, **119**, 11094–11095.
- 345 J.N. Moorthy, S.L. Monahan, R.B. Sunoj, J. Chandrasekhar and C. Bohne, *J. Am. Chem. Soc.*, 1999, **121**, 3093–3103.
- 346 D. Ng, Z. Yang and M.A. Garcia-Garibay, *Tetrahedron Lett.*, 2001, **42**, 9113–9116.
- 347 S. Samanta, B.K. Mishra, T.C.S. Pace, N. Sathyamurthy, C. Bohne and J.N. Moorthy, *J. Org. Chem.*, 2006, **71**, 4453–4459.
- 348 O. Anamimoghadam, M.D. Symes, C. Busche, D.L. Long, S. T. Caldwell, C. Flors, S. Nonell, L. Cronin and G. Bucher, *Org. Lett.*, 2013, **15**, 2970–2973.
- 349 J.G. Luis, W.Q. Fletcher, F. Echeverri and T.A. Grillo, *Tetrahedron*, 1994, **50**, 10963–10970.
- 350 L.I. Rosquete, M.G. Cabrera-Serra, J.E. Piñero, P. Martín-Rodríguez, L. Fernández-Pérez, J.G. Luis, G. McNaughton-Smith and T. Abad-Grillo, *Bioorg. Med. Chem.*, 2010, **18**, 4530–4.
- 351 R. Boch, C. Bohne, J.C. Netto-Ferreira and J. C. Scaiano, *Can. J. Chem.*, 1991, **69**, 2053–2058.
- 352 C. Reichardt, *Chem. Rev.*, 1994, **94**, 2319–2358.
- 353 C. Reichardt, *Solvents and Solvent Effects in Organic Chemistry*, Wiley-VCH Verlag GmbH, 2002.
- 354 F.M. Page and J. Kay, *Nature*, 1963, **199**, 483–483.
- 355 D.N. Dhar, *Chem. Rev.*, 1967, **67**, 611–622.
- 356 M. Stevens and S. Merilaita, *Philos. Trans. R. Soc. B Biol. Sci.*, 2009, **364**, 423–427.
- 357 W. Szymański, J.M. Beierle, H.A.V. Kistemaker, W.A. Velema and B.L. Feringa, *Chem. Rev.*, 2013, **113**, 6114–6178.
- 358 J. Broichhagen, J.A. Frank and D. Trauner, *Acc. Chem. Res.*, 2015, **48**, 1947–1960.
- 359 M. Russew and S. Hecht, *Adv. Mater.*, 2010, **22**, 3348–3360.
- 360 M. Irie, *Chem. Rev.*, 2000, **100**, 1685–1716.
- 361 J. Requejo-Isidro, *J. Chem. Biol.*, 2013, **6**, 97–120.
- 362 T.J. Chozinski, L.A. Gagnon and J.C. Vaughan, *FEBS Lett.*, 2014, **588**, 3603–3612.
- 363 M. El Gemayel, K. Börjesson, M. Herder, D. T. Duong, J.A. Hutchison, C. Ruzie, M. El Gemayel, K. Bo, G. Schweicher, A. Salleo, Y. Geerts, S. Hecht, E. Orgiu and P. Samori, *Nat. Commun.*, 2015, **6**, 6330.
- 364 K. Smaali, S. Karpe, P. Blanchard, D. Deresmes, S. Godey, A. Rochefort, J. Roncali, D. Vuillaume and C. Hc, *ACS Nano*, 2010, **4**, 2411–2421.
- 365 H. Moustroph, M. Stollenwerk and V. Bressau, *Angew. Chem. Int. Ed.*, 2016, **45**, 2016–2035.
- 366 S. Venkataramani, U. Jana, M. Dommaschk, F. D. Sönnichsen, F. Tuzcek and R. Herges, *Science*, 2013, **331**, 445–448.
- 367 C. Jin, R. Yan and J. Huang, *J. Mater. Chem.*, 2011, **21**, 17519–17525.
- 368 G. Mayer and A. Heckel, *Angew. Chem. Int. Ed.*, 2006, **45**, 4900–4921.
- 369 H. Bouas-Laurent and H. Dürr, *Pure Appl. Chem.*, 2001, **73**, 639–665.
- 370 J. García-Amorós and D. Velasco, *Beilstein J. Org. Chem.*, 2012, **8**, 1003–17.
- 371 D. H. Waldeck, *Chem. Rev.*, 1991, **91**, 415–436.
- 372 R. S. Becker and J. Michl, *J. Am. Chem. Soc. Commun.*, 1966, 5931–5933.

- 373 G. Berkovic, V. Krongauz and V. Weiss, *Chem. Rev.*, 2000, **100**, 1741–1753.
- 374 N. A. Murugan, S. Chakrabarti and H. Ågren, *J. Phys. Chem. B*, 2011, **115**, 4025–4032.
- 375 M. Irie, *Photochem Photobiol Sci.*, 2010, **9**, 1535–1542.
- 376 L.F.V. Pinto, S. Kundu, P. Brogueira, C. Cruz, S. N. Fernandes, A. Aluculesei and M.H. Godinho, *Langmuir*, 2011, **27**, 6330–6337.
- 377 Q. Shen, L. Wang, S. Liu, Y. Cao, L. Gan, X. Guo, L. Michael, Z. Shuai, Z. Liu and C. Nuckolls, *Adv. Mater.*, 2010, **22**, 3282–3287.
- 378 M. Sauer, *Proc. Natl. Acad. Sci.*, 2005, **102**, 9433–9434.
- 379 J. Buback, M. Kullmann, F. Langhojer, P. Nuernberger, R. Schmidt, F. Würthner and T. Brixner, *J. Am. Chem. Soc.*, 2010, **132**, 16510–16519.
- 380 J. Garcia-Amorós, M. Díaz-Lobo, S. Nonell and D. Velasco, *Angew. Chemie Int. Ed.*, 2012, **51**, 12820–12823.
- 381 S. Steinwand, T. Halbritter, D. Rastädter, J. M. Ortiz-Sánchez, I. Burghardt, A. Heckel and J. Wachtveitl, *Chem. Eur. J.*, 2015, **21**, 15720–15731.
- 382 F. Renth, J. Bahrenburg and F. Temps, *Photon-Working Switches*, Springer Japan, 2017.
- 383 O. Anamimoghadam, D.L. Long and G. Bucher, *RSC Adv.*, 2014, **4**, 56654–56657.
- 384 G. Bucher, R. Bresolí-Obach, C. Brosa, C. Flors, J. G. Luis, T. A. Grillo and S. Nonell, *Phys. Chem. Chem. Phys.*, 2014, **16**, 18813–18820.
- 385 P.J. Coelho, L.M. Carvalho, S. Abrantes, M.M. Oliveira, A.M.F. Oliveira-Campos and R. Guglielmetti, *Tetrahedron*, 2002, **58**, 9505–9511.
- 386 S.A. Ahmed, M. Tanaka, H. Ando, H. Iwamoto and K. Kimura, *European J. Org. Chem.*, 2003, **52**, 2437–2442.
- 387 W. Zhao and E. M. Carreira, *Org. Lett.*, 2011, **13**, 1609–1612.
- 388 M. Hu, S. Kawachi, M. Satoh, J. Komiyama, J. Watanabe, S. Kobatake and M. Irie, *J. Photochem Photobiol. A*, 2002, **150**, 131–141.
- 389 J.N. Moorthy, P. Venkatakishnan, S. Samanta and D.K. Kumar, *Org. Lett.*, 2007, **9**, 919–922.
- 390 M. Uchidal and M. Irie, *J. Am. Chem. Soc. Commun.*, 1993, **115**, 6442–6443.
- 391 M. Uchida and M. Irie, *Chem. Lett.*, 1995, 323–324.
- 392 S. Abbruzzetti, S. Bruno, S. Faggiano, E. Grandi, A. Mozzarelli and C. Viappiani, *Photochem. Photobiol. Sci.*, 2006, **5**, 1109.
- 393 M. Fujitsuka, O. Ito, T. Yamashiro, Y. Aso and T. Otsubo, *J. Phys. Chem. A*, 2000, **104**, 4876–4881.
- 394 R.A. McClelland, V.M. Kanagasabapathy and S. Steenken, *J. Am. Chem. Soc.*, 1988, **110**, 6913–6914.
- 395 A.H. Zewail, *Angew. Chem. Int. Ed.*, 2000, **39**, 2586–2631.
- 396 O. Stern and M. Volmer, *Phys. Zeitschrift*, 1919, **20**, 183–188.
- 397 M.J. Frisch, G.W. Trucks, H.B. Schlegel, G.E. Scuseria, M.A. Robb, J.R. Cheeseman, G. Scalmani, V. Barone, B. Mennucci, G.A. Petersson, H. Nakatsuji, M. Caricato, X. Li, H. P. Hratchian, A.F. Izmaylov, J. Bloino, G. Zheng, J.L. Sonnenberg, M. Hada, M. Ehara, K. Toyota, R. Fukuda, J. Hasegawa, M. Ishida, T. Nakajima, Y. Honda, O. Kitao, H. Nakai, T. Vreven, Montgomery, J.E. Peralta, F. Ogliaro, M. Bearpark, J.J. Heyd, E. Brothers, K.N. Kudin, V.N. Staroverov, R. Kobayashi, J. Normand, K. Raghavachari, A. Rendell, J.C. Burant, S.S. Iyengar, J. Tomasi, M. Cossi, N. Rega, J.M. Millam, M. Klene, J.E. Knox, J.B. Cross, V. Bakken, C. Adamo, J. Jaramillo, R. Gomperts, R.E. Stratmann, O. Yazyev, A.J. Austin, R. Cammi, C. Pomelli, J.W. Ochterski, R.L. Martin, K. Morokuma, V.G. Zakrzewski, G.A. Voth, P. Salvador, J.J. Dannenberg, S. Dapprich, A.D. Daniels, Ö. Farkas, J.B. Foresman, J.V. Ortiz, J. Cioslowski and D.J. Fox, Gaussian INC; 2009.
- 398 A. D. Becke, *J. Chem. Phys.*, 1993, **98**, 5648–5652.
- 399 M. Cossi, G. Scalmani, N. Rega and V. Barone, *J. Chem. Phys.*, 2002, **117**, 43–54.
- 400 G.C.R. Ellis-Davies, *Nat. Methods*, 2007, **4**, 619–628.
- 401 G. Mayer and A. Heckel, *Angew. Chemie Int. Ed.*, 2006, **45**, 4900–4921.
- 402 A.P. Pelliccioli and J. Wirz, *Photochem. Photobiol. Sci.*, 2002, **1**, 441–458.
- 403 J.H. Kaplan, B. Forbush and J. F. Hoffman, *Biochemistry*, 1978, **16**, 1929–35.
- 404 Y.V. Il'ichev, M.A. Schwörer and J. Wirz, *J. Am. Chem. Soc.*, 2004, **126**, 4581–4595.

- 405 R. Schmidt, D. Geissler, V. Hagen and J. Bendig, *J. Phys. Chem. A*, 2007, **111**, 5768–5774.
- 406 A. Barth, K. Hauser, W. Maentele, J.E.T. Corrie and D.R. Trentham, *J. Am. Chem. Soc.*, 1995, **117**, 10311–10316.
- 407 S. Walbert, W. Pfeleiderer and U.E. Steiner, *Helv. Chim. Acta*, 2001, **84**, 1601–1611.
- 408 B. Schade, V. Hagen, R. Schmidt, R. Herbrich, E. Krause, T. Eckardt and J. Bendig, *J. Org. Chem.*, 1999, **64**, 9109–9117.
- 409 T. Furuta, S.S.H. Wang, J.L. Dantzker, T.M. Dore, W.J. Bybee, E.M. Callaway, W. Denk and R.Y. Tsien, *Proc. Natl. Acad. Sci.*, 1999, **96**, 1193–1200.
- 410 M.J. Hansen, W.A. Velema, M.M. Lerch, W. Szymanski and B.L. Feringa, *Chem. Soc. Rev.*, 2015, **44**, 3358–3377.
- 411 M. Matsuzaki, G.C.R. Ellis-Davies, T. Nemoto, Y. Miyashita, M. Iino and H. Kasai, *Nat. Neurosci.*, 2001, **4**, 1086–1092.
- 412 K. Deisseroth, *Nat. Methods*, 2011, **8**, 26–29.
- 413 L. Fenno, O. Yizhar and K. Deisseroth, *Annu. Rev. Neurosci.*, 2011, **34**, 389–412.
- 414 S.S. Agasti, A.M. Laughney, R.H. Kohler and R. Weissleder, *Chem. Commun.*, 2013, **49**, 11050.
- 415 M.V. Westphal, M.A. Schafroth, R.C. Sarott, M.A. Imhof, C.P. Bold, P. Leippe, A. Dhopeswarkar, J.M. Grandner, V. Katritch, K. Mackie, D. Trauner, E.M. Carreira and J.A. Frank, *J. Am. Chem. Soc.*, 2017, **139**, 18206–18212.
- 416 J. Font, M. López-Cano, S. Notartomaso, P. Scarselli, P. Di Pietro, R. Bresolí-Obach, G. Battaglia, F. Malhaire, X. Rovira, J. Catena, J. Giraldo, J.-P. Pin, V. Fernández-Dueñas, C. Goudet, S. Nonell, F. Nicoletti, A. Llebaria and F. Ciruela, *Elife*, 2017, **6**, e23545.
- 417 K. Fukuhara, N. Miyata and S. Kamiya, *Tetrahedron Lett.*, 1990, **31**, 3743–3744.
- 418 P. Huang, J. Lin, X. Wang, Z. Wang, C. Zhang, M. He, K. Wang, F. Chen, Z. Li, G. Shen, D. Cui and X. Chen, *Adv. Mater.*, 2012, **24**, 5104–5110.
- 419 A. Nadler and C. Schultz, *Angew. Chemie*, 2013, **52**, 2408–2410.
- 420 Y. Hori and K. Kikuchi, *Curr. Opin. Chem. Biol.*, 2013, **17**, 644–50.
- 421 S. Mizukami, Y. Hori and K. Kikuchi, *Acc. Chem. Res.*, 2014, **47**, 247–56.
- 422 Q. Yan, S.L. Schwartz, S. Maji, F. Huang, C. Szent-Gyorgyi, D.S. Lidke, K.A. Lidke and M. P. Bruchez, *Chemphyschem*, 2014, **15**, 687–95.
- 423 J. Lippincott-Schwartz, *Science*, 2003, **300**, 87–91.
- 424 R. Hudson, M. Carcenac, K. Smith, L. Madden, O.J. Clarke, A. Pèlegri, J. Greenman and R.W. Boyle, *Br. J. Cancer*, 2005, **92**, 1442–1449.
- 425 S. Ohkuma and B. Poole, *Proc. Natl. Acad. Sci.*, 1978, **75**, 3327–3331.
- 426 S.S. Ghosh, P.M. Kao, A.W. McCue and H.L. Chappelle, *Bioconjug. Chem.*, 1990, **1**, 71–76.
- 427 M. Mitsunaga, M. Ogawa, N. Kosaka, L.T. Rosenblum, P.L. Choyke and H. Kobayashi, *Nat. Med.*, 2011, **17**, 1685–1691.
- 428 M. Kobayashi and Y. Chiba, *Anal. Biochem.*, 1994, **219**, 189–194.
- 429 <https://www.thermofisher.com/es/es/home/life-science/cell-analysis/cell-analysis-learning-center/molecular-probes-school-of-fluorescence/imaging-basics/labeling-your-samples/different-ways-to-add-fluorescent-labels.html>, Visited on: 8th March 2018.
- 430 T. Nakajima, K. Sato, H. Hanaoka, R. Watanabe, T. Harada, P. L. Choyke and H. Kobayashi, *BMC Cancer*, 2014, **14**, 389.
- 431 O. Planas, T. Gallavardin and S. Nonell, *Chem. Commun.*, 2015, **51**, 5586–5589.
- 432 K. Sato, R. Watanabe, H. Hanaoka, T. Harada, T. Nakajima, I. Kim, C. H. Paik, P. L. Choyke and H. Kobayashi, *Mol. Oncol.*, 2014, **8**, 620–632.
- 433 O. Planas, T. Gallavardin and S. Nonell, Unusual properties of asymmetric porphycenes, in *Handbook of Porphyrin Science*, Ed. R. Guillard, K.M. Smith and K.M. Kadish, Volume 41, 2016, 299–349.
- 434 O. Planas, D. Fernández-Llaneza, I. Nieves, R. Ruiz-Gonzalez, E. Lemp, A. L. Zanoocco and S. Nonell, *Phys. Chem. Chem. Phys.*, 2017, **19**, 25537–25543.
- 435 S. Kim and K.Y. Yi, *J. Org. Chem.*, 1986, **51**, 2613–2615.
- 436 F. Wilkinson, W.P. Helman and A.B. Ross, *J. Phys. Chem. Ref. Data*, 1993, **22**, 113–262.
- 437 R.W. Redmond and J.N. Gamlin, *Photochem. Photobiol.*, 1999, **70**, 391–475.
- 438 E.W. Hansen and C.A. Martiarena, *Rev. Invest. Agropecu.*, 1967, **4**, 81–113.

- 439 https://www.sib.gov.ar/archivos/thumbs/472x_20141222195840_Heterophyllaea_pustulata.jpg, Visited on: 18th March 2018.
- 440 S.C. Núñez-Montoya, A.M. Agnese and J.L. Cabrera, *J. Nat. Prod.*, 2006, **69**, 801–803.
- 441 S.C. Núñez-Montoya, A.M. Agnese, C. Pérez, I.N. Tiraboschi and J.L. Cabrera, *Phytomedicine*, 2003, **10**, 569–574.
- 442 M. Rajendran, *Photodiagnosis Photodyn. Ther.*, 2016, **13**, 175–187.
- 443 S.C. Núñez-Montoya, L.R. Comini, M. Sarmiento, C. Becerra, I. Albesa, G.A. Argüello and J.L. Cabrera, *J. Photochem. Photobiol. B Biol.*, 2005, **78**, 77–83.
- 444 L.R. Comini, S.C. Núñez-Montoya, M. Sarmiento, J.L. Cabrera and G.A. Argüello, *J. Photochem. Photobiol. A Chem.*, 2007, **188**, 185–191.
- 445 B.S. Konigheim, L.R. Comini, S. Grasso, J.J. Aguilar, J. Marioni, M.S. Contigiani and S.C. Núñez-Montoya, *Lat. Am. J. Pharm.*, 2012, **31**, 51–56.
- 446 J. Marioni, J.E. Arce, J.L. Cabrera, M.G. Paraje and S.C. Núñez-Montoya, *Pharm. Biol.*, 2016, **54**, 2791–2801.
- 447 J. Marioni, M.A. da Silva, J.L. Cabrera, S.C. Núñez-Montoya and M.G. Paraje, *Phytomedicine*, 2016, **23**, 1321–1328.
- 448 L.R. Comini, I.M. Fernandez, N.B.R. Vittar, S. C. Núñez-Montoya, J.L. Cabrera and V.A. Rivarola, *Phytomedicine*, 2011, **18**, 1093–1095.
- 449 G.A. O'Toole and R. Kolter, *Mol. Microbiol.*, 1998, **28**, 449–461.
- 450 D. Berry, E. Mader, T.K. Lee, D. Woebken, Y. Wang, D. Zhu, M. Palatinszky, A. Schintlmeister, M.C. Schmid, B.T. Hanson, N. Shterzer, I. Mizrahi, I. Rauch, T. Decker, T. Bocklitz, J. Popp, C.M. Gibson, P.W. Fowler, W.E. Huang and M. Wagner, *Proc. Natl. Acad. Sci.*, 2015, **112**, 194–203.
- 451 T. Shida, *Phys. Sci. Data*, 1988, **34**, 1–345.
- 452 W. Bors, *Biochim. Biophys. Acta*, 1979, **582**, 537–542.
- 453 L. Zhang, F. Gu, J. Chan, A. Wang, R. Langer and O. Farokhzad, *Clin. Pharmacol. Ther.*, 2008, **83**, 761–769.
- 454 V. J. Mohanraj and Y. Chen, *Trop. J. Pharm. Res.*, 2006, **5**, 561–573.
- 455 X. Huang, X. Teng, D. Chen, F. Tang and J. He, *Biomaterials*, 2010, **31**, 438–448.
- 456 K.L. Kelly, E. Coronado, L.L. Zhao and G.C. Schatz, *J. Phys. Chem. B*, 2003, **107**, 668–677.
- 457 I.I. Slowing, B.G. Trewyn, S. Giri and V.S.Y. Lin, *Adv. Funct. Mater.*, 2007, **17**, 1225–1236.
- 458 V. Mamaeva, C. Sahlgren and M. Lindén, *Adv. Drug Deliv. Rev.*, 2013, **65**, 689–702.
- 459 L.A. Lane, X. Qian and S. Nie, *Chem. Rev.*, 2015, **115**, 10489–10529.
- 460 W. Lin, *Chem. Rev.*, 2015, **115**, 10407–10409.
- 461 D. Bechet, P. Couleaud, C. Frochot, M.L.L. Viriot, F. Guillemain and M. Barberi-Heyob, *Trends Biotechnol.*, 2008, **26**, 612–621.
- 462 S. Perni, P. Prokopovich, J. Pratten, I. P. Parkin and M. Wilson, *Photochem. Photobiol. Sci.*, 2011, **10**, 712–720.
- 463 M. Qin, H.J. Hah, G. Kim, G. Nie, Y.E.K. Lee and R. Kopelman, *Photochem. Photobiol. Sci.*, 2011, **10**, 832–41.
- 464 F. Giuntini, F. Dumoulin, R. Daly, V. Ahsen, E. M. Scanlan, A.S.P. Lavado, J.W. Aylott, G.A. Rosser, A. Beeby and R.W. Boyle, *Nanoscale*, 2012, **4**, 2034–45.
- 465 E. Boix-Garriga, P. Acedo, A. Casadó, A. Villanueva, J.C. Stockert, M. Cañete, M. Mora, M.L. Sagristá and S. Nonell, *Nanotechnology*, 2015, **26**, 365104.
- 466 N. Husain, T.T. Ndou, A. Muñoz de la Peña and I.M. Warner, *Appl. Spectrosc.*, 1992, **46**, 652–658.
- 467 M.K. Khaing, Y. Yang, Y. Hu, M. Gomez, H. Du and H. Wang, *ACS Nano*, 2012, **6**, 1939–1947.
- 468 O. Planas, N. Macia, M. Agut, S. Nonell and B. Heyne, *J. Am. Chem. Soc.*, 2016, **138**, 2762–2768.
- 469 O. Planas, R. Bresolí-Obach, J. Nos, T. Gallavardin, R. Ruiz-González, M. Agut and S. Nonell, *Molecules*, 2015, **20**, 6284–6298.
- 470 E. Huynh and G. Zheng, *Nano Today*, 2014, **9**, 212–222.
- 471 J.F. Lovell, C.S. Jin, E. Huynh, H. Jin, C. Kim, J. L. Rubinstein, W.C.W. Chan, W. Cao, L.V. Wang and G. Zheng, *Nat. Mater.*, 2011, **10**, 324–332.
- 472 A. Jańczyk, E. Krakowska, G. Stochel and W. Macyk, *J. Am. Chem. Soc.*, 2006, **128**, 15574–15575.
- 473 R. Misra, S. Acharya and S.K. Sahoo, *Drug Discov. Today*, 2010, **15**, 842–50.

- 474 B.E. Smith, P.B. Roder, J.L. Hanson, S. Manandhar, A. Devaraj, D.E. Perea, W.J. Kim, A.L.D. Kilcoyne and P.J. Pauzauskie, *ACS Photonics*, 2015, **2**, 559–564.
- 475 R.D. Badley, W.T. Ford, F.J. McEnroe and R. A. Assink, *Langmuir*, 1990, **6**, 792–801.
- 476 W. Stöber, A. Fink and E. Bohn, *J. Colloid Interface Sci.*, 1968, **26**, 62–69.
- 477 E. M. Winyall, US1927120A1, 1971.
- 478 T. Yanagisawa, T. Shimizu, K. Kuroda and C. Kato, *Bull. Chem. Soc. Jpn.*, 1990, **63**, 988–992.
- 479 C.T. Kresge, M.E. Leonowicz, W.J. Roth, J.C. Vartuli and J.S. Beck, *Nature*, 1992, **359**, 710–712.
- 480 J.S. Beck, J.C. Vartuli, W.J. Roth, M.E. Leonowicz, C.T. Kresge, K.D. Schmitt, C.T.W. Chu, D.H. Olson, E.W. Sheppard, S.B. McCullen, J.B. Higgins and J.L. Schlenker, *J. Am. Chem. Soc.*, 1992, **114**, 10834–10843.
- 481 P. Kipkemboi, A. Fogden, V. Alfredsson and K. Flodström, *Langmuir*, 2001, **17**, 5398–5402.
- 482 D. Zhao, Q. Huo, J. Feng, B. F. Chmelka and G. D. Stucky, *J. Am. Chem. Soc.*, 1998, **120**, 6024–6036.
- 483 H.P. Lin and C.Y. Mou, *Acc. Chem. Res.*, 2002, **35**, 927–935.
- 484 F. Lu, S.H. Wu, Y. Hung and C.Y. Mou, *Small*, 2009, **5**, 1408–1413.
- 485 F. Tang, L. Li and D. Chen, *Adv. Mater.*, 2012, **24**, 1504–1534.
- 486 K.O. Yu, C.M. Grabinski, A.M. Schrand, R.C. Murdock, W. Wang, B. Gu, J.J. Schlager and S.M. Hussain, *J. Nanoparticle Res.*, 2009, **11**, 15–24.
- 487 L.M. Rossi, P.R. Silva, L.L.R. Vono, A.U. Fernandes, D.B. Tada and M.S. Baptista, *Langmuir*, 2008, **24**, 12534–12538.
- 488 V. Simon, C. Devaux, A. Darmon, T. Donnet, E. Thianot, M. Germain, J. Honnorat, A. Duval, A. Pottier, E. Borghi, L. Levy and J. Marill, *Photochem. Photobiol.*, 2010, **86**, 213–222.
- 489 T.Y. Ohulchanskyy, I. Roy, L.N. Goswami, Y. Chen, E.J. Bergoy, R.K. Pandey, A.R. Oseroff and P.N. Prasad, *Nano Lett.*, 2007, **7**, 2835–2842.
- 490 B.S. Pattni and V.P. Torchilin, *Targeted Drug Delivery: Concepts and Design*, RSC Publishing, 2015.
- 491 [Http://www.basf.com/tw/en/we-create-chemistry/creating-chemistry-magazine/quality-of-life/pioneer-thinker-then-and-now-methylene-blue.html](http://www.basf.com/tw/en/we-create-chemistry/creating-chemistry-magazine/quality-of-life/pioneer-thinker-then-and-now-methylene-blue.html) Visited on: 18th March 2018.
- 492 D. Claus, *World J. Microbiol. Biotechnol.*, 1992, **8**, 451–452.
- 493 W.B. Wendel, *J. Clin. Invest.*, 1939, **18**, 179–185.
- 494 J.P. Tardivo, A. Del Giglio, C.S. de Oliveira, D. S. Gabrielli, H.C. Junqueira, D.B. Tada, D. Severino, R. de Fátima-Turchiello and M.S. Baptista, *Photodiagnosis Photodyn. Ther.*, 2005, **2**, 175–191.
- 495 H.C. Junqueira, D. Severino, L.G. Dias, M.S. Gugliotti and M.S. Baptista, *Phys. Chem. Chem. Phys.*, 2002, **4**, 2320–2328.
- 496 M. Wainwright, D.A. Phoenix, M. Gaskell and B. Marshall, *J. Antimicrob. Chemother.*, 1999, **44**, 823–825.
- 497 V. Klepac-Ceraj, N. Patel, X. Song, C. Holewa, C. Patel, R. Kent, M.M. Amiji and N.S. Soukos, *Lasers Surg. Med.*, 2011, **43**, 600–606.
- 498 S.H. Siddiqui, K.H. Awan and F. Javed, *Photodiagnosis Photodyn. Ther.*, 2013, **10**, 632–643.
- 499 A. Gollmer, A. Felgenträger, W. Bäuml, T. Maisch and A. Späth, *Photochem. Photobiol. Sci.*, 2015, **14**, 335–351.
- 500 M. Wainwright, *Int. J. Antimicrob. Agents*, 2000, **16**, 381–394.
- 501 R.H. Young, R.L. Martin, D. Feriozi, D. Brewer and R. Kayser, *Photochem. Photobiol.*, 1973, **17**, 233–244.
- 502 B.M. Monroe, *J. Phys. Chem.*, 1977, **81**, 1861–1864.
- 503 K.K. Iu and J. Kerry Thomas, *J. Photochem. Photobiol. A Chem.*, 1993, **71**, 55–60.
- 504 B. Cojocar, M. Laferrière, E. Carbonell, V. Parvulescu, H. García and J.C. Scaiano, *Langmuir*, 2008, **24**, 4478–4481.
- 505 K. Ghnem, DE32584, 1882.
- 506 E. Gandin, Y. Lion and A. Van de Vorst, *Photochem. Photobiol.*, 1983, **37**, 271–278.
- 507 B.F. Minaev, S. Knuts and H. Ågren, *Chem. Phys.*, 1994, **181**, 15–28.
- 508 K.N. Solovov and E.A. Borisevich, *Physicochem. Uspekhi*, 2005, **48**, 231–253.

- 509 M. Rae, F. Perez-Balderas, C. Baleizão, A. Fedorov, J.A.S. Cavaleiro, A.C. Tomé and M. N. Berberan-Santos, *J. Phys. Chem. B*, 2006, **110**, 12809–12814.
- 510 J.J.M. Lamberts and D.C. Neckers, *Tetrahedron*, 1985, **41**, 2183–2190.
- 511 G. Amescua, A. Arboleda, N. Nikpoor, H. Durkee, N. Relhan, M.C. Aguilar, H.W. Flynn, D. Miller and J.M. Parel, *Cornea*, 2017, **36**, 1141–1144.
- 512 E. Panzarini, V. Inguscio, G.M. Fimia and L. Dini, *PLoS One*, 2014, **9**, e105778.
- 513 R.P. Feenstra and S.C. Tseng, *Ophthalmology*, 1992, **99**, 605–617.
- 514 R.P. Feenstra and S.C. Tseng, *Acta Ophthalmol.*, 1992, **110**, 984–93.
- 515 N. Sugita, K. Kawabata, K. Sasaki, I. Sakata and S. Umemura, *Bioconjug. Chem.*, 2007, **18**, 866–873.
- 516 H. Wang, P. Agarwal, S. Zhao, J. Yu, X. Lu and X. He, *Biomaterials*, 2016, **97**, 62–73.
- 517 I. Postiglione, A. Chiaviello and G. Palumbo, *Cancers*, 2011, **3**, 2597–2629.
- 518 M.F. Zuluaga and N. Lange, *Curr. Med. Chem.*, 2008, **15**, 1655–1673.
- 519 C. M. Peterson, J.M. Lu, Z.W. Gu, J.G. Shiah, K. Lythgoe, C.A. Peterson, R.C. Straight and J. Kopecek, *J. Soc. Gynecol. Investig*, 1995, **2**, 772–777.
- 520 S.N. Datta, R. Allman, C. Loh, M. Mason and P.N. Matthews, *Br. J. Cancer*, 1997, **76**, 312–317.
- 521 M. Nonaka, H. Ikeda, T. Inokuchi, Y. Nonaka, A. Nanashima, T. Nonaka, M. Uehara, H. Isomoto, T. Abo, T. Nagayasu, M. Nonaka, H. Ikeda and T. Inokuchi, *Cancer Lett.*, 2002, **184**, 171–178.
- 522 E. Crescenzi, A. Chiaviello, G. Canti, E. Reddi, B.M. Veneziani and G. Palumbo, *Mol. Cancer Ther.*, 2006, **5**, 776–785.
- 523 E. Crescenzi, L. Varriale, M. Lovino, A. Chiaviello, B.M. Veneziani and G. Palumbo, *Mol. Cancer Ther.*, 2004, **3**, 537–544.
- 524 R. Ge, J.C. Ahn, J.I. Shin, C.W. Bahk, P. He and P.S. Chung, *Photomed. Laser Surg.*, 2011, **29**, 155–160.
- 525 A. Weyergang, P.K. Selbo and K. Berg, *Biochim. Biophys. Acta*, 2013, **1830**, 2659–2670.
- 526 O.A. Bamodu, W.C. Huang, D.T.W. Tzeng, A. Wu, L.S. Wang, C.T. Yeh and T.Y. Chao, *Cancer Lett.*, 2015, **364**, 125–134.
- 527 J.F. Lovell and G. Zheng, *J. Innov. Opt. Health Sci.*, 2008, **1**, 45–61.
- 528 A.M. Bugaj, *Photochem. Photobiol. Sci.*, 2011, **10**, 1097–1109.
- 529 C. Schweitzer and R. Schmidt, *Chem. Rev.*, 2003, **103**, 1685–1758.
- 530 S. Jayaraman, D.L. Gantz and O. Gursky, *Biophys. J.*, 2005, **88**, 2907–2918.
- 531 C.E. Matz and A. Jonas, *J. Biol. Chem.*, 1982, **257**, 4535–4540.
- 532 T. Förster, *Ann. Phys.*, 1948, **437**, 55–75.
- 533 M.R. Wasielewski, *Chem. Rev.*, 1992, **92**, 435–461.
- 534 P. Piotrowiak, *Chem. Soc. Rev.*, 1999, **28**, 143–150.
- 535 N. Noguchi, H. Yamashita, N. Gotoh, Y. Yamamoto, R. Numano and E. Niki, *Free Radic. Biol. Med.*, 1998, **24**, 259–268.
- 536 T.D. Poulsen, P.R. Ogilby and K.V. Mikkelsen, *J. Phys. Chem. A*, 1998, **102**, 8970–8973.
- 537 R. Schmidt, F. Shafii and M. Hild, *J. Phys. Chem. A*, 1999, **103**, 2599–2605.
- 538 R. Schmidt and E. Afshari, *J. Phys. Chem.*, 1990, **94**, 4377–4378.
- 539 A.P. Losev, I.N. Nichiporovich, I.M. Byteva, N.N. Drozdov and I.F. Al Jghami, *Chem. Phys. Lett.*, 1991, **181**, 45–50.
- 540 A.P. Darmany, *Chem. Phys. Lett.*, 1993, **215**, 477–482.
- 541 X. Ragàs, A. Gallardo, Y. Zhang, W. Massad, C.D. Geddes and S. Nonell, *J. Phys. Chem. C*, 2011, **115**, 16275–16281.
- 542 R. Toftegaard, J. Arnbjerg, K. Daasbjerg, P.R. Ogilby, A. Dmitriev, D.S. Sutherland and L. Poulsen, *Angew. Chem. Int. Ed.*, 2008, **47**, 6025–6027.
- 543 [Http://www.hamamatsu.com/resources/pdf/etd/PMT_handbook_v3aE-Chapter4.pdf](http://www.hamamatsu.com/resources/pdf/etd/PMT_handbook_v3aE-Chapter4.pdf), Visited on: 26th March 2018.
- 544 [Http://www.euromillones.com/euromillions.asp](http://www.euromillones.com/euromillions.asp), Visited on: 2nd April 2018.
- 545 J.W. Snyder, I. Zebger, Z. Gao, L. Poulsen, P. K. Frederiksen, E. Skovsen, S.P. McIlroy, M. Klinger, L.K. Andersen and P.R. Ogilby, *Acc. Chem. Res.*, 2004, **37**, 894–901.

- 546 M. Scholz, R. Dēdic, J. Hála and S. Nonell, *EUCMOS XXXI*, 2013, **1044**, 303–307.
- 547 J. Zhang, R.E. Campbell, A.Y. Ting and R.Y. Tsien, *Nat. Rev. Mol. Cell Biol.*, 2002, **3**, 906–918.
- 548 E.C. Jensen, *Anat. Rec. Adv. Integr. Anat. Evol. Biol.*, 2012, **295**, 2031–2036.
- 549 J. Mérian, J. Gravier, F. Navarro and I. Texier, *Molecules*, 2012, **17**, 5564–5591.
- 550 X. He, J. Gao, S. S. Gambhir and Z. Cheng, *Trends Mol. Med.*, 2010, **16**, 574–583.
- 551 X. Li, Y. Qin, C. Liu, S. Jiang, L. Xiong and Q. Sun, *Food Chem.*, 2016, **199**, 356–363.
- 552 Y. Wei, K.J.M. Bishop, J. Kim, S. Soh and B.A. Grzybowski, *Angew. Chemie Int. Ed.*, 2009, **48**, 9477–9480.
- 553 G.T. Hermanson, *Bioconjugate Techniques*, Elsevier, 2013.
- 554 Y.-E. Koo Lee and R. Kopelman, *Meth. Enzym.*, 2012, **218**, 419–470.
- 555 Y. Cao, Y.E. Koo, S.M. Koo and R. Kopelman, *Photochem. Photobiol.*, 2005, **81**, 1489–1498.
- 556 [Http://www.thermofisher.com/order/catalog/product/S36002](http://www.thermofisher.com/order/catalog/product/S36002), Visited on: 26th March 2018.
- 557 I. Johnson, W.Y. Leung, J. Liu and R. Patch, *US2005/0214807 A1*, 2005.
- 558 K. Tanaka, T. Miura, N. Umezawa, Y. Urano, K. Kikuchi, T. Higuchi and T. Nagano, *J. Am. Chem. Soc.*, 2001, **123**, 2530–2536.
- 559 S.K. Pedersen, J. Holmehave, F.H. Blaikie, A. Gollmer, T. Breitenbach, H.H. Jensen and P.R. Ogilby, *J. Org. Chem.*, 2014, **79**, 3079–3087.
- 560 S. Kim, M. Fujitsuka and T. Majima, *J. Phys. Chem. B*, 2013, **117**, 13985–13992.
- 561 M. Marazzi, V. Besancenot, H. Gattuso, H.P. Lassalle, S. Grandemange and A. Monari, *J. Phys. Chem. B*, 2017, **121**, 7586–7592.
- 562 H. Lin, Y. Shen, D. Chen, L. Lin, B.C. Wilson, B. Li and S. Xie, *J. Fluoresc.*, 2012, **23**, 41–47.
- 563 K. Welsler, M.D.A. Perera, J.W. Aylott and W.C. Chan, *Chem. Commun.*, 2009, 6601–6603.
- 564 N. Barbero, E. Barni, C. Barolo, P. Quagliotto, G. Viscardi, L. Napione, S. Pavan and F. Bussolino, *Dye. Pigment.*, 2009, **80**, 307–313.
- 565 J.M. Beechem and L. Brand, *Annu. Rev. Biochem.*, 1985, **54**, 43–71.
- 566 J.R. Lakowicz, E. Gratton, H. Cherek, B.P. Maliwal and G. Laczko, *J. Biol. Chem.*, 1984, **259**, 10967–10972.
- 567 M. Bardhan, J. Chowdhury and T. Ganguly, *J. Photochem. Photobiol. B Biol.*, 2011, **102**, 11–19.
- 568 E.J. Olson and P. Bühlmann, *J. Org. Chem.*, 2011, **76**, 8406–8412.
- 569 X. Ragàs, A. Jiménez-Banzo, D. Sanchez-Garcia, X. Batllori, S. Nonell and D. Sánchez-García, *Chem. Commun.*, 2009, **20**, 2920–2922.
- 570 R. Ruiz-González, J.H. White, M. Agut, S. Nonell and C. Flors, *Photochem. Photobiol. Sci.*, 2012, **11**, 1411–1413.
- 571 R. Ruiz-González, J.H. White, A.L. Cortajarena, M. Agut, S. Nonell and C. Flors, *Progress in Biomedical Optics and Imaging - Proceedings of SPIE*, 2013, **8596**, 1–7.
- 572 K. Berg, A. Weyergang, M. Vikdal and P.S. Maria-Berstad, *Photodiagnosis Photodyn. Ther.*, 2011, **8**, 155–156.
- 573 M. Wagner, P. Weber, T. Bruns, W.S.L. Strauss, R. Wittig and H. Schneckenburger, *Int. J. Mol. Sci.*, 2010, **11**, 956–966.
- 574 D. Gao, R.R. Agayan, H. Xu, M.A. Philbert and R. Kopelman, *Nano Lett.*, 2006, **6**, 2383–2386.
- 575 H.K. Yoon, X. Lou, Y. Chen, Y.E. Koo Lee, E. Yoon and R. Kopelman, *Chem. Mater.*, 2014, **26**, 1592–1600.
- 576 B.A. Lindig, M.A.J. Rodgers and A.P. Schaap, *J. Am. Chem. Soc.*, 1980, **102**, 5590–5593.
- 577 M.S. Oliveira, D. Severino, F.M. Prado, J.P.F. Angeli, F.D. Motta, M.S. Baptista, M.H.G. Medeiros and P. Di Mascio, *Photochem. Photobiol. Sci.*, 2011, **10**, 1546–1555.
- 578 D. Kessel and M. Price, *Photochem. Photobiol.*, 2012, **88**, 717–720.
- 579 X.D. Wang, Z.X. Shen, T. Sang, X.B. Cheng, M.F. Li, L.Y. Chen and Z.S. Wang, *J. Colloid Interface Sci.*, 2010, **341**, 23–29.
- 580 C.A. Schneider, W.S. Rasband and K.W. Eliceiri, *Nat. Methods*, 2012, **9**, 671–675.
- 581 J. Schindelin, I. Arganda-Carreras, E. Frise, V. Kaynig, M. Longair, T. Pietzsch, S. Preibisch, C. Rueden, S. Saalfeld, B. Schmid, J.-Y. Tinevez, D.J. White, V. Hartenstein, K. Eliceiri, P. Tomancak and A. Cardona, *Nat. Methods*, 2012, **9**, 676–682.
- 582 B. Neises and W. Steglich, *Angew. Chemie Int. Ed. English*, 1978, **17**, 522–524.

- 583 M. Nemoto, H. Kokubun and M. Koizumi, *Bull. Chem. Soc. Jpn.*, 1969, **42**, 2464–2470.
- 584 M.A.J. Rodgers and P.T. Snowden, *J. Am. Chem. Soc.*, 1982, **104**, 5541–5543.
- 585 F. Wilkinson, W.P. Helman and A.B. Ross, *J. Phys. Chem. Ref. Data*, 1995, **24**, 663–677.
- 586 R.W. Redmond and J.N. Gamlin, *Photochem. Photobiol.*, 1999, **70**, 391–475.
- 587 H.A. Benesi and J.H. Hildebrand, *J. Am. Chem. Soc.*, 1949, **71**, 2703–2707.
- 588 F.M. Pimenta, R.L. Jensen, T. Breitenbach, M. Etzerodt and P.R. Ogilby, *Photochem. Photobiol.*, 2013, **89**, 1116–1126.
- 589 H. Kotani, K. Ohkubo and S. Fukuzumi, *J. Am. Chem. Soc.*, 2004, **126**, 15999–16006.
- 590 L. Crovetto and S.E. Braslavsky, *J. Phys. Chem.*, 2006, **110**, 7307–7315.
- 591 Y. Barbieri, W.A. Massad, D.J. Díaz, J. Sanz, F. Amat-Guerri and N.A. García, *Chemosphere*, 2008, **73**, 564–571.
- 592 J. Baier, T. Maisch, M. Maier, E. Engel, M. Landthaler and W. Bäuml, *Biophys. J.*, 2006, **91**, 1452–1459.
- 593 D.C. Neckers, *J. Photochem. Photobiol. A Chem.*, 1989, **47**, 1–29.
- 594 Y.Y. He, S.E. Council, L. Feng, M.G. Bonini and C.F. Chignell, *Photochem. Photobiol.*, 2008, **84**, 69–74.
- 595 I.B.C. Matheson and J. Lee, *Chem. Phys. Lett.*, 1970, **7**, 475–476.
- 596 P.B. Merkel and D.R. Kearns, *Chem. Phys. Lett.*, 1971, **12**, 120–122.
- 597 P. Di Mascio, M.H.G. Medeiros, H. Sies, S. Bertolotti, S.E. Braslavsky, D. Piló-Veloso, B.H.L.N. Sales, E. Magalhães, R. Braz-Filho and E.J.H. Bechara, *J. Photochem. Photobiol. B Biol.*, 1997, **38**, 169–173.
- 598 R.H. Young, D. Brewer and R.A. Keller, *J. Am. Chem. Soc.*, 1973, **95**, 375–379.
- 599 A.L. Zanocco, G. Gunther, E. Lemp and J.R. de la Fuente, *Photochem. Photobiol.*, 1998, **68**, 487–493.
- 600 E.L. Clennan and M.E. Mehrsheikh-Mohammadi, *J. Am. Chem. Soc.*, 1984, **106**, 7112–7118.
- 601 G. Günther, E. Lemp and A.L. Zanocco, *Boletín Soc. Chil. Quim.*, 2000, **45**, 637–644.
- 602 J. Yu, J. Chen, C. Li, X. Wang, B. Zhang and H. Ding, *J. Phys. Chem. B*, 2004, **108**, 2781–2783.
- 603 J.M. Burns, W.J. Cooper, J.L. Ferry, D.W. King, B.P. DiMento, K. McNeill, C.J. Miller, W.L. Miller, B.M. Peake, S.A. Rusak, A.L. Rose and T.D. Waite, *Aquat. Sci.*, 2012, **74**, 683–734.
- 604 A. Gomes, E. Fernandes and J.L.F.C. Lima, *J. Biochem. Biophys.*, 2005, **65**, 45–80.
- 605 X. Chen, F. Wang, J.Y. Hyun, T. Wei, J. Qiang, X. Ren, I. Shin and J. Yoon, *Chem. Soc. Rev.*, 2016, **45**, 2976–3016.
- 606 R.R. Nazarewicz, A. Bikineyeva and S.I. Dikalov, *J. Biomol. Screen.*, 2013, **18**, 498–503.
- 607 M. Price, J.J. Reiners, A.M. Santiago and D. Kessel, *Photochem. Photobiol.*, 2009, **85**, 1177–1181.
- 608 A.S. Keston and R. Brandt, *Anal. Biochem.*, 1965, **11**, 1–5.
- 609 X. Chen, Z. Zhong, Z. Xu, L. Chen and Y. Wang, *Free Radic. Res.*, 2010, **44**, 587–604.
- 610 I. Kalousek, D. Jandová and Z. Vodrážka, *Int. J. Biol. Macromol.*, 1980, **2**, 284–288.
- 611 Y.E. Koo-Lee, R. Smith and R. Kopelman, *Annu. Rev. Anal. Chem.*, 2009, **2**, 57–76.
- 612 R. Ruiz-González, R. Bresolí-Obach, Ò. Gulías, M. Agut, H. Savoie, R. W. Boyle, S. Nonell and F. Giuntini, *Angew. Chemie Int. Ed.*, 2017, **56**, 2885–2888.
- 613 R. Bresolí-Obach, J. Nos, M. Mora, M. L. Sagristà, R. Ruiz-González and S. Nonell, *Methods*, 2016, **109**, 64–72.
- 614 K. Kundu, S.F. Knight, N. Willett, S. Lee, W.R. Taylor and N. Murthy, *Angew. Chemie Int. Ed.*, 2009, **48**, 299–303.
- 615 Y.Q. O'Malley, K.J. Reszka and B.E. Britigan, *Free Radic. Biol. Med.*, 2004, **36**, 90–100.
- 616 K. Takeda, K. Fujisawa, H. Nojima, R. Kato, R. Ueki and H. Sakugawa, *J. Photochem. Photobiol. A Chem.*, 2017, **340**, 8–14.
- 617 S.E. Page, W.A. Arnold and K. McNeill, *J. Environ. Monit.*, 2010, **12**, 1658.
- 618 A. Verma and F. Stellacci, *Small*, 2010, **6**, 12–21.
- 619 I. Brigger, C. Dubernet and P. Couvreur, *Adv. Drug Deliv. Rev.*, 2002, **54**, 631–651.
- 620 R. Brandt and A.S. Keston, *Anal. Biochem.*, 1965, **11**, 6–9.

- 621 P. Agostinis, A. Vantiegheem, W. Merlevede and P.A.M. De Witte, *Int. J. Biochem. Cell Biol.*, 2002, **34**, 221–241.
- 622 [Http://www.thermofisher.com/order/catalog/product/C10448](http://www.thermofisher.com/order/catalog/product/C10448), Visited on: 26th March 2018.
- 623 C.J. Hall, R.H. Boyle, X. Sun, S.M. Wicker, J.P. Misa, G.W. Krissansen, C.G. Print, K.E. Crosier and P.S. Crosier, *Nat. Commun.*, 2014, **5**, 3880–3882.
- 624 H.Y. Ahn, K.E. Fairfull-Smith, B.J. Morrow, V. Lussini, B. Kim, M.V. Bondar, S.E. Bottle and K.D. Belfield, *J. Am. Chem. Soc.*, 2012, **134**, 4721–4730.
- 625 M. Latil, P. Rocheteau, L. Châtre, S. Sanulli, S. Mémet, M. Ricchetti, S. Tajbakhsh and F. Chrétien, *Nat. Commun.*, 2012, **3**, 903.
- 626 L. Liu, J. Ulbrich, J. Müller, T. Wüstefeld, L. Aeberhard, T.R. Kress, N. Muthalagu, L. Rycak, R. Rudalska, R. Moll, S. Kempa, L. Zender, M. Eilers and D. J. Murphy, *Nature*, 2012, **483**, 608–612.
- 627 W.T. Harkcom, A.K. Ghosh, M.S. Sung, A. Matov, K.D. Brown, P. Giannakakou and S.R. Jaffrey, *Proc. Natl. Acad. Sci.*, 2014, **111**, 2443–2452.
- 628 E. Runge and E.K.U. Gross, *Phys. Rev. Lett.*, 1984, **52**, 997–1000.
- 629 W.H. Koppenol, *Free Radic. Biol. Med.*, 1993, **15**, 645–651.
- 630 A.C. Soares, R. Leite, M.A.K. . Tatsuo and I.D. Duarte, *Eur. J. Pharmacol.*, 2000, **400**, 67–71.
- 631 M. Kim, S.K. Ko, H. Kim, I. Shin and J. Tae, *Chem. Commun.*, 2013, **49**, 7959–7961.
- 632 L. Lin, D. Xiao, H. Yuan, M.M.F. Choi and W. Chan, *J. Chem. Educ.*, 2005, **82**, 1231.
- 633 N. Yoshito, N. Yusuke and O. Nobumoto, WO2012/061403 A1, 2012.
- 634 F.H. Westheimer, *Chem. Rev.*, 1961, **61**, 265–273.
- 635 H. Muchalski, A.J. Levonyak, L. Xu, K.U. Ingold and N.A. Porter, *J. Am. Chem. Soc.*, 2015, **137**, 94–97.
- 636 D.A. Bass, J.W. Parce, L.R. Dechatelet, P. Szejda, M.C. Seeds and M. Thomas, *J. Immunol.*, 1983, **130**, 1910–1917.
- 637 P. Breeuwer, J.L. Drocourt, N. Bunschoten, M.H. Zwietering, F.M. Rombouts and T. Abee, *Appl. Environ. Microbiol.*, 1995, **61**, 1614–1619.
- 638 L.D. Lavis, T. Chao and R.T. Raines, *Chem. Sci.*, 2011, **2**, 521–530.
- 639 T. Macrides, A. Shihata, N. Kalafatis and P. Wright, *IUBMB Life*, 1997, **42**, 1249–1260.
- 640 M.Y. Li, C.S. Cline, E.B. Koker, H.H. Carmichael, C.F. Chignell and P. Bilski, *Photochem. Photobiol.*, 2001, **74**, 760–764.
- 641 A. Rodríguez-Pulido, A.L. Cortajarena, J. Torra, R. Ruiz-González, S. Nonell and C. Flors, *Chem. Commun.*, 2016, **52**, 8405–8408.
- 642 A.G. Bell, *Am. J. Sci.*, 1880, **3**, 305–324.
- 643 A.G. Bell, *Philos. Mag.*, 1881, **11**, 510–587.
- 644 W.R. Harshbarger and M.B. Robin, *Acc. Chem. Res.*, 1973, **6**, 329–334.
- 645 A. Rosencwaig, *Science*, 1973, **181**, 657–658.
- 646 A. Rosencwaig and A. Gersho, *J. Appl. Phys.*, 1976, **47**, 64–69.
- 647 L. B. Kreuzer, *Anal. Chem.*, 1974, **46**, 235–244.
- 648 A.C. Tam and C.K.N. Patel, *Appl. Phys. Lett.*, 1979, **35**, 843–845.
- 649 E. Voigtman, A. Jurgensen and J.D. Winefordner, *Anal. Chem.*, 1981, **53**, 1921–1923.
- 650 T. Kitamori and T. Sawada, *Spectrochem. Acta Rev.*, 1991, **14**, 275–279.
- 651 V.E. Anderson, H.Z. Cheng, G.J. Diebold, A. Mahmood and D.A. Sweigart, *J. Am. Chem. Soc.*, 1987, **109**, 6191–6193.
- 652 O.V. Puchenkov and S. Malkin, *Rev. Sci. Instrum.*, 1996, **67**, 672–680.
- 653 O.V. Puchenkov, Z. Kopf and S. Malkin, *Biochim. Biophys. Acta*, 1995, **1231**, 197–212.
- 654 G.J. Edens, M.R. Gunner, Q. Xu and D. Mauzerall, *J. Am. Chem. Soc.*, 2000, **122**, 1479–1485.
- 655 O.V. Puchenkov, *Biophys. Chem.*, 1995, **56**, 241–261.
- 656 R.M. Williams, A.F. McDonagh and S.E. Braslavsky, *Photochem. Photobiol.*, 1998, **68**, 433–437.
- 657 T. Gensch and S.E. Braslavsky, *J. Phys. Chem. B*, 1997, **101**, 101–108.
- 658 C. Liu, X. Gong, R. Lin, F. Liu, J. Chen, Z. Wang, L. Song and J. Chu, *Theranostics*, 2016, **6**, 2414–2430.

- 659 S.K. Herbert, T. Han and T.C. Vogelmann, *Photosynth. Res.*, 2000, **66**, 13–31.
- 660 C. Viappiani, S. Abbruzzetti, J.R. Small, L.J. Libertini and E.W. Small, *Biophys. Chem.*, 1998, **73**, 13–22.
- 661 E. Oliveros, S.H. Bossmann, S. Nonell, C. Martí, G. Heit, G. Tröschler, A. Neuner, C. Martínez and A.M. Braun, *New J. Chem.*, 1999, **23**, 85–93.
- 662 T. Gensch, M.S. Churio, S.E. Braslavsky and K. Schaffner, *Photochem. Photobiol.*, 1996, **63**, 719–725.
- 663 S. Abbruzzetti, E. Crema, L. Masino, A. Veccli, C. Viappiani, J.R. Small, L.J. Libertini and E.W. Small, *Biophys. J.*, 2000, **78**, 405–415.
- 664 C.J. Reinhardt and J. Chan, *Biochemistry*, 2018, **57**, 194–199.
- 665 J. Yao and L.V. Wang, *Contrast Media Mol. Imaging*, 2011, **6**, 332–345.
- 666 P. Beard, *Interface Focus*, 2011, **1**, 602–631.
- 667 M. Xu and L.V. Wang, *Rev. Sci. Instrum.*, 2006, **77**, 41101.
- 668 L.V. Wang and H.I. Wu, *Biomedical Optics*, John Wiley & Sons, 2009.
- 669 L.V. Wang, *Nat. Photonics*, 2009, **3**, 503–509.
- 670 L.M. Kabeya, M.F. Andrade, F. Piatasi, A.E.C. S. Azzolini, A.C.M. Polizello and Y.M. Lucisano-Valim, *Anal. Biochem.*, 2013, **437**, 130–132.
- 671 S. Madersbacher and P. Berger, *J. Immunol. Methods*, 1991, **138**, 121–124.
- 672 D. Josephy, T. Eling and R. Mason, *J. Biol. Chem.*, 1982, **257**, 3669–3675.
- 673 L.A. Marquez and H.B. Dunford, *Biochemistry*, 1997, **36**, 9349–9355.
- 674 K. Pu, A.J. Shuhendler, J.V. Jokerst, J. Mei, S. S. Gambhir, Z. Bao and J. Rao, *Nat. Nanotechnol.*, 2014, **9**, 233–239.
- 675 C. Yin, X. Zhen, Q. Fan, W. Huang and K. Pu, *ACS Nano*, 2017, **11**, 4174–4182.
- 676 X. Zhang, C. Huang, S. Xu, J. Chen, Y. Zeng, P. Wu and X. Hou, *Chem. Commun.*, 2015, **51**, 14465–14468.
- 677 J.J. Jankowski, D.J. Kieber and K. Mopper, *Photochem. Photobiol.*, 1999, **70**, 319–328.
- 678 J.C. Barreto, G.S. Smith, N.H.P. Strobel, P.A. McQuillin and T.A. Miller, *Life Sci.*, 1994, **56**, 89–96.
- 679 X. Ragàs, M. Agut and S. Nonell, *Free Radic. Biol. Med.*, 2010, **49**, 770–776.
- 680 B. Li, L. Lin, H. Lin and B.C. Wilson, *J. Biophotonics*, 2016, **9**, 1314–1325.
- 681 B.W. Pogue, J.T. Elliott, S.C. Kanick, S.C. Davis, K.S. Samkoe, E.V. Maytin, S.P. Pereira and T. Hasan, *Phys. Med. Biol.*, 2016, **61**, 57–89.
- 682 M. A. Weston and M. S. Patterson, Singlet Oxygen dosimetry in biological media, in *Singlet Oxygen : Applications in Biosciences and Nanosciences*, Ed. S. Nonell and C. Flors, 2016, 151–168.
- 683 B.C. Wilson, M.S. Patterson and L. Lilge, *Lasers Med. Sci.*, 1997, **12**, 182–199.
- 684 J.S. Dysart, M.S. Patterson, T.J. Farrell and G. Singh, *Photochem. Photobiol.*, 2002, **75**, 289–295.
- 685 J.S. Dysart, G. Singh and M.S. Patterson, *Photochem. Photobiol.*, 2005, **81**, 196–205.
- 686 J.C. Finlay, S. Mitra, M.S. Patterson and T.H. Foster, *Phys. Med. Biol.*, 2004, **49**, 4837–4860.
- 687 M.T. Jarvi, M.S. Patterson and B.C. Wilson, *Biophys. J.*, 2012, **102**, 661–671.
- 688 W.R. Potter, T.S. Mang and T.J. Dougherty, *Photochem. Photobiol.*, 1987, **46**, 97–101.
- 689 M.T. Jarvi, M.J. Niedre, M.S. Patterson and B.C. Wilson, *Photochem. Photobiol.*, 2006, **82**, 1198–1204.
- 690 T. Hirano, E. Kohno and M. Nishiwaki, *J. Japan Soc. Laser Surg. Med.*, 2001, **22**, 99–108.
- 691 M. Niedre, M.S. Patterson and B.C. Wilson, *Photochem. Photobiol.*, 2002, **75**, 382–91.
- 692 M.J. Niedre, A.J. Secord, M.S. Patterson and B.C. Wilson, *Cancer Res.*, 2003, **63**, 7986–7994.
- 693 S. Erbas-Cakmak and E.U. Akkaya, *Org. Lett.*, 2014, **16**, 2946–2949.
- 694 Y. Yuan, C.J. Zhang, S. Xu and B. Liu, *Chem. Sci.*, 2016, **7**, 1862–1866.
- 695 Y. You, E.J. Cho, H. Kwon, J. Hwang and S.E. Lee, *Chem Commun*, 2015, **52**, 780–783.
- 696 Y. Wei, J. Song and Q. Chen, *Photochem. Photobiol. Sci.*, 2011, **10**, 1066–1071.
- 697 Y. Qin, D. Xing, S. Luo, J. Zhou, X. Zhong and Q. Chen, *Photochem. Photobiol.*, 2005, **81**, 1534–1538.

- 698 Y. Wei, D. Xing, S. Luo, W. Xu and Q. Chen, *J. Biomed. Opt.*, 2008, **13**, 24023-24025.
- 699 A.F. Olea and F. Wilkinson, *J. Phys. Chem.*, 1995, **99**, 4518-4524.
- 700 A.H. Delcour, *Biochim. Biophys. Acta*, 2009, **1794**, 808-816.
- 701 A.L. Harvey, *Drug Discov. Today*, 2008, **13**, 894-901.
- 702 J.G. Luis, W.Q. Fletcher, F. Echeverri, T.A. Grillo, M.P. Kishi and A. Perales, *Nat. Prod. Lett.*, 1994, **6**, 23-28.
- 703 M. Irie, *Chem. Rev.*, 2000, **100**, 1683-1684.
- 704 I. Tochitsky, Z. Helfft, V. Meseguer, R.B. Fletcher, K.A. Vessey, M. Telias, B. Denlinger, J. Malis, E.L. Fletcher and R.H. Kramer, *Neuron*, 2016, **92**, 100-113.
- 705 M. Izquierdo-Serra, A. Bautista-Barrufet, A. Trapero, A. Garrido-Charles, A. Díaz-Tahoces, N. Camarero, S. Pittolo, S. Valbuena, A. Pérez-Jiménez, M. Gay, A. García-Moll, C. Rodríguez-Esrich, J. Lerma, P. de la Villa, E. Fernández, M. À. Pericàs, A. Llebaria and P. Gorostiza, *Nat. Commun.*, 2016, **7**, 12221-12223.
- 706 S.E. Stein and R.L. Brown, *J. Am. Chem. Soc.*, 1991, **113**, 787-793.
- 707 S. Gronert, *J. Org. Chem.*, 2006, **71**, 1209-1219.
- 708 L. Duque, C. Restrepo, J. Sáez, J. Gil, B. Schneider and F. Otálvaro, *Tetrahedron Lett.*, 2010, **51**, 4640-4643.
- 709 B. Schneider, L. Duque, C. Zapata and F. Ot, *Org. Lett.*, 2013, **15**, 2011-2014.
- 710 D. Holscher, S. Dhakshinamoorthy, T. Alexandrov, M. Becker, T. Bretschneider, A. Buerkert, A.C. Crecelius, D. De Waele, A. Elsen, D.G. Heckel, H. Heklau, C. Hertweck, M. Kai, K. Knop, C. Krafft, R. K. Maddula, C. Matthäus, J. Popp, B. Schneider, U. S. Schubert, R.A. Sikora, A. Svato, R.L. Swennen, D. Hölscher, S. Dhakshinamoorthy, T. Alexandrov, M. Becker, T. Bretschneider, A. Buerkert, A.C. Crecelius, D. De Waele, A. Elsen, D.G. Heckel, H. Heklau, C. Hertweck, M. Kai, K. Knop, C. Krafft, R.K. Maddula, C. Matthäus, J. Popp, B. Schneider, U.S. Schubert, R.A. Sikora, A. Svatoš and R.L. Swennen, *Proc. Natl. Acad. Sci.*, 2014, **111**, 105-110.
- 711 R. Dosselli, C. Tampieri, R. Ruiz-González, S. De Munari, X. Ragàs, D. Sánchez-García, M. Agut, S. Nonell, E. Reddi and M. Gobbo, *J. Med. Chem.*, 2013, **56**, 1052-1063.
- 712 E. Rosàs, P. Santomá, M. Duran-Frigola, B. Hernández, M.C. Llinàs, R. Ruiz-González, S. Nonell, D. Sánchez-García, E.R. Edelman and M. Balcells, *Langmuir*, 2013, **29**, 9734-9743.
- 713 J.E. Bachman, L.A. Curtiss and R.S. Assary, *J. Phys. Chem. A*, 2014, **118**, 8852-8860.
- 714 G. Zampini, O. Planas, F. Marmottini, O. Gulías, M. Agut, S. Nonell and L. Latterini, *RSC Adv.*, 2017, **7**, 14422-14429.
- 715 E.J. Hong, D.G. Choi and M.S. Shim, *Acta Pharm. Sin. B*, 2016, **6**, 297-307.
- 716 P. García-Calavia, I. Chambrier, M.J. Cook, A. H. Haines, R.A. Field and D.A. Russell, *J. Colloid Interface Sci.*, 2018, **512**, 249-259.
- 717 A.F. Monteiro, M. Rato and C. Martins, *Clin. Dermatol.*, 2016, **34**, 571-581.
- 718 V. Brezova, M. Valko, M. Breza, H. Morris, J. Telser, D. Dvoranova, K. Kaiserova, L. Varecka, M. Mazur and D. Leibfritz, *J. Phys. Chem. B*, 2003, **107**, 2415-2425.
- 719 O. Molins-Molina, R. Bresolí-Obach, G. Garcia-Lainez, I. Andreu, S. Nonell, M. A. Miranda and M.C. Jiménez, *J. Phys. Org. Chem.*, 2017, **30**, 1-7.
- 720 R. Ruiz-González, P. Milán, R. Bresolí-Obach, J. Stockert, A. Villanueva, M. Cañete and S. Nonell, *Cancers*, 2017, **9**, 18.
- 721 M.T. Piccolo, C. Menale and S. Crispi, *Anticancer. Agents Med. Chem.*, 2015, **15**, 408-422.
- 722 P.A. Cowled, L. Mackenzie and I.J. Forbes, *Cancer Res.*, 1987, **47**, 971-974.
- 723 P.F. Brophy and S.M. Keller, *J. Surg. Res.*, 1992, **52**, 631-634.
- 724 V. Kirveliėne, G. Grazeleėne, D. Dabkeviciėne, I. Micke, D. Kirvelis, B. Juodka and J. Didziapetriėne, *Cancer Chemother. Pharmacol.*, 2006, **57**, 65-72.
- 725 S. Zakaria, A.M. Gamal-Eldeen, S.M. El-Daly and S. Saleh, *Photodiagnosis Photodyn. Ther.*, 2014, **11**, 227-238.
- 726 T.A. Shewmake, F.J. Solis, R.J. Gillies and M. R. Caplan, *Biomacromolecules*, 2008, **9**, 3057-3064.
- 727 P. Yang, S. Gai and J. Lin, *Chem. Soc. Rev.*, 2012, **41**, 3679-3685.
- 728 R. Ruiz-González, A.L. Cortajarena, S.H. Mejias, M. Agut, S. Nonell and C. Flors, *J. Am. Chem. Soc.*, 2013, **135**, 9564-9567.
- 729 B. Gómez-Reyes and A.K. Yatsimirsky, *Org. Lett.*, 2003, **5**, 4831-4834.

- 730 B. Halliwell, M.V. Clement and L.H. Long, *FEBS Lett.*, 2000, **486**, 10–13.
- 731 S. Mallidi, G.P. Luke and S. Emelianov, *Trends Biotechnol.*, 2011, **29**, 213–221.
- 732 M.V. Cattaneo and J.H.T. Luong, *Electroanalysis*, 1996, **8**, 223–228.
- 733 A. Rodríguez-Pulido, A.L. Cortajarena, J. Torra, R. Ruiz-González, S. Nonell and C. Flors, *Chem. Commun.*, 2016, **52**, 8405–8408.
- 734 J.L. Smith and J.A. Alford, *Lipids*, 1970, **5**, 795–799.
- 735 Z. Chen, X.L. Deán-Ben, S. Gottschalk and D. Razansky, *Biomed. Opt. Express*, 2018, **9**, 2229.
- 736 S.S. Kelkar and T.M. Reineke, *Bioconjugate Chem.*, 2011, **22**, 1879–903.
- 737 A.A. Krasnovsky Jr., *J. Photochem. Photobiol. A Chem.*, 2018, **354**, 11–24.
- 738 M.K. Kuimova, G. Yahioglu and P.R. Ogilby, *J. Am. Chem. Soc.*, 2009, **131**, 332–340.
- 739 K. Świderek and P. Paneth, *Chem. Rev.*, 2013, **113**, 7851–7879.
- 740 L. Gille, U. Prösch and R. Stoesser, *Int. J. Radiat. Appl. Instr. Radiat. Phys. Chem.*, 1992, **40**, 461–468.
- 741 J.A. Weil, K.V. Sane and J.M. Kinkade, *J. Phys. Chem.*, 1961, **65**, 710–712.
- 742 S. Goldschmidt and K. Renn, *Berichte der Dtsch. Chem. Gesellschaft*, 1922, **55**, 628–643.
- 743 R.H. Poirier, E.J. Kahler and F. Benington, *J. Org. Chem.*, 1952, **17**, 1437–1445.
- 744 P. Griess, *Berichte der Dtsch. Chem. Gesellschaft*, 1879, **12**, 426–428.
- 745 K. Schulz, S. Kerber and M. Kelm, *Nitric oxide*, 1999, **3**, 225–234.
- 746 J.C. Kennedy, S.L. Marcus and R.H. Pottier, *Photomed. Laser Surg.*, 1996, **14**, 289–293.
- 747 N.H. Bui-Xuan, P.M.K. Tang, C.K. Wong, J.Y.W. Chan, K.K.Y. Cheung, J.L. Jiang and K.P. Fung, *Cell. Immunology*, 2011, **269**, 60–67.
- 748 J. Chan, P. Tang, P.M. Hon, S. Au, S. Tsui, M. Waye, S.K. Kong, T. Mak and K.P. Fung, *Planta Med.*, 2006, **72**, 28–33.
- 749 L.E. Xodo, V. Rapozzi, M. Zacchigna, S. Drioli and S. Zorzet, *Curr. Med. Chem.*, 2012, **19**, 799–807.
- 750 W.Y. Lee, D.S. Lim, S.H. Ko, Y.J. Park, K.S. Ryu, M.Y. Ahn, Y.R. Kim, D.W. Lee and C.W. Cho, *J. Photochem. Photobiol. B.*, 2004, **75**, 119–126.
- 751 P.M.K. Tang, J.Y.W. Chan, S.W.N. Au, S.K. Kong, S.K.W. Tsui, M.M.Y. Waye, T.C.W. Mak, W.P. Fong and K.P. Fung, *Cancer Biol. Ther.*, 2006, **5**, 1111–1116.
- 752 D. Lebrecht and U.A. Walker, *Cardiovasc. Toxicol.*, 2007, **7**, 108–113.
- 753 A. Eisfeld and J.S. Briggs, *Chem. Phys.*, 2006, **324**, 376–384.
- 754 F. Valeriote and H. Lin, *Cancer Chemother. reports*, 1975, **59**, 895–900.
- 755 C. Lorente, E. Arzoumanian, C. Castaño, E. Oliveros and A.H. Thomas, *RSC Adv.*, 2014, **4**, 10718–10725.

Chapter IX

Annex

Mentre estaven conversant sobre aquest tema, un especialista en l'Art es va presentar davant del papa i li va dir que a causa de la diversificació de les ciències (en teologia, en filosofia, en dret i en medicina) s'havien generat multitud d'opinions diverses en cadascuna d'aquestes ciències; i això es devia al fet que els autors i els mestres escrivien obres sobre les ciències en les quals els uns divergien de les opinions dels altres. Per això l'especialista en l'Art va dir al papa i als cardenals que totes les ciències s'havien de sotmetre a uns mateixos breus principis necessaris que funcionessin d'acord amb el mètode de l'Art per tal que, si sorgia algun error o alguna falsa opinió, aplicant l'Art es pogués posar ordre als principis de cada ciència i s'eliminessin les falses opinions, contràries a aquestes ciències.

Ramon Llull

List of articles derived from the thesis

Publications derived from this thesis (together with my contributions to each manuscript) are listed below by chronological order:

(*These authors contributed equally to this work.)

“S'ha d'entendre allò que estimes i s'ha d'estimar allò que entens”

Ramon Llull

1) G. Bucher, **R. Bresolí-Obach**, C. Brosa, C. Flors, J.G. Luis, T.A. Grillo, S. Nonell; β -Phenyl quenching of 9-phenylphenalenones: a novel photocyclisation reaction with biological implications; *Phys. Chem. Chem. Phys.*, **2014**, 16, 18813-18820.

Roger Bresolí Obach has synthesized the 9-perdeuterophenylphenalenone, characterized their photophysical and photochemical properties, unravelled the β -phenyl quenching mechanism for 9-phenylphenalenones, participated in data analysis and discussion, and participated in the critical revision and final approval of the manuscript.

2) O. Planas,⁺ **R. Bresolí-Obach**,⁺ J. Nos,⁺ T. Gallavardin, R. Ruiz-González, M. Agut, S. Nonell; Synthesis, Photophysical characterization, and photoinduced antibacterial activity of methylene blue-loaded amino- and mannose-targeted mesoporous silica nanoparticles; *Molecules*, **2015**, 20, 6284-6298.

Roger Bresolí Obach has characterized the photophysical and photosensitizing properties of the methylene blue silica nanoconjugates, assisted in the assessment of the biological activity of the nanoconjugates in microbial samples, participated in data analysis and discussion, participated in the preparation of the first draft of the manuscript and participated in its critical revision and final approval.

3) **R. Bresolí-Obach**, S. Nonell; A modern view on the beta phenyl quenching of aromatic ketones; *Afinidad*, **2016**, 574, 90-95.

Roger Bresolí Obach has written the first draft of the manuscript and participated in its critical revision and final approval.

4) **R. Bresolí-Obach**, J. Nos, M. Mora, M.L. Sagristà, R. Ruiz-González, S. Nonell; Anthracene-based fluorescent nanoprobe for singlet oxygen detection in biological media; *Methods*, **2016**, 109, 64-72.

Roger Bresolí Obach has participated in the design and conception of the nanoprobe presented in this manuscript.

Roger Bresolí Obach has synthesized and characterized the physico-chemical, photophysical properties of the anthracene dipropionic acid nanoconjugates, explored their reactivity towards $^1\text{O}_2$, studied the interaction between the nanoprobe and proteins (BSA and miniSOG), assisted in the assessment of the $^1\text{O}_2$ detection inside HeLa cells, participated in data analysis and discussion, prepared the first draft of the manuscript and participated in its critical revision and final approval.

5) R. Ruiz-González, ⁺ **R. Bresolí-Obach**, ⁺ O. Gulias, M. Agut, H. Savoie, R.W. Boyle, S. Nonell, F. Giuntini; NanoSOSG: a nanostructured fluorescent probe for the detection of intracellular singlet oxygen; *Angew. Chem. Int. Ed.*, **2017**, 56, 2885-2888.

R. Ruiz-González, ⁺ **R. Bresolí-Obach**, ⁺ O. Gulias, M. Agut, H. Savoie, R.W. Boyle, S. Nonell, F. Giuntini; NanoSOSG: ein nanostrukturiertes fluoreszenzsonde zur detektion von intrazellulärer singulett-sauerstoff; *Angew. Chem.*, **2017**, 129, 2931-2934.

Roger Bresolí Obach has studied the interaction between SOSG (or its nanoparticulate form) and bovine serum albumin, designed and performed the experiments of the $^1\text{O}_2$ detection with *E. coli* bacterial cells, participated in data analysis and discussion, participated in the preparation of the first draft of the manuscript and participated in its critical revision and final approval.

6) R. Ruiz-González, P. Millán, **R. Bresolí-Obach**, J.C. Stockert, A. Villanueva, M. Cañete, S. Nonell; Photodynamic synergistic effect of pheophorbide a and doxorubicin in combined treatment against tumoral cells; *Cancers*, **2017**, 9, 18.

Roger Bresolí Obach has characterized the photophysical and photosensitizing properties of the drugs used in this work (Pheophorbide a and doxorubicin), studied the interaction between doxorubicin and DNA, participated in data analysis and discussion and participated in its critical revision and final approval of the manuscript.

7) J. Marioni, ⁺ **R. Bresolí-Obach**, ⁺ M. Agut, L.R. Comini, J.L. Cabrera, M.G. Paraje, S. Nonell, S.C. Nuñez-Montoya; On the mechanism of *Candida tropicalis* biofilm reduction by the combined action of naturally-occurring anthraquinones and blue light; *PLoS ONE*, **2017**, 12, e0181517.

Roger Bresolí Obach has characterized the photophysical, photochemical and photosensitizing properties of the anthraquinones used in this work either free in solution or adsorbed onto *C. tropicalis* biofilms, participated in data analysis and discussion, participated in the preparation of the first draft of the manuscript and participated in its critical revision and final approval.

8) **R. Bresolí-Obach**,[†] I. Gispert,[†] D. García-Peña,[†] S. Boga, Ó. Gulias, M. Agut, M.E. Vázquez, S. Nonell; Triphenylphosphonium cation: a valuable functional group for antimicrobial photodynamic therapy; *J. Biophotonics*, **2018**, e201800054.

Roger Bresolí Obach has participated in the design and conception of the two triphenylphosphonium derivatized PS presented in this manuscript.

Roger Bresolí Obach has characterized the photophysical and photosensitizing properties of the two triphenylphosphonium derivatized PS, assisted in the assessment of the biological activity of them, participated in data analysis and discussion, participated in the preparation of the first draft of the manuscript and participated in its critical revision and final approval.

9) **R. Bresolí-Obach**,[†] L. Busto-Moner,[†] C. Muller, M. Reina, S. Nonell; NanoDCFH-DA: a silica-based nanostructured fluorogenic probe for the detection of reactive oxygen species; *Photochem. Photobiol.*, under revision.

Roger Bresolí Obach has participated in the design and conception of the nanoprobe presented in this manuscript.

Roger Bresolí Obach has assisted in the synthesis, characterization of the physico-chemical and the photophysical properties of the DCFH-DA nanoconjugates, the study of their reactivity towards ROS, the assessment of interaction between the nanoprobe and proteins and the assessment of the ROS detection inside HeLa cells. He has participated in data analysis and discussion, prepared the first draft of the manuscript and participated in its critical revision and final approval.

Publications not directly-derived from this thesis (together with my contributions to each manuscript) are listed below by chronological order:

“L'home és esclau de les seves paraules i amo dels seus silencis”

Refrany popular

10) E. Anaya-Plaza, E. van de Winckel, J. Mikkilä, J.M. Malho, O. Ikkala, O. Gulías, **R. Bresolí-Obach**, M. Agut, S. Nonell, T. Torres, M.A. Kostianen, A. de la Escosura; Photoantimicrobial biohybrids by supramolecular immobilization of cationic phthalocyanines onto cellulose nanocrystals; *Chem. Eur. J.*, **2017**, 23, 4320-4326.

Roger Bresolí Obach has characterized the photophysical and photosensitizing properties of the free phthalocyanines and phthalocyanines-cellulose biohybrids, assisted in the assessment of the biological activity of the biohybrids, participated in data analysis and discussion, participated in the preparation of the first draft of the manuscript and participated in its critical revision and final approval.

11) J. Font, M. López-Cano, S. Notartomaso, P. Scarselli, P. Di Pietro, **R. Bresolí-Obach**, G. Battaglia, F. Malhaire, X. Rovira, J. Catena, J. Giraldo, J.P. Pin, V. Fernández-Dueñas, C. Goudet, S. Nonell, F. Nicoletti, A. Llebaria, F. Ciruela; Optical control of pain in vivo with a photoactive mGlu₅ receptor negative allosteric modulator; *eLife*, **2017**, 6, e23545.

Roger Bresolí Obach has characterized the photochemical properties of some caged compounds, determined their photouncaging quantum yields, participated in data analysis and participated in the critical revision and final approval of the manuscript.

12) O. Molins-Molina, **R. Bresolí-Obach**, G. Garcia-Lainez, I. Andreu, S. Nonell, M.A. Miranda, M.C. Jiménez; Singlet oxygen production and in vitro phototoxicity studies on fenofibrate, mycophenolate mofetil, trifusal, and their active metabolites; *J. Phys. Org. Chem.*, **2017**, e3722.

Roger Bresolí Obach has assisted in the assessment of the photosensitizing properties of the drugs and metabolites studied in this work, participated in data analysis and discussion, participated in the preparation of the first draft of the manuscript and participated in its critical revision and final approval.

13) A. Gandioso, **R. Bresolí-Obach**, A. Nin-Hill, M. Bosch, M. Palau, A. Galindo, S. Contreras, A. Rovira, C. Rovira, S. Nonell, V. Marchán; Redesigning the coumarin scaffold into small bright fluorophores with far-red to NIR emission and large Stokes' shifts useful for cell imaging; *J. Org. Chem.*, **2018**, 83, 1185-1195.

Roger Bresolí Obach has characterized the photophysical properties of the different fluorophores, participated in data analysis and discussion, participated in the preparation of the first draft of the manuscript and participated in its critical revision and final approval.

14) R.P. Zanocco, **R. Bresolí-Obach**, S. Nonell, E. Lemp, A.L. Zanocco; Structure–activity study of furyl aryloxazole fluorescent probes for the detection of singlet oxygen; *PLoS ONE*, **2018**, 13, e0200006.

Roger Bresolí Obach has assisted in the assessment of the reactivity of furyl-aryloxazole towards $^1\text{O}_2$ and participated in its critical revision and final approval.

15) A. Gandioso,[†] M. Palau-Requena,[†] **R. Bresolí-Obach**,[†] A. Galindo, A. Rovira, M. Bosch, S. Nonell, V. Marchán; Unprecedented high photostability in non-conventional coumarins with far-red/NIR emission through azetidiny substitution; *J. Org. Chem.*, submitted.

Roger Bresolí Obach has characterized the photophysical properties of the different fluorophores, participated in data analysis and discussion, participated in the preparation of the first draft of the manuscript and participated in its critical revision and final approval.

Book chapters derived from this thesis (together with my contributions to each chapter) are listed below by chronological order:

“Not everything that is more difficult is more meritorious”

Tommaso d'Aquino

B1) O. Planas, E. Boix-Garriga, B. Rodriguez-Amigo, J. Torra, **R. Bresolí-Obach**, C. Flors, C. Viappiani, M. Agut, R. Ruiz-González, S. Nonell; Chapter 9: Newest approaches to singlet oxygen photosensitisation in biological media. In *Photochemistry: Volume 42*; Fasani, E.; Albini, A., Eds.; Photochemistry; Royal Society of Chemistry, **2015**, 42, 233-278. ISBN: 978-1-84973-956-6.

Roger Bresolí Obach has written the first draft of the section “Switchable PSs” and participated in its critical revision and final approval.

B2) **R. Bresolí-Obach**, C. Hally, S. Nonell; Chapter 8: Activatable photosensitizers. In *Singlet oxygen: Applications in biosciences and nanosciences Volume 1*; Nonell, S.; Flors, C., Eds.; Comprehensive Series in photochemical and photobiological sciences; Royal Society of Chemistry, **2016**, 163-181. ISBN: 978-1-78262-038-9.

Roger Bresolí Obach has written the first draft of the chapter and participated in its critical revision and final approval.

B3) B. Rodriguez-Amigo, O. Planas, J. Torra, **R. Bresolí-Obach**, R. Ruiz-González, S. Nonell; Chapter 2: Photosensitisers for Photodynamic Therapy: State of the Art and Perspectives. In *Photodynamic Medicine: From Bench to Clinic*; Kostron, H.; Hasan, T., Eds.; Royal Society of Chemistry, **2016**, 23-62. ISBN: 978-1-78262-451-6.

Roger Bresolí Obach has written the first draft of the sections “Preclinical PSs of natural origin” and “Activatable PSs” and participated in its critical revision and final approval

B4) C. Hally, B. Rodríguez-Amigo, **R. Bresolí-Obach**, O. Planas, J. Nos, E. Boix-Garriga, R. Ruiz-González, S. Nonell; Photodynamic Therapy. In *Theranostics and Image Guided Drug Delivery*; Thanou, A. Ed.; Royal Society of Chemistry, **2018**, 86-122. ISBN: 978-178-2624-66-0.

Roger Bresolí Obach has written the first draft of the section “¹O₂ Dosimetry” and participated in its critical revision and final approval.

Communications in congresses derived from this thesis are listed below by chronological order:

“Vergonya, cavallers, vergonya”

Jaume I El Conqueridor (a la batalla de Portopí)

C1) **R. Bresolí-Obach**, G. Bucher, C. Brosa, C. Flors, J.G. Luis, T.A. Grillo, S. Nonell; β -Phenyl quenching of 9-phenylphenalenones: a novel photocyclisation reaction with biological implications; 3rd ESP Photobiology School, June 16-21, **2014**.

C2) **R. Bresolí-Obach**, G. Bucher, C. Brosa, C. Flors, J.G. Luis, T.A. Grillo, S. Nonell; β -Phenyl quenching of 9-phenylphenalenones: a novel photocyclisation reaction with biological implications; 25th IUPAC Symposium on Photochemistry, Bordeaux (France), July 13-18, **2014**.

C3) **R. Bresolí-Obach**, R. Ruiz-González, O. Gulias, M. Agut, H. Savoie, R.W. Boyle, S. Nonell, F. Giuntini; Polyacrylamide nanoprobe: a new scaffold for assessing singlet oxygen production in biological environments. 16th Congress of the European Society for Photobiology, Aveiro (Portugal), August 31- September 4, **2015**.

C4) **R. Bresolí-Obach**, J. Nos, M. Mora, M.L. Sagristà, R. Ruiz-González, S. Nonell; Anthracene-based fluorescent nanoprobe for singlet oxygen detection in biological media. 5th HRSMC Photochemistry School, Maastricht (Holland), August 27-31, **2016**. **Best poster prize**.

C5) **R. Bresolí-Obach**, R. Zanocco, J. Nos, Ò. Gulías, M. Mora, M.L. Sagristà, F. Nájera, E. Pérez-Inestrosa, A.L. Zanocco, E. Lemp, M. Agut, R. Ruiz-González, S. Nonell; Singlet oxygen nanoprobe: a new scaffold for assessing singlet oxygen production in biological environments. Vth Spanish-Portuguese Workshop on Photochemistry, Toledo (Spain), September 7-10, **2016**.

C6) No communication presented but I assisted to: XXI International school of pure and applied biophysics: Time-resolved methods in biophysics, Venezia (Italy), January 9-13, **2017**.

C7) **R. Bresolí-Obach**, R. Zanocco, F. Nájera, E. Pérez-Inestrosa, A.L. Zanocco, E. Lemp, R. Ruiz-González, S. Nonell; Small particles, big improvement: a two-photon singlet oxygen fluorescent nanoprobe. XXXVI Biennial Meeting of the spanish royal society of chemistry, Sitges (Spain), June 25-29, **2017**.

C8) **R. Bresolí-Obach**, R. Zanocco, L. Busto, F. Nájera, E. Pérez-Inestrosa, A.L. Zanocco, E. Lemp, R. Ruiz-González, Santi Nonell; Small particles, big improvement: the use of nanoprobe for reactive oxygen species detection in biological media. 17th Congress of the European Society for Photobiology, Pisa (Italy), September 4-8, **2017**.

C9) **R. Bresolí-Obach**, C. Flors, A. Abudulimu, L. Lüer, J.G. Luis, T.A. Grillo, G. Bucher, S. Nonell; Beta-phenyl quenching in 9-arylphenalenones: a novel photocyclisation reaction with different implications; 27th IUPAC Symposium on Photochemistry, Dublin (Ireland), July 8-13, **2018**. **Best poster prize**.